Factors required to enhance water recycling at two major Australian industrial manufacturing sites

A thesis submitted for the degree of

Doctor of Philosophy

by

Bernard A. Agana

Victoria University

College of Engineering and Science

September 2013

Preface

I, Bernard A. Agana, declare that the PhD thesis entitled, **Factors required to enhance water recycling at two major Australian industrial manufacturing sites** is no more than 100,000 words in length including quotes and exclusive of tables, figures, appendices, bibliography, references and footnotes. This thesis contains no material that has been submitted previously, in whole or in part, for the award of any other academic degree or diploma. Except otherwise indicated, this thesis is my own work.

Signature  Date 27th August 2013

Journal publications, conference proceedings and conference presentations relevant to the scope of this thesis

Refereed Journal Publications (copies attached at the end of the thesis and also available in the accompanying CD)

[1] Agana, B. A., Reeve, D. & Orbell, J. D. 2011. Optimization of the operational parameters for a 50 nm ZrO_2 ceramic membrane as applied to the ultrafiltration of post-electrodeposition rinse wastewater. *Desalination,* 278**,** 325-332.

[2] Agana, B. A., Reeve, D. & Orbell, J. D. 2012. The influence of an applied electric field during ceramic ultrafiltration of post-electrodeposition rinse wastewater. *Water Research,* 46, 3574 – 3584.

[3] Agana, B. A., Reeve, D. & Orbell, J. D. 2013. An approach to industrial water conservation – A case study involving two large manufacturing companies based in Australia. *Journal of Environmental Management,* 114**,** 445-460.

[4] Agana, B. A., Reeve, D. & Orbell, J. D. 2013. Performance optimization of a 5 nm TiO2 ceramic membrane with respect to beverage production wastewater. *Desalination,* 311**,** 162-172.

[5] Agana, B. A., Reeve, D. & Orbell, J. D. (In press). Industrial water reclamation using low-pressure polymeric membranes – case studies involving a car

manufacturer and a beverage producer. *Journal of Water Reuse and Desalination*, doi:10.2166/wrd.2013.004.

Refereed Conference Proceedings (copies available in the accompanying CD)

[1] Agana, B.A., McKenzie-McHarg, G., Orbell, J. D. & Reeve, D. 2010. Towards optimal water reuse at Toyota Motor Corporation Australia Ltd. *In:* Ozwater'10, March 8-10, 2010, Brisbane, Queensland, Australia. Australian Water Association.

[2] Agana, B.A., Orbell, J. D. & Reeve, D. 2010. Optimizing process water use at two large Australian manufacturing companies. *In:* 3rd International Conference on Environmental and Computer Science, October 17-19, 2010, Kunming China. IEEE Press, 33-38.

[3] Agana, B.A., Orbell, J. D. & Reeve, D. 2011. Laboratory scale evaluation of ultrafiltration membranes for distributed wastewater treatment at an Australian car manufacturer's production site. *In:* Membranes and Desalination Specialty Conference IV, February 9-11, 2011, Gold Coast, Queensland, Australia. Australian Water Association (AWA).

[4] Agana, B. A., Orbell, J. D. & Reeve, D. 2011. Ceramic electro-ultrafiltration of post-electrodeposition paint rinse wastewater. *In:* 6th IWA Specialist Conference on Membrane Technology for Water & Wastewater Treatment, October 4-7, 2011, Aachen, Germany. IWA, 671-672.

[5] Agana, B. A., Reeve, D. & Orbell, J. D. 2012. Pre–treatment of Beverage Production Wastewater using a 5 nm TiO2 Ceramic Ultrafiltration Membrane. *Procedia Engineering,* 44**,** 666-669.

Conference Presentations (copies available in the accompanying CD)

[1] Agana, B.A., McKenzie-McHarg, G., Orbell, J. D. & Reeve, D. 2010. Towards optimal water reuse at a car manufacturing company. Ozwater'10, March 8-10, 2010, Brisbane, Queensland, Australia. Australian Water Association. *(Oral presentation).*

[2] Agana, B.A., Orbell, J. D. & Reeve, D. 2010. Optimizing process water use at two large Australian manufacturing companies. 2010, 3rd International Conference on Environmental and Computer Science. Kunming China. IEEE Press. *(Oral presentation).*

[3] Agana, B.A., Orbell, J. D. & Reeve, D. 2011. Laboratory scale evaluation of ultrafiltration membranes for distributed wastewater treatment at an Australian car manufacturer's production site. Membranes and Desalination Specialty Conference IV, February 9-11, 2011, Gold Coast, Queensland, Australia. Australian Water Association. *(Oral presentation).*

[4] Agana, B. A., Orbell, J. D. & Reeve, D. 2011. Ceramic electro-ultrafiltration of post-electrodeposition paint rinse wastewater. 6th IWA Specialist Conference on

Membrane Technology for Water & Wastewater Treatment, October 4-7, 2011, Aachen, Germany. IWA. *(Poster presentation).*

[5] Agana, B. A., Reeve, D. and Orbell, J.D. 2012. Pre-treatment of beverage production wastewater using a 5 nm TiO_2 ceramic ultrafiltration membrane. Euromembrane 2012, 23 – 27 September, 2012, London UK. (*Poster presentation).*

ABSTRACT

This study presents the application of an integrated water management strategy at two large Australian manufacturing companies that are contrasting in terms of their respective products and wastewater generation. The integrated strategy, consisting of water audit, pinch analysis and membrane process application, was deployed in series to systematically identify water conservation opportunities. Initially, a water audit was deployed to completely characterize all water streams found at each production site. This led to the development of a water balance diagram which, together with water test results, served as a basis for subsequent enquiry. After the water audit, commercially available water pinch software was utilized to identify possible water reuse opportunities, some of which were subsequently implemented on site. Finally, utilizing a laboratory-scale test rig, membrane processes such as UF, NF and RO were evaluated for their suitability to treat the various wastewater streams.

Experiments involving the reclamation of wastewater containing positively charged paint particles were carried out using a 50 nm ZrO_2 ceramic membrane. Results showed that paint particle deposition on the membrane surface is inhibited by a high crossflow velocity and low transmembrane pressure. Likewise, the effect of an applied electric field on the positively charged paint particles was also evaluated. The influence of an applied electric field was dependent on both the applied voltage and transmembrane pressure (TMP). At a TMP of 100 kPa, the application of different magnitudes of voltages generally improved filtration efficiency with the most significant improvement obtained at an applied voltage of 60 V. The specific energy consumption for both ultrafiltration and electro-ultrafiltration was comparable with each other. Similarly, a 5 nm TiO2 ceramic membrane was evaluated with respect to beverage production

wastewater. Results also reveal that certain combination of higher crossflow velocities and transmembrane pressures provide significant improvements in permeate flux and contaminant rejection rates.

In general, the findings reveal that, for both companies, although there is considerable potential for an enhancement of the recycling of significant volumes of process water, other factors need to be considered in order to move towards the goal of total process water recycling. For example, both companies would need to make significant process changes in order to increase water use efficiency and be prepared to invest in water recycling technologies. Currently, in Australia, there is little financial incentive to do this since the cost of water tariffs is generally cheaper than the cost of investing in process changes and water reclamation technologies. However, this situation may well change in the future.

Acknowledgements

The research work was completed with the help of many individuals and organizations. In connection with this, I wish to express my sincerest gratitude to the following:

1. The Australian Agency for International Development (AusAID) for the Australian Leadership Awards (ALA) Scholarship. This scholarship gave me the opportunity to undertake a PhD degree at Victoria University, Melbourne.
2. The two large manufacturing companies studied, Victoria University, and City West Water for providing the necessary research funds. The funds were vital to the success of this research undertaking.
3. My principal supervisor, Professor John D. Orbell for being continuously supportive and very helpful throughout my PhD journey.
4. My associate supervisor, Mr. Darrel Reeve, and my industry supervisors Audra Liubinas, Randa Kondos, Geraldine McKenzie-McHarg, Doug Anderson, and Graeme Kentish for all their valuable advice and guidance during the data gathering stages of the research work.
5. The technical staff at Victoria University (Werribee campus) for their support during the experiment stages of the research work.
6. My wife, daughter, parents, sister, and friends for their support and understanding throughout the duration of my PhD studies.

This thesis is dedicated to my wife and daughter

Abbreviations and Terms

ā	Adhesive distance
AATSE	Australian Academy of Technological Sciences and Engineering
Adhesive forces	Forces that tend to hold two bodies together
Agglomeration	Process of gathering into a mass
AHUs	Air Handling Units; utilized to condition and circulate incoming air supply
C_E	Equipment cost
CED	Cathodic Electrodeposition; rust proofing automotive bodies using positively charged paint
Ceramic membrane	Formed from inorganic materials such as alumina, titania and zirconia
CFV	Crossflow velocity; velocity of the fluid inside the test cell or module
C_I	Total initial cost of equipment installation
CIP	Clean-in-place; method of automatically cleaning without the need for disassembly and assembly of equipment
C_M	Miscellaneous cost
COD	Chemical oxygen demand; oxygen reducing capabilities of wastewater
Conductivity	Electrical conductance per unit distance
C_W	Cost of freshwater per m^3
C_{WW}	Cost of wastewater discharge per m^3
Deionization	Process of removing mineral ions in water

ΔP	Pressure drop
$Ø_{CM}$	Internal diameter of ceramic membrane
$Ø_P$	Particle diameter
E	Electric field strength
E_{CR}	Critical electric field strength
EC_T	Total energy consumption
EC_{SP}	Specific energy consumption
ED	Electrodeposition; method of rust proofing automotive bodies
EDTA	Ethylenediaminetetraacetic acid
Electro-filtration	Membrane filtration performed with the aid of either direct current (DC) or alternating current (AC)
Electrostatic interaction	Interaction between two bodies based on surface charges
Electro-ultrafiltration	Electro-filtration using an ultrafiltration (UF) membrane
ε	Dielectric permittivity of water
ε_O	Permittivity of a vacuum
F_{DI}	Deposition-inhibiting force
F_{DP}	Deposition-promoting force
F_E	Electrophoretic force
F_{EDL}	Electrostatic double-layer force
FESEM	Field Emission Scanning Electron Microscope
F_{FD}	Filtrate drag force
F_G	Gravitational force
Filtrate	Liquid that has passed through a filter
F_L	Lift force
Fouling	A phenomenon where solute or particles deposit onto a

	membrane surface resulting in reduced membrane performance
F_{VD}	Velocity drag force
F_{VDW}	Van der Waals force
FW_S	Freshwater savings per year
G	Gravitational acceleration constant
γ	Particle adhesion probability
GL	Gigaliter; unit of volume; 1 GL = 1 billion liters
η_F	Viscosity of feed water
$h\varpi$	Lifschitz-van der Waals constant
Heavy metals	Metallic chemical elements that are toxic to living organisms even at low concentrations
Hydrodynamic forces	Forces created by a liquid in motion
Hydrophilicity	Having an affinity for water
Hydrophobicity	Having a tendency to repel water
J	Actual permeate flux
J_C	Flux through the cake in the absence of an electric field
J_M	Membrane flux in the absence of an electric field
$J_{20°C}$	Permeate flux standardized at 20°C
$J_{25°C}$	Permeate flux standardized at 25°C
kPa	Kilopascal; unit of pressure; 1 kPa = 1000 Pa
kV	Kilovolt; unit of potential difference; 1kV = 1000 Volt
kWh	Kilowatt-hr
L_{CM}	Length of the ceramic membrane
MTB	Mass-transfer-based; processes that utilize water as a mass

	separating agent
MPa	Megapascal; unit of pressure; 1 MPa = 1 million Pa
μ_C	Cake electro-osmotic mobility
MF	Microfiltration; membrane filtration process that rejects suspended solids in a size range of 1 to 0.1 μm
μ_M	Membrane electro-osmotic mobility
μ_P	Electrophoretic mobility
μS/cm	Microsiemen per centimeter; unit of conductivity
mg/L	Milligram per liter; measurement of mass concentration
mV	Millivolt; unit of potential difference; 1 mV = 0.001 Volt
NF	Nanofiltration; membrane filtration process that rejects multivalent ions and certain charged particles
Nm	Nanometer; unit of length; 1 nm = 1 billionth of a meter
NATA	National Association of Testing Authorities
NTU	Nephelometric turbidity unit; unit of turbidity
N	Newton; unit of force
$\aleph$	Inverse Debye length
NMTB	Non-mass-transfer-based; processes that may utilize water as a cooling or heating medium, or a raw material that eventually becomes part of a product
N_D	Number of days the manufacturing facility operates
ν_V	Velocity field
O&G	Oil and grease; common components include petroleum oils, vegetable oils and natural oils

P	Power consumption
pH	Water quality parameter that measures the activity of hydrogen ion
Φ	Resistance index
Polymeric membrane	Microporous film acting as a semi-permeable barrier
P_P	Payback period
% P_R	Reduction/rejection rates of critical water quality parameters
PWF	Pure water flux; volume of pure water that passes through a membrane per unit area · time
PWP	Pure water permeability; volume of pure water that passes through a membrane per unit area · time · TMP
R	Particle radius
% R_C	Contaminant rejection rate
Re	Reynolds number
R_{EC}	Concentration polarization resistance in the presence of an electric field
R_{EF}	Adsorption resistance in the presence of an electric field
R_{EM}	Membrane resistance in the presence of an electric field
R_F	Adsorption resistance on inner pore fibre
$R_{G/C}$	Concentration polarization resistance
ρ_F	Density of feed water
ρ_P	Particle density
R_M	Intrinsic membrane resistance
RO	Reverse osmosis; membrane filtration process that rejects majority of dissolved constituents in water

R_T	Total resistance
R_{Turb}	Turbidity rejection rate
% R_{WW}	Wastewater recycling rate
SDI	Silt density index; measurement of the fouling potential of suspended solids in wastewater
SEM	Scanning electron microscope
σ	Surface charge density
Sinks	Streams going into processes often having specific water quality requirements
Sources	Streams coming out of processes often carrying multiple contaminants
SS	Suspended solids; particles that remain in suspension in wastewater
S_T	Total savings per year
τ_w	Shear stress
TDS	Total dissolved solids; combined content of all dissolved organic and inorganic material in wastewater
TiO_2	Titanium dioxide (Titania)
TL	Teraliter; unit of volume; 1 TL = one trillion liter
TMP	Transmembrane pressure; average applied pressure from the feed to the filtrate side of the membrane module
TOC	Total organic carbon; amount of carbon in an organic compound
Tradewaste	Liquid wastes from any business, industry, trade or manufacturing process approved for sewer disposal

	(excluding domestic sewage)
TSS	Total suspended solids; quantity of solid particles contained in wastewater
Turbidity	Cloudiness of water due to suspended solids
UF	Ultrafiltration; membrane filtration process that rejects large dissolved molecules and colloidal particles in the size range 0.1 to 0.01 μm
V_P	Permeate volume
VSD	Variable speed drive
v/v %	Volume percent concentration
Water audit	Process of documenting the quantity and quality of water inputs and outputs for a process or set of processes, assumed to be operating at a steady-state and within a defined boundary
Water flow diagram	Provides an easy to understand representation of process systems
Water Pinch	Process integration tool widely used for water use optimization
WaterTarget™	Commercially available water pinch software with trademark registered to KBC Advanced Technologies plc
W_R	Volume of treated water for reuse per day
WW_S	Actual wastewater savings per year
WW_{SI}	Initial wastewater savings per year
Zeta potential (ζ)	Measure of particle-particle and particle-surface interactions
ZrO_2	Zirconium dioxide (Zirconia)

Table of Contents

Chapter One: Introduction

Figure

Tables

Figures

Tables

Figures

Tables

Chapter Four: The application of a 50 nm ZrO_2 ceramic membrane for the ultrafiltration of post-electrodeposition rinse wastewater

Figures

Tables

Chapter Five: Ceramic electro-ultrafiltration of post-electrodeposition rinse wastewater

Figures

Tables

Figures

Tables

Chapter Seven: Recommendations and Conclusions

Tables

Attached Appendices

Accompanying CD

Chapter One: Introduction

1.1 Industrial water

Industrial water may be defined as wastewater generated by industrial or commercial facilities [1]. Its quality and quantity may depend on factors such as operating conditions, process raw materials, types of water-using processes and product characteristics [1]. A good example of industrial water is the significant amount of wastewater that is generated by the manufacturing industry. The manufacturing industry uses water in production processes, process utilities and a range of other production related activities [2]. Production processes may utilize water as a cleaning agent, contaminant diluter or as part of the final product. Process utilities, such as cooling towers, boilers and air handling units (AHUs), utilize water to carry out heat transfer, steam production or to make up water loss due to evaporation. General plant cleaning and employee sanitation usually constitute most of the water used for other production related activities.

Since water is extensively used in the manufacturing industry, it is not surprising that the volume of industrial wastewater generated is substantial. Furthermore, industrial wastewater generated from the enormous diversity of manufacturing processes that exist worldwide leads to equally diverse water qualities and characteristics. This presents an ongoing challenge to those who are interested in devising strategies and technologies for water conservation and reuse.

1.2 Industrial water generated by the manufacturing industry

Water discharged by manufacturing industries may be divided into three broad categories – oily, metals and general wastewater streams. Of these, the oily and metals wastewater streams are generally the most harmful to the environment.

Oily streams commonly contain oil and grease (O&G) in the form of free oil (characterized by droplet size > 150 μm), dispersed oil (droplet size 20 – 150 μm), or emulsified oil (droplet size < 20 μm) [3]. A wide range of water treatment processes are commercially available to treat oily wastewater streams. Such processes include skimming, gravity oil-water separation, chemical treatment, flotation, coagulation and flocculation, and membrane filtration [3].

For the metals wastewater streams, the heavy metals are of primary concern. These are non-biodegradable and have the tendency to bioaccumulate in living organisms. At elevated levels, the heavy metals that emanate from manufacturing industries such as zinc (Zn), copper (Cu), nickel (Ni), mercury (Hg), cadmium (Cd), lead (Pb) and chromium (Cr) are toxic to living organisms [4] and, in humans, excessive intake of heavy metals can cause serious health problems or even death [5]. For example, ingestion of Ni above the critical level can result in serious lung and kidney problems, gastrointestinal distress, pulmonary fibrosis and skin dermatitis [6], while ingestion of Hg above the critical level can result in impairment of pulmonary and kidney function, chest pain and dyspnoea [7]. Similarly, excessive Pb intake can damage the nervous system, kidney, liver, reproductive system, basic cellular processes and brain functions [8], whilst excessive Cr intake can affect human physiology and can also cause severe health problems ranging from skin irritation to lung carcinoma [9]. Since heavy metals pose such a serious risk to human beings, their removal prior to wastewater discharge is considered essential. Heavy metal removal in wastewater can be facilitated by water treatment processes such as precipitation, ion exchange, adsorption, membrane filtration, coagulation/flocculation, electrodialysis, flotation, and electrochemical techniques [4].

General wastewater streams that originate from blowdown and condensates of air handling units (AHUs), boilers and cooling towers have relatively good water quality and the contaminants present do not usually pose health risks to human beings.

1.3 Industrial water recycling and reuse

Due to increasing water scarcity and costs, manufacturing industries around the world are moving towards the recycling of their process wastewater. However, the amount of wastewater that is recycled and reused in most manufacturing industries is still quite low compared to the amount of freshwater they consume. As mentioned previously, such consumption is typically substantial. For example, Table 1.1 shows the approximate water demand for various representative industrial sectors in the United Kingdom [10].

Table 1.1: Approximate water demands for various industrial sectors in the United Kingdom (Note: $1m^3 = 1000L$)

INDUSTRY	WATER DEMAND
Paper	29 m^3/t paper produced
Newspaper	9 m^3/t paper produced
Brewing	10-15 m^3/m^3 beer
Dairy	140 m^3/m^3 milk
Sugar	8 m^3/t sugar
Automotive	450 m^3/car (metal production)
Automotive	760 m^3/car (tire production)
Dying	100 m^3/t fabric processed
Soap	2 m^3/t soap produced
Power	3 m^3/MWh for steam; 60 m^3/MWh for cooling

In a 2007 survey conducted by Statistics Canada [11], around 2,885 million cubic meters of water (approx. 2.9 TL) used by different manufacturing processes, was reported as recirculated water – i.e. water coming out of a process and reused within the same process or by other processes. The primary metals industry accounted for 46.6 % of this volume, the paper industry represented 31.6 % of the total and the petroleum and coal industries had 14.9 % share of the total. The remaining percentage was distributed amongst the other manufacturing industries. As a whole, the percentage of recirculated water used by the manufacturing industry was approximately 55.0 % of the total water intake.

In 2004, Japan derived 79 % of their overall industrial water use from recycled water [12]. Wastewater recycling rates reached 80-90 % in the chemical and steel industries and about 45 % in the pulp/paper industry. In the food and textile industry, recycling rates were about 40 % and 15 % respectively.

Surprisingly, unlike Japan and Canada, Australia has no detailed data on water recycling and reuse in the manufacturing industry. Nonetheless, State Governments have started directing recycled water from sewage treatment plants to industry. According to the Australian Bureau of Statistics, in 2009-10, the total volume of recycled water supplied to different industries was 374 GL. Of this volume, around 127 GL (34 %) was supplied within New South Wales while around 98 GL was supplied within Victoria [13]. The largest users of the recycled water were the agricultural and water supply industries – with the latter having a total consumption of 105 GL and the former having a total consumption of 126 GL. The remaining volume (78 GL) of recycled water supplied was used by other industries [13].

The fact that Japan's chemical and steel industry was able to exceed an overall recycling rate of 70 % as long ago as 2004, clearly shows that there is still great potential for other countries to further reduce their fresh water usage. Indeed, increasing the industrial wastewater-recycling rate by at least another 30 percentage points should be achievable worldwide.

1.4 Trends in industrial water management

In recent years, industrial water reuse and recycling have focused intensively on methods such as process integration and the use of advanced water treatment technologies. Process integration is an holistic approach to the analysis, synthesis, and retrofit of process plants [14, 15]. One simple process integration tool widely used for water use optimization is known as "water pinch analysis". Water pinch analysis considers water reuse opportunities by carefully analyzing the flows and qualities of different streams. Possible water reuse options are identified by matching different "sources" and "sinks". Counter-intuitively, "sources" are defined as streams coming out of processes carrying, often multiple, contaminants - whilst "sinks" are streams going into processes that often have specific water quality requirements [16]. Water pinch fundamentals developed by Wang & Smith [17] and El-Halwagi & Manousiouthakis [18] have been the basis of many water use optimization methods deployed in industry in recent times.

A number of researchers have shown the effectiveness of process integration in reducing freshwater consumption and wastewater discharge [19-26]. Although this is the case, reduction in freshwater consumption and wastewater discharge is highly dependent on the processes involved. For example, in a case study involving a

brewhouse [21], the integration of the water system yielded freshwater savings and wastewater reduction of 8 % and 13 % respectively. In another case study involving a Chinese steel plant [24], the integration of the water system yielded freshwater savings and wastewater reduction of approximately 58 % and 82 % respectively.

Advanced water treatment technologies such as membrane filtration processes play a major role in the reclamation of water in manufacturing industries worldwide. They have been shown to be applicable to a wide variety of wastewaters generated by industries such as food & beverage, car manufacturing, metal plating, tannery, carpet manufacturing, textile, and glass manufacturing [27-38]. Since industrial wastewater characteristics are quite diverse, the use of membrane filtration processes for water reclamation is preferred over conventional water treatment technologies since they can deliver more consistent permeate water qualities despite the variations in the quality of feed water [39]. They are also more energy efficient and have smaller footprints compared to conventional water treatment technologies [40]. However, the major setback with membrane filtration is fouling – a phenomenon that can greatly affect the performance and life of the membrane [41].

Membrane filtration includes four major separation processes; namely, microfiltration (MF), ultrafiltration (UF), nanofiltration (NF) and reverse osmosis (RO) [42, 43]. In general, MF rejects suspended solids in a size range of 1 to 0.1 μm, including micro-organisms such as bacteria and protozoa, whilst UF rejects large dissolved molecules and colloidal particles in the size range 0.1 to 0.01 μm. On the other hand, NF rejects multivalent ions and certain charged particles whilst RO rejects the majority of dissolved constituents in water [39, 44].

1.5 Water recycling and reuse in Australia

Australia tends to apply a holistic approach to water recycling and reuse due to the fact that it is one of the driest continents in the world. A key feature of its environment is that water is relatively scarce when compared to other inhabited lands. In March 2004, the Australian Academy of Technological Sciences and Engineering (AATSE) published an extensive review of water recycling in Australia. Since then, many developments have occurred including the formulation of National Water Initiatives and new strategies aimed at increasing the use of recycled water, stormwater, and rainwater in Australia's capital cities [13, 45].

One of the most notable water use optimization tools for water resource allocation in Australia was developed by Higgins *et al.* [46]. The purpose of this tool is to produce solutions for water resource allocation under inflow uncertainty by using a stochastic non-linear programming model with multiple objectives. The tool was primarily applied to a case study in South East Queensland, which at that time was facing severe drought prospects. The application of this tool significantly reduced the risk of reservoirs running dry. Additionally, the tool was also used to assess a new water initiative of the Queensland State Government to overcome the water crisis. Another work presented by Marks *et al.* [47] showed a water management plan demonstrating the integration of local water resources – rainwater, stormwater, and sewage effluent. In their work, rainwater tanks were assessed to be adequate for in-house uses with the exception of toilet flushing. A combination of reclaimed sewage and harvested stormwater was found to be adequate for non-potable uses including toilet flushing, gardens, and public open space.

Innovative ways of recycling or reusing wastewater has become a common practice in the Australian manufacturing industry. Some good examples are the works of Wijesinghe *et al.* [48], Bryant *et al.* [49], and Hatt *et al.* [50]. The work of Wijesinghe *et al.* investigated acceptable technologies for the use of secondary effluent as cooling water "make up" for inland manufacturing industries. The outcome showed that the use of treated secondary effluent for cooling water make up is technically feasible. Bryant *et al.* demonstrated that by installing a reverse osmosis system to treat cooling tower blowdown, the usage of brine concentrators can be minimized. Hatt *et al.* showed that if the costs and benefits of recycling systems compare favorably with the costs and benefits of conventional practices then a widespread adoption of stormwater recycling in industry is possible.

Although the Australian manufacturing industry is developing innovative ways of wastewater recycling or reuse, much more in-depth research needs to be carried out, as suggested by Al-Rifai *et al.* [51]. In an investigation conducted by these researchers on three Australian recycling schemes (two employing RO technology and the other a combination of ozonation and biological activated carbon filtration), it was found that that natural and synthetic chemicals in the form of hormones and pharmaceuticals, as well as different kinds of compounds with domestic and industrial applications, can enter wastewater treatment plants and cause a wide variety of environmental and health problems. Such scenario complicates the deployment of water reclamation strategies.

1.6 This study

Since water is a vital input to many manufacturing processes and activities, water scarcity and increasing water tariffs have prompted manufacturing industries within

Australia to implement on-site water recycling programs. Although this initiative is producing favorable results in terms of freshwater savings and wastewater reduction, there is considerable scope for the identification of further water conservation measures. In this regard, this research project was undertaken in order to investigate the opportunities that exist for moving towards total wastewater recycling with respect to larger manufacturing industries. Thus, two large and contrasting (in terms of product – and hence processes) manufacturing companies based in Melbourne, Australia (i.e. an automobile manufacturer and a beverage manufacturer) were approached (in conjunction with their common water retailer) with the goal of carrying out an extended research project aimed at identifying general and specific strategies for moving towards the total recycling of process water. It is also worth mentioning that the two companies have different waste distribution streams (i.e. separate vs. comingled) and therefore the water treatment approach to be deployed at each site will be different. The agreement and full co-operation of all parties was secured with a view to integrating the comprehensive analysis of water use efficiency within both companies together with the identification and laboratory-scale testing of potential water treatment membrane technologies. The devised integrated water management strategy is depicted schematically in Figure 1.1.

It was anticipated that the integration of the three central components of: WATER AUDIT, PROCESS INTEGRATION and WATER RECYCLING, would result in a synergistic approach to industrial water conservation.

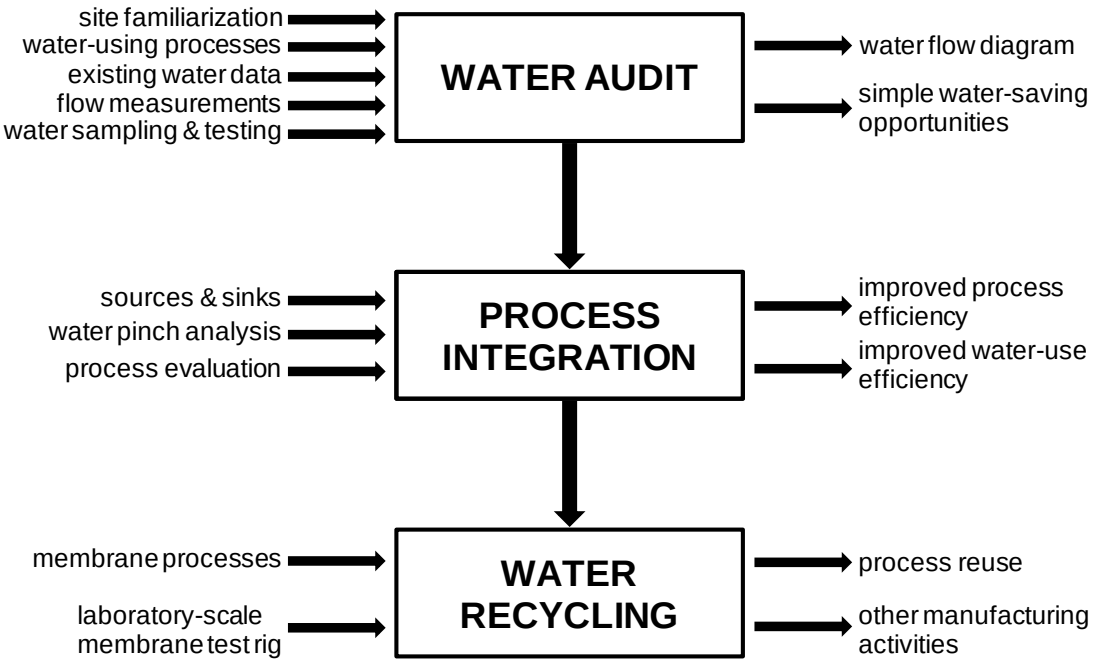

Figure 1.1: Schematic diagram of the integrated water management strategy applied in this study to two large manufacturing companies based in Victoria, Australia.

Details of the inputs and outputs to the three components depicted in Figure 1.1 are provided in subsequent Chapters. For convenience, the contents of these Chapters are summarized in Table 1.2, and briefly outlined as follows:

Table 1.2: Contents of Chapters 2 – 7

Chapter	Contents
2	Water audit and process integration
3	Evaluation of flat sheet polymeric membranes
4	Operating parameter optimization of ceramic ultrafiltration membrane with respect to wastewater containing cathodic electrodeposition (CED) paint
5	Operating parameter optimization of ceramic electro-ultrafiltration membrane with respect to wastewater containing cathodic electrodeposition (CED) paint

6	Operating parameter optimization of ceramic ultrafiltration membrane with respect to beverage production wastewater
7	Summary of results, recommendations to companies, cost analysis, and recommendations for future research work

---

Chapter 2 describes the application of the water audit and process integration method with respect to both companies. The water optimization method was carried using commercially available water pinch software known as WaterTarget^{TM}. This process allowed simple water saving opportunities to be identified and also allowed key wastewater streams within both companies to be considered for the testing and implementation of appropriate membrane technologies. Subsequently, Chapters 3 - 6 describe laboratory scale experiments that trial various organic and inorganic membranes.

Specifically, Chapter 3 employs a test rig, designed and constructed as an integral part of this project, to examine the suitability of different flat sheet polymeric membranes consisting of ultrafiltration (UF), nanofiltration (NF) and reverse osmosis (RO) with respect to various wastewaters generated at the two production facilities. Chapters 4 and 5 describe the optimization of operating parameters for ceramic ultrafiltration and ceramic electro-ultrafiltration with respect to wastewater containing CED paint. Chapter 6 describes the optimization of operating parameters for ceramic ultrafiltration with respect to beverage production wastewater.

A summary of the overall outcomes and appropriate recommendations to both companies are provided in Chapter 7. Chapter 7 also contains some cost-benefit analysis and recommendations for future research work.

1.7 References

[1] EPA-Victoria. 2009. *IWRG 632: Industrial water reuse* [Online]. Melbourne: EPA-Victoria. Available: http://epanote2.epa.vic.gov.au/EPA/publications.nsf /PubDocsLU/ IWRG632?OpenDocument [Accessed 13/5/11].

[2] Dupont, D. P. & Renzetti, S. 2001. The Role of Water in Manufacturing. *Environmental and Resource Economics,* 18**,** 411-432.

[3] Kajitvichyanukul, P., Hung, Y.-T. & Wang, L. K. 2006. Oil Water Separation: Advanced Physicochemical Treatment Processes. *In:* Wang, L. K., Hung, Y.-T. & Shammas, N. K. (eds.). Humana Press.

[4] Fu, F. & Wang, Q. 2011. Removal of heavy metal ions from wastewaters: A review. *Journal of Environmental Management,* 92**,** 407-418.

[5] Oyaro, N., Juddy, O., Murago, E. N. M. & Gitonga, E. 2007. The contents of Pb, Cu, Zn and Cd in meat in Nairobi, Kenya. *Journal of Food, Agriculture and Environment,* 5**,** 119-121.

[6] Borba, C. E., Guirardello, R., Silva, E. A., Veit, M. T. & Tavares, C. R. G. 2006. Removal of nickel(II) ions from aqueous solution by biosorption in a fixed bed column: Experimental and theoretical breakthrough curves. *Biochemical Engineering Journal,* 30**,** 184-191.

[7] Namasivayam, C. & Kadirvelu, K. 1999. Uptake of mercury (II) from wastewater by activated carbon from an unwanted agricultural solid by-product: Coirpith. *Carbon,* 37**,** 79-84.

[8] Naseem, R. & Tahir, S. S. 2001. Removal of Pb(II) from aqueous/acidic solutions by using bentonite as an adsorbent. *Water Research,* 35**,** 3982-3986.

[9] Khezami, L. & Capart, R. 2005. Removal of chromium(VI) from aqueous solution by activated carbons: Kinetic and equilibrium studies. *Journal of Hazardous Materials,* 123**,** 223-231.

[10] Judd, S. 2003. Introduction. *In:* Judd, S. & Jefferson, B. (eds.) *Membranes for industrial wastewater recovery and re-use.* Oxford, UK: Elsevier Advanced Technology.

[11] Statistics Canada. 2010. *Industrial water use 2007* [Online]. Ottawa, Canada: Ministry of Industry. Available: http://www.statcan.gc.ca/pub/16-401-x/16-401-x2010001-eng.pdf [Accessed 05/02/12].

[12] Japan External Trade Organization. 2004. *Categories of water use and related technologies/products* [Online]. Tokyo, Japan: JETRO. Available: http:www3.jetro.go.jp/ttppoas/special/envrepenglish/envrep02.html [Accessed 22/07/08].

[13] Australian Bureau of Statistics. 2011. *Water Account, Australia, 2009-10: Reuse water* [Online]. Canberra, Australia: Australian Bureau of Statistics. Available: http://www.abs.gov.au/ausstats/abs@.nsf/Lookup/0780E126E46A5507CA257956000E6586 [Accessed 05/02/12].

[14] Mann, J. & Liu, Y. 1999. *Industrial water reuse and wastewater minimization,* New York, McGraw-Hill.

[15] Foo, D. C. Y. 2009. State-of-the-art review of pinch analysis techniques for Water network synthesis. *Industrial and Engineering Chemistry Research,* 48**,** 5125-5159.

[16] Brauns, E., Helsen, J., Schiettecatte, W. & Genné, I. 2008. Pragmatic software tools for water reuse evaluation in a factory. *Clean Technologies and Environmental Policy,* 10**,** 189-201.

[17] Wang, Y. P. & Smith, R. 1994. Wastewater minimisation. *Chemical Engineering Science,* 49**,** 981-1006.

[18] El-Halwagi, M. M. & Manousiouthakis, V. 1989. Synthesis of mass exchange networks. *AIChE Journal,* 35**,** 1233-1244.

[19] Chan, J. H., Foo, D. C. Y., Kumaresan, S., Aziz, R. A. & Abu-Hassan, M. A. 2008. An integrated approach for water minimisation in a PVC manufacturing process. *Clean Technologies and Environmental Policy,* 10**,** 67-79.

[20] Dakwala, M., Mohanty, B. & Bhargava, R. 2009. A process integration approach to industrial water conservation: a case study for an Indian starch industry. *Journal of Cleaner Production,* 17**,** 1654-1662.

[21] Feng, X., Huang, L., Zhang, X. & Liu, Y. 2009. Water system integration of a brewhouse. *Energy Conversion and Management,* 50**,** 354-359.

[22] Tewari, P. K., Batra, V. S. & Balakrishnan, M. 2009. Efficient water use in industries: Cases from the Indian agro-based pulp and paper mills. *Journal of Environmental Management,* 90**,** 265-273.

[23] Thevendiraraj, S., Klemes, J., Paz, D., Aso, G. & Cardenas, G. J. 2003. Water and wastewater minimisation study of a citrus plant. *Resources, Conservation and Recycling,* 37**,** 227-250.

[24] Tian, J. R., Zhou, P. J. & Lv, B. 2008. A process integration approach to industrial water conservation: A case study for a Chinese steel plant. *Journal of Environmental Management,* 86**,** 682-687.

[25] Žbontar Zver, L. & Glavič, P. 2005. Water minimization in process industries: Case study in beet sugar plant. *Resources, Conservation and Recycling,* 43**,** 133-145.

[26] Zheng, P., Feng, X., Qian, F. & Cao, D. 2006. Water system integration of a chemical plant. *Energy Conversion and Management,* 47**,** 2470-2478.

[27] Kang, S.-K. & Choo, K.-H. 2003. Use of MF and UF membranes for reclamation of glass industry wastewater containing colloidal clay and glass particles. *Journal of Membrane Science,* 223**,** 89-103.

[28] Bennett, A. Automotive: Innovative filtration applications in the auto industry. *Filtration & Separation,* 47**,** 28-31.

[29] Bes-Piá, A., Cuartas-Uribe, B., Mendoza-Roca, J. A., Galiana-Aleixandre, M. V., Iborra-Clar, M. I. & Alcaina-Miranda, M. I. 2008. Pickling wastewater reclamation by means of nanofiltration. *Desalination,* 221**,** 225-233.

[30] Bes-Piá, A., Cuartas-Uribe, B., Mendoza-Roca, J.-A. & Alcaina-Miranda, M. I. 2010. Study of the behaviour of different NF membranes for the reclamation of a secondary textile effluent in rinsing processes. *Journal of Hazardous Materials,* 178**,** 341-348.

[31] Capar, G., Yetis, U. & Yilmaz, L. 2006. Reclamation of printing effluents of a carpet manufacturing industry by membrane processes. *Journal of Membrane Science,* 277**,** 120-128.

[32] Chmiel, H., Kaschek, M., Blöcher, C., Noronha, M. & Mavrov, V. 2003. Concepts for the treatment of spent process water in the food and beverage industries. *Desalination,* 152**,** 307-314.

[33] Holmes, D. 2002. Water and chemicals recovery in the German automotive industry. *Membrane Technology,* 2002**,** 6-10.

[34] Qin, J.-J., Maung Nyunt, W., Maung Htun, O. & Lee, H. 2004. A pilot study for reclamation of a combined rinse from a nickel-plating operation using a dual-membrane UF/RO process. *Desalination,* 161**,** 155-167.

[35] Tay, J.-H. & Jeyaseelan, S. 1995. Membrane filtration for reuse of wastewater from beverage industry. *Resources, Conservation and Recycling,* 15**,** 33-40.

[36] Van der Bruggen, B., Curcio, E. & Drioli, E. 2004. Process intensification in the textile industry: the role of membrane technology. *Journal of Environmental Management,* 73**,** 267-274.

[37] Wu, H.-Z., Hsu, Y.-L., Lee, Y.-J. & Lin, P. H.-P. 2005. Reclamation of textile dyeing wastewater for process use via a highly efficient integration system. *Desalination,* 172**,** 293-307.

[38] Zuo, W., Zhang, G., Meng, Q. & Zhang, H. 2008. Characteristics and application of multiple membrane process in plating wastewater reutilization. *Desalination,* 222**,** 187-196.

[39] Bennett, A. 2005. Membranes in industry: facilitating reuse of wastewater. *Filtration & Separation,* 42**,** 28-30.

[40] Zhang, Y., Ma, C., Ye, F., Kong, Y. & Li, H. 2009. The treatment of wastewater of paper mill with integrated membrane process. *Desalination,* 236**,** 349-356.

[41] Cheryan, M. 1998. *Ultrafiltration and microfiltration handbook*, Lancaster, Pennsylvania, Technomic Publishing Company, Inc.

[42] Chen, J. P., Mou, H., Wang, L. K. & Matsuura, T. 2006. Membrane Filtration. *In:* Wang, L. K., Hung, Y.-T. & Shammas, N. K. (eds.) *Advanced Physicochemical Treatment Processes.* Humana Press.

[43] Pinnekamp, J. & Friedrich, H. (eds.) 2006. *Municipal Water and Waste Management : Membrane Technology for Waste Water Treatment,* Aachen, FiW VERLAG.

[44] Wintgens, T., Melin, T., Schäfer, A., Khan, S., Muston, M., Bixio, D. & Thoeye, C. 2005. The role of membrane processes in municipal wastewater reclamation and reuse. *Desalination,* 178**,** 1-11.

[45] Radcliffe, J. C. 2006. Future directions for water recycling in Australia. *Desalination,* 187**,** 77-87.

[46] Higgins, A., Archer, A. & Hajkowicz, S. 2008. A stochastic non-linear programming model for a multi-period water resource allocation with multiple objectives. *Water Resources Management,* 22**,** 1445-1460.

[47] Marks, R., Clark, R., Rooke, E. & Berzins, A. 2006. Meadows, South Australia: Development through integration of local water resources. *Desalination,* 188**,** 149-161.

[48] Wijesinghe, B., Kaye, R. B. & Fell, C. J. D. 1996. Reuse of treated sewage effluent for cooling water make up: A feasibility study and a pilot plant study.

[49] Bryant, T., Stuart, J., Fergus, I. & Lesan, R. 1987. The use of reverse osmosis as a 35,600m3/day concentrator in the waste water management scheme at 4640 MW Bayswater/Liddell Power Station complex - Australia. *Desalination,* 67**,** 327-353.

[50] Hatt, B. E., Deletic, A. & Fletcher, T. D. 2006. Integrated treatment and recycling of stormwater: A review of Australian practice. *Journal of Environmental Management,* 79**,** 102-113.

[51] Al-Rifai, J. H., Gabelish, C. L. & Schäfer, A. I. 2007. Occurrence of pharmaceutically active and non-steroidal estrogenic compounds in three different wastewater recycling schemes in Australia. *Chemosphere,* 69**,** 803-815.

Chapter Two: Water audit and process integration at two large manufacturing companies based in Australia

2.1 Introduction

A water audit of a company is carried out in order to document the quantity and quality of water inputs and outputs for a process or set of processes, assumed to be operating at a steady-state and within a defined boundary [1]. One of the most useful outcomes of a water audit is the creation of a water flow diagram – which provides an easy to understand representation of (usually complex) process systems. A water flow diagram also documents the amount of water that is being used by each process - including the volume and quality of the wastewater being generated. A water audit may reveal abnormalities in water usage which cannot be identified during normal operations and it can also, in itself, facilitate the identification of water-saving opportunities within processes [2].

Water use optimization methods deployed in industry are commonly based on "water pinch" technology, which is a tool used for the systematic analysis of water networks and for the identification of measures for increasing water use efficiency in processes [3]. The development of water pinch technology has progressed in two main directions [4]; namely, graphical methods [5-9] and mathematical-based methods [10, 11]. Both methods have proven to be effective in simultaneously reducing freshwater consumption and wastewater discharge in a number of process industries [12-17]. The choice of which method to use depends on the nature of the problem to be addressed. For example, if one were to tackle a single contaminant problem, a graphical method would be recommended, but where there are multiple contaminants, a mathematical-based method would be a better choice in terms of accuracy. Types of industry that have achieved significant freshwater usage and wastewater reductions by applying

water pinch technology include oil refining, chemical, pulp & paper and food & drink [3, 4, 18].

Wang & Smith [19] initially introduced a graphical method of targeting water systems that has the potential for regeneration or recycling. Their work became the basis of many combined methods that have been successfully used in industrial practices [20]. In 2007, Feng X. *et al.* [9] showed in their work that optimal regeneration concentration does not necessarily point to the pinch concentration as suggested by water pinch analysis. Although both aforementioned researchers were correct to a certain extent, their work primarily dealt with fixed contaminant load operations (e.g. washing, scrubbing, and extraction) without considering water loss [21]. Meanwhile, El-Halwagi *et al.* [6] developed a single stage, systematic, and graphical method for identifying targets for the maximum recycle/reuse of process streams. In their work, optimum conditions were derived using dynamic program formulation and a solution for parametric optimization. The mathematical analysis is used as a guide in developing a new pinch-based graphical representation of the most optimum composite load versus flow. Similar research by Almutlaq *et al.* [10] demonstrated an algebraic procedure that targets wastewater recycle networks. This approach is valid for both pure and impure sources and plays a pivotal role in managing process water sources, freshwater usage, and wastewater discharge.

Studies dealing with fixed flow rate problems (e.g. boilers, cooling towers, reactors) based on water pinch analysis have also been reported [21]. Some notable examples of these are the works of Manan *et al.* [7] and Foo *et al.* [8], which used the concept of Hallale [5] in determining the maximum water recovery network. In their

investigations, the maximum water recovery network turned out to be across the pinch concentration. This means that in order to achieve maximum water recovery, a concentration range of critical water quality parameters should be considered. For example, the conductivity of inlet feed water to boilers can be set from 0 to 10 μS/cm. Such a scenario will facilitate more opportunities for water recovery compared to setting a single feed water conductivity limit (say 5 μS/cm). Manan *et al.* [7] proposed a water cascade analysis to minimize freshwater use by providing important insights into the pinch-causing streams and water allocations. This represented an enhancement of Hallale's [5] water surplus diagram technique. Foo *et al.* [8] showed that zero liquid discharge is achievable using the water cascade analysis developed by Manan *et al.* [7]. Similarly, Koppol *et al.* [22] presented a mathematical programming method to analyze the feasibility of zero liquid discharge in four different industries. Their work showed that factors such as regeneration cost, freshwater cost, and wastewater concentration generally contribute to the feasibility of zero liquid discharge. Van der Bruggen & Braeken [2] discussed three consecutive approaches to zero liquid discharge in the brewing industry. These researchers investigated the current water balance, optimized water-consuming processes and developed an overall concept for the optimized processes. Although the three consecutive approaches proved useful in significantly reducing water consumption, zero liquid discharge was not achieved. However, according to Agrawal & Shenoy [23], zero liquid discharge can be realized if the regeneration output concentration meets the criteria of the lowest water concentration demand.

The effectiveness of water pinch technology in reducing freshwater consumption and wastewater discharge in manufacturing facilities has been demonstrated in recent years.

However, manual analysis of complex water networks can be a daunting task, even with the availability of this technology. In this regard, commercially available software packages based on the water pinch technique are a viable alternative. Such software packages analyze water networks as steady-state processes and work within the boundaries of sources and sinks [24]. One such package, which has been selected for the current project, is described as follows.

2.2 Materials and methods

2.2.1 Selected case studies

Two large manufacturing companies in the area of Western Melbourne were approached and agreed to fully collaborate on this project as case studies. Due to confidentiality agreements, their names cannot be divulged and for the purpose of this thesis they will be referred to as Companies A & B. Company A is an automobile manufacturer and Company B is a major producer of non-alcoholic drinks and cordials (beverages). Since both companies are within the same locality, they are subject to similar water tariffs and water restrictions. Furthermore, both companies have Tradewaste (or industrial water) discharge agreements with the same local water retailer who was also enlisted as a partner on the project.

The recruited companies were selected for the following reasons: 1) both use substantial amounts of freshwater in their processes; 2) the manner of freshwater consumption at each company is different; 3) contrasting types of wastewater are generated by each company, and 4) the companies are contrasting in terms of their respective products.

2.2.2 Water audit

Components of the water audit deployed for both companies include (i) site familiarization; (ii) classification of water-using processes – water flow diagrams; (iii) analysis of existing water data; (iv) flow measurements; (v) water sampling and testing.

Site familiarizations were undertaken prior to commencing actual flow measurements and water sampling to ensure that issues relating to occupational health and safety (OH&S) were addressed in advance. Meanwhile, the classification of all water-using processes facilitated the systematic development of the water flow diagram. These were classified as either mass-transfer-based (MTB) or non-mass-transfer-based (NMTB) processes. MTB processes utilize water as a mass separating agent (e.g. product cleaning), while NMTB processes may utilize water as a cooling or heating medium (e.g. cooling towers, boilers, etc.), or a raw material that eventually becomes part of a product (e.g. soft drinks production) [4]. After site familiarization, existing water data obtained from both companies were analyzed. These data provided insights on the quantity and quality of water consumed and wastewater generated. These were subsequently used as guidelines in flow measurements and subsequent wastewater sampling.

Flow measurements were carried out using multiple portable clamp-on ultrasonic flow meters (GE TransPort PT878), which were installed at different locations within the manufacturing site and which were programmed to log flow rates and accumulated volumes from periods ranging from days to weeks. The logged data were downloaded and were graphed and analyzed for trends and irregularities. The complete technical

details of the flow meter used are shown in Appendix 2.1 – attached at the end of the thesis.

Wastewater samples were taken from strategic points within the manufacturing site to ensure that every type of wastewater stream is represented in the study. Samples were collected in plastic and glass containers provided by a contracted analysis laboratory and were tested for a range of water quality parameters including, pH, conductivity, Total Dissolved Solids (TDS), Suspended Solids (SS), Oil & Grease (O&G), Chemical Oxygen Demand (COD) and various metals. Water sampling was carried out in that part of the production week that captured the worst-case scenario in terms of contamination levels. Actual test results are provided in the accompanying CD – Appendices 2.2 and 2.3.

2.2.3 Process integration

The process integration method used in this study consists of water pinch analysis and process evaluation. Water pinch analysis was carried out using commercially available software known as WaterTarget^{TM}. The software uses mathematical calculations to theoretically identify water reuse opportunities by matching the different flow rates and water qualities of sources and sinks. In this case, the sources and sinks used in the analysis were obtained from the water audit. On the other hand, process evaluation involves the use of fundamental engineering concepts to assess the applicability of the water pinch results on actual plant conditions. Process evaluations were done in conjunction with the management team and process engineers of both companies. The evaluations involve actual pilot plant trials of processes were possible water conservation opportunities exist. Such trials were held for a number of days (and even

months) during actual production operations. The data gathered were subsequently analyzed and presented to top management for approval and actual implementation. Samples of these pilot plant trials are shown in Section 2.3.4 of this Chapter.

2.3 Results and discussion

2.3.1 Irregularities in water use as identified by the water audit

A number of irregularities in water use, some associated with employees' work practices, were detected during the water audits. Such irregularities emanate from work practices performed during manually controlled addition of freshwater into processes, equipment cleaning and general plant cleaning. Since these irregularities were mostly due to employees' work practices, it was decided that this could best be resolved through direct management intervention. This would include the provision of appropriate training and seminars aimed at changing employees' perception on water use. Figure 2.1 illustrates an example of an irregularity in freshwater consumption identified at the paint shop pretreatment stage of Company A.

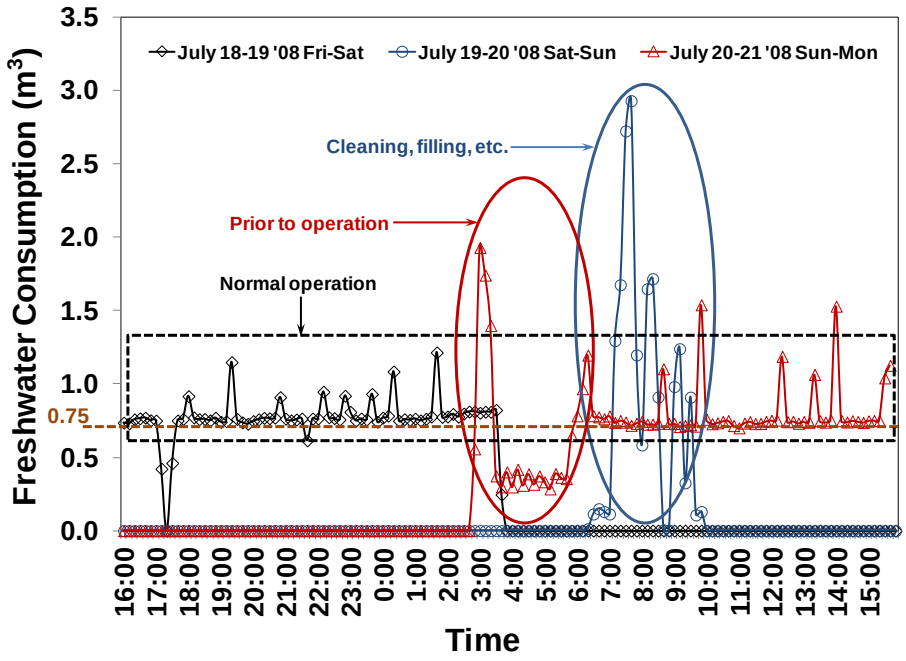

Figure 2.1: Water consumption at the pretreatment stages of Company A.

The pretreatment stage acts as the preparation stage for car bodies prior to electrocoating and painting. Such stage includes processes such as car body dip washing, spray rinsing and metal surface conditioning. Freshwater supply to these processes was measured for a period of three days – capturing normal operation, shutdown, and then back to normal operation. Normal operation ceases on Saturday morning between 3-4 am, and therefore freshwater consumption at this point should be zero. However, it is found that freshwater is continuously being consumed as shown in Figure 2.1 (spikes encircled in red). Such consumption is unnecessary since the processes at this stage is already in shutdown mode and therefore freshwater supplied to the baths would only continue to overflow. Prior to re-starting the processes, baths and tanks are drained, cleaned and then refilled with freshwater again. Since this is the case, it is expected that freshwater consumption would increase – as shown in Figure 2.1 (spikes encircled in blue).

After cleaning and filling activities, the processes are restarted and go back into normal operation. During normal operation (Figure 2.1, rectangle in black dashed lines), the spikes in consumption were due mainly to the manual addition of freshwater supply into the processes. Such manual additions of freshwater were mainly based on "customary work practices" carried out by operators over a number of years. If the water uses of processes at the paint shop's pretreatment stage will be standardized (i.e. defined volume of water use per hour), freshwater consumption during normal operation should be at an average of 0.75 m^3 hr^{-1} – based on the trends shown in Figure 2.1. The standardized freshwater supply will reduce consumption by approximately 69.0 %. The type of irregularity shown in Figure 2.1 also exists at company B – as shown in Figure 2.2.

Figure 2.2 shows the freshwater consumption at the syrup room of company B. The syrup room facilitates the mixing of sugar and treated Citywater in order to produce a sweetener additive for beverage products. At the end of every production run, tanks in this area are cleaned thoroughly using clean-in-place (CIP) systems. Water used by the CIP systems was measured for a period of three days – capturing normal operation, shutdown and back to normal operation. As shown in Figure 2.2, unusual spikes (encircled in red) in freshwater consumption were recorded during the first day of measurement. Such spikes in freshwater consumption were not evident in subsequent days of measurement. Although the reasons for the spikes in freshwater consumption were not verified on-site, it is suspected that this maybe due to variations in cleaning activities. For example, a standardized cleaning procedure (i.e. CIP duration) for tanks does not exist and therefore freshwater consumption during cleaning is dependent on the worker performing the task.

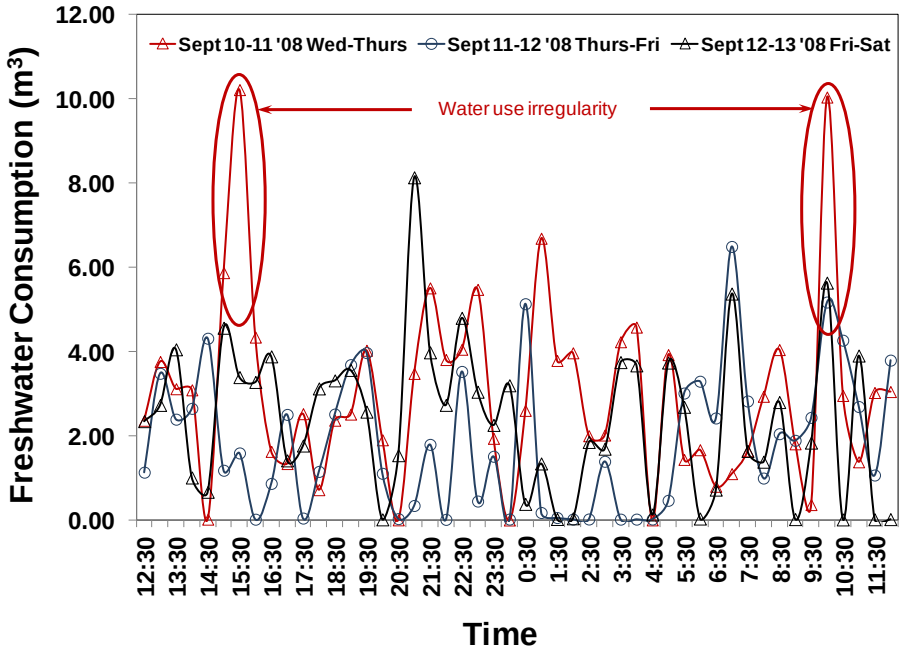

Figure 2.2: Treated Citywater consumption of CIP systems at the syrup room of Company B.

The complete water use logs for the different processes found at Companies A and B are available in the accompanying CD (Appendices 2.4, 2.5 and 2.6).

2.3.2 Water flow diagrams and usages

The main source of water used at the production sites of both companies is "Citywater" – i.e. freshwater supplied by the local water retailer. Rainwater is also used at both sites but is only available during certain periods of the year and therefore is not considered a reliable source. Average water quality parameters of the Citywater used at each site is shown in Table 2.1.

Table 2.1: Average water qualities of Citywater supplied to Companies A and B

Category	pH	TDS (mg/L)	Conductivity (μS/cm)	SS (mg/L)	O&G (mg/L)	COD (mg/L)
Citywater to A	7.3	79	129	<1	<5	<5
Citywater to B	7.2	36	83	<1	<5	<5

The different uses of Citywater at the production sites of companies A and B are shown in their respective simplified Water Flow Diagrams, Figures 2.3a and b. Likewise, these uses are also summarized in Table 2.2 and subsequently discussed in Sections 2.3.2.1 and 2.3.2.2. The comprehensive water flow diagrams developed for both companies are shown in Appendices 2.7 and 2.8 – attached at the end of the thesis.

Table 2.2: Summary of water uses at the production sites of Companies A and B

Co.	Citywater supply				Water uses				
	Untreated	Treated			Washing/rinsing of products/equipment		Make-up for products/equipment		Plant and employee sanitation
		DI	RO	CV	Treated	Untreated	Treated	Untreated	Untreated
A	75.9 %	19.1 %	5.0 %	-	22.0 %	15.2 %	2.1 %	34.6 %	26.1 %
B	33.7 %	-	-	66.3 %	12.1 %	13.6 %	54.2 %	10.5 %	9.6 %

a)

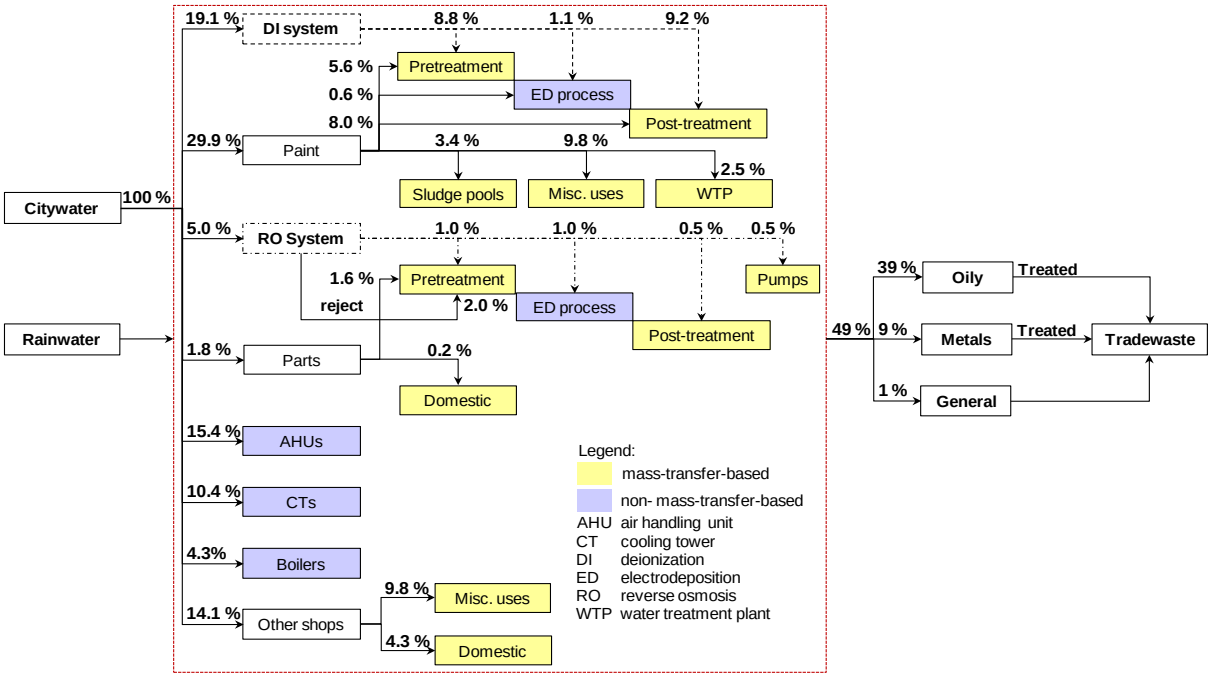

b)

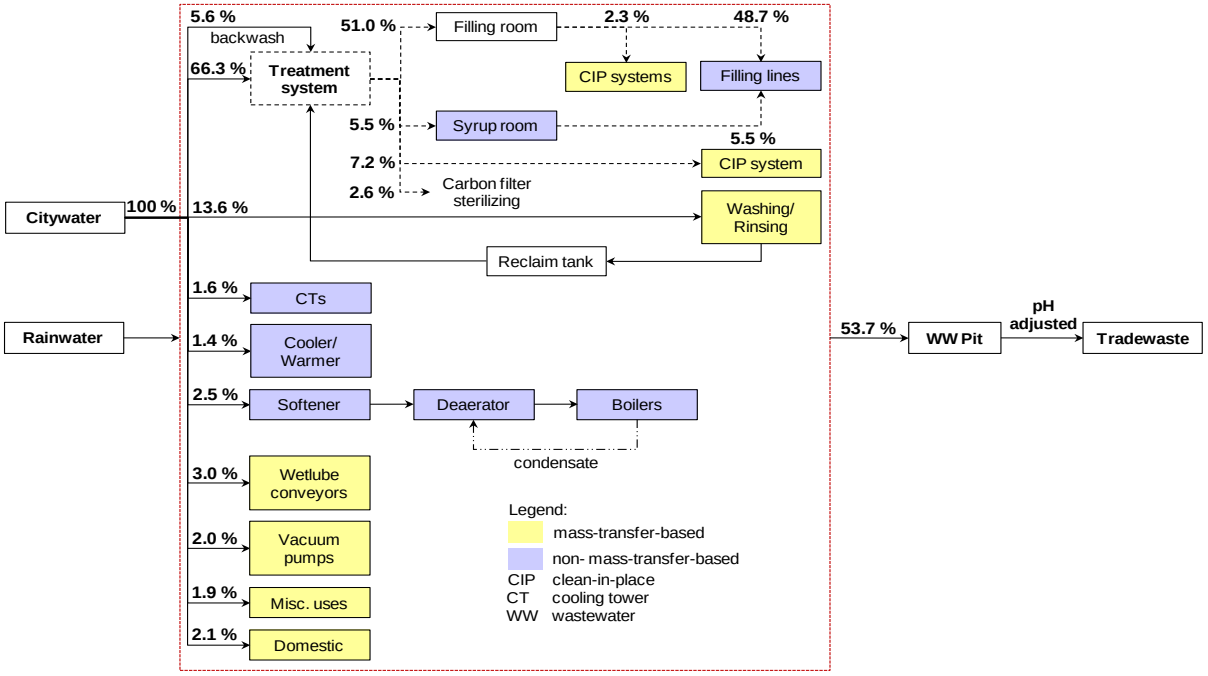

Figure 2.3: Water flow diagrams for (a) Company A and (b) Company B.

2.3.2.1 Company A (automobile manufacturer)

- Of the total Citywater supplied, 19.1 % is treated via a deionization (DI) system while 5.0 % is treated via a reverse osmosis (RO) system. DI and RO water are mainly used for product washing/rinsing at the paint shop's final pretreatment and post-treatment stages for car bodies. Likewise both types of treated water are also used to replenish the electrocoat bath. Approximately 15.2 % of the total Citywater supplied is used for product washing/rinsing at the initial pretreatment and post-treatment stages while 26.1 % is used for personal sanitation and miscellaneous plant cleaning. A small portion (0.6 %) of the total Citywater supplied is also used to replenish the electrocoat bath. The remaining 34.0 % of the total Citywater supplied is used as either feed or make up water to process utilities such as air handling units, boilers, cooling towers, pumps, and sludge pools.
- Mass-transfer-based (MTB) processes account for 67.7 % of the total Citywater consumption while non-mass-transfer-based (NMTB) processes account for 32.3 % of the total Citywater consumption.
- The area with the highest water consumption is paint shop – utilizing 49.0 % of the total Citywater supplied.

2.3.2.2 Company B (beverage company)

- Approximately 66.3 % of the total Citywater supplied is treated via a conventional (CV) system consisting of clarifier, sand filter, carbon filter, bag filter, and UV sterilizer. The treated water is mainly used for clean-in-place (CIP) systems, product mix, syrup mix, and sterilizing carbon filters. Roughly 13.6 % of the total Citywater supplied is used for washing/rinsing product containers while 9.6 % is used for personal sanitation and miscellaneous plant cleaning. The remaining 10.5 % of the

total Citywater supplied is used as either feed or make up water to process utilities such as boilers, cooling towers, coolers/warmers, wet lube conveyors, and vacuum pumps.

- MTB processes account for 40.3 % of total Citywater consumption while NMTB processes account for 59.7 % of total Citywater consumption.
- Approximately 48.7 % of the total Citywater supplied is used for beverage production.

2.3.3 Wastewater characteristics

As mentioned previously, the wastewater streams generated at each company's production site differ markedly from each other. Contaminants generally present in Company A's wastewater streams include paint particles and metals while cleaning chemicals and product components are the contaminants generally present at Company B's wastewater streams. The average water qualities of these streams are described as follows.

2.3.3.1 Company A

Approximately 49% of the total Citywater supplied ends up as Tradewaste while the remainder is either discharged directly into the sewer or is lost due to evaporation. Wastewater streams generated at the manufacturing site are segregated upon collection and are classified into three categories – namely, oily, metals and general streams (as shown in Figure 2.3a). The segregation of wastewater streams facilitates the treatment of specific contaminants. For example, oil & grease and electrodeposition (ED) paint emulsions are removed from the oily stream prior to discharge. Likewise, metals such as nickel (Ni), zinc (Zn) and manganese (Mn) are also removed from the metals stream

prior to discharge. All streams are mixed together after undergoing the relevant treatment and eventually discharged as Tradewaste. Table 2.3 presents the average water qualities of the different wastewater streams found in company A's manufacturing site. Only the main parameters limiting water reuse are shown.

Table 2.3: Average water qualities of different wastewater streams found at Company A's manufacturing site

Category	pH	Conductivity (μS/cm)	SS (mg/L)	O&G (mg/L)	COD (mg/L)
Oily stream	8.8	545	130	45	575
Metals stream	3.7	1595	188	21	250
General stream	6.7	187	7	<5	14
Tradewaste	8.4	1555	28	7	280

2.3.3.2 Company B

Of the total amount of Citywater used on production site, approximately 53.7 % ends up as wastewater while the remaining 46.3% is either mixed with the final products or is lost due to evaporation. A substantial amount of the total wastewater can be traced to discharges generated by process utilities such as boilers, CIP systems, cooling towers, wet lube conveyors, coolers/warmers, vacuum pumps, and washer/rinsers. Contaminants commonly found on Company B's wastewater streams include cleaning chemicals, product mixes and concentrates, and sugars. All wastewater streams are mixed together and discharged as Tradewaste after the pH level has been adjusted. The average water quality of Tradewaste discharge is shown on Table 2.4. Similar to Company A, only the main parameters limiting water reuse are shown.

Table 2.4: Average water quality of Tradewaste discharge at Company B's production site

Category	pH	TDS (mg/L)	SS (mg/L)	O&G (mg/L)	COD (mg/L)
Tradewaste	8.3	2369	41	9	2950

The complete wastewater test results for the representative streams identified at Companies A and B are shown in Appendices 2.9 and 2.10 respectively (attached at the end of the thesis).

2.3.4 Water pinch and process evaluation

The commercially available water pinch software WaterTarget^{TM} [25] was used in analyzing Company A and B's water networks, under steady-state conditions. The mass balance equations used in analyzing the water-using processes found in these networks are as follows:

$$\sum \text{Mass flow}_{IN} = \sum \text{Mass flow}_{OUT} \quad (1)$$

$$\sum \text{Mass flow}_{IN} = \sum \text{Mass flow}_{OUT} + \sum \text{Evaporative losses} + \sum \text{Misc. Losses} \quad (2)$$

Eq. 1 assumes that water losses are negligible and best represents MTB processes. Eq. 2 suggests that there are losses to be accounted for such as evaporative and other miscellaneous losses. This mass balance equation best represents NMTB processes. Since the mass balance equations are steady-state representation of process types, average steady flows were used [25]. These averages represented 2 - 4 days of real time data logging.

The identified sources and sinks together with their mass flow rates and water quality data were encoded into the water pinch software prior to starting the analysis. The comprehensive water pinch analyses for Companies A and B are available in the accompanying CD (Appendices 2.11 and 2.12).

Water pinch analysis for Company A was focused on "shops" with the most number of water-using processes (paint and parts) while water pinch analysis for Company B focused on the whole production site. The results of the analyses are as follows:

2.3.4.1 Company A

Results of the water pinch analysis for Company A identified three main processes where possible water saving opportunities can be achieved. These processes include air handling units (AHUs), car body preparation and car parts preparation – as highlighted in Figure 2.4.

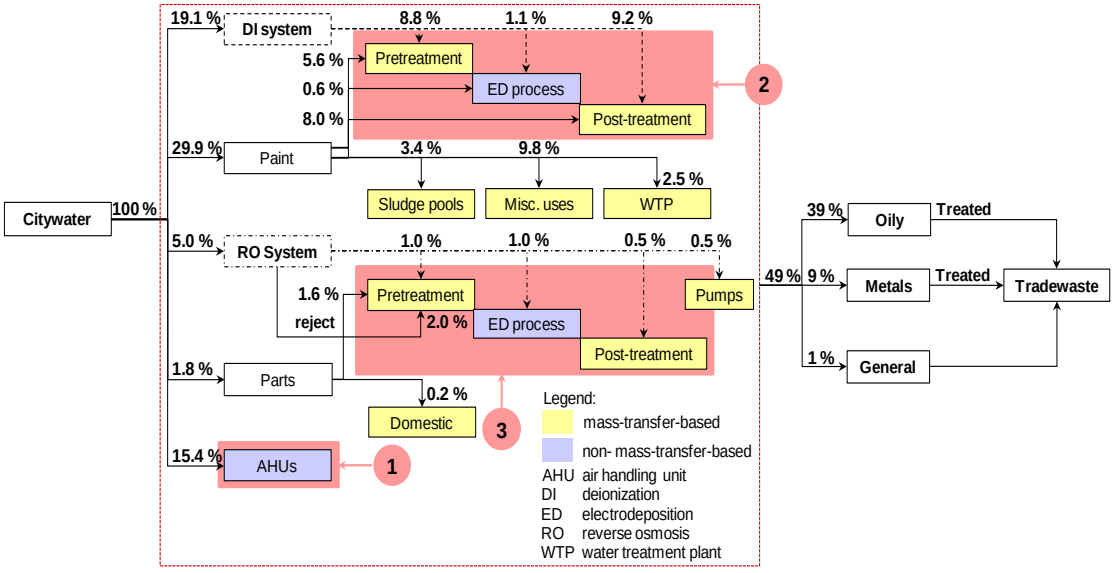

Figure 2.4: Water flow diagram of shops with the most number of water-using processes. Processes identified as having the potential for water saving opportunities are highlighted in light red.

2.3.4.1.1 Air handling units (AHUs)

The AHUs for Company A's manufacturing site are mainly used to condition the incoming air supply of the painting booths. The main users of Citywater in the AHUs are the humidifiers. Citywater is continuously supplied to the humidifiers to offset evaporation and bleed-off losses.

Evaporation loss occurs during the humidification process while bleed-off loss takes place continuously in order to maintain the quality of the water being recirculated in the system. Maintaining the correct quality of water recirculated in the system prevents the build-up of solids and scale on the humidifier pads. Such water quality must be similar to Citywater supply shown in Table 2.1.

A portion of the bleed-off volume is currently being utilized as make-up water for the sludge pools. Bleed-off that goes into the sludge pools is controlled via solenoid valves. Once the level of the water in the sludge pools fall under the control level limits, the solenoid valves open for a specific length of time and shut off once the Citywater supply comes on-line. The moment the solenoid valves shut off, all bleed-off is diverted back into the drain. The current set-up decreases the Citywater consumption but further reuse of the bleed-off is still possible.

Further use of the bleed-off was trialed on two sludge pools. The trial lasted for more than a month. Citywater usage was recorded prior to changes in control settings. The changes involved delaying Citywater fill by 30 s in order to utilize more AHUs' bleed-off and setting the Citywater fill time to 60 s. Prior to control modifications, the average Citywater use for the two sludge pools was 28 tonnes/day. After the

modifications, Citywater use for the two sludge pools decreased to 15 tonnes/day. This translated to approximately 13 tonnes/day of Citywater savings.

It is also worth mentioning that reuse of all the bleed-off into the sludge pools may not be viable because this may increase the conductivity level of the pools. Therefore, at any time, only an optimum volume of bleed-off should be diverted into the sludge pools. This optimum volume should not increase the conductivity level above the specified operating limit – currently maintained within a range of 400 - 450 µs/cm.

2.3.4.1.2 Car body preparation

Car body preparation prior to electrodeposition (ED) painting involves a number of pretreatment processes. Pretreatment increases a car body's resistance to corrosion and facilitates better adhesion of the electrodeposition paint. It is commonly made up of different stages which include degreasing, rinsing, phosphating, and deionized (DI) water rinsing [26]. Electrodeposition painting is a process commonly used in car manufacturing to render car bodies virtually rustproof. Deposition of electrocoat paint is achieved by immersing car bodies into an electrocoat tank connected to a rectifier. A voltage of more than 300 volts is then applied to the electrodes in the tank to facilitate the diffusion and migration of dispersed electrocoat paint particles onto the car body [27]. After ED painting, car bodies are subjected to a series of post-treatment rinses utilizing Citywater, ultrafiltration water and DI water. Rinsing of car bodies after ED painting is primarily carried out to remove non-adhered electrocoat paint.

Figure 2.5 shows the water flow diagram at Company A's car body preparation section. The types of wastewater generated from this section are considered to be the "oily and

metals" streams. These streams are collected separately and treated prior to discharge. The main water quality parameters limiting water reuse in this section include conductivity, suspended solids (SS) and oil & grease (O&G). Each of the water quality parameters mentioned are carefully monitored because they can affect ED paint quality. For example, oil contamination in the ED bath can increase the risk of craters being produced in the paint film. Similarly, tiny particles such as welding pearls not completely removed from car bodies can lead to paint defects like paint splits or rust [27].

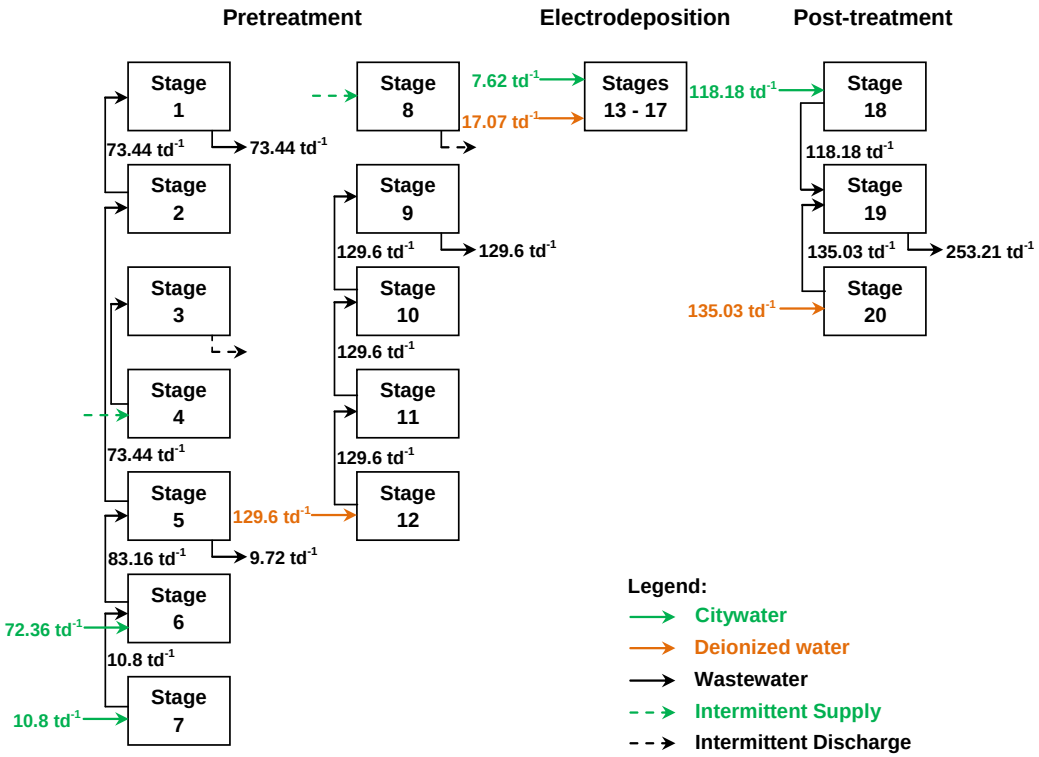

Figure 2.5: Current water flow diagram for Company A's car body preparation section. The amount of Citywater used and wastewater discharged is given in tonnes per day.

An initial water pinch analysis revealed that direct water reuse within the current car body preparation section was not possible due to contamination of the wastewater

streams – as shown in Table 2.5. For example, DI water fed to stage 12 cascades down to stages 11 to 9 (Figure 2.5) and eventually gets discharged down the drain from stage 9. The contamination level changes within each stage and is highest upon discharge. Although this was generally the case, water test results showed that wastewater generated at Stage 19 (Figure 2.5) has the best water quality among the different wastewater streams found at the car body preparation section (Table 2.5). Obviously, the removal of suspended solids (mainly paint particles) as well as O&G will facilitate the reuse of stage 19's wastewater into other stages.

Table 2.5: Average water qualities of wastewater streams generated at Company A's car body preparation section

Wastewater	pH	Conductivity (μS/cm)	SS (mg/L)	O&G (mg/L)
Stage 1	10.4	6160	706	342
Stage 3	11.1	16410	74	62
Stage 5	9.94	849	52	6
Stage 9	3.58	1280	46	9
Stage 19	**6.7**	**56.2**	**12**	**10**

The water pinch analysis was repeated to incorporate the installation of a 50 nm ceramic ultrafiltration system on Stage 19. Results of the analysis showed that the membrane filtrate quality matched the quality of the Citywater input to Stages 6 & 7. Therefore, Citywater supply into stages 6 & 7 can be completely replaced by the ceramic membrane filtrate – as shown in Figure 2.6. Such modifications will result to water savings of 83.16 tonnes/day.

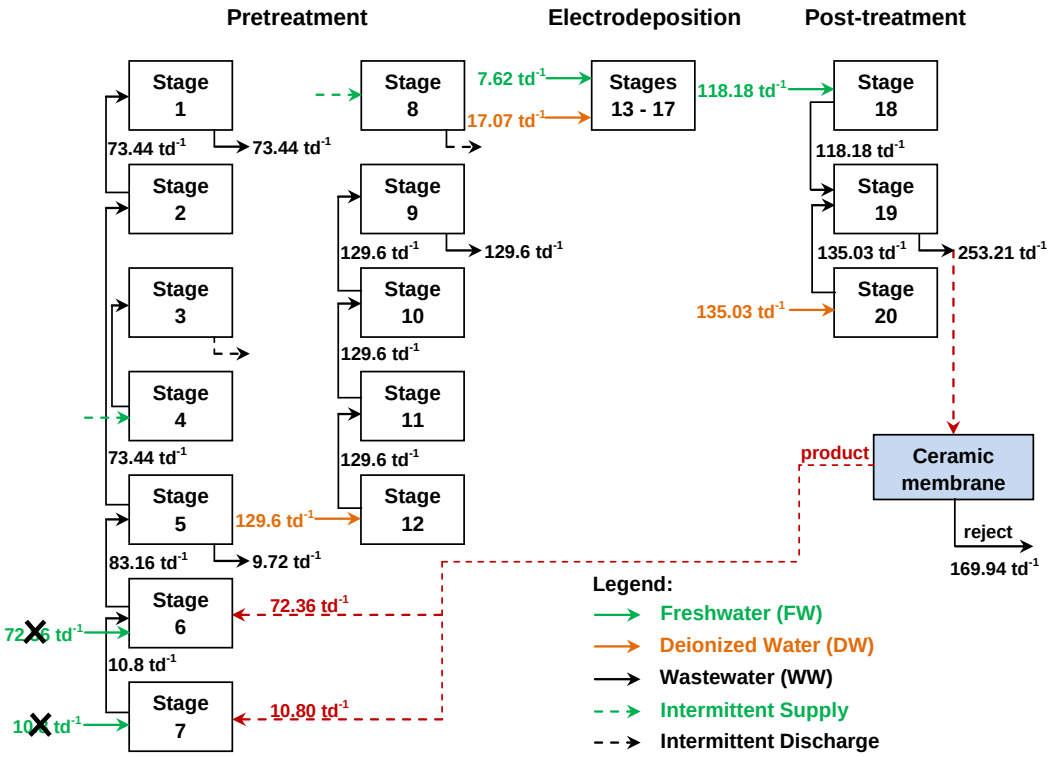

Figure 2.6: Proposed new water flow diagram for car body preparation section. The amount of Citywater used and wastewater discharged is given in tonnes per day.

The ability of the 50 nm ceramic ultrafiltration membrane to remove the paint particle contaminant is explained in detail in Chapter 4.

2.3.4.1.3 Car parts preparation

The car parts preparation section found at the parts shop is similar in operation to the car body preparation section at the paint shop. Main processes found at this section include pretreatment, ED and post-treatment. The current water flow diagram for this section is shown in Figure 2.7. A potential for water savings was identified at Stage 2 of this section based on the water pinch analysis and operator feedbacks. The Stage 2 process was subsequently pilot- trialed for two weeks. Details of these trials are mentioned below.

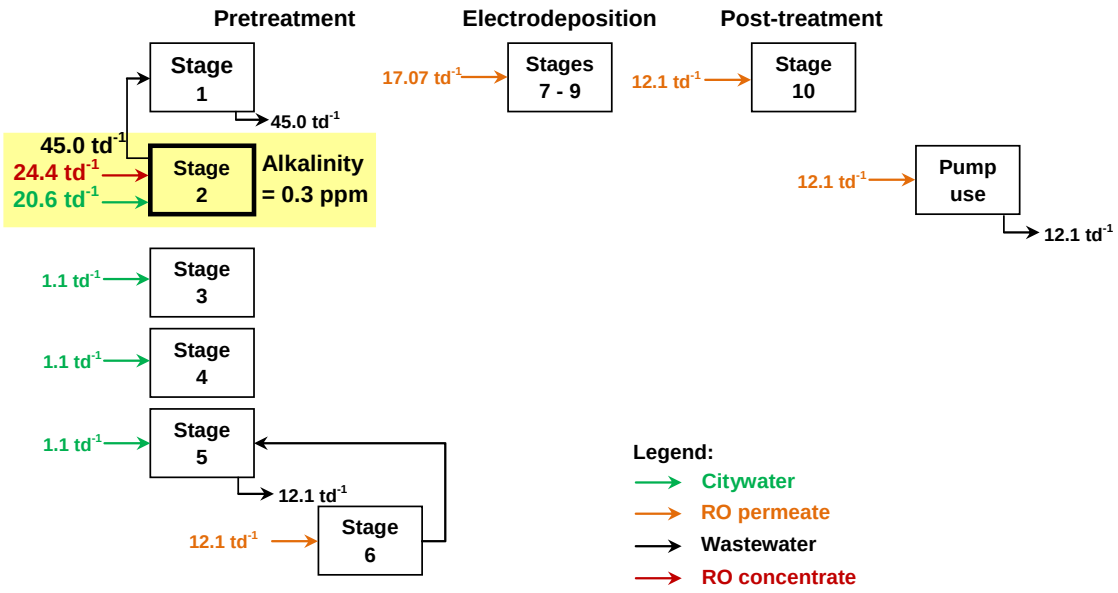

Figure 2.7: Current water flow diagram for Company A's car parts preparation section. The amount of Citywater used and wastewater discharged is given in tonnes per day.

The largest user of water in the car parts section is Stage 2 (Figure 2.7). It utilizes an average of 20.6 tonnes/day of Citywater and 24.4 tonnes/day of RO concentrate as make-up water. The existing overflow rate for this stage is set at 45 tonnes/day to maintain a bath alkalinity concentration of 0.3 ppm.

Water pinch analysis for Stage 2 suggests that by maintaining a higher bath alkalinity level, less make-up water will be needed by the process because the overflow rate can be decreased. A discussion with Company A's subcontractor confirmed that the bath at Stage 2 can operate within an alkalinity range of 0 to 1 ppm. Although the bath alkalinity can go up to 1 ppm, actual changes must be within the range of 0 to 0.8 ppm to have a 20 % safety factor. The 20 % safety factor is a standard operating buffer incorporated by the company in every design project they undertake.

After consulting with appropriate staff at the car parts preparation section, an actual trial at Stage 2 was commenced. The overflow rate at Stage 2 was initially reduced to 28.0 tonnes/day and the alkalinity reading increased to 0.7 ppm. A further reduction of the overflow rate to 25.0 tonnes/day resulted in the same alkalinity reading of 0.7 ppm. At this point, the adjustment was stopped since further reducing the overflow rate will only result in an alkalinity level equal to or above the maximum operating value identified.

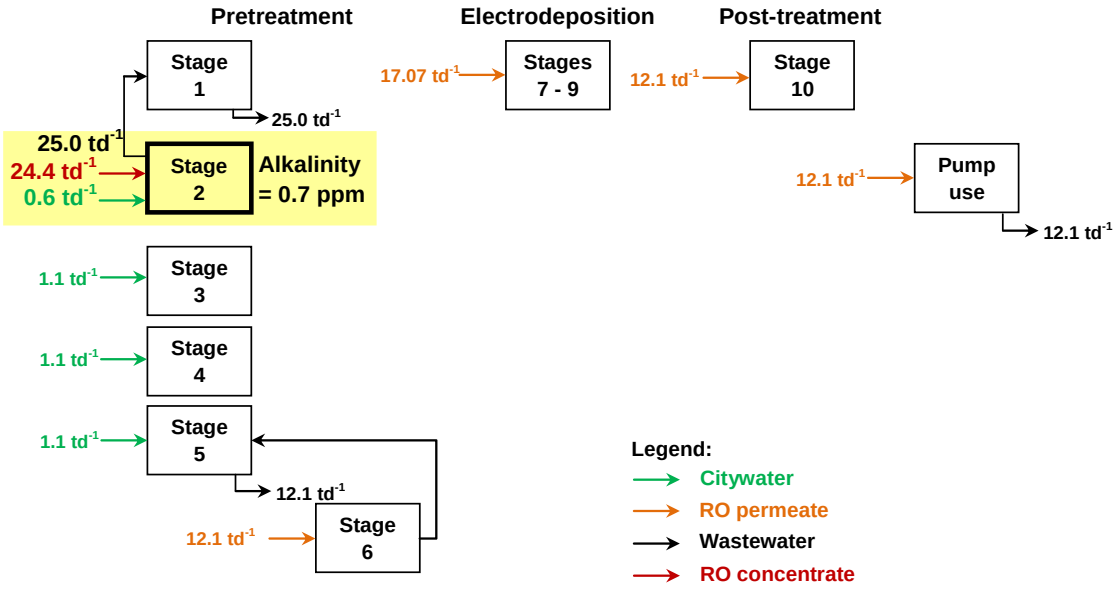

Figure 2.8: Proposed new water flow diagram for car parts preparation area. The amount of Citywater used and wastewater discharged is given in tonnes per day.

With the latest overflow rate, Stage 2 presently utilizes approximately 24.4 tonnes/day of RO concentrate and 0.6 tonnes/day of Citywater – as shown in Figure 2.8. The adjustment of the overflow rate at Stage 2 resulted in a Citywater saving of approximately 20.0 tonnes /day.

2.3.4.2 Company B

Company B's current water flow diagram with actual flow measurements is shown in Figure 2.9a. The results from the water pinch analysis suggest that a number of

wastewater streams generated by some process utilities can be collected at the reclaim tank (Figure 2.9b, red broken lines) and re-supplied back into production processes via the water treatment system. Sources of these streams include vacuum pumps, boilers and washer/rinsers. These wastewater streams have been found to have equal or better water quality compared to the current water collected in the reclaim tank – as shown (in bold) in Table 2.6.

Table 2.6: Average water qualities of wastewater generated by process utilities at Company B's production site

Process utilities	pH	TDS (mg/L)	SS (mg/L)	O&G (mg/L)	COD (mg/L)
Reclaim tank	6.4	92.0	120.0	7.0	81.0
Boiler condensate	**7.1**	**60**	**3.0**	**<5**	**9.0**
Conveyor	4.4	550.0	290.0	7.0	1800.0
Vacuum pumps	**6.5**	**46.0**	**<2**	**<5**	**68.0**
Washer/rinsers	**6.0**	**84.0**	**2.0**	**<5**	**11.0**

The wastewater streams identified above as having the potential for reuse need only minimal treatment prior to redirection into the reclaim tank. For example, boiler condensate must pass through a heat exchanger before being collected, in order to bring down the temperature to ambient level. By reclaiming the wastewater streams generated from the processes mentioned above, a Citywater saving of 80.8 tonnes/day can be achieved. Other wastewater streams in Company B's production site are identified as needing some form of major treatment before they can be reused in the production processes.

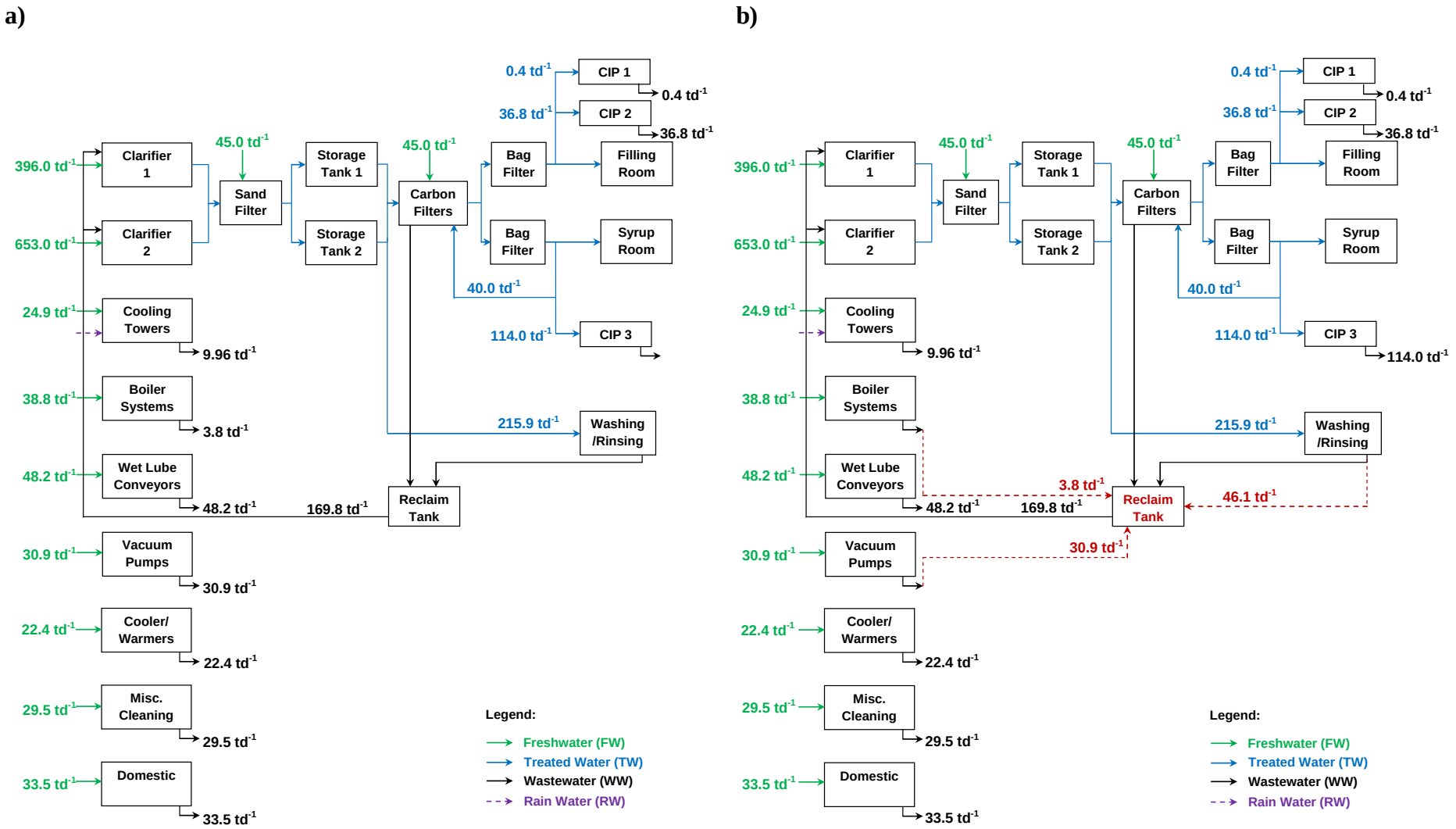

Figure 2.9: Company B's (a) current water flow diagram and; (b) proposed new water flow diagram.

2.4 Conclusions

The synergy of the different water management strategies deployed in this Chapter can bring about substantial reduction of Citywater consumption and wastewater discharge. For example, it was shown at Company A that 33 tonnes/day (2.2 % of total input) of Citywater consumption was saved by directly reusing wastewater generated from other processes. Likewise, it was also shown at Company A that a further 83.16 tonnes/day (5.7 % of total input) of freshwater consumption can be saved through treatment of the post-electrodeposition rinse wastewater using an ultrafiltration process. The combined value of the Citywater savings for Company A will eventually translate to a wastewater reduction of approximately 16.1%. Meanwhile, for Company B, approximately 83.2 tonnes/day (5.25 % of total input) of Citywater can be saved just by reclaiming wastewater generated from different identified processes. The reclaimed wastewater will be treated by the conventional treatment system currently in operation at the production site and reused back into different water-using processes. This will translate into a wastewater reduction of approximately 8.6% for Company B.

In general, results of the water audit and the pinch analysis for both companies suggest that the biggest opportunity for water reuse comes from the most contaminated wastewater streams - although this is not necessarily a general rule. Here, these wastewater streams happen to represent the largest portion of the total wastewater volume generated at each company as shown in Figure 2.10. The reclamation and reuse of these streams will necessarily involve the introduction of some form of water treatment equipment capable of efficiently removing water contaminants in a cost effective manner.

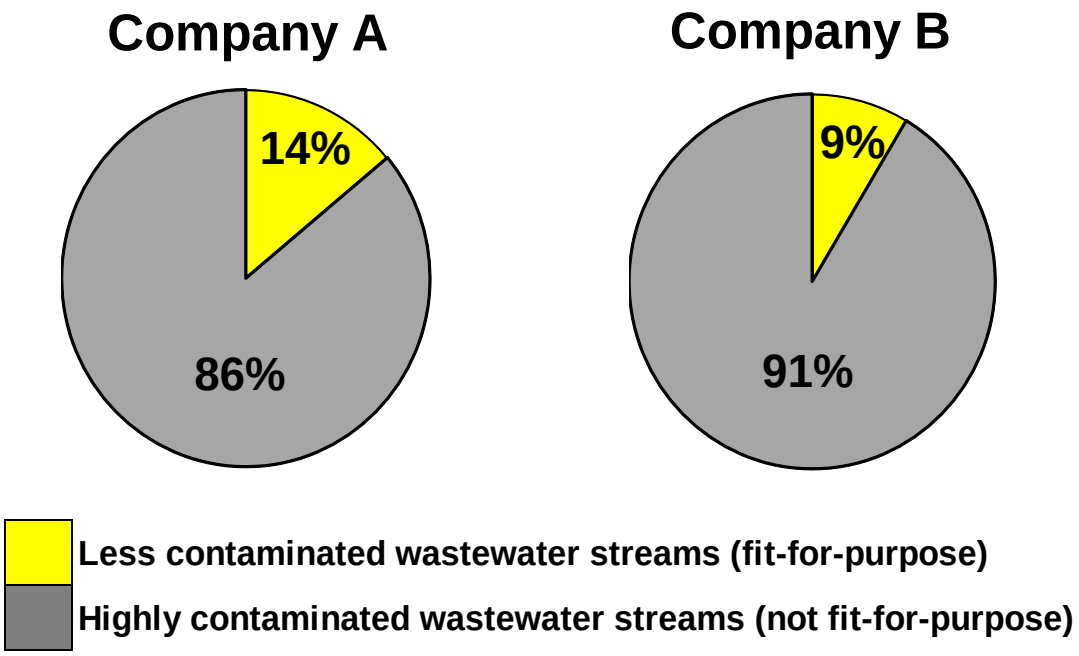

Figure 2.10: General categories of wastewater generated at the two manufacturing companies studied based on degree of contamination.

Not unexpectedly perhaps, the wastewater treatment approaches that are best suited to each of the contrasting manufacturers differ. Overall, for Company A, a distributed effluent treatment approach is found to be appropriate, since the wastewater streams that are generated by the different processes are segregated upon collection. The segregation of streams facilitates the installation of specific water treatment equipment suitable for the type of contaminants that are present in the wastewater. However, a distributed effluent approach is not appropriate for Company B due to the lack of existing infrastructure that would enable the wastewater streams to be collected separately. All wastewater streams at Company B's production site are mixed in drains and end up at a single wastewater collection pit. With Company B's current set-up, the appropriate option for water reclamation is to treat the mixed stream - that is currently discharged as Tradewaste.

Having completed the comprehensive water audits and pinch analyses for both companies, as described above, the selection of the most appropriate technology for the treatment of a particular waste stream may be addressed by conducting controlled experiments in laboratory scale experimental membrane test rig . This approach has been adopted in this thesis whereby a rig has been designed and constructed for the purpose of evaluating the performance of a number of different low-energy membranes on specific wastewater streams generated at both companies. These experiments and evaluations are described in subsequent chapters and provide recommendations on the applicability of different membranes with respect to the reclamation of the specific wastewater streams.

The work described in this chapter has since been published in the international literature [28].

2.5 References

[1] Sturman, J., Ho, G. & Mathew, K. 2004. *Water auditing and water conservation*, Cornwall, UK, IWA Publishing.

[2] Van der Bruggen, B. & Braeken, L. 2006. The challenge of zero discharge: from water balance to regeneration. *Desalination,* 188**,** 177-183.

[3] Natural Resources Canada. 2003. *Pinch analysis: for the efficient use of energy, water and hydrogen* [Online]. Ottawa, Canada. Available: http://198.103.48.154/fichier.php/codectec/En/2009-052/2009-052_PM-FAC_404-DEPLOI_e.pdf [Accessed 24/04/08].

[4] Manan, Z. A. & Alwi, S. R. W. 2007. Water pinch analysis evolution towards a holistic approach for water minimization. *Asia-Pacific Journal of Chemical Engineering,* 2**,** 544-553.

[5] Hallale, N. 2002. A new graphical targeting method for water minimisation. *Advances in Environmental Research,* 6**,** 377-390.

[6] El-Halwagi, M. M., Gabriel, F. & Harell, D. 2003. Rigorous graphical targeting for resource conservation via material recycle/reuse networks. *Industrial and Engineering Chemistry Research,* 42**,** 4319-4328.

[7] Manan, Z. A., Tan, Y. L. & Foo, D. C. Y. 2004. Targeting the minimum water flow rate using water cascade analysis technique. *AIChE Journal,* 50**,** 3169-3183.

[8] Foo, D. C. Y., Manan, Z. A. & Tan, Y. L. 2006. Use cascade analysis to optimize water networks. *Chemical Engineering Progress,* 102**,** 45-52.

[9] Feng, X., Bai, J. & Zheng, X. 2007. On the use of graphical method to determine the targets of single-contaminant regeneration recycling water systems. *Chemical Engineering Science,* 62**,** 2127-2138.

[10] Almutlaq, A. M., Kazantzi, V. & El-Halwagi, M. M. 2005. An algebraic approach to targeting waste discharge and impure fresh usage via material recycle/reuse networks. *Clean Technologies and Environmental Policy,* 7**,** 294-305.

[11] Keckler, S. E. & Allen, D. T. 1998. Material Reuse Modeling: A Case Study of Water Reuse in an Industrial Park. *Journal of Industrial Ecology,* 2**,** 79-92.

[12] Tian, J. R., Zhou, P. J. & Lv, B. 2008. A process integration approach to industrial water conservation: A case study for a Chinese steel plant. *Journal of Environmental Management,* 86**,** 682-687.

[13] Zheng, P., Feng, X., Qian, F. & Cao, D. 2006. Water system integration of a chemical plant. *Energy Conversion and Management,* 47**,** 2470-2478.

[14] Thevendiraraj, S., Klemes, J., Paz, D., Aso, G. & Cardenas, G. J. 2003. Water and wastewater minimisation study of a citrus plant. *Resources, Conservation and Recycling,* 37**,** 227-250.

[15] Dakwala, M., Mohanty, B. & Bhargava, R. 2009. A process integration approach to industrial water conservation: a case study for an Indian starch industry. *Journal of Cleaner Production,* 17**,** 1654-1662.

[16] Feng, X., Wang, N. & Chen, E. 2006. Water System Integration in a Catalyst Plant. *Chemical Engineering Research and Design,* 84**,** 645-651.

[17] Feng, X., Huang, L., Zhang, X. & Liu, Y. 2009. Water system integration of a brewhouse. *Energy Conversion and Management,* 50**,** 354-359.

[18] Foo, D. C. Y. 2009. State-of-the-art review of pinch analysis techniques for Water network synthesis. *Industrial and Engineering Chemistry Research,* 48**,** 5125-5159.

[19] Wang, Y. P. & Smith, R. 1994. Wastewater minimisation. *Chemical Engineering Science,* 49**,** 981-1006.

[20] Liu, Z. Y., Yang, Y. Z. & Zhang, Y. 2007. Determining the pinch point and calculating the freshwater target for water-using systems with single contaminant. *Chemical Engineering Research and Design,* 85**,** 1485-1490.

[21] Deng, C., Feng, X. & Bai, J. 2008. Graphically based analysis of water system with zero liquid discharge. *Chemical Engineering Research and Design,* 86**,** 165-171.

[22] Koppol, A. P. R., Bagajewicz, M. J., Dericks, B. J. & Savelski, M. J. 2004. On zero water discharge solutions in the process industry. *Advances in Environmental Research,* 8**,** 151-171.

[23] Agrawal, V. & Shenoy, U. V. 2006. Unified conceptual approach to targeting and design of water and hydrogen networks. *AIChE Journal,* 52**,** 1071-1082.

[24] Brauns, E., Helsen, J., Schiettecatte, W. & Genné, I. On the use of alternative and pragmatic software tools during process water reuse evaluation in a factory. *In:* CHISA 2006 - 17th International Congress of Chemical and Process Engineering, 2006 Prague.

[25] Brauns, E., Helsen, J., Schiettecatte, W. & Genné, I. 2008. Pragmatic software tools for water reuse evaluation in a factory. *Clean Technologies and Environmental Policy,* 10**,** 189-201.

[26] Gehmecker, H. 2007. Pretreatment of multimetal car bodies. *In:* Streitberger, H. & Dossel, K. (eds.) *Automotive paints and coatings.* 2nd ed. Weinheim: Wiley-VCH.

[27] Streitberger, H. 2007. Electrodeposition coatings. *In:* Streitberger, H. & Dossel, K. (eds.) *Automotive paints and coatings.* 2nd ed. Weinheim: Wiley-VCH.

[28] Agana, B. A., Reeve, D. & Orbell, J. D. 2013. An approach to industrial water conservation – A case study involving two large manufacturing companies based in Australia. *Journal of Environmental Management,* 114**,** 445-460.

Chapter Three: Low-pressure polymeric membranes for reclamation of industrial water generated by Company A (automobile manufacturer) and Company B (beverage producer)

3.1 Introduction

A number of researchers have shown that certain types of membrane can be employed for treating the various wastewaters generated during car manufacturing and beverage production. For example, Anderson et al. [9] have shown that a cellulose acetate RO membrane can work successfully in reclaiming wastewater generated from an automotive electrocoat painting process. In terms of beverage production, Tay and Jeyaseelan [29] have demonstrated the viability of a combined UF and RO treatment system in the reclamation of bottle-washing wastewater. They concluded that the combined UF and RO system not only reduces freshwater consumption but also conserves energy.

Membranes have also been shown to work successfully in treating similar wastewater streams generated by different production facilities. For example, in an experiment involving the treatment of vegetable oil-contaminated factory wastewater, using a polysulfone UF membrane [22], reductions in water quality parameters such as COD, TOC, TSS, and phosphate concentration exceeded 85 %. Similarly, good retention rates for emulsified solvent and oil and grease were obtained when a cellulose acetate UF membrane was used for treatment of spent solvent rinses from nickel-plating operations [26]. The retention rates for emulsified solvent and oil and grease were reported to be 96 % and 80 % respectively.

Aside from water reclamation, membranes have also been shown to be an effective means of recovering valuable resources such as coating materials and metals. For example, Lipnizki [19] discussed the potential for recovering coating materials such as paper coatings, latex and flexographic ink. This concept is similar to what might be

applied to the recovery of electrodeposition (ED) paint. Diluted coating materials are recovered using UF to obtain a solid-free permeate stream that can easily be treated and reused. Such a set-up can translate into less than two years payback periods for UF systems. Meanwhile, metals recovery through membrane filtration is slowly becoming a viable alternative. Some of the most valuable metals being recovered from wastewater using membrane filtration systems include copper [6, 12], chromium [23, 27] and silver [18].

The work described in this chapter was aimed at determining the suitability of selected low-pressure polymeric membranes (UF, NF and RO) for the reclamation of wastewater generated at the production facilities of a car manufacturer and a beverage producer. Wastewater streams generated at both of these two production facilities have substantial volumes – making wastewater reclamation desirable in order to reduce excessive water consumption. The main challenge to wastewater reclamation at these facilities is the level of contamination present in the wastewater. In the case of the car manufacturer, wastewater streams are generally classified as "oily" and "metals" streams. Contaminants commonly found in the oily wastewater stream include electrodeposition (ED) paint emulsions and oil & grease. Metals such as Iron (Fe), Nickel (Ni), Manganese (Mn), and Zinc (Zn) are the dominant contaminants found in the metals wastewater stream – together with phosphate. On the other hand, contaminants commonly found on the beverage producer's wastewater include cleaning chemicals, product mixes and concentrates, and sugars.

The suitability of the selected low-pressure membranes was evaluated based on reduction/rejection rates in relation to critical water quality parameters, permeate flux

decline rates and power usage. Likewise, to visualize the degree of fouling on the membrane surface, fouled membranes were analysed using a scanning electron microscope (SEM). In general, the UF membranes were evaluated for pretreatment of wastewater whilst the NF and RO membranes were evaluated for wastewater reclamation.

3.2 Materials and methods

3.2.1 Wastewater samples

Actual wastewater samples were obtained from a car manufacturer and a beverage producer operating in the western suburbs of Melbourne, Australia. The wastewater samples were collected in 20 L containers and kept in a cold room at a temperature of 4 °C. Prior to every experiment, a specified volume of wastewater sample is transferred into a stainless steel container. The stainless steel container is then left for a couple of hours inside the laboratory to bring up the wastewater temperature to ambient level. All wastewater samples were used within 48 hours of collection.

3.2.2 UF membranes

Two types of polymeric flat sheet UF membranes, supplied by GE Osmonics, were used in the experiments – namely, JW (polyvinylidine-difluoride, PVDF) membrane with MWCO of 30 kD (pore size = 3.25 nm) and MW (polyacrylonitrile, PAN) membrane with MWCO of 100 kD (pore size = 10 nm) [3, 4]. The JW membrane is hydrophobic (contact angle = 66°) while the MW membrane is extremely hydrophilic (contact angle = 4°). UF membranes used for experiments were soaked in deionized water overnight to remove any surface impurities.

3.2.3 NF and RO membranes

Both the NF (DL series) and low–pressure RO (AK series) membranes used in the experiments were supplied by GE Osmonics. The NF membrane is a thin-film membrane having an approximate MWCO of 0.15 – 0.30 kD for uncharged organic molecules [2]. Similar to the NF membrane, the RO membrane is also a thin-film membrane having high flux and a NaCl rejection rate of approximately 99.0 % [1]. The NF membrane was specifically tested on the metals wastewater sample while the RO membrane was tested on all the wastewater samples.

3.2.4 NF and RO membranes preparation

All NF and RO membranes used in the experiments were soaked in deionized water overnight to remove any surface impurities. Prior to using the NF and RO membranes, a wetting protocol was followed [17, 20]. In this case, deionized water having an average conductivity of 2 μS/cm was pumped into the membrane for 15 minutes. The pressure and temperature of the deionized water was maintained at 2.5 MPa and 25 °C respectively throughout the wetting period.

3.2.5 Membrane filtration system

Central to this research project was the design and construction of a versatile, experimental test rig, shown in Figure 3.1. This rig was employed for a range of different experiments relating to different recycling issues for both companies and is depicted schematically in subsequent Chapters, as required.

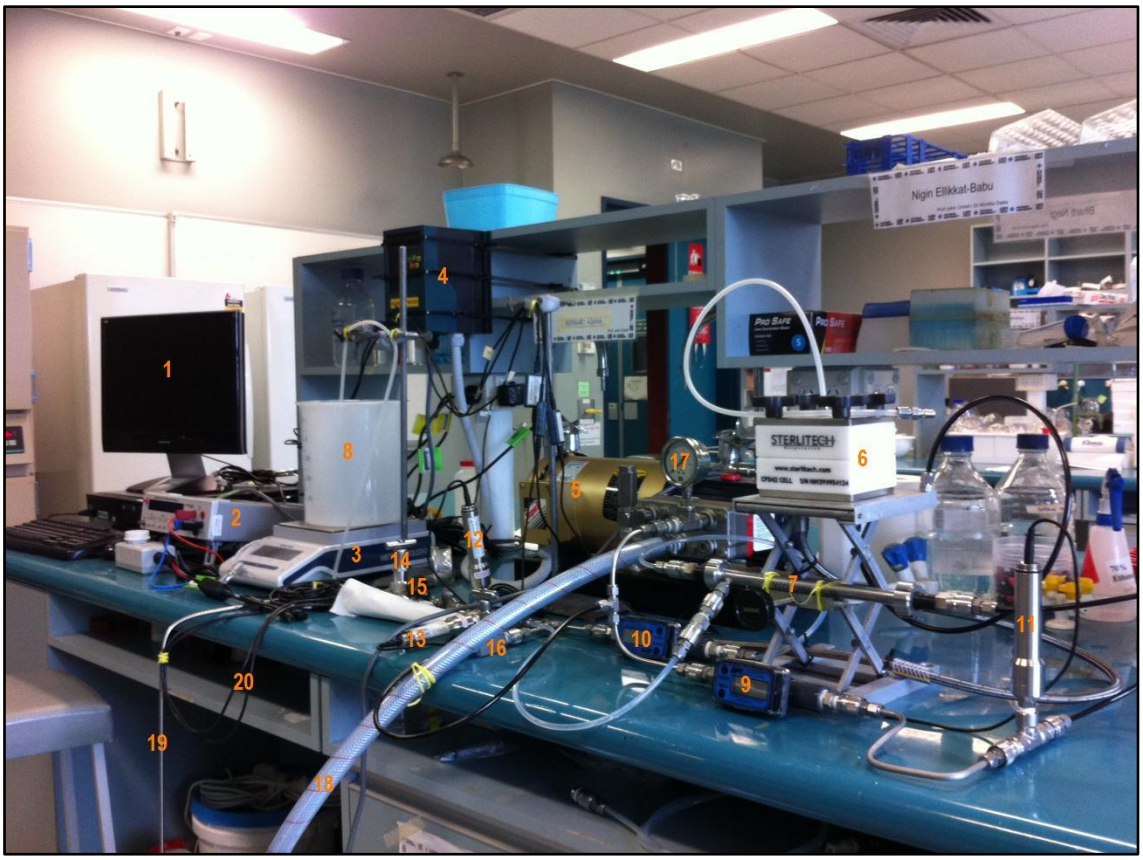

Figure 3.1: Experimental test rig used during membrane experiments. 1 – desktop computer for data logging, 2 – power meter, 3 – balance, 4 – variable speed drive, 5 – positive displacement pump, 6 – flat sheet test cell, 7 – ceramic membrane module, 8 – plastic container, 9 – feedwater flowmeter, 10 – reject water flowmeter, 11 – feedwater pressure recorder, 12 – reject water pressure recorder, 13 – product water pressure recorder, 14 – product water valve, 15 – reject water valve, 16 – recirculation valve, 17 – discharge pressure gauge, 18 – inlet line, 19 – reject line, 20 – pH and conductivity probes.

The experimental test rig shown in Figure 3.1 has a crossflow configuration (i.e. flow is parallel to the surface of the membrane). The crossflow velocity (CFV, m s^{-1}) for the system was approximated using Eq. (1):

$$CFV = Q / A \quad (1)$$

where Q is the flow rate ($m^3 s^{-1}$) and A is the area of pipe or tube (m^2). The area of the pipe or tube can be calculated using Eq. (2):

$$A = \pi Ø_i^2 / 4 \quad (2)$$

where $Ø_i$ is the inside diameter of the pipe or tube. For experiments involving flat sheet membranes, $Ø_i$ is equal to the inside diameter of the feed tube. On the other hand, for experiments involving ceramic membranes, $Ø_i$ is equal to the inside diameter of the tubular ceramic membrane.

The feed pump used in the system is connected to a variable speed drive (VSD). The VSD acts as a mechanism that regulates the flowrate of the pump. Such a mechanism is very important, especially in membrane experiments requiring the precise delivery of feed flowrate and pressure. Monitoring equipment such as balance, flowmeters, power meter, probes, and recorders were also fitted into the system to continuously monitor operating parameters such as permeate weight, feed flowrate, power usage, conductivity, pH, and pressure. Data acquisition and storage of operating parameters were facilitated by computer software provided by equipment manufacturers.

Table 3.1 shows the specifications of the main components of the experimental test rig. The polymeric and ceramic membranes used in the experiments are all commercially available.

Table 3.1: Specifications of the main components of the experimental test rig

Equipment	Manufacturer / Supplier	Specifications
Balance	Mettler-Toledo	MS 4002S New Classic Balance 4200g x 0.01g
Ceramic membrane module	Pall Australia Pty Ltd	Membralox 1T1-70 stainless steel module with EPDM O-rings
Desktop computer	Generic	Intel Core 2 Duo; loaded with data acquisition software from Mettler-Toledo, Hach, Hameg, and Madgetech
Flat sheet test cell	GE Osmonics	CF042 Development Cell; Delrin Acetal
Flowmeter	GPI	Model No. TM050-N; ½" NPT; 0.0 – 38.0 Lpm
Multimeter	Hach	IM6700 Multi-parameter; digital dual-input model; pH probe (PHC101030); conductivity probe (CDC 40103)
Power meter	Hameg	Model No. 8115-2; 8 kW power meter with simultaneous display of voltage, current & power
Positive displacement pump	Hydracell	M-03S Hydracell CC pump with stainless steel head and valves; Viton diaphragms; 1.8 GPM
Pressure recorder	Madgetech	PST-PRTEMP1000 rugged temperature & pressure recorder; 1/4" NPT fitting; stainless steel enclosure; 0-1000 psi
Pump motor	Baldor	CEM 3554; premium efficiency; C-Face; ½ hp; 3 phase; 230 V; 50Hz
Variable speed controller	Generic	Output of 230 V; Input – 230 V; single phase; 7 amp rated

3.2.6 UF experiments

Wastewater samples collected were directly used as feed into the UF membranes. UF membrane experiments were carried out at a crossflow velocity (CFV) of 2.4 m s^{-1} and at transmembrane pressures (TMPs) of 0.2 and 0.4 MPa. A crossflow velocity configuration was chosen because at this mode, particle deposition onto the membrane surface is inhibited. Meanwhile, the TMPs used represent 30 % and 60 % of the maximum operating pressure stated by the manufacturer. Such TMPs offer the best permeate quality based on a number of preliminary experiments conducted. The temperature range during the experiments was maintained within 19 – 24 °C. This range represents the actual temperature in the manufacturing processes. Operating parameters mentioned in Section 3.2.5 were continuously monitored at 15 minute intervals. Samples of feedwater and membrane permeate were collected into containers and sent to a NATA (National Association of Testing Authorities) accredited laboratory for analysis on water quality parameters such as oil & grease (O&G) and total organic carbon (TOC). Actual test results are available in the accompanying CD – Appendices 3.1, 3.2 and 3.3. Aside from O&G and TOC, feedwater and membrane permeate turbidity were also measured during the experiments to estimate suspended particle rejection rates. The volume of wastewater sample used for each experiment is 6 L while filtration area for all UF membranes used is 0.0042 m^2. Each experimental run lasted for approximately 6 hrs.

3.2.7 NF and RO experiments

Prior to NF and RO experiments, wastewater samples collected were filtered through a 0.3 micron filter to remove any suspended particles present. Both the NF and RO membrane experiments were carried out at a CFV of 2.7 m s^{-1} and at TMPs of 0.69,

1.03 and 1.38 MPa. The temperature range during the experiments was maintained within 25 – 29 °C. Operating parameters mentioned in Section 2.5 were continuously monitored at 5 minute intervals. Similar to the UF experiments, samples of feedwater and membrane permeate were collected into containers and sent to a NATA accredited laboratory for analysis on water quality parameters such as chemical oxygen demand (COD), conductivity and metals content. Actual test results are available in the accompanying CD – Appendices 3.4 and 3.5. The volume of filtered wastewater sample used in each experiment is 3 L while filtration area for both the NF and RO membranes is 0.0042 m^2. Each experiment run lasted for approximately 2 hrs.

3.2.8 Analytical methods

The size distribution and zeta potential (ζ) of particles in the actual wastewater samples were measured using a Malvern Zetasizer Nano Series (Nano-ZS). Turbidity measurements were carried out using a La Motte 2020 Series Turbidity meter. The reduction/rejection rates of the critical water quality parameters (% P_R) mentioned in Sections 2.6 and 2.7 were calculated using Eq. (3):

$$\% P_R = [(P_F - P_P) / P_F] \times 100 \% \quad (3)$$

where P_F is the parameter concentration in the feedwater (mg L^{-1}) and P_P is the parameter concentration in the membrane permeate (mg L^{-1}).

After each experiment, used flat sheet membranes were washed with deionized water and air dried at ambient temperature. Representative portions of each air dried membranes were cut (approximately 1 cm^2) and mounted on aluminum stubs with

carbon tape. They were then coated with a layer of gold and analysed under a Field Emission Scanning Electron Microscope (FESEM, Philips XL30 FEG). The accelerating voltages used during the analysis ranged from 2 to 15 kV while magnifications used ranged from 20,000 to 25,000 times.

3.3 Results and discussion

3.3.1 Pure water flux (PWF)

Experiments aimed at establishing the relationship between pure water flux (PWF) and TMP were carried out prior to commencing actual wastewater experiments. Distilled water having a conductivity of 2 μS/cm was used as feed to ensure that no form of fouling will occur during filtration. Results showed that PWFs of the polymeric membranes were highly correlated ($R^2 > 0.99$) with TMP as shown in Figures 3.2a and b. A high correlation between PWF and TMP is expected since the only resistance present during the experiments is the intrinsic membrane resistance. The slopes of the line shown in Figures 3.2a and b give the pure water permeabilities (PWPs) of the membranes. Figure 3.2a shows that the PWF of the MW membrane was higher than the JW membrane. The disparity between the pure water fluxes of the two UF membranes can be attributed to the relative membrane structure and properties (i.e. hydrophilicity/hydrophobicity). For example, the MW membrane was designed to be extremely hydrophilic and it might be expected to have higher water fluxes than the hydrophobic JW membrane. This scenario is similar to the pure water fluxes obtained for NF and RO membranes (Figure 3.2b). An NF membrane has relatively looser pores compared to an RO membrane and is expected to have a higher pure water flux. The data used for plotting Figures 3.2a and b are available in the accompanying CD (Appendix 3.6).

a)

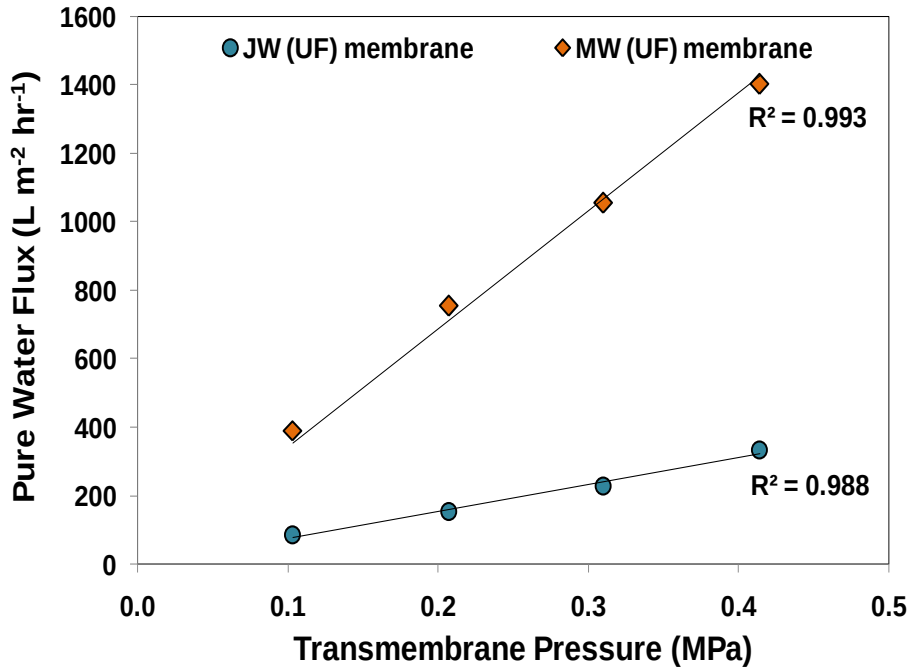

b)

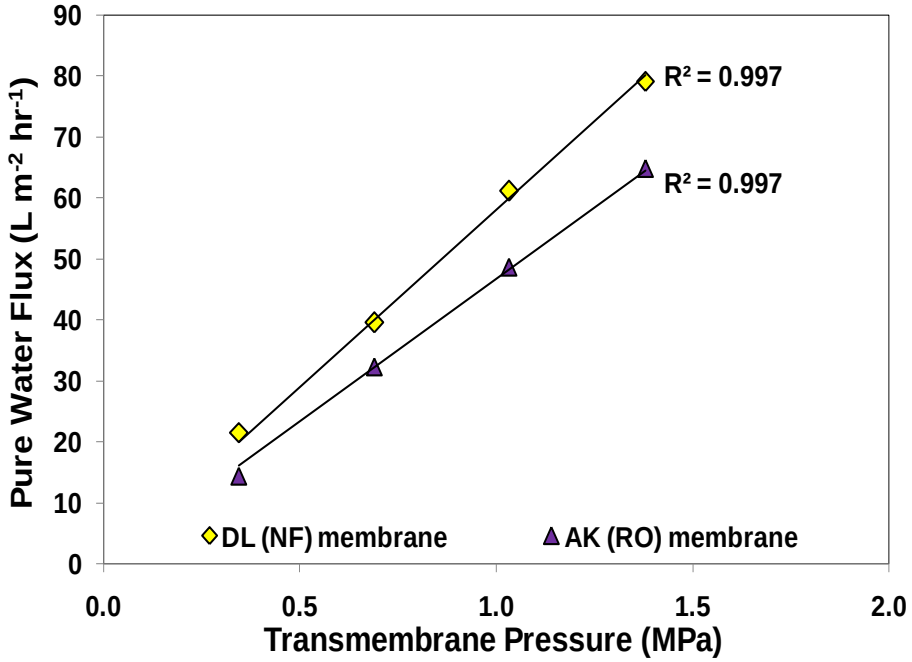

Figure 3.2: Pure water fluxes of: a) UF membranes as a function of TMP at a CFV of 2.4 m s^{-1} and standard temperature of 20 °C and b) NF and RO membranes as a function of TMP at a CFV of 2.7 m s^{-1} and standard temperature of 25 °C. The PWP of the membrane is given by the slope of the line.

The calculated intrinsic resistance of the JW and MW membranes are 4.16E+12 m^{-1} and 3.44E+11m^{-1} respectively. Such resistances are lower as compared to the intrinsic resistances obtained for the ceramic membranes used. The difference may be due to the relative thickness of the membranes. The intrinsic resistance calculated have values close to the ones indirectly obtained by Akdemir and Ozer [8]. Similarly, the intrinsic resistances calculated for both the AK and NF membranes (8.28E+12 m^{-1} and 1.01E+13 m^{-1}) are well within the range of results obtained in literature [14].

3.3.2 Characteristics of wastewater samples

The particle size distributions for the wastewater samples collected are shown in Figure 3.3. The oily and metals wastewater samples obtained from the car manufacturer have particle sizes ranging from 90 – 532 nm and 18 – 397 nm respectively. The mean diameter of the particle sizes found on the oily wastewater sample is 245.5 nm while the mean diameter of particle sizes found on the metals wastewater sample is 134.1 nm. On the other hand, wastewater samples from the beverage producer have particle sizes in the range of 24 to 5560 nm – with a mean diameter of 161.4 nm.

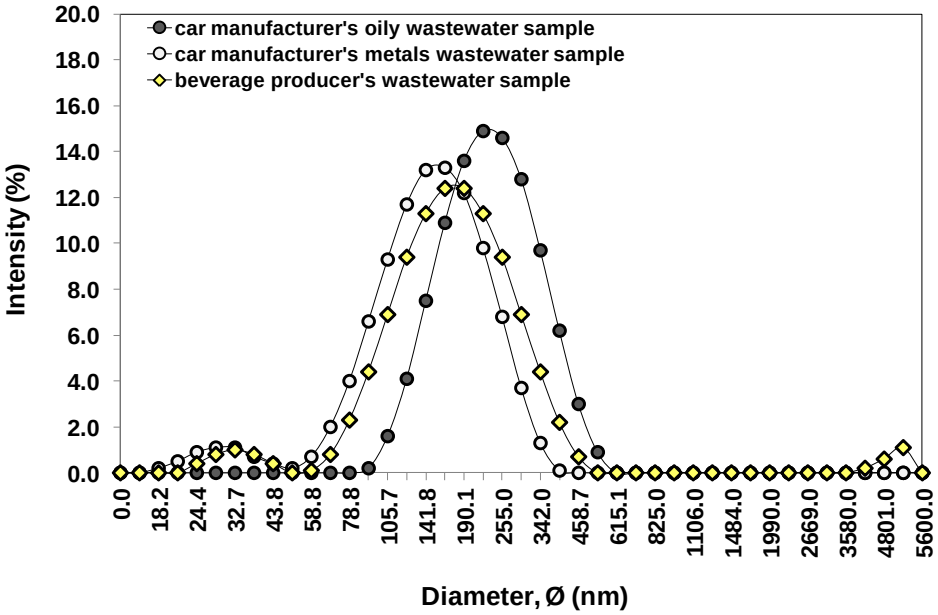

Figure 3.3: Particle size distributions for wastewater samples used.

The average zeta potential (ζ) of the particles present in the wastewater samples collected are shown in Table 3.2 while the data used for plotting Figure 3.3 are available in the accompanying CD (Appendix 3.7).

Table 3.2: Average zeta potential (ζ) of particles found on the wastewater samples used in the experiments

Wastewater sample	pH	Particle zeta potential (ζ)
Car manufacturer's oily wastewater sample	7.5	56 ± 2 mV
Car manufacturer's metals wastewater sample	3.8	- 21± 2 mV
Beverage producer's wastewater sample	8.3	- 23 ± 2 mV

The values of the zeta potential for both the metals and beverage production wastewater samples suggest that the particles present have incipient instability [10]. Because particles present in these wastewater samples are likely to exhibit instability, particle aggregation may occur. Particle aggregation is not considered to be a problem during ultrafiltration because the more the particles aggregate, the better. Larger particles have higher hydrodynamic forces acting on them and therefore are more likely to be swept away from the membrane surface. In contrast, the zeta potential of particles found in the oily wastewater sample suggests that the particles have good stability and are well dispersed in solution. Since particles are well dispersed in solution, particle aggregation is unlikely to happen. In this particular case, the particle sizes present in the oily wastewater sample can be assumed to be the same throughout the experiments. Therefore, the possibility for the finer suspended particles to deposit on the membrane surface is high. The typical characteristics of the wastewater samples used in the experiments are shown in Table 3.3.

Table 3.3: Typical characteristics of wastewater samples used in the experiments

Water quality parameters	Oily wastewater	Metals wastewater	Beverage production wastewater
pH	7.5	3.8	8.3
Conductivity, μS cm^{-1}	979	1579	1129
COD, mg L^{-1}	230	91	4900
O&G, mg L^{-1}	21	<5	17
TOC, mg L^{-1}	120	16	140
Turbidity, NTU	294	43	58
Color	light gray	hazy white	murky, yellowish
Iron (Fe), mg L^{-1}	1.13	4	-
Manganese (Mn), mg L^{-1}	0.06	23	-
Nickel (Ni), mg L^{-1}	0.02	40	-
Zinc (Zn), mg L^{-1}	1.23	98	-

3.3.3 UF experiments

Permeate fluxes (J, $m^3\ m^{-2}\ s^{-1}$) were calculated using Eq. (4):

$$J = (0.001 \times W) / (A_M \times t) \quad (4)$$

where W is the weight measured by the balance (kg), A_M is the effective membrane area (m^2), t is the sampling time (s). To account for temperature variations, all permeate fluxes were standardized at a temperature of 20 °C using Eq. (5) [11]:

$$J_{20°C} = J\ (1.03)^{T_S - T_M} \quad (5)$$

where $J_{20°C}$ is the flux at a standard temperature of 20 °C ($m^3\ m^{-2}\ s^{-1}$), T_S is the standard temperature (20 °C), T_M is the measured temperature (°C).

Both the JW and MW membranes showed the same flux decline profiles when tested on the oily wastewater sample (Figure 3.4a). A rapid decline in flux was observed after 2 hrs followed by a gradual decline throughout the remainder of the experiment run. Of the two membranes tested for this specific wastewater sample, the MW membrane showed the worst flux decline rates at all TMPs used, which can be explained by considering the membrane's permeability. As noted previously, the pure water permeability of the MW membrane is significantly higher than for the JW membrane (Figure 3.2a). Howe et al. [16] showed that membranes with higher permeability fouled faster than membranes with lower permeability. Membranes with higher permeability have bigger pores compared to those with lower permeability. Initially, membranes with bigger pores will have higher fluxes but once particles start to deposit on the pores, fluxes obtained will drastically be reduced until such time that the pore openings have become smaller. Consequently, the smaller pore openings will inhibit further deposition of particles – resulting in gradual flux decline.

a)

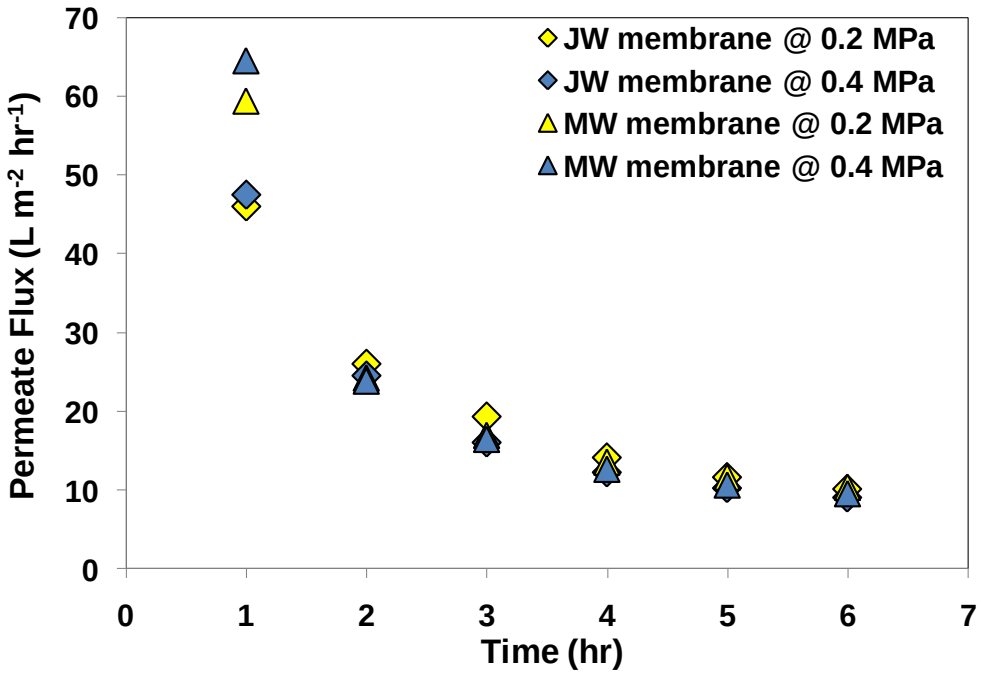

b)

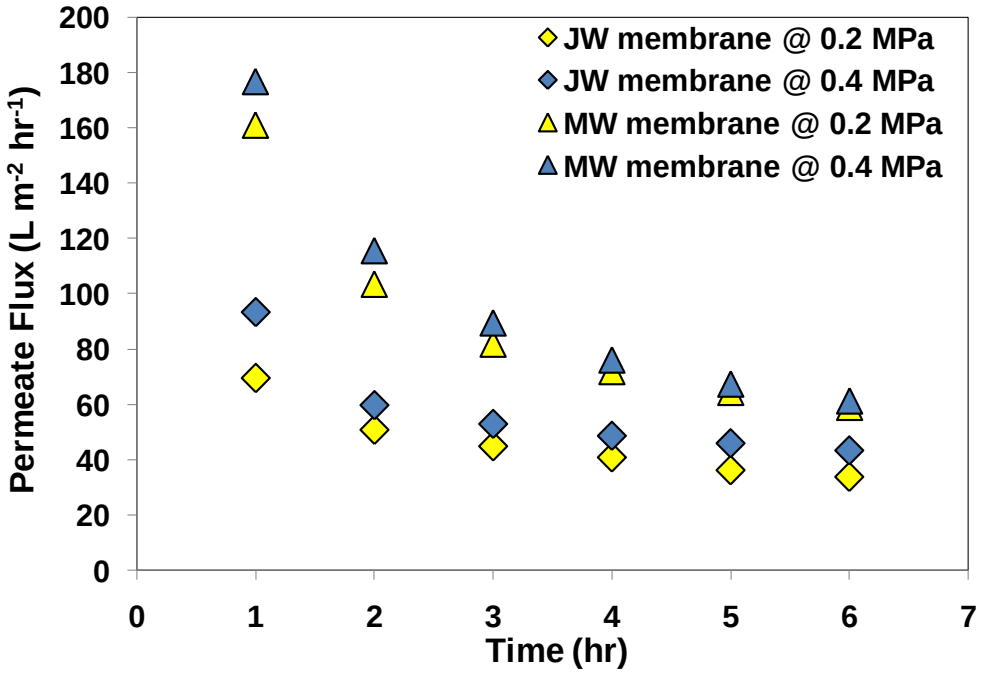

c)

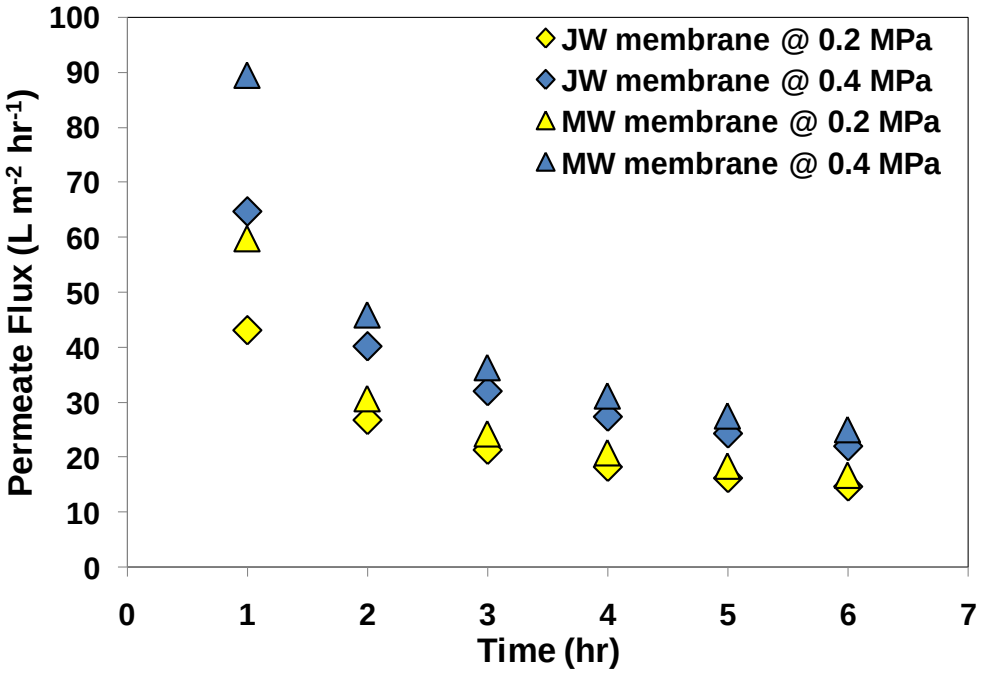

Figure 3.4: JW and MW membranes' permeate fluxes with respect to: a) oily wastewater sample (automobile manufacturer), b) metals wastewater sample (automobile manufacturer) and c) beverage production wastewater sample.

Fouling rates during the experiments that involved the oily wastewater sample were greatly influenced by the presence of suspended cathodic electrodeposition (CED) paint particles. These particles include paint pigment, unstable resins and polymers. Positively charged cathodic electrodeposition paint particles deposit rapidly on the surfaces of the JW and MW membranes. The combination of membrane surface-particle interaction and applied transmembrane pressure (TMP) resulted in intense fouling of both membranes. Fouling mechanisms observed during the oily wastewater experiments include intermediate pore blocking and cake layer formation. Intermediate pore blocking occured during the first two hours of the experiments resulting in rapid flux decline (Figure 3.4a). Subsequently, cake layer formation was the prevailing fouling mechanism during the remaining experiment time. Deposition of paint particles happen initially on the membrane pores and was followed by accumulation of particles on the membrane surface, resulting in cake layer formation. Fouling of the MW membrane was more severe than for the JW membrane because it has larger pore sizes and higher surface porosity, as shown in Figures 3.5a & b. Aside from membrane structure, charge attraction can also be a contibuting factor in the rapid deposition of CED paint particles on the pores and surface of the MW membrane. Since the CED paint particles are positively charged [28], they are attracted to the negatively charged surface of the MW membrane. The MW membrane was modified by its manufacturer to become extremely hydrophilic [4]. Such membrane modification usually involves the partial hydrolysis of the membrane material with NaOH – resulting in improved hydrophilicity and a negative surface charge [30]. The data used for plotting Figures 3.4a to c are available in the accompanying CD (Appendix 3.8).

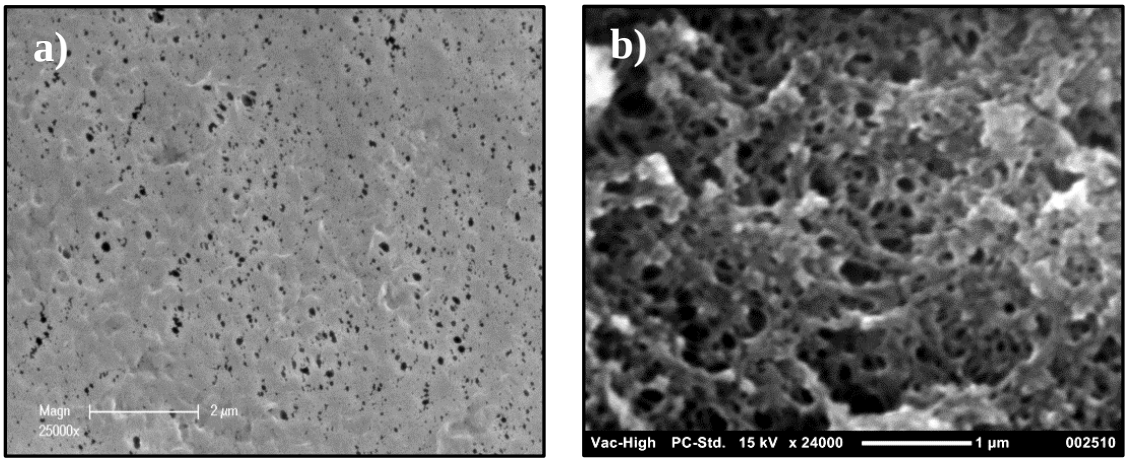

Figure 3.5: Scanning electron microscope (SEM) images of: a) new JW membrane and b) new MW membrane. The images show the surface pore structures of new JW and MW ultrafiltration membranes.

The degree of deposition of CED paint particles on the surfaces of the JW and MW membranes are shown in Figures 3.6a and b.

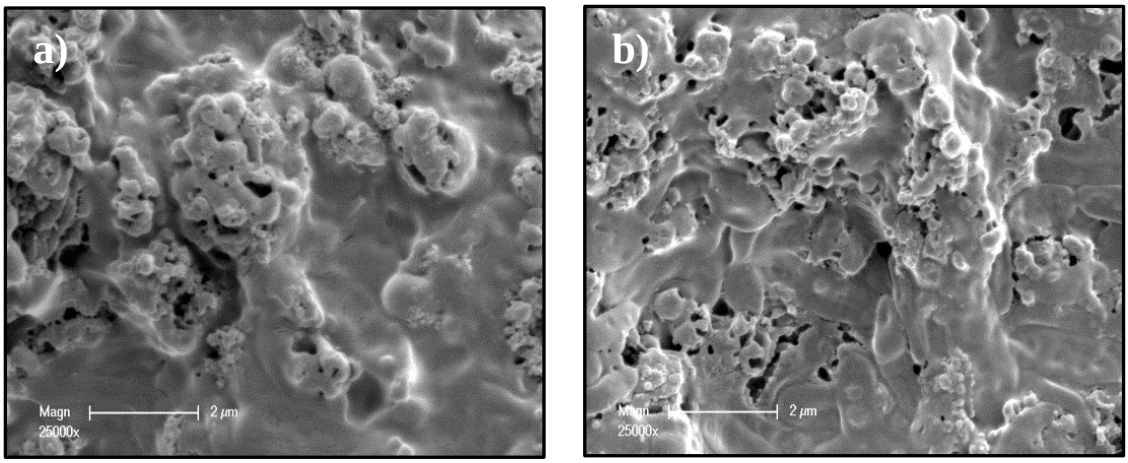

Figure 3.6: Scanning electron microscope (SEM) images of membranes used for oily wastewater sample – a) JW membrane and b) MW membrane. Fouling occurred at a CFV of 2.4 m s^{-1} and TMP of 0.2 MPa. A build up of cathodic electrodeposition (CED) paint particles can be seen on the membrane surfaces.

As previously mentioned, surface-particle interaction and applied TMP resulted in intense fouling of the membranes. During the ultrafiltration of the oily wastewater sample, CED paint particles continuously deposit on the membrane surface. The particles that have already deposited on the membrane surface are then compressed leading to higher cake resistance and low permeate flux. The reduction of permeate flux is further magnified at higher TMPs as shown in Figure 3.4a. Higher pressures cause the cake layer on the membrane surface to compress further resulting in a much lower permeate flux.

For the three different kinds of wastewater stream, the JW and MW membranes performed better for the metals wastewater sample (automobile manufacturer), as shown in Figure 3.4b – with a relativley higher permeate flux being achieved for both membranes. This was particularly noticeable for the MW membrane which achieved steady-state permeate fluxes of approximately 57.6 and 61.2 L m^{-2} hr^{-1} at TMPs of 0.2 and 0.4 MPa respectively. However, although the MW membrane had higher permeate fluxes, its flux decline rates were relatively higher than for the JW membrane – as shown in Figure 3.4b. This suggests that a JW membrane is more suitable for the metals wastewater sample than the MW membrane. The higher flux decline rates experienced by the MW membrane is a sign of intense fouling. An intensely fouled membrane may require a longer cleaning time and the use of aggresive chemicals in order to be regenerated. Such a scenario may lead to premature degradation and a shorter lifespan.

The relatively improved performance of both membranes for the metals wastewater sample can be attributed to the instability of the particles present in this type of

wastewater. As mentioned previously, Section 3.3.2, the instability of the suspended particles will promote aggregation. Once particles have formed into larger masses, their deposition into the membrane surface is inhibited. Larger particles have higher hydrodynamic forces acting on them and therefore are more likely to be swept away from the membrane surface.

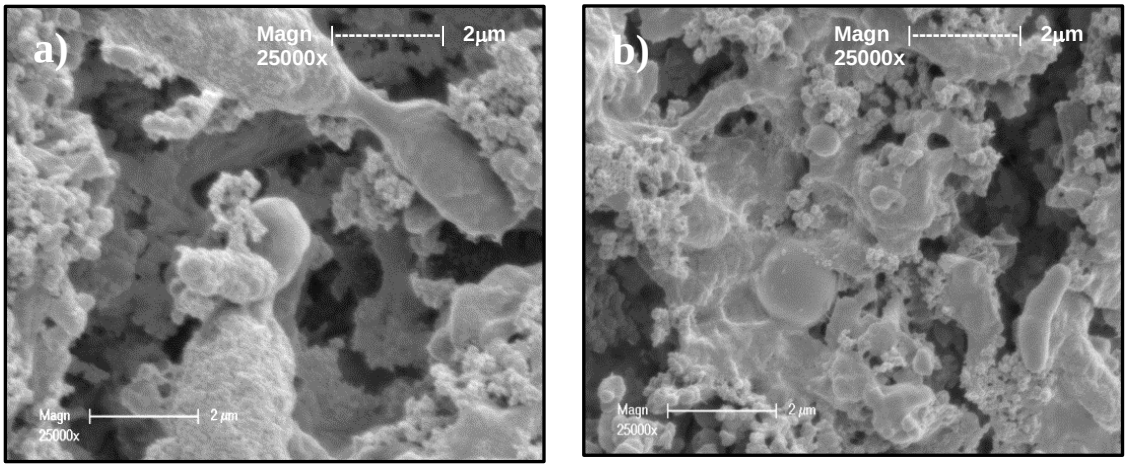

Figure 3.7: Scanning electron microscope (SEM) images of membranes used for metals wastewater sample – a) JW membrane and b) MW membrane. Fouling occurred at a CFV of 2.4 m s^{-1} and TMP of 0.2 MPa. A build up of suspended particles can be seen on the membrane surfaces.

It may be argued that because particles present in the metals wastewater sample have a tendency to aggregate, the cake layers formed on the surfaces of both membranes (Figures 3.7a and b) were more porous compared to the cake layers formed during experiments involving the oily wastewater sample. Likewise, the dominant fouling mechanism involved during the experiments can be deduced to be cake layer formation.

Improvement in permeate fluxes for both the JW and MW membranes during experiments involving the beverage production wastewater were not significant as

compared to permeate fluxes obtained during experiments on the metals wastewater sample from the automobile manufacturer (Figure 3.4c). Although the particles present have the tendency to aggregate due to instability, surface-particle interaction and applied TMP negated the effects of hydrodynamic forces on the larger particles formed. Suspended particles commonly made up of dirt and beverage pigments rapidly deposit on the membrane surface. The deposited particles are then continuously compressed resulting in low membrane porosity (Figure 3.8a and b) and permeate flux. Such a scenario was also observed at a TMP of 0.4 MPa – although permeate fluxes obtained were slightly higher.

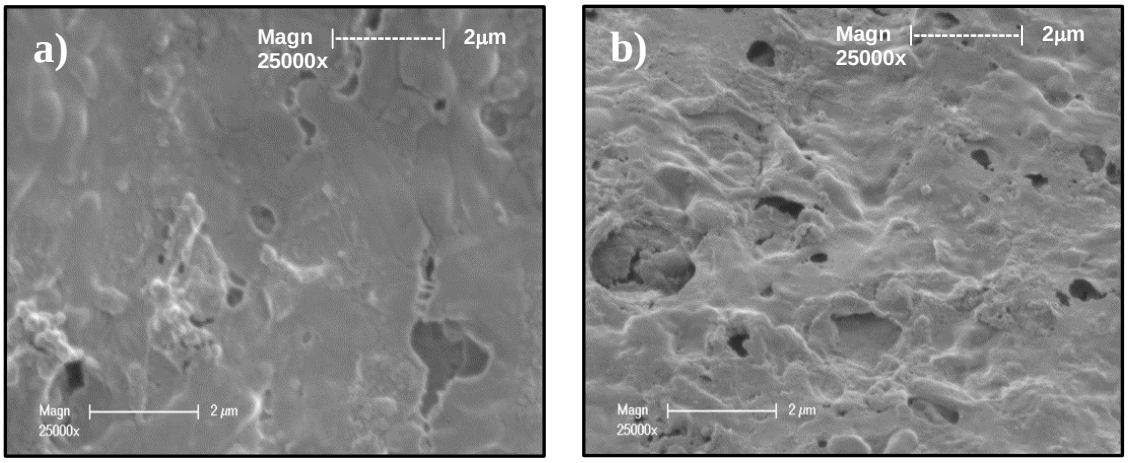

Figure 3.8: Scanning electron microscope (SEM) images of membranes used for beverage production wastewater sample – a) JW membrane and b) MW membrane. Fouling occurred at a CFV of 2.4 m s^{-1} and TMP of 0.2 MPa. A build up of suspended particles such as dirt and beverage pigment can be seen on the membrane surfaces.

Of the two UF membranes used for the beverage production wastewater, the JW membrane showed slightly lower flux decline rates – as shown in Figure 3.4c. In general, the fouling mechanisms involved can be deduced as being a combination of intermediate pore blocking and cake layer formation. Deposition of suspended

particles occurs initially in the membrane pores, followed by accumulation of particles on the membrane surface.

The raw SEM images of all polymeric membranes used in the experiments are available in the accompanying CD (Appendix 3.9).

Turbidity and O&G reduction rates obtained for both the JW and MW membranes show minimal variations – as shown in Figures 3.9a to c. In general, for all types of wastewater samples used, both membranes achieved turbidity reduction rates of above 98%. Likewise, both membranes also achieved 100% removal of O&G for all wastewater samples used. In terms of TOC reduction, the performance of the two membranes varied with TMP. When evaluated on the oily wastewater sample, the JW membrane's TOC reduction rate appeared to increase with an increase in TMP, while the MW membrane's TOC reduction rate appeared to decrease with an increase in TMP (Figure 3.9a). Although these experiments were not performed in replicate, such a TOC rejection characteristic, as exhibited by the MW membrane for an oily wastewater sample, is consistent with the results obtained by Akdemir and Ozer [8]. On the other hand, when the membranes were evaluated on the metals and beverage production wastewater samples, TOC reduction rates for both membranes appeared to show a slight increase when the TMP was increased from 0.2 to 0.4 MPa (Figures 3.9b and c). Notably, the highest TOC reduction for both membranes were obtained from UF experiments involving the beverage production wastewater sample; the TOC reduction rates being above 80% - suggesting that most of the TOC content of the beverage production wastewater is associated with suspended solids. The data used for plotting Figures 3.9a to c are available in the accompanying CD (Appendix 3.10)

a)

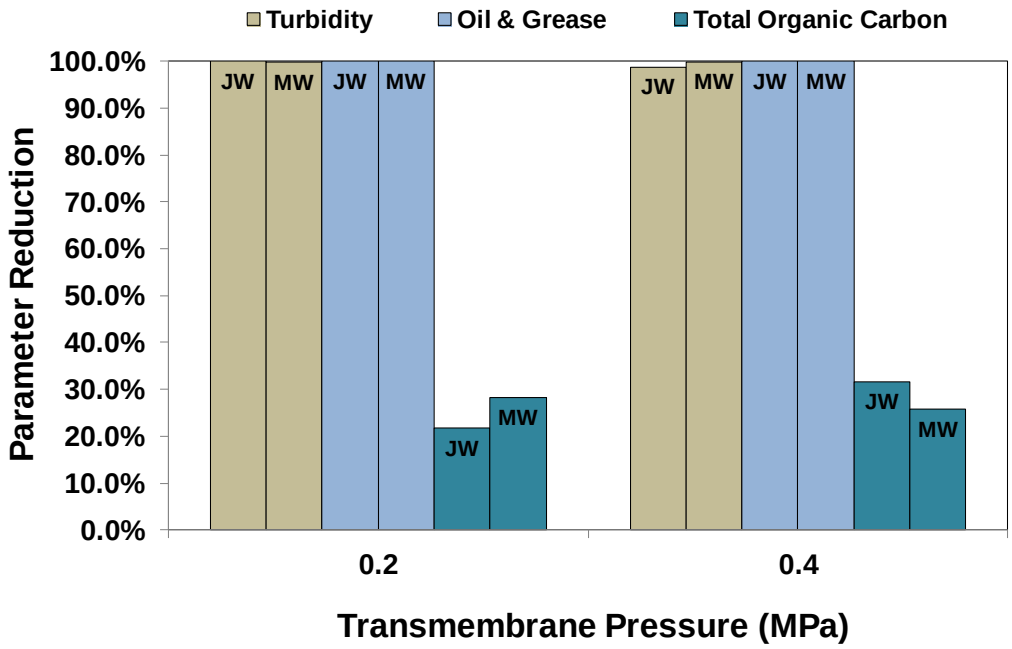
Turbidity
Oil & Grease
Total Organic Carbon
100.0%
90.0%
80.0%
70.0%
60.0%
50.0%
40.0%
30.0%
20.0%
10.0%
0.0%
Parameter Reduction
JW
MW
0.2
0.4
Transmembrane Pressure (MPa)

b)

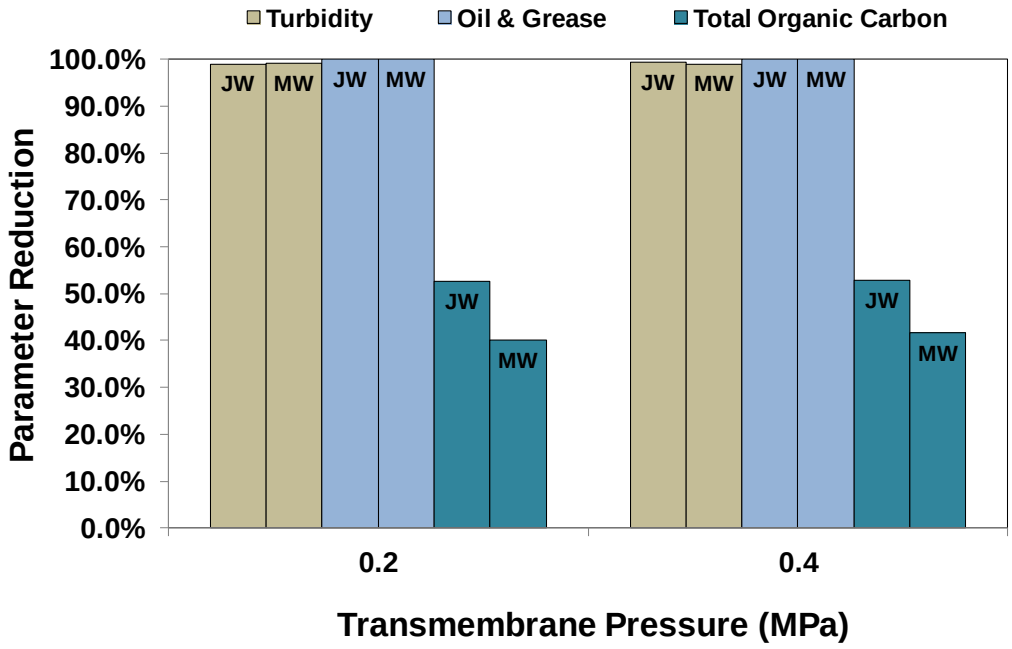
Turbidity
Oil & Grease
Total Organic Carbon
100.0%
90.0%
80.0%
70.0%
60.0%
50.0%
40.0%
30.0%
20.0%
10.0%
0.0%
Parameter Reduction
JW
MW
0.2
0.4
Transmembrane Pressure (MPa)

c)

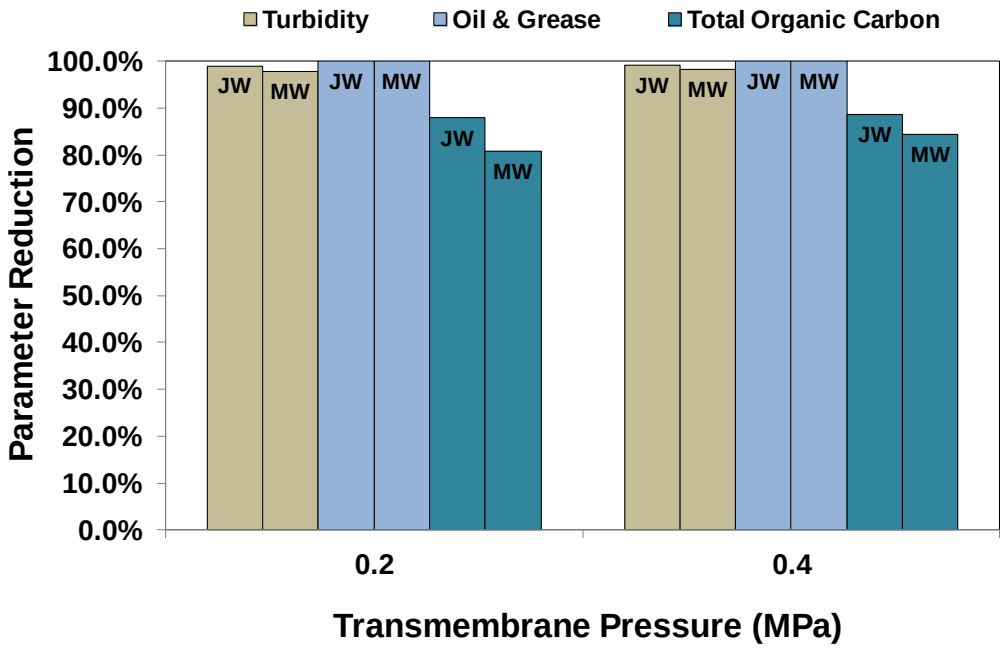

Figure 3.9: Performance of the JW and MW membranes on the reduction of water quality parameters such as turbidity, O&G and TOC. Feedwater used include: a) oily wastewater sample, b) metals wastewater sample and c) beverage production wastewater sample.

3.3.4 NF and RO experiments

Similar to the UF experiments, the permeate fluxes for both the NF and RO membranes were calculated using Eq. (2). To account for temperature variations, all permeate fluxes were standardized at a temperature of 25 °C using Eq. (6):

$$J_{25°C} = J / TCF \quad (6)$$

where $J_{25°C}$ is the flux at a standard temperature of 25 °C ($m^3\ m^{-2}\ s^{-1}$), J is the actual flux measured ($m^3\ m^{-2}\ s^{-1}$) and TCF is the temperature correction factor (dimensionless). The TCF can be estimated using eq. (7) [11]:

$$TCF = (1.03)^{T_M - 25} \quad (7)$$

Where T_M is the measured temperature (°C).

For the three different wastewater types, the permeate fluxes obtained for the RO (AK) membrane at different TMPs are shown in Figures 3.10a to c. In general, as the TMP is increased, significant improvements in permeate fluxes were measured for all types of wastewater samples used. The highest permeate fluxes were measured for the beverage production wastewater whilst the lowest permeate fluxes were measured for the metals wastewater sample (automobile manufacturer).

a)

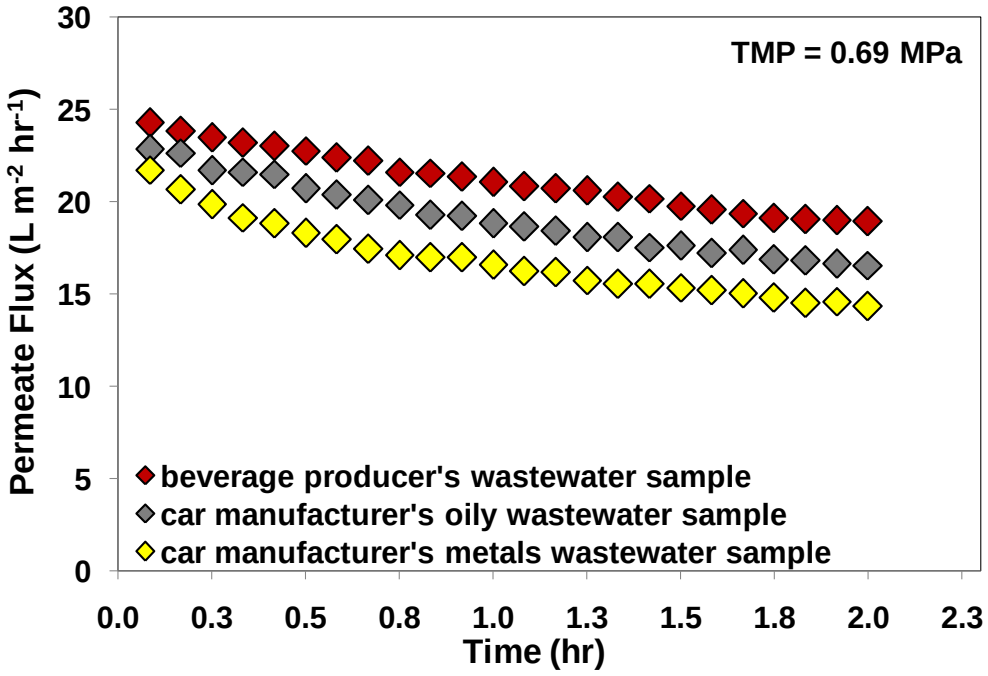

b)

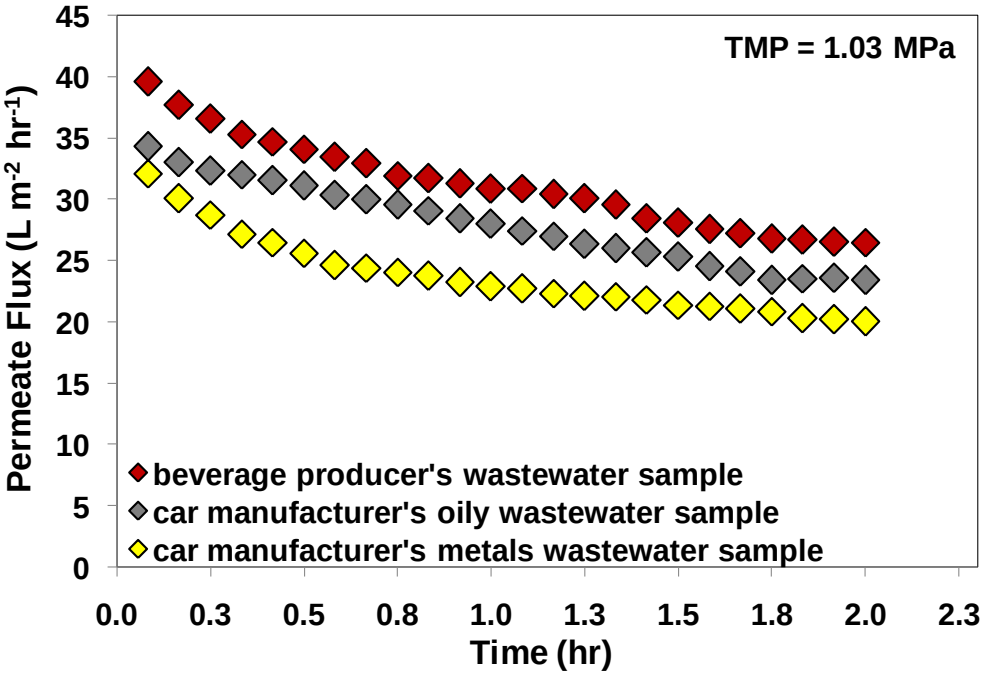

c)

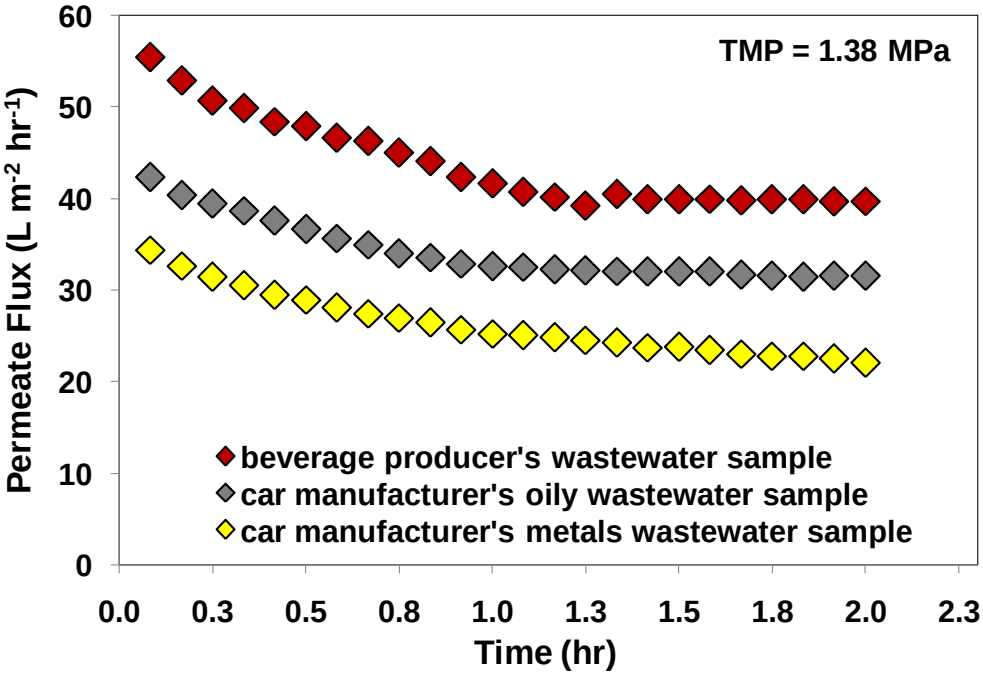

Figure 3.10: RO (AK) membrane's permeate fluxes obtained at TMPs of: a) 0.69 MPa, b) 1.03 MPa and c) 1.38 MPa. Feedwater used include: a) oily wastewater sample, b) metals wastewater sample and c) beverage production wastewater sample.

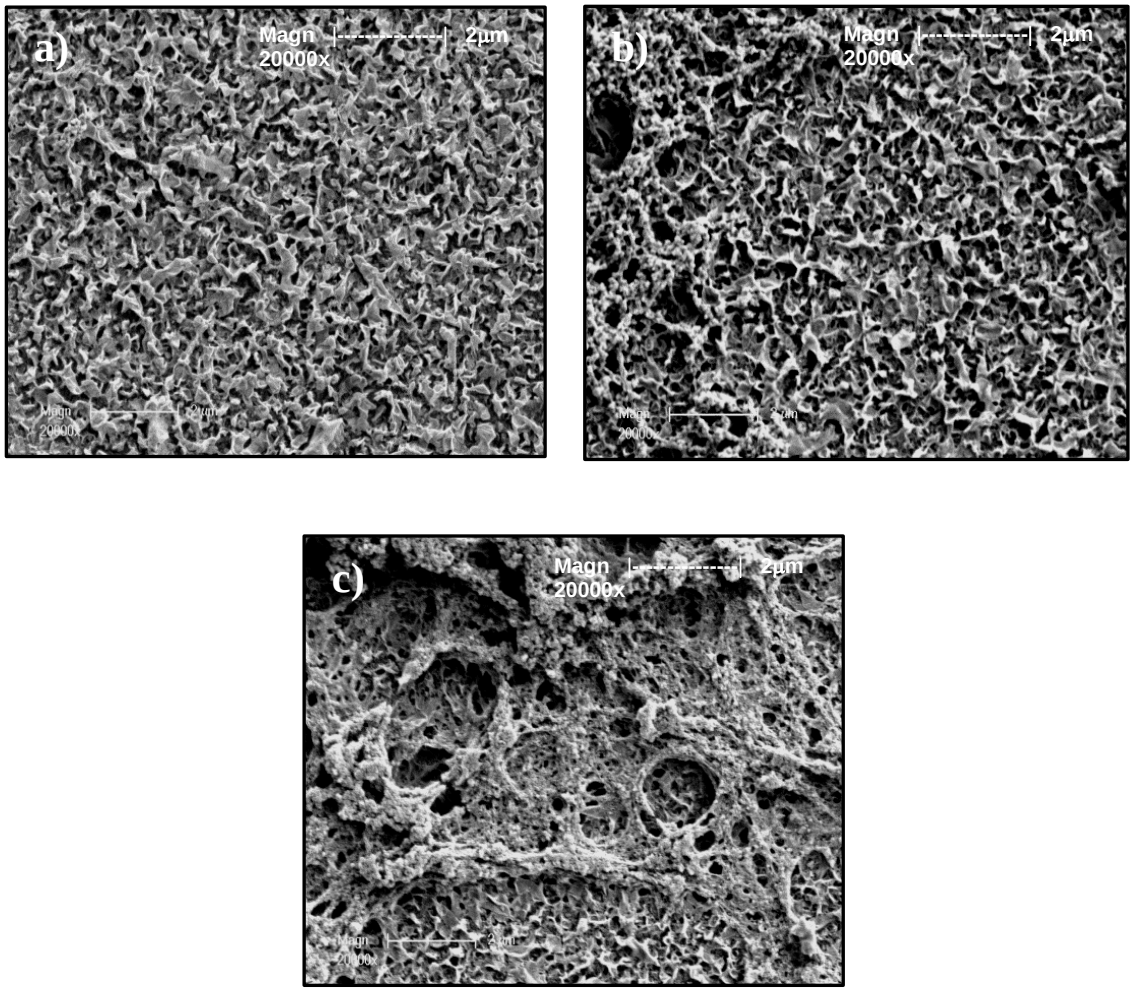

Figure 3.11: Scanning electron microscope (SEM) images of RO (AK) membranes used for metals wastewater sample – a) new AK membrane, b) AK membrane used at a TMP of 0.69 MPa and c) AK membrane used at a TMP of 1.38 MPa. Fouling occurred at a CFV of 2.7 m s^{-1}.

Figure 3.11a shows the surface structure of a fresh AK membrane while Figures 3.11 b and c show possible deposition of metal oxides on the membrane surfaces. Such deposition appears to intensify as pressure increases.

It is proposed that the low permeate fluxes obtained for the metals wastewater sample could be due to metal oxide fouling. The metals wastewater sample contains elevated

concentrations of heavy metals such as Fe, Mn, Ni, and Zn, Table 3.3. Iron (Fe), in particular, is known to be susceptible to oxidation [11] and since the apparatus shown in Figure 3.1 is a closed loop system, the flow of the concentrate back into the feed tank promotes rapid mixing of the wastewater sample. This rapid mixing is similar to aerating a pond to increase dissolved oxygen content. As a result, the process may facilitate the formation of insoluble iron, and other metal oxides, resulting in the deposition of oxide particles onto the surface of the RO membrane (Figures 3.11b and c). Such fouling would be expected to be further intensified as the pressure increases (Figure 3.11c).

On the other hand, the highly organic character of the oily and beverage production wastewater samples resulted in relatively higher permeate fluxes for the RO membrane. Such a wastewater characteristic could be considered to be appropriate for the RO membrane given that RO is known to be effective in the separation of organic molecules [24].

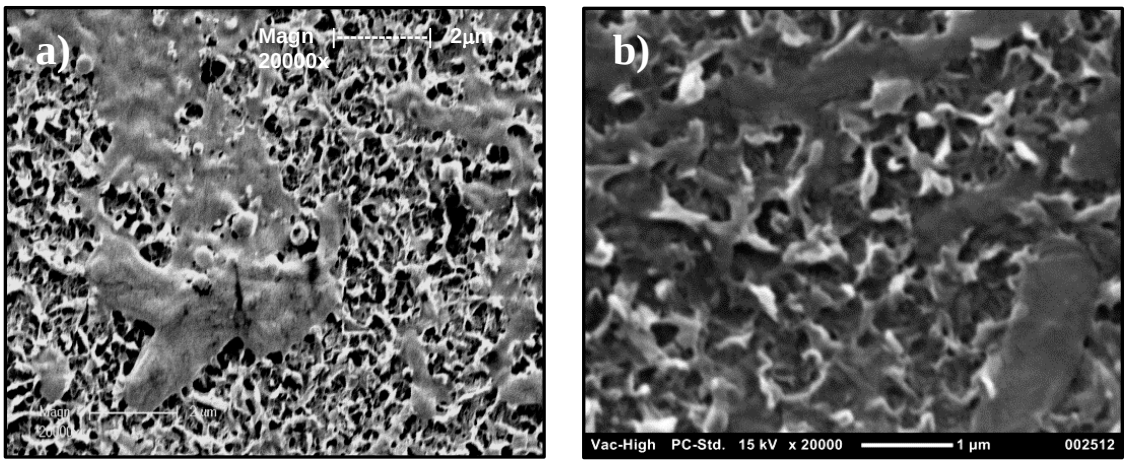

Figure 3.12: Scanning electron microscope (SEM) images of RO (AK) membranes used for: a) oily wastewater sample at a TMP of 1.38 MPa and b) beverage production wastewater sample at a TMP of 1.38 MPa. Fouling occurred at a CFV of 2.7 m s^{-1}. The figures show the deposition of contaminants on the membrane surfaces.

Because the two wastewater samples mentioned mostly contain organic contaminants, a less severe membrane fouling might be expected, even at a high TMP of 1.38 MPa, and this appears to be evident from the electron micrographs shown in Figures 3.12a and b.

Aside from higher permeate fluxes, the RO membrane used also had high conductivity and COD reduction rates. With respect to the oily wastewater sample, conductivity and COD reduction rates were more than 96.0 % and 98.0 % respectively. With respect to the beverage production wastewater sample, conductivity and COD reduction rates were both more than 98.0 %. Conductivity and COD reduction rates obtained appeared to be almost invariant with respect to applied TMP for both the beverage production wastewater and the oily wastewater, Figures 3.13a and b.

a)

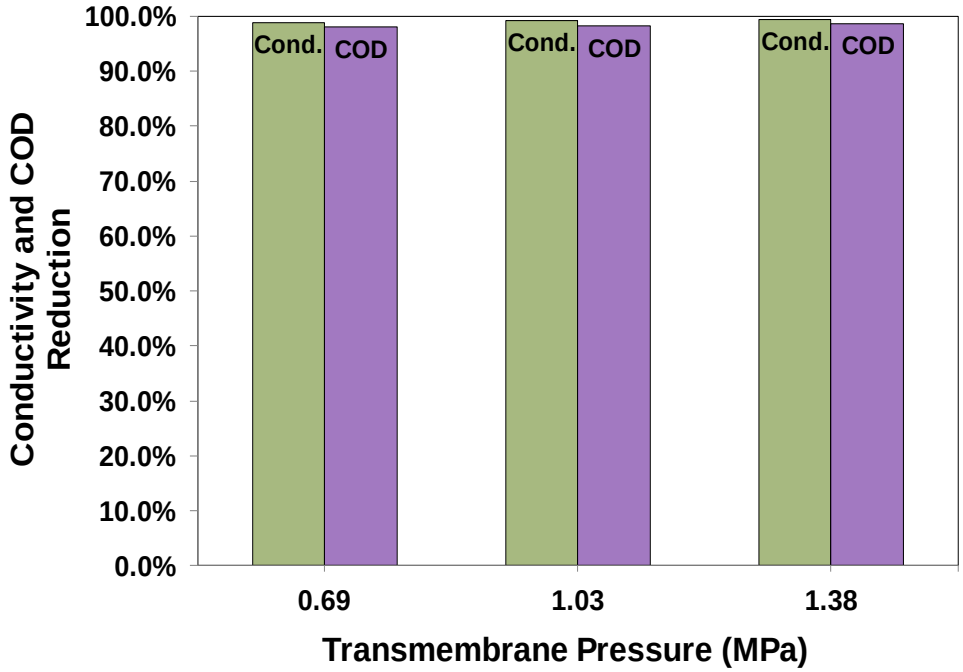

b)

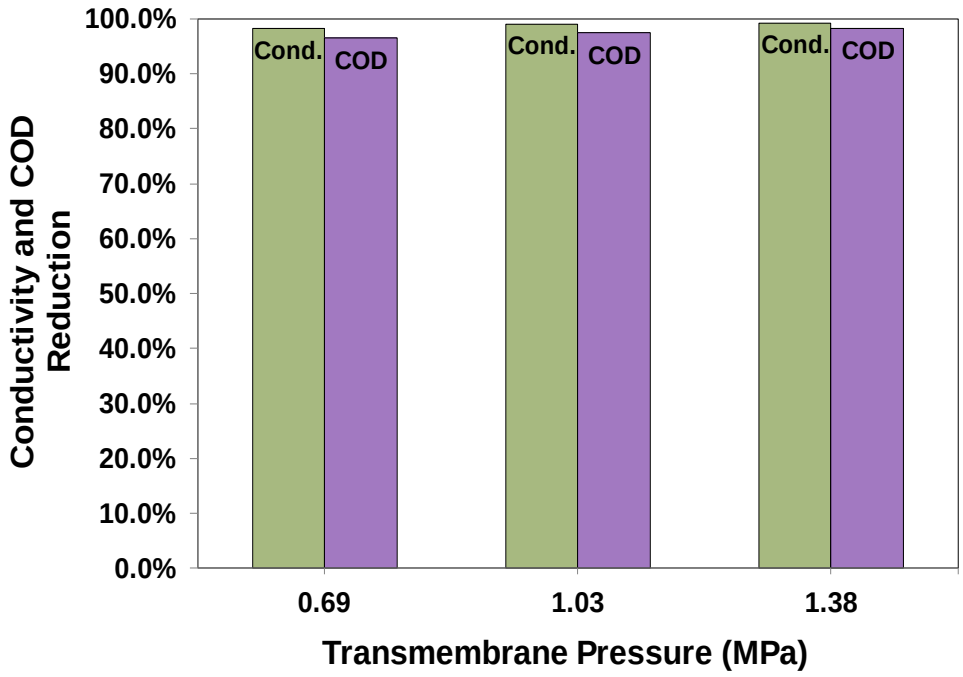

Figure 3.13: RO (AK) membrane's conductivity and COD reduction rates with respect to: a) beverage production wastewater sample and b) oily wastewater sample.

An NF (DL series) membrane was also evaluated with respect to the metals wastewater sample since this type of membrane has been reported in literature to be effective in removing heavy metals present in wastewater streams [7, 15, 21, 25]. The results of our experiments show that permeate fluxes obtained for the NF membrane were approximately two times higher than the permeate fluxes obtained for the RO membrane, as shown in Figures 3.14a to c. The superior performance of the NF membrane for the metals wastewater sample can be attributed to its separation mechanism. Unlike an RO membrane, whose primary separation mechanism is solution-diffusion, an NF membrane combines solution-diffusion and charge repulsion mechanisms to separate dissolved organic molecules and polyvalent inorganic ions [21, 24].

a)

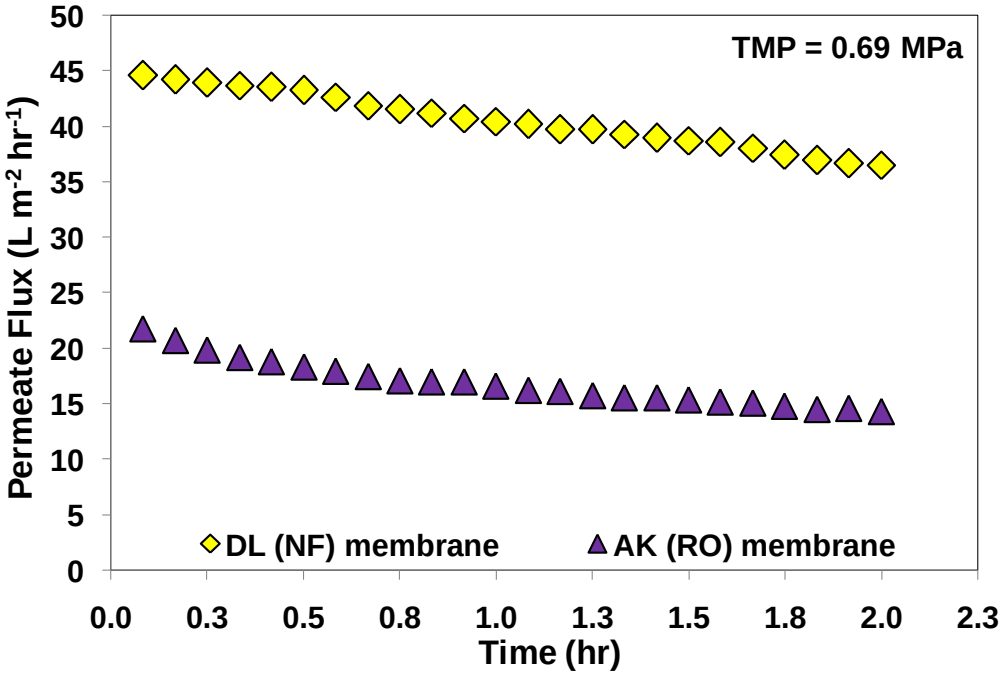
TMP = 0.69 MPa
Permeate Flux (L m-2 hr-1)
50
45
40
35
30
25
20
15
10
5
0
DL (NF) membrane
AK (RO) membrane
0.0
0.3
0.5
0.8
1.0
1.3
1.5
1.8
2.0
2.3
Time (hr)

b)

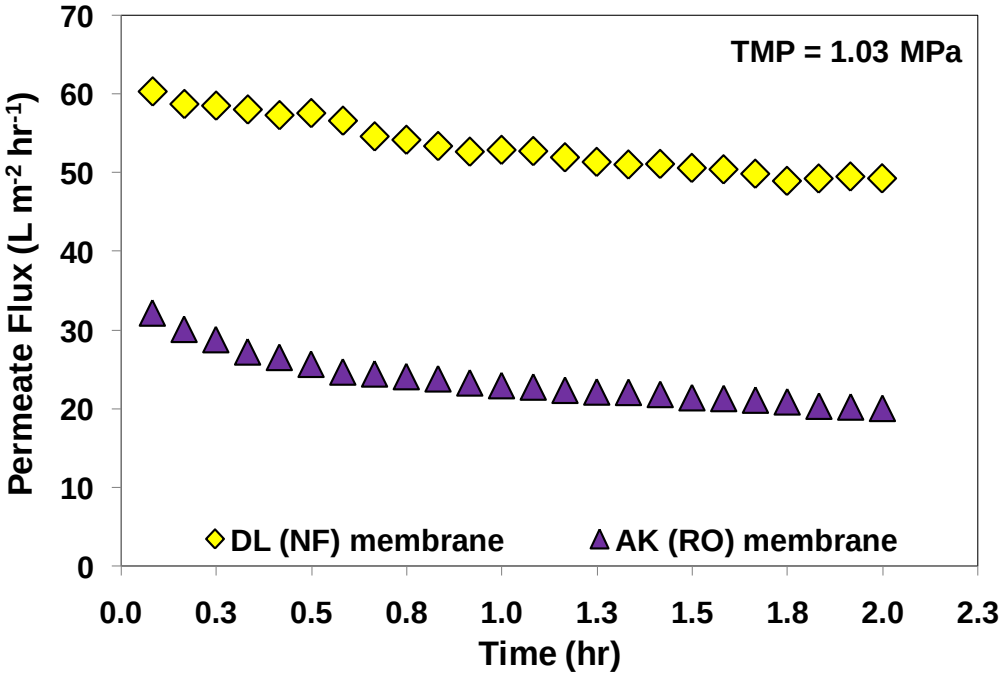
TMP = 1.03 MPa
Permeate Flux (L m-2 hr-1)
70
60
50
40
30
20
10
0
DL (NF) membrane
AK (RO) membrane
0.0
0.3
0.5
0.8
1.0
1.3
1.5
1.8
2.0
2.3
Time (hr)

c)

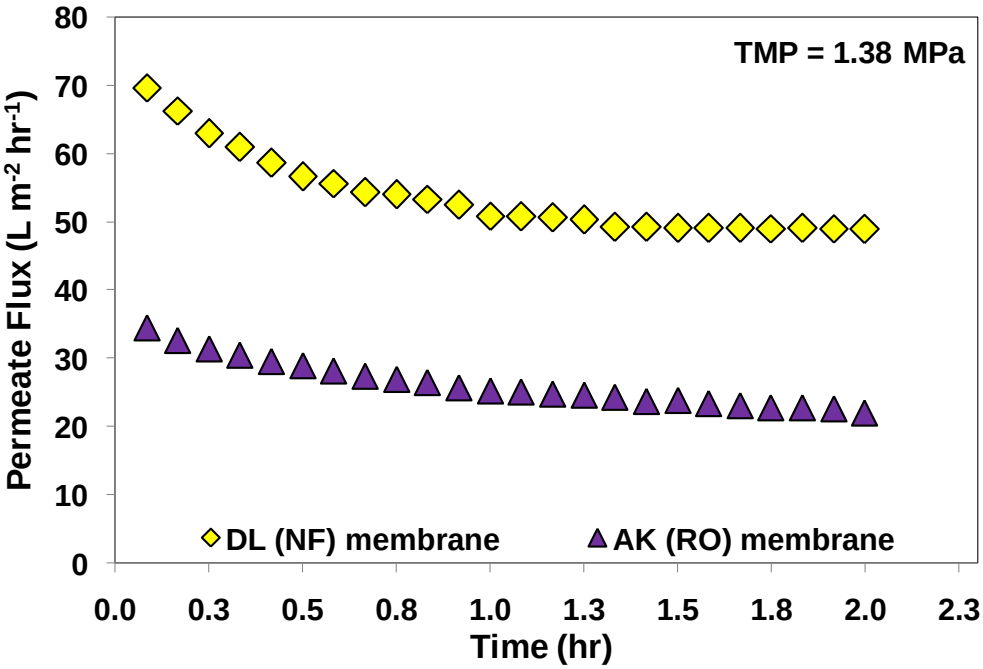

Figure 3.14: Comparison of permeate fluxes measured for RO (AK) and NF (DL) membranes with respect to metals wastewater sample at TMPs of: a) 0.69 MPa, b)1.03 MPa and c) 1.38 MPa.

The inherent charge on the NF membrane's surface would be expected to facilitate the rejection of similarly charged solutes. Likewise, because of this surface charge, it is also able to effectively reject similarly charged metal species [21] and metal oxide particles present in the metals wastewater sample. Consequently, fouling of the NF membrane due to the formation of insoluble metal oxide particles would be expected to be inhibited. Assuming that the observed deposition on the membrane surface is primarily metal oxide, Figures 3.15b and c demonstrate that, even at high TMP, the material does not appear to be significantly compressed onto the surface.

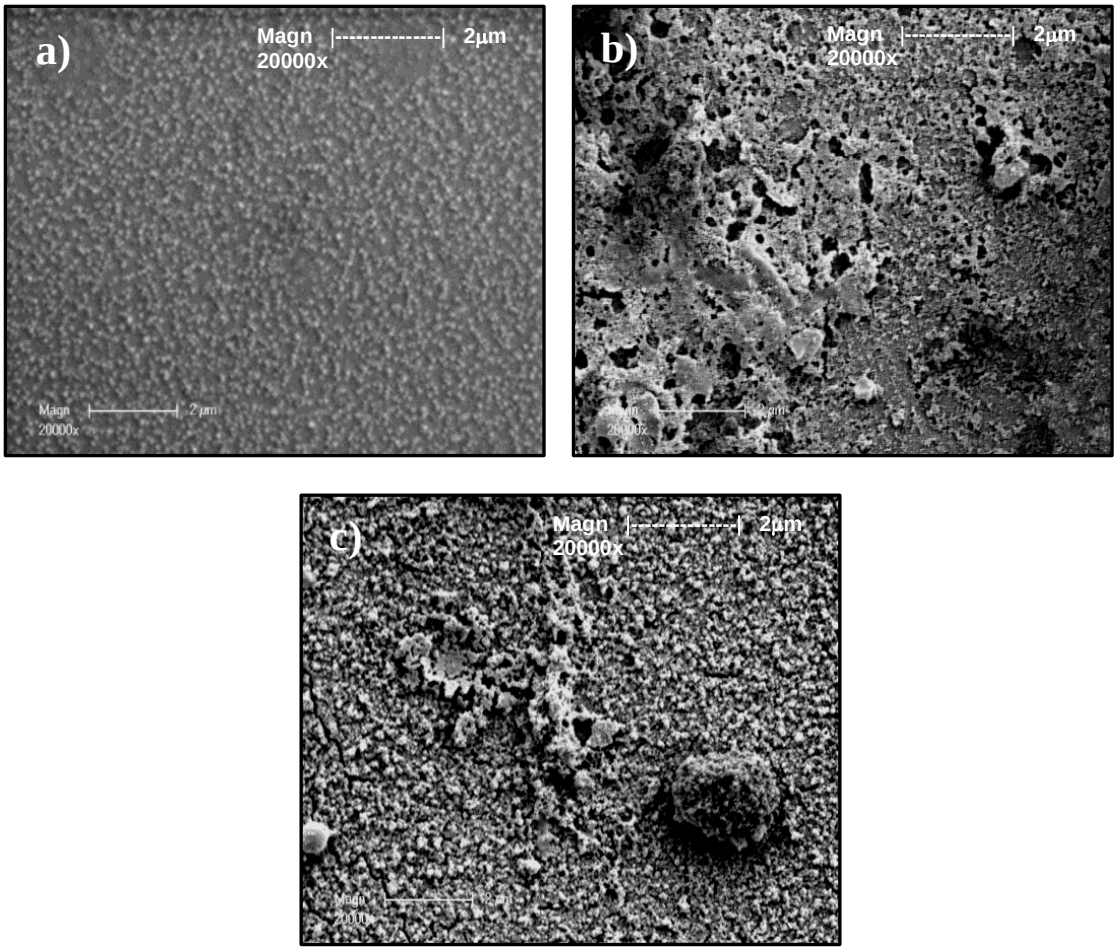

Figure 3.15: Scanning electron microscope (SEM) images of NF (DL) membranes used for metals wastewater sample – a) new DL membrane, b) DL membrane used at a TMP of 0.69 MPa and c) DL membrane used at a TMP of 1.38 MPa. Fouling occurred at a CFV of 2.7 m s^{-1}. Figure 3.15a shows the surface structure of a new DL membrane while Figures 3.15b and c show possible deposition of metal oxides on the membrane surfaces. Such deposition appears loose and also appears not to compress significantly at higher pressures.

The conductivity reduction for both the NF (DL) and RO (AK) membranes with respect to the metals wastewater sample show values of more than 60.0 % at all TMPs used (Figure 3.16a). This suggests that a single pass system is not enough if water reclamation is aimed at replacing Citywater to be supplied to processes. In terms of

COD reduction, the RO membrane appears to have relatively higher reduction rates than the NF membrane (Figure 3.16b).

a)

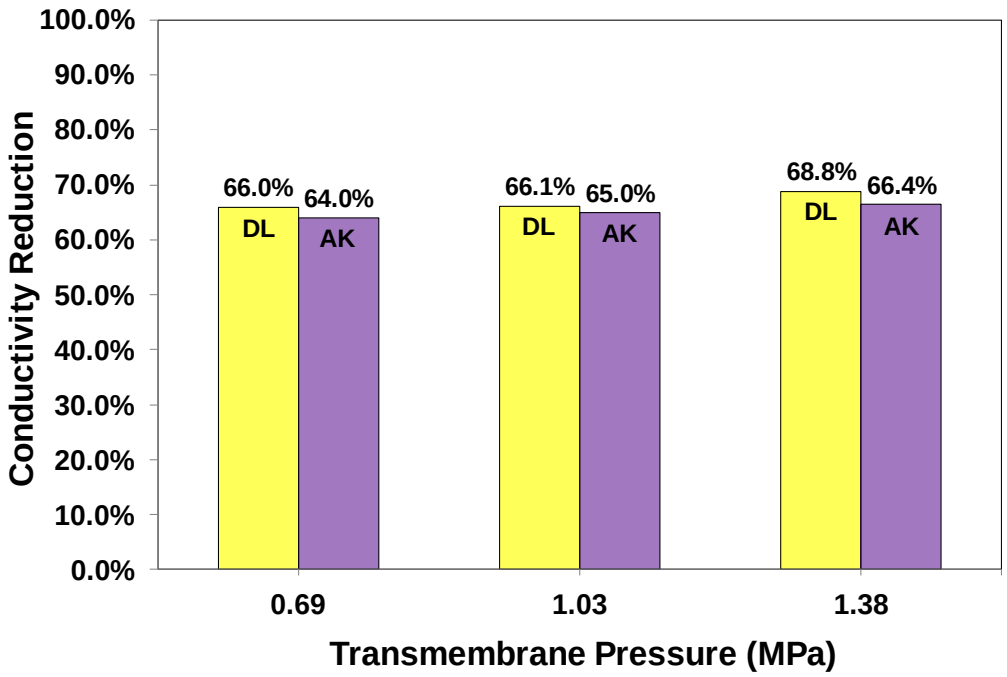

b)

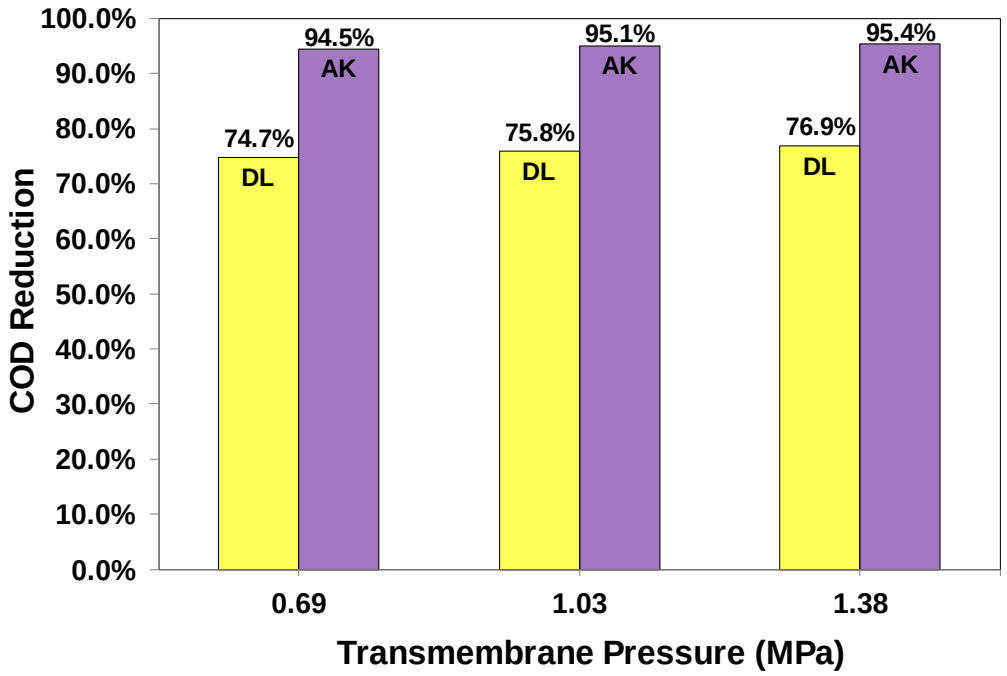

Figure 3.16: NF (DL) and RO (AK) membranes' a) conductivity and b) COD reduction rates with respect to metals wastewater sample.

For the RO membrane, COD reduction rates were more than 94.0 %, while for the NF membrane, COD reduction was just above 74.0 %. In general, conductivity and COD reduction rates show a slight dependency on TMP – as TMP increased, reduction rates slightly increased.

a)

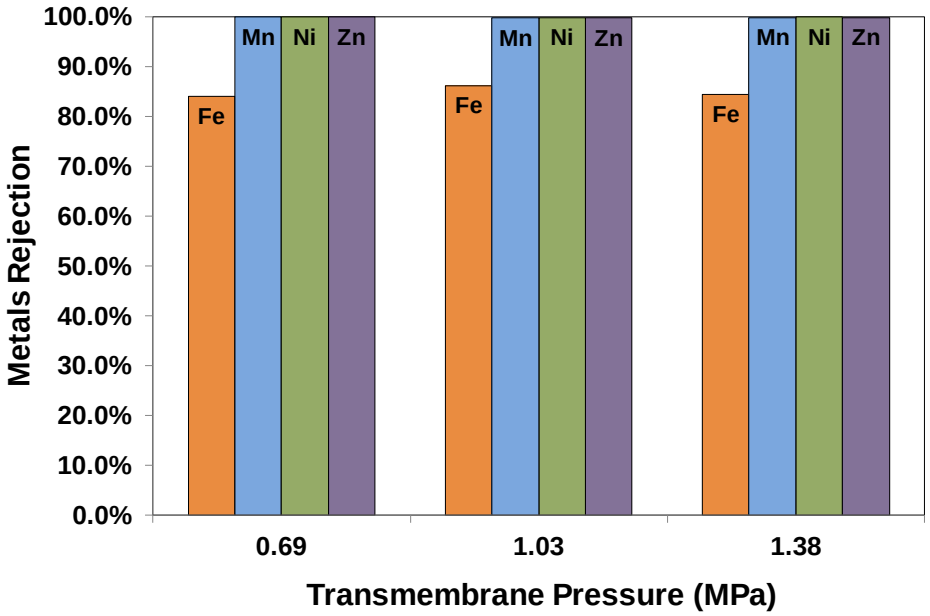

b)

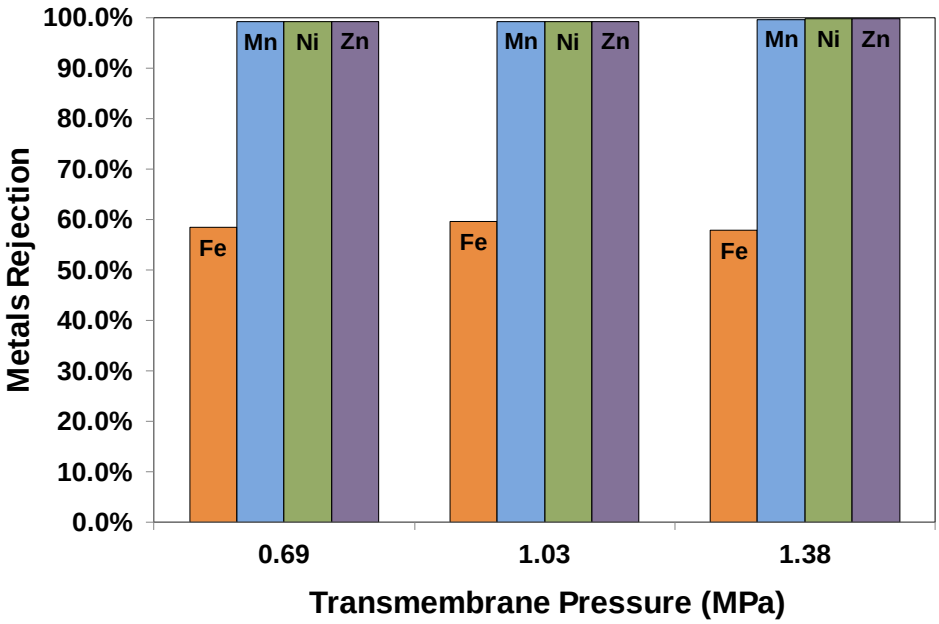

Figure 3.17: a) NF (DL) and b) RO (AK) membranes' metals rejection rates with respect to metals wastewater sample.

Both NF and RO membranes showed rejection rates of more than 99.0 % for the metals Mn, Ni and Zn. Interestingly, with respect to Fe, the NF membrane had rejection rates of 84.0 %, 86.2 % and 87.5 % while the RO membrane had lower rejection rates – 58.3 %, 59.6 % and 62.2 % (Figures 3.17a and b).

The selective passage of iron through both membranes, although intriguing, has not been investigated further in this study. However, it is tempting to relate this to the fact that the iron is likely to be trivalent whereas the other metals are all divalent. The phenomenon might also be related to the relative speciation profiles of the different metals in the wastewater. Another possibility may be the fouling of iron on the membrane surface. Once a membrane is fouled with iron, the local concentration at the surface will be higher, hence the amount of iron passing through will be higher. Additionally, the work conducted by Diallo *et al.* [13] showed that at high acid concentration, chloride retention is negative – suggesting that electrostatic interactions can have an influence in the transfer mechanism during nanofiltration. This result was based on a model solution of iron chloride (18.6×10^{-3} mol L^{-1} $FeCl_3$) mixed in different concentrations of phosphoric acid (H_3PO_4: 0.12, 1.2 and 5.9 mol L^{-1}) [13].

The data used for plotting the AK (RO) and DL (NF) membranes' permeate fluxes and contaminant reduction/rejection rates are available in the accompanying CD (Appendices 3.11 and 3.12).

A summary of the average membrane permeate quality with respect to specific wastewater samples is shown in Table 3.3.

Table 3.4: Average membrane permeate quality with respect to specific wastewater samples

Water quality parameters	UF – Oily		UF – Metals		UF – Bev.		RO			DL - Metals
	JW	MW	JW	MW	JW	MW	Oil	Metals	Bev.	
pH	7.3	7.5	3.5	3.3	7.0	7.3	8.5	3.5	7.8	3.3
Conductivity, μS cm^{-1}	-	-	-	-	-	-	9.5	546	9.5	526
COD, mg L^{-1}	-	-	-	-	-	-	6.0	4.6	84.5	22
O&G, mg L^{-1}	<5	<5	<5	<5	<5	<5	-	-	-	-
TOC, mg L^{-1}	88	88	8.5	8	16.5	24.5	-	-	-	-
Turbidity, NTU	1.9	0.5	0.4	0.4	0.3	0.6	-	-	-	-
Iron (Fe), mg L^{-1}	-	-	-	-	-	-	-	1.8	-	1.4
Manganese (Mn), mg L^{-1}	-	-	-	-	-	-	-	0.1	-	0.04
Nickel (Ni), mg L^{-1}	-	-	-	-	-	-	-	0.2	-	0.05
Zinc (Zn), mg L^{-1}	-	-	-	-	-	-	-	0.5	-	0.2

3.3.5 Energy consumption

In general, slight improvements in permeate fluxes and reduction/rejection rates of critical water quality parameters were achieved at higher TMPs. However, maintaining higher TMPs usually involve the consumption of substantial amounts of energy, especially for systems requiring larger pumps [5]. To investigate this further at a laboratory-scale level, the average power consumption (P, kW) of the pump motor for each experiment run was recorded. The recorded power consumptions were subsequently used to calculate specific energy consumptions (EC_{SP}, kWh/m^3) using Eq. (8):

$$EC_{SP} = Pt / V_P \quad (8)$$

where t is the experiment duration (hr) and V_P is the volume of permeate produced (m^3).

Tables 3.5 and 3.6 show the energy consumptions of all the membranes used on specific wastewater samples. The detailed calculations for the membrane specific energy consumptions are available in the accompanying CD (Appendix 3.13).

In general, the specific energy consumption (kWh/m^3) is directly related to transmembrane pressure, permeate flowrate and system efficiency. For the UF experiments, minimal changes in energy consumptions were obtained when TMP was increased from 0.2 to 0.4 MPa (Table 3.5). In general, at a higher pressure of 0.4 MPa, the efficiency of the UF system is higher as evidenced by the reduction in specific energy consumption.

Table 3.5: Specific energy consumptions for all ultrafiltration membranes used. The CFV used in every experiment is 2.4 m s^{-1}. Considered duration of each experiment run is 2 hrs

Sample	JW		MW	
	Specific energy consumption, kWh/m^3			
	@ 0.2 MPa	@ 0.4 MPa	@ 0.2 MPa	@ 0.4 MPa
Car manufacturer's oily wastewater	210	227	196	198
Car manufacturer's metals wastewater	95	78	48	46
Beverage producer's wastewater	186	129	154	106

On the other hand, a significant difference in specific energy consumption (kWh/m^3) between the NF and RO membranes were obtained during experiments involving the metals wastewater stream – as shown in Table 3.6. In general, the specific energy consumption of the RO membrane doubles that of the NF membrane.

Table 3.6: Specific energy consumptions for NF and RO membranes used. The CFV used in every experiment is 2.7 m s^{-1}. Duration of each experiment run is 2 hrs

Sample	DL			AK		
	Specific energy consumption, kWh/m^3					
	@ 0.69 MPa	@ 1.03 MPa	@1.38 MPa	@ 0.69 MPa	@ 1.03 MPa	@1.38 MPa
Car manufacturer's oily wastewater	-	-	-	1259	1006	960
Car manufacturer's metals wastewater	562	491	578	1347	1112	1150
Beverage producer's wastewater	-	-	-	1094	785	734

3.4 Conclusions

The above experiments demonstrated the suitability of different low-pressure polymeric membranes for the reclamation of different wastewater streams generated by a car manufacturer and a beverage producer. Based on these results, the following conclusions may be made:

1. Both the JW and MW ultrafiltration membranes cannot be used directly as pretreatment for the oily wastewater stream due to the presence of suspended CED paint particles. Although particle deposition can be minimized by increasing the CFV, membrane cleaning of the deposited CED paint particles is the main problem. The nature and frequency of cleaning to remove the deposited CED paint particles may significantly degrade the membrane material – leading to a shorter membrane lifespan. In this instance, an inorganic membrane such as a ceramic membrane will be a better choice for pretreatment of the oily wastewater stream.

2. Of the two ultrafiltration membranes tested on the beverage production wastewater stream, the JW membrane proved more suitable for pretreatment than the MW membrane. Flux decline rates for the JW membrane were relatively lower as compared to the MW membrane. Likewise, for this specific wastewater stream, the JW membrane showed higher reduction rates with respect to critical water parameters such as turbidity and TOC.

3. The JW membrane was also suitable for pretreatment of the metals wastewater stream. It showed significantly lower flux decline rates and higher turbidity and TOC reduction rates – as compared to the MW membrane.

4. The RO (AK) membrane was suitable for use in the reclamation of two wastewater streams – the oily and beverage production wastewaters. Fouling rates of the RO membrane at these two wastewater streams were slow as reflected on the permeate flux decline rates. Furthermore, reduction rates of critical water quality parameters such as conductivity and COD were high.

5. Permeate fluxes obtained for the NF membrane at all TMPs used were significantly higher compared to the RO membrane. In terms of metals rejection, the NF membrane generally had higher metals rejection rates than the RO membrane. Although the NF membrane had relatively higher permeate fluxes, its conductivity and COD reduction rates were just above 66.0 and 74.0% respectively. The data obtained for RO and NF membranes with respect to the treatment of the metals wastewater stream are not consistent with the literature since RO membranes are known to have greater capacity to remove dissolved salts as compared to an NF membrane. Therefore, before a

conclusion on whether an RO or NF membrane is suitable for the reclamation of the metals wastewater stream, a comprehensive study should be conducted.

6. Not unexpectedly, the specific energy consumptions for all the membranes used were dependent on transmembrane pressure, permeate flowrate and system efficiency. It also worth mentioning that the specific energy consumption of the RO membrane doubles that of the NF membrane when evaluated with respect to the metals wastewater stream.

3.5 References

[1] *GE Water and Process Technologies: AK Series Fact Sheet* [Online]. http://www.gewater.com/pdf/Fact%20Sheets_Cust/Americas/English/FS1263EN.pdf. [Accessed 16/12/11/].

[2] *GE Water and Process Technologies: DL Series Fact Sheet* [Online]. http://www.gewater.com/pdf/Fact%20Sheets_Cust/Americas/English/FS1248EN.pdf. [Accessed 16/12/11/].

[3] *GE Water and Process Technologies: JW Series Fact Sheet* [Online]. http://www.gewater.com/pdf/Fact%20Sheets_Cust/Americas/English/FSpsJWSeries_EN.pdf. [Accessed 16/12/11/].

[4] *GE Water and Process Technologies: MW Series Fact Sheet* [Online]. http://www.gewater.com/pdf/Fact%20Sheets_Cust/Americas/English/AM-FSpwMWSeries_EN.pdf. [Accessed 16/12/11/].

[5] Agana, B. A., Reeve, D. & Orbell, J. D. 2011. Optimization of the operational parameters for a 50 nm ZrO2 ceramic membrane as applied to the ultrafiltration of post-electrodeposition rinse wastewater. *Desalination,* 278**,** 325-332.

[6] Ahmad, A. L. & Ooi, B. S. 2010. A study on acid reclamation and copper recovery using low pressure nanofiltration membrane. *Chemical Engineering Journal,* 156**,** 257-263.

[7] Ahn, K. H., Song, K. G., Cha, H. Y. & Yeom, I. T. 1999. Removal of ions in nickel electroplating rinse water using low-pressure nanofiltration. *Desalination,* 122**,** 77-84.

[8] Akdemir, E. O. & Ozer, A. 2009. Investigation of two ultrafiltration membranes for treatment of olive oil mill wastewater. *Desalination,* 249**,** 660-666.

[9] Anderson, J. E., Springer, W. S. & Strossberg, G. G. 1981. Application of reverse osmosis to automotive electrocoat paint wastewater recycling. *Desalination,* 36**,** 179-188.

[10] ASTM 1985. Zeta Potential of Colloids in Water and Waste Water. *ASTM Standard D 4187-82.*

[11] Crittenden, J. C., Trussell, R. R., Hand, D. W., Howe, K. J. & Tchobanoglous, G. 2005. *Water treatment: Principles and design,* Hoboken, NJ, John Wiley & Sons, Inc.

[12] Cséfalvay, E., Pauer, V. & Mizsey, P. 2009. Recovery of copper from process waters by nanofiltration and reverse osmosis. *Desalination,* 240**,** 132-142.

[13] Diallo, H., Rabiller-Baudry, M., Khaless, K. & Chaufer, B. 2013. On the electrostatic interactions in the transfer mechanisms of iron during nanofiltration in high concentrated phosphoric acid. *Journal of Membrane Science,* 427**,** 37-47.

[14] Dolar, D., Košutić, K. & Vučić, B. 2011. RO/NF treatment of wastewater from fertilizer factory — removal of fluoride and phosphate. *Desalination,* 265**,** 237-241.

[15] Frarès, N. B., Taha, S. & Dorange, G. 2005. Influence of the operating conditions on the elimination of zinc ions by nanofiltration. *Desalination,* 185**,** 245-253.

[16] Howe, K. J., Marwah, A., Chiu, K.-P. & Adham, S. S. 2007. Effect of membrane configuration on bench-scale MF and UF fouling experiments. *Water Research,* 41**,** 3842-3849.

[17] Jezowska, A., Schipolowski, T. & Wozny, G. 2006. Influence of simple pre-treatment methods on properties of membrane material. *Desalination,* 189**,** 43-52.

[18] Koseoglu, H. & Kitis, M. 2009. The recovery of silver from mining wastewaters using hybrid cyanidation and high-pressure membrane process. *Minerals Engineering,* 22**,** 440-444.

[19] Lipnizki, F. 2008. Opportunities and challenges of using ultrafiltration for the concentration of diluted coating materials. *Desalination,* 224**,** 98-104.

[20] Mänttäri, M., Pihlajamäki, A., Kaipainen, E. & Nyström, M. 2002. Effect of temperature and membrane pre-treatment by pressure on the filtration properties of nanofiltration membranes. *Desalination,* 145**,** 81-86.

[21] Mohammad, A. W., Othaman, R. & Hilal, N. 2004. Potential use of nanofiltration membranes in treatment of industrial wastewater from Ni-P electroless plating. *Desalination,* 168**,** 241-252.

[22] Mohammadi, T. & Esmaeelifar, A. 2004. Wastewater treatment using ultrafiltration at a vegetable oil factory. *Desalination,* 166**,** 329-337.

[23] Ortega, L. M., Lebrun, R., Noël, I. M. & Hausler, R. 2005. Application of nanofiltration in the recovery of chromium (III) from tannery effluents. *Separation and Purification Technology,* 44**,** 45-52.

[24] Pinnekamp, J. & Friedrich, H. (eds.) 2006. *Municipal Water and Waste Management : Membrane Technology for Waste Water Treatment,* Aachen: FiW VERLAG.

[25] Qdais, H. A. & Moussa, H. 2004. Removal of heavy metals from wastewater by membrane processes: A comparative study. *Desalination,* 164**,** 105-110.

[26] Qin, J.-J., Wong, F.-S., Li, Y.-Q., Nyunt Wai, M. & Lian, Y.-T. 2004. The use of ultrafiltration for treatment of spent solventcleaning rinses from nickel-plating operations: membrane material selection study. *Desalination,* 170**,** 169-175.

[27] Religa, P., Kowalik, A. & Gierycz, P. 2011. Application of nanofiltration for chromium concentration in the tannery wastewater. *Journal of Hazardous Materials,* 186**,** 288-292.

[28] Streitberger, H. 2007. Electrodeposition coatings. *In:* Streitberger, H. & Dossel, K. (eds.) *Automotive paints and coatings.* 2nd ed. Weinheim: Wiley-VCH.

[29] Tay, J.-H. & Jeyaseelan, S. 1995. Membrane filtration for reuse of wastewater from beverage industry. *Resources, Conservation and Recycling,* 15**,** 33-40.

[30] Wang, Z. G., Wan, L. S. & Xu, Z. K. 2007. Surface engineerings of polyacrylonitrile-based asymmetric membranes towards biomedical applications: An overview. *Journal of Membrane Science,* 304**,** 8-23.

Chapter Four: The application of a 50 nm ZrO_2 ceramic membrane for the ultrafiltration of post-electrodeposition rinse wastewater

4.1 Introduction

Cathodic electrodeposition (CED) paint is the most widely-used anti-corrosion coating in the modern automotive industry [1]. Deposition of electrocoat paint is achieved by immersing car bodies into an electrocoat tank connected to a rectifier. A voltage of more than 300 volts is then applied to the electrodes in the tank to facilitate the diffusion and migration of dispersed electrocoat paint particles onto the car body surface [1]. Car bodies are then subjected to a series of rinses after the electrodeposition process to remove excess paint particles. Such rinses are often arranged in series and include the use of ultrafiltered water rinse, freshwater rinse and deionized water rinse.

The ultrafiltration of post-electrodeposition rinse wastewater in the automotive industry commonly involves the use of polymeric membranes. Such membranes are resistant to electrocoat solvents, acids, and electrolytes [1]. The membranes are flushed with a special solution prior to use in order to remove impurities and to establish surface cationic charges. This helps to prevent the deposition of the positively charged paint particles on the surface of the membrane [1]. However, polymeric membranes are subject to material instability and their operating life is very much affected by the frequency and nature of cleaning. For example, exposure to strong doses of chlorine can cause significant degradation [2].

Ceramic membranes are known to have better chemical and thermal stability than polymeric membranes [3, 4]. They work well within a pH range of 1 to 14 and can be operated at temperatures as high as 500 °C [5]. One of the distinctive characteristics of ceramic membranes is their ability to endure strong doses of chlorine – an extremely effective cleansing agent at alkaline pH [2]. Other advantages of ceramic membranes

include longer lifespan, higher average flux and lower cleaning frequency [3]. Although ceramic membranes may offer some advantages compared to polymeric membranes, their use in industrial wastewater treatment has been limited to date by their higher cost and by their intrinsic brittleness. In regard to the latter, undue vibrations caused by pump cavitations or pressure surges can cause damage and sudden temperature changes can result in thermal shocks causing crack damage [2].

Therefore, for a particular application, the relative advantages and disadvantages need to be carefully assessed. In some situations, the advantages mentioned above can make ceramic membranes more favourable than polymeric membranes despite the high initial cost.

Crossflow filtration is the common mode of operation for ceramic membranes. Cake layer formation during this mode is commonly governed by mechanisms such as surface shear forces, the crossflow velocity (CFV) and the velocity gradient [6]. These mechanisms draw the particles away from the membrane surface resulting in a decrease in cake formation. Some of the well-known models that describe particle behaviour during crossflow filtration include the inertial migration model, the shear-induced hydrodynamic convection model, the shear-induced hydrodynamic diffusion model, the erosion model, the turbulent burst model, the friction force model, the particle adhesion model, the surface renewal model and the particle-particle interaction model. A comprehensive discussion of the models enumerated above can be found in a review paper written by Bowen and Jenner [7].

The type of ceramic membrane tested in this experiment is under consideration for the

treatment of wastewater generated at the final rinsing stage of a car manufacturer's post-electrodeposition process. Wastewater generated at this stage represents a substantial volume of the total wastewater discharged by the company. A combination of the feedwater supplies (townswater and deionized water) and non-adhered CED paint particles commonly make up the wastewater generated. Typical wastewater quality generated by the final rinsing stage is shown in Table 4.1.

Table 4.1: Typical wastewater quality generated at the final rinsing stage of a car manufacturer's post-electrodeposition process

pH	Conductivity (μS/cm)	TDS (mg/L)	Turbidity (NTU)	Zeta Potential, ζ (mV)
6.7	56.2	44.0	262.0	56 ± 2 mV

The reuse or further treatment of wastewater generated at the final rinsing stage is restricted by the presence of suspended CED paint particles. Removing these paint particles from the wastewater will result in a better water quality suitable for direct reuse or further water treatment.

A model wastewater containing CED paint (5% v/v) was used in the experiments. The model wastewater has been prepared to have a worse water quality compared to the actual wastewater generated at the final rinsing stages and hence represents a worst-case scenario. The primary reason for using model wastewater in lieu of the actual wastewater is to control the size of the CED paint particles present in the feed. CED paint particles present in the actual wastewater can go up to several microns due to paint particle agglomeration. These larger particles are not of great concern to our present investigations since they are unlikely to deposit on the membrane surface due to high

velocity drag and lift forces. Smaller or finer particles are the real concern because they have been reported to be the main components of the cake layer formed during crossflow filtration [8]. These smaller or finer particle sizes have been shown in this study to be present in pure CED paint.

This chapter has analysed the detailed performance of a 50 nm ZrO_2 ceramic ultrafiltration membrane with respect to model wastewater containing CED paint particles. Hence, the influence of different operating parameters such as transmembrane pressure (TMP), CFV, and particle size on filtration performance were systematically investigated. Hydrodynamic and adhesive forces were calculated to investigate their effects on the CED paint particles present in the feed water. Likewise, particle adhesion probability and membrane resistances were calculated to give a thorough understanding of permeate flux behaviour. Results obtained from this work have provided an insight into the applicability of ceramic membranes for the treatment of post-electrodeposition rinse wastewater.

4.2 Materials and methods

4.2.1 Model wastewater

Pure CED paint was obtained directly from the electrocoat bath of a car manufacturer. A volume of 250 mL of CED paint was mixed with 4,750 mL of distilled water to make up a 5 % v/v model wastewater suspension. The average water quality for the model wastewater is shown in Table 4.2.

Table 4.2: Average water quality of model wastewater containing 5 % v/v CED paint

pH	Conductivity (µS/cm)	TDS (mg/L)	Turbidity (NTU)	Zeta Potential, ζ (mV)
5.7	102	79.9	4644.3	58 ± 2 mV

4.2.2 Ceramic membrane

A Membralox T1-70 single channel ceramic membrane with a zirconium dioxide (ZrO_2) active layer was used in all the experiments. The membrane has a nominal pore size of 50 nm and an effective membrane area of 0.005 m^2. Its dimensions are as follows – internal diameter, i.d. = 7 mm; outside diameter, o.d. = 10 mm; length, l = 250 mm. The isoelectric point of the active layer is approximately 7 [9] and therefore the membrane surface charge is positive or negative respectively below or above a pH of 7. This membrane was supplied by Pall Corporation Australia.

4.2.3 Ceramic ultrafiltration system

The ceramic ultrafiltration rig used in the experiments is similar to the system shown in Section 3.2.5 of Chapter 3. The only difference is that the flat sheet test cell was replaced by a ceramic membrane module – as shown in Figure 4.1. A variable speed pump was used to deliver wastewater into the stainless steel ceramic module at different CFVs (2.4 m s^{-1}, 2.8 m s^{-1} and 3.2 m s^{-1}) and TMPs (100 kPa, 200kPa and 300 kPa). Membrane permeate was collected into a container and weighed while reject water was returned into the feed tank to facilitate increase of feed water concentration and fast track the rate of membrane fouling. The feed tank was submerged halfway into a water bath to maintain the temperature within 19 – 24 °C. The conductivity and the pH of the feedwater were also maintained within the ranges of 100.0 – 120.0 µS cm^{-1} and 5.0 – 6.0, respectively. Parameters such as pressures, temperatures, weights, and water qualities (pH and conductivity) were monitored at 2 minute intervals using probes and recorders connected to a computer. Each experiment run was performed in duplicate and lasted for ~ 140 minutes.

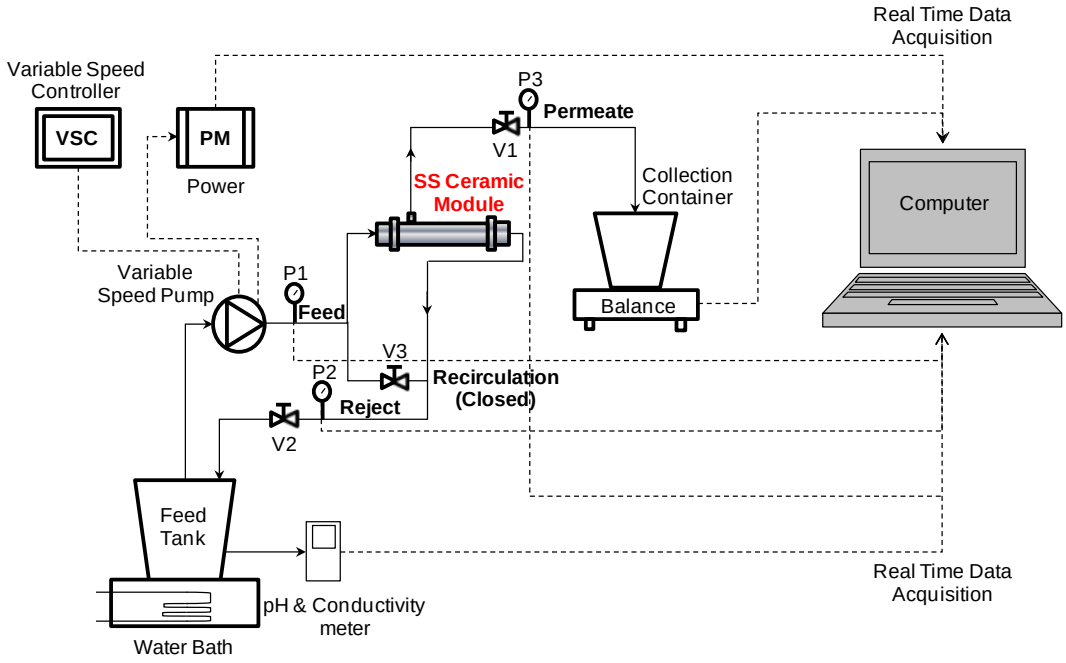

Figure 4.1: Schematic diagram of ceramic ultrafiltration rig used in the experiments. P1 – feed pressure; P2 – concentrate pressure; P3 – permeate pressure; V1 – permeate valve; V2 – concentrate valve; V3 – recirculation valve. Solid lines represent water flow while broken lines represent real time data acquisition.

4.2.4 Analytical methods

Particle size distributions in the model and actual wastewater samples were determined using a Malvern Zetasizer Nano Series (Nano-ZS). The results were then compared to each other to ascertain that the particle sizes present in the model wastewater reflected those in the actual wastewater. Turbidity measurements were used to estimate total paint particle rejection rates. Feed and permeate water turbidity were measured using a La Motte 2020 Series Turbidity Meter. Turbidity rejection rates (R_{Turb}) were calculated using Eq. (1):

$$R_{Turb} = [(T_F - T_P) / T_F] \times 100\ \% \quad (1)$$

where T_F is the feed turbidity (NTU) and T_P is the permeate turbidity (NTU).

4.2.5 Membrane cleaning

The ceramic membrane used in the experiments was cleaned after each trial. The membrane cleaning procedure consists of tap water flushing, chemical cleaning and deionized water rinsing. Tap water flushing was carried out for 15 minutes at a temperature of 45 °C. It was then followed by chemical cleaning using Ultrasil 10 – a commercially available cleaning chemical containing Sodium Hydroxide (NaOH) and Tetrasodium EDTA. Chemical cleaning parameters used were as follows: 1.5% v/v Ultrasil 10 solution, pH range 11 –12, temperature range 45 – 50 °C, pressure of 100 kPa, cross flow velocity 2.4 m s^{-1} and cleaning time 45 – 60 minutes. After chemical cleaning, the membrane was rinsed with deionized water for 15 minutes at a temperature of 21 °C. Chemical cleaning and deionized water rinsing were repeated when the pure water flux of the regenerated membrane was below its initial measured value. The cleaning chemical used was supplied by ECOLAB Australia.

4.3 Results and discussion

4.3.1 Pure water flux (PWF)

The pure water flux (PWF) of the ceramic membrane used in all experiments was found to be highly correlated with the TMP as shown in Figure 4.2. This is not unexpected since the only resistance present during the pure water flux experiments is the intrinsic membrane resistance (R_M). The use of high quality feed water such as distilled water ensures that no form of fouling will occur during the determination of the pure water flux. In this case, distilled water having an average conductivity of 2 µS cm^{-1} was used.

The data used for plotting Figure 4.2 are available in the accompanying CD (Appendix 4.1).

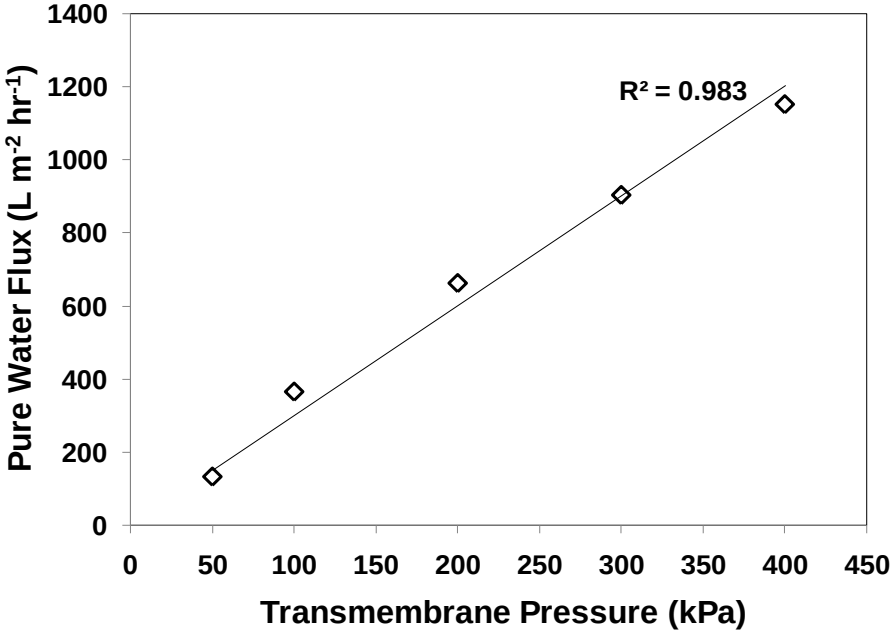

Figure 4.2: Pure water flux of 50 nm ceramic membrane as a function of TMP at a CFV of 2.4 m s^{-1} and temperature of 20 °C. The pure water permeability (J_{PWP}, $m^3 m^{-2} s^{-1} kPa^{-1}$) of the membrane is given by the slope of the graph.

The intrinsic membrane resistance (R_M) is calculated according to Eq. (2) [2]:

$$R_M = TMP / \eta_F PWF \quad (2)$$

where η_F is the dynamic viscosity of the feed water at 20 °C (0.001002 Pa·s). The calculated intrinsic membrane resistance (R_M) for the 50 nm ceramic membrane is equal to 1.14E+12 m^{-1}.

4.3.2 Influence of particle size distribution

Results of the particle analysis on the model and actual wastewater samples are shown

in Figure 4.3. The paint particles present in both samples ranged from 91 nm to 342 nm in size. These particle sizes can be found in the electrocoat bath where pure electrodeposition paint samples used in the experiments were obtained. The presence of larger particles in the actual wastewater generated was due to particle agglomeration of non-adhered electrodeposition paint. The data used for plotting Figure 4.3 are available in the accompanying CD (Appendix 4.2).

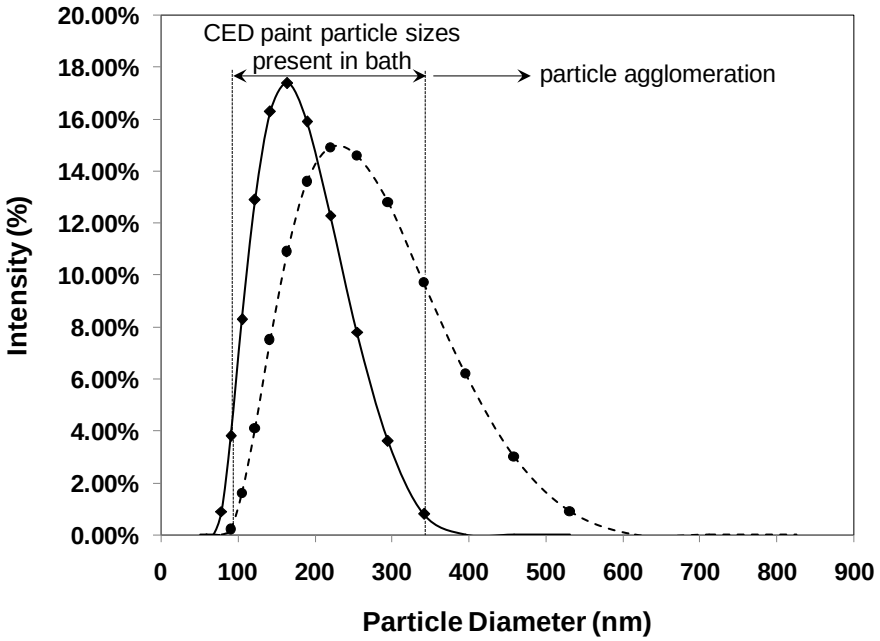

Figure 4.3: Particle size distribution for model and actual wastewater samples. Solid line represents the model wastewater while dashed line represents actual wastewater generated by post-electrodeposition rinses.

The deposition behaviour of particles on the membrane surface is governed by hydrodynamic and surface interaction forces [8]. Components of hydrodynamic forces include drag and lift forces while surface interaction forces include electrostatic interactions and Van der Waals forces. The magnitudes of hydrodynamic forces acting on CED paint particles during crossflow ultrafiltration depend on particle size. Larger

CED paint particles present in the feed stream will have higher drag and lift forces compared to smaller ones. Likewise, larger CED paint particles are more likely to stay in the flow field region while smaller particles have the tendency to deposit on the membrane surface during crossflow ultrafiltration.

Electrostatic interaction between the particles and the membrane surface are due to inherent surface charges. CED paint particles are positively charged and therefore it is expected that particles will repel each other when suspended in solution. The surface charge of the ceramic membrane depends on the isoelectric point of the active layer. For the ceramic membrane used in the experiments, the isoelectric point of the active layer (ZrO_2) is 7, *vide supra*. At a feedwater pH of 5.7 (the pH of the model wastewater), the active surface of the ceramic membrane has a net positive charge. This means that electrostatic repulsive forces are expected to be in effect between the membrane surface and the CED paint particles during ultrafiltration. However, it is found that significant adhesion of CED paint particles onto the membrane surface still occurs during these experiments. The presence of CED paint particles on the surface of the membrane demonstrates that the potential electrostatic repulsion is not sufficient to preclude adhesion. Since the CED paint particles deposit on the membrane surface irrespective of such charge considerations, electrostatic interactions have been disregarded in our modelling and the adhesive forces between the particles and the membrane have been attributed to Van der Waals interactions alone.

Figure 4.4 illustrates the different forces acting on the CED paint particles during crossflow ultrafiltration of model wastewater.

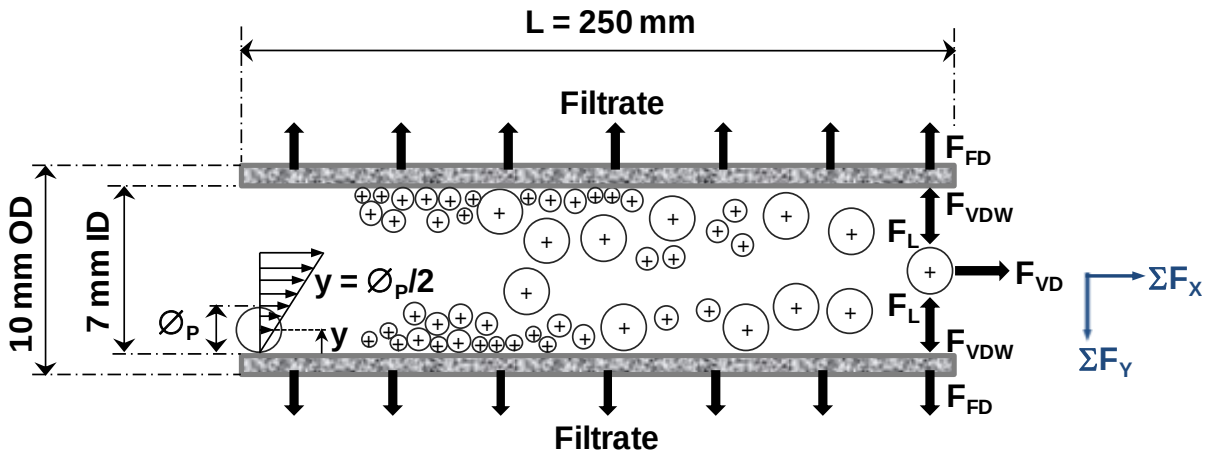

Figure 4.4: Different forces acting on CED paint particles during crossflow ultrafiltration of model wastewater – $\varnothing_P$ is the particle diameter (m); F_L is the lift force (N); F_{FD} is the filtrate drag force (N); F_{VD} is the velocity drag force (N); and F_{VDW} is the Van der Waals force (*vide supra*).

Drag forces experienced by particles during crossflow filtration are due to filtrate flow and feed velocities. The filtrate drag force (F_{FD}) can be calculated using the general form of Stoke's equation, Eq. (3) and the feed velocity drag force can be calculated using Eq. (4) [10] :

$$F_{FD} = 3\pi\eta_F\varnothing_P J \quad (3)$$

where η_F is the viscosity of the feed water at 20 °C (0.001002 Pa s); $\varnothing_P$ is the particle diameter (m); J is the permeate flux ($m^3\ m^{-2}\ s^{-1}$).

$$F_{VD} = 1.7009\ [3\pi\eta_F\varnothing_P\nu_V\ (y = \varnothing_P / 2) \quad (4)$$

where ν_V is the velocity field ($m\ s^{-1}$).

The term ν_V ($y=Ø_P/2$) in Eq. (4) is defined as the undistributed velocity at position $y = Ø_P/2$. The value of this term is given by Eq. (5):

$$\nu_V (y=Ø_P/2) = \tau_W Ø_P / 2\eta_F \quad (5)$$

The shear stress (τ_W, Pa) acting on the cake boundary can be calculated using Eq. (6) [11]:

$$\tau_W = \Delta P Ø_{CM} / 4L_{CM} \quad (6)$$

where ΔP is the pressure drop in the ceramic membrane during filtration (Pa); $Ø_{CM}$ is the internal diameter of the ceramic membrane (m); and L_{CM} is the length of the ceramic membrane (m).

Therefore, Eq. (4) can be rewritten as

$$F_{VD} = 0.638 (\pi \Delta P Ø_{CM} Ø_P^2 / L_{CM}) \quad (7)$$

The lift force (F_L) which is commonly due to shear flow can be estimated using Eq. (8) [12] while the adhesive force (F_{VDW}), which is assumed to be purely Van der Waals (*vide supra*), can be estimated using Eq. (9) [12, 13]:

$$F_L = 0.761 (\tau_W^{1.5} Ø_P^3 \rho_F / \eta_F) \quad (8)$$

where ρ_F is the density of the feed water at 20 °C (998.2 kg m^{-3}).

$$F_{VDW} = h\varpi Ø_P / 32\pi\bar{a}^2 \quad (9)$$

where $h\varpi$ is the Lifschitz-van der Waals constant (1.0E-20 J); and ā is the adhesive distance (4.0E-10 m)[14].

Utilizing the above equations, the magnitudes of the forces acting on the different sizes of CED paint particles present in the model wastewater have been calculated. These are represented in Figure 4.5. The calculations of these forces are shown in Appendix 4.3 – attached at the end of the thesis.

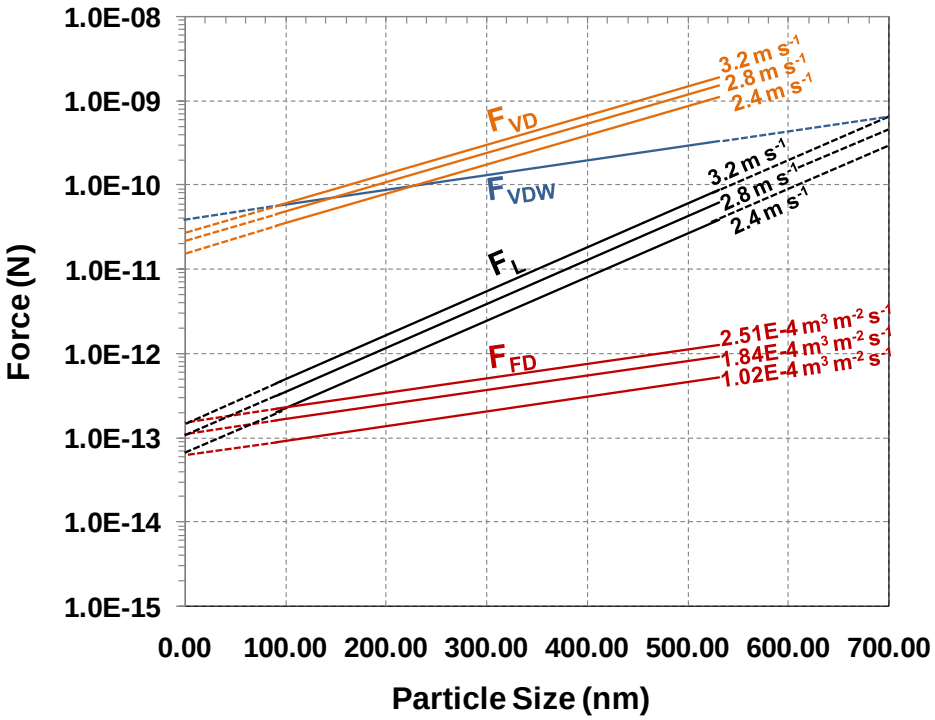

Figure 4.5: Magnitudes of forces acting on the CED paint particles during crossflow ultrafiltration of model wastewater. Solid lines represent the forces on the CED paint particle sizes while the broken lines represent the extension of forces on either the smaller or larger CED paint particle sizes. CFVs are indicated on the graph for F_{VD} and F_L and permeate fluxes are indicted for F_{FD}.

As can been seen from Figure 4.5, the deposition of CED paint particles on the surface of the ceramic membrane depends on the balance between the velocity drag force (F_{VD}) and the Van der Waals adhesive force (F_{VDW}). The effects of the lift force (F_L) and the filtrate drag force (F_{FD}) on the particle sizes present in the model wastewater are relatively insignificant. However, with larger CED paint particles, > 700 nm, the lift force at a CFV of 3.2 m s^{-1} overcomes the Van der Waals adhesive force. Likewise, as the particle sizes increase, the filtrate drag force, F_{FD}, also increases but not enough to overcome the lift force. The filtrate drag force only overcomes the lift force at smaller particle sizes (approximately < 70 nm) and at a CFV of 2.4 m s^{-1}.

The effects of velocity drag and adhesive forces on the particle sizes present in the model wastewater are the following: a) at a CFV of 2.4 m s^{-1}, the adhesive force on particle sizes less than 240 nm is greater than the velocity drag force; b) at a CFV of 2.8 m s^{-1}, the adhesive force on particles less than 160 nm is greater than the velocity drag force; c) at a CFV of 3.2 m s^{-1}, the adhesive force on particles less than 100 nm is greater than the velocity drag force; and d) the velocity drag force at all CFVs is greater than the adhesive force when the particle sizes are larger than the ones mentioned in a) to c). Therefore, as the CFV increases, the range of particle sizes that are likely to be deposited on the membrane surface gets smaller.

4.3.3 Particle adhesion probability

A simple model for particle adhesion probability (γ) was developed by Stamatakis and Chi [8]. This model assumes that only a fraction of particles present in the feed water deposit on the membrane surface. Based on this model, particle deposition is due to the

effects of various forces acting on particles near the cake-suspension interface. Eq. (10) shows the general form of the particle adhesion probability formula:

$$\gamma = 1 - [1 - (1 / ((F_X / F_Y)^2 + 1)^{0.5})] [Ø_P / 2h_{max}] \quad (10)$$

The symbols F_X and F_Y represent the summation of forces with respect to the x and y axes, as shown in Figure 4.4, and h_{max} represents the maximum protrusion height of the cake layer that is formed (m). The protrusion height is assumed to be of uniform distribution over the range of heights defined by $0 \leq h \leq h_{max}$. Complete deposition of particles will occur when γ is equal to 1 while no deposition occurs when γ is equal to zero [15]. For γ to vary from 0 to 1, $Ø_P/2$ is assumed to be equal to h_{max}, and therefore Eq. (10) can be simplified to,

$$\gamma = 1 - [1 - (1 / ((F_X / F_Y)^2 + 1)^{0.5})] \quad (11)$$

Figure 4.6 shows the calculated particle adhesion probability of the CED paint particles as a function of particle sizes at a TMP of 100 kPa and CFVs of 2.4, 2.8, and 3.2 m s^{-1}.

In general, the adhesion probability of CED paint particles present in the model wastewater decreases as particle sizes increase (Figure 4.6). As mentioned before, larger particles are likely to be swept away from the surface of the cake layer because they have higher velocity drag and lift forces. A decrease of particle adhesion probabilities is observed as CFV increases, and as expected the highest CFV of 3.2 m s^{-1} showed the lowest particle adhesion probabilities.

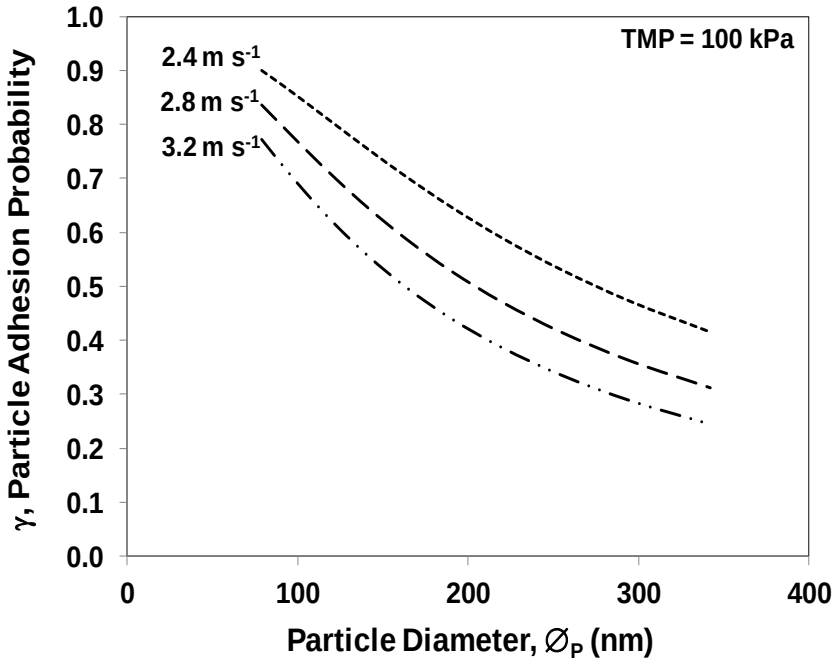

Figure 4.6: Particle adhesion probability (γ) as a function of particle size diameter at a TMP of 100 kPa and CFVs of 2.4, 2.8, and 3.2 m s^{-1}. The calculations for the particle adhesion probability are shown in Appendix 4.4 – attached at the end of the thesis.

4.3.4 Influence of transmembrane pressure (TMP) and crossflow velocity (CFV)

In order to determine the influence of TMP and CFV on the performance of the 50 nm ceramic membrane during ultrafiltration of the model wastewater, duplicate experiments (each of 140 minutes duration) were carried out as follows.

Permeate flux (J, $m^3\ m^{-2}\ s^{-1}$) was calculated using Eq. (12):

$$J = 0.001W / A_M t \quad (12)$$

where W is the weight measured by the balance (kg), A_M is the effective membrane area (m^2), t is the sampling time (s).

To account for temperature variations, all permeate fluxes were standardized at a temperature of 20 °C using Eq. (13) [6]:

$$J_{20°C} = J\,(1.03)^{T_S - T_M} \qquad (13)$$

where $J_{20°C}$ is the flux at a standard temperature of 20 °C ($m^3\ m^{-2}\ s^{-1}$), T_S is the standard temperature (20 °C), T_M is the measured temperature (°C).

Figures 4.7a to c show the measured permeate fluxes of the 50 nm ceramic ultrafiltration membrane at different combinations of TMP and CFV. The steady-state permeate flux measured at a TMP of 100 kPa (Figure 4.7a) was generally higher than the ones measured at 200 and 300 kPa. In fact the highest steady-state permeate flux for all experiments was obtained at a TMP of 100 kPa and CFV of 3.2 m s^{-1}. As the TMP is increased, the initial measured flux increases but rapidly declines afterwards until the steady-state permeate flux is reached (Figures 4.7b and c).

a)

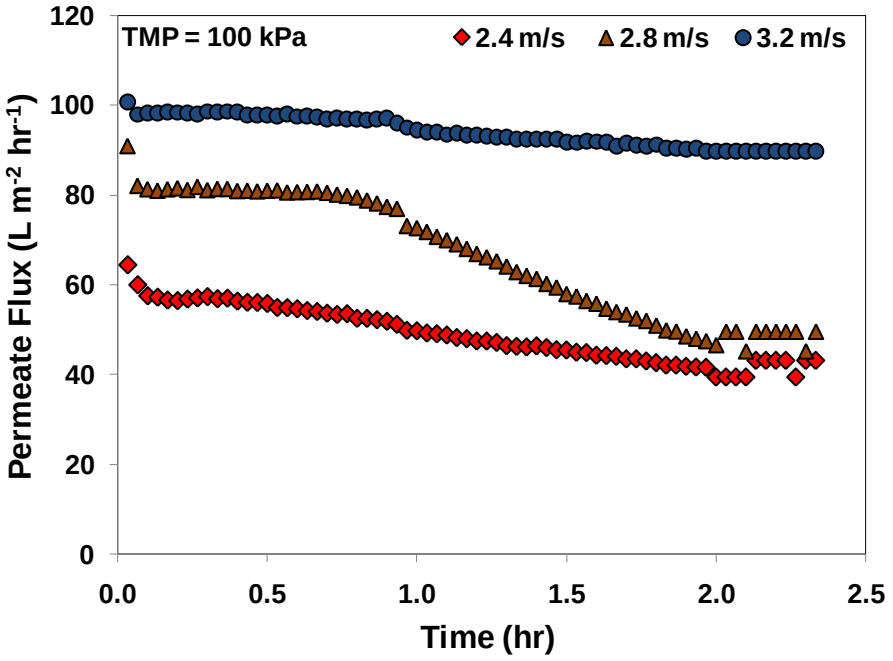

b)

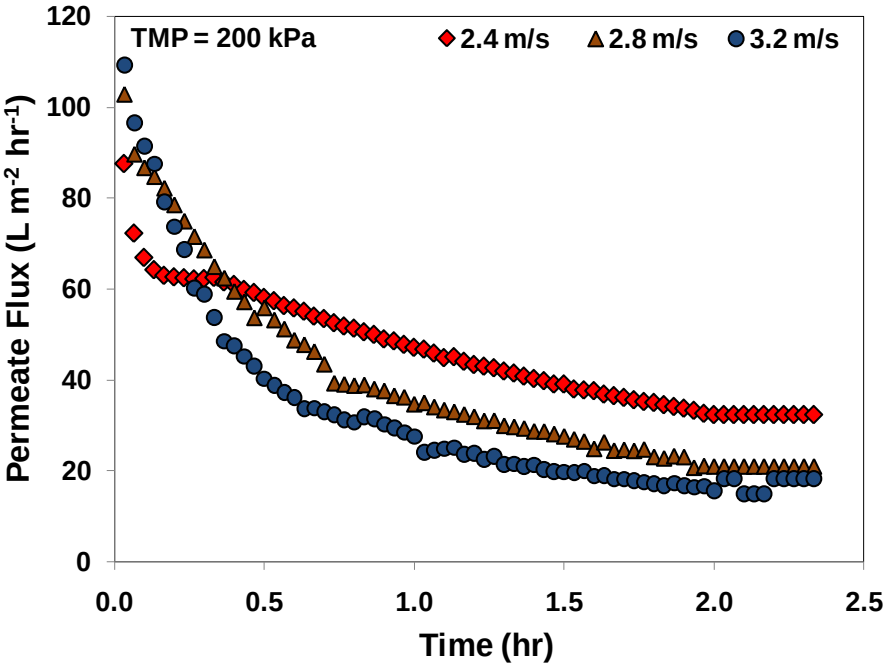

c)

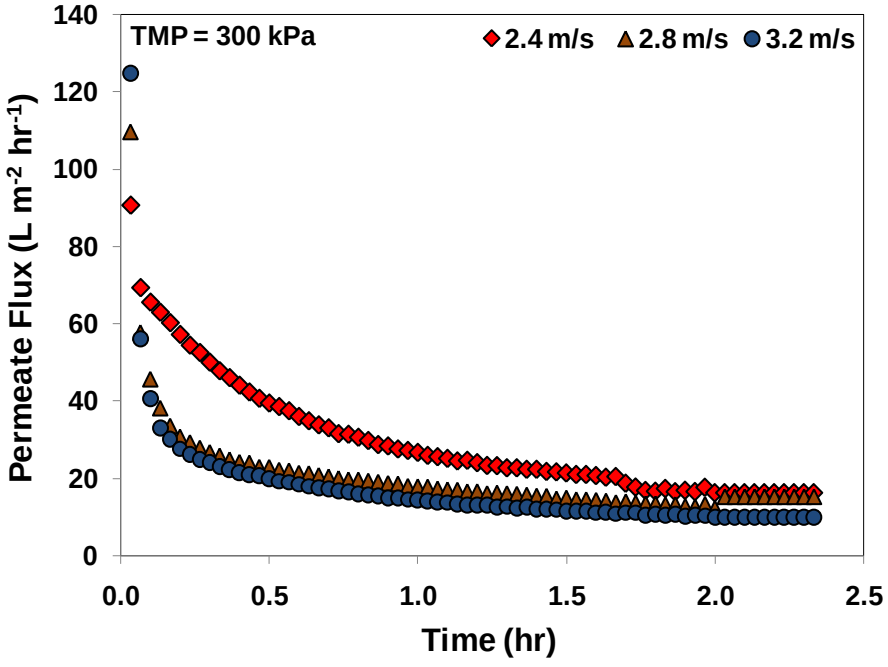

Figure 4.7: Permeate flux as a function of time at TMPs of: a) 100 kPa, b) 200 kPa, and c) 300 kPa; and CFVs of 2.4, 2.8, and 3.2 kPa.

The data used for plotting Figures 4.7a to c are available in the accompanying CD (Appendix 4.5).

The results from the experiments clearly show that permeate flux improvement is dependent on both CFV and TMP. At a TMP of 100 kPa, the steady-state permeate fluxes increase as CFVs are increased. But at higher pressures of 200 and 300 kPa, the steady-state permeate fluxes decrease as CFVs are increased. Table 4.3 shows the steady-state fluxes measured at the end of each experiment run.

Table 4.3: Steady-state permeate fluxes and turbidity rejection rates measured during ceramic ultrafiltration of model wastewater containing 5 % v/v CED paint. The calculations for the turbidity rejection rates are available in the accompanying CD (Appendix 4.6)

TMP (kPa)	CFV ($m\ s^{-1}$)	Permeate Flux ($L\ m^2\ hr^{-1}$)	Turbidity Rejection (%)
100	2.4	43.2	99.96
	2.8	50.4	99.96
	3.2	90.0	99.98
200	2.4	32.4	99.98
	2.8	21.6	99.98
	3.2	18.0	99.98
300	2.4	18.0	99.98
	2.8	14.4	99.99
	3.2	10.8	99.98

The flux behaviour at pressures of 200 and 300 kPa can be explained by considering the geometry of the filter cake formed on the surface of the ceramic membrane during the experiments. At different CFVs, different ranges of particle sizes are deposited on the surface of the membrane as mentioned in Section 4.3.2. Figures 4.8a – c show the different geometries of filter cakes formed during ceramic ultrafiltration of CED paint particles at different CFVs. Obviously, the filter cake formed at a cross-flow velocity of 3.2 m s^{-1} is likely to be thinner compared to ones formed at 2.8 and 2.4 m s^{-1} due to the preponderance of relatively smaller particles.

a)

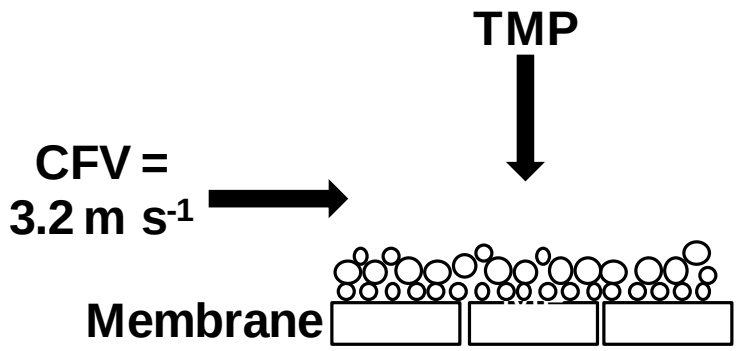

b)

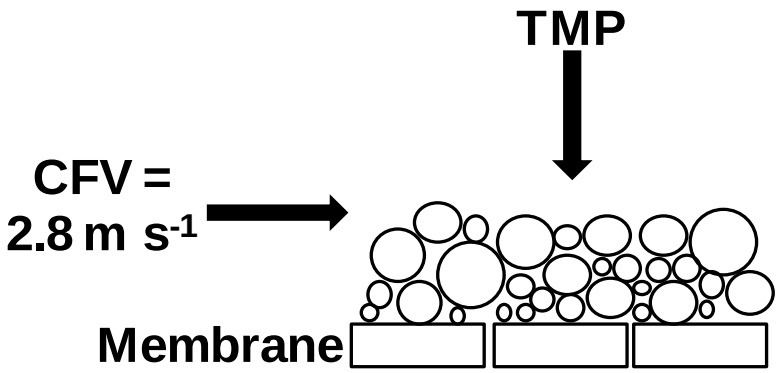

c)

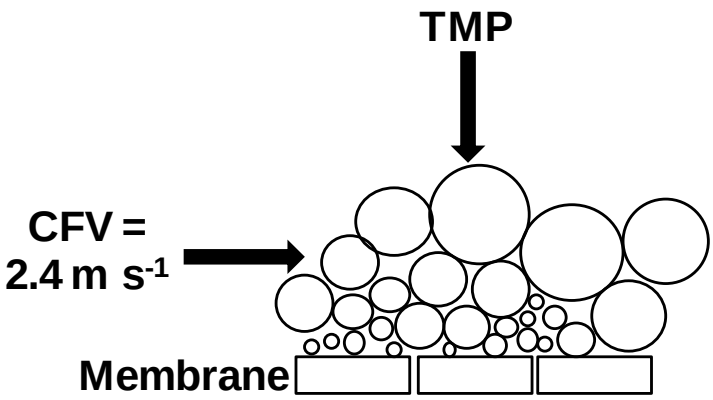

Figure 4.8: Geometry of filter cake formed during ceramic ultrafiltration of CED paint particles at different CFVs.

The thin cake layer formed at a CFV of 3.2 m s^{-1} is only favourable at low TMP. A relatively thinner cake layer allows the passage of water into the membrane at a faster rate compared to a much thicker cake layer. This can be seen in the permeate flux results shown in Figure 4.7a. The permeate flux produced at a CFV of 3.2 m s^{-1} is higher compared to the permeate fluxes produced at CFVs of 2.8 and 2.4 m s^{-1}.

At higher pressures, the thinner cake layer which is primarily composed of smaller particles becomes a liability. Higher pressures will cause the cake layer to compress thereby reducing cake porosity. The reduction in porosity will be more pronounced on the cake layer composed of smaller and less diverse particle sizes than on the cake layer composed of larger and more diverse particle sizes. The cake layer formed from smaller and less diverse particle sizes has a compact structure (Figure 4.8a) and subjecting them further to higher pressures makes them more compact resulting in very low porosity. In contrast, the cake layer formed from larger and more diverse particle sizes has a loose structure (Figures 4.8b to c) and when subjected to higher pressures

will still have high porosity. This explains the behaviour of the permeate fluxes obtained at higher pressures. The permeate fluxes shown in Figures 4.7b and c are more dependent on TMP rather than CFV. The effect of a higher CFV at pressures of 200 and 300 kPa is negated. In fact as CFV is increased, the steady-state permeate fluxes measured decreased. At pressures of 200 and 300 kPa, the steady-state permeate fluxes measured at the highest CFV of 3.2 m s^{-1} was the lowest. The highest measured steady-state permeate fluxes at both pressures came from the lowest CFV of 2.4 m s^{-1} (Table 4.3).

The effect of different CFVs and TMPs on particle rejection is negligible. Turbidity rejection rates measured for all experiments are greater than 99.95 % (Table 4.3). Based on turbidity rejection rates, CED paint particle removal in the model wastewater is just a function of membrane pore size. It also shows that the chosen membrane pore size is suitable for wastewater containing CED paint particles.

Based on the results shown above, the combination of a high CFV and low pressure gives the highest steady-state permeate flux. However, maintaining a high CFV usually involves the consumption of a substantial amount of energy [16]. To look into this aspect at a laboratory scale level, the energy consumption (kWh) of the feed pump was monitored during the ultrafiltration experiments of the model wastewater. Table 4.4 shows the specific energy consumption (kWh/m^3) as a function of different CFVs and TMPs.

In general, the specific energy consumption (kWh/m^3) of the 50 nm ultrafiltration membrane increases as TMP is increased. Such results were consistent for all CFVs

used. Additionally, at a TMP of 100 kPa, the specific energy consumption of the membrane decreases as the CFV is increased. In contrast, at temperatures of 200 and 300 kPa, the specific energy consumption increases as CFV is increased.

Table 4.4: Energy consumption as a function of different CFVs and TMPs

CFV (m/s)	Pressure (kPa)	Energy Consumption (kWh)	Volume (m^3)	Specific energy consumption (kWh/m^3)
2.4	100	0.332	0.00063	527
	200	0.347	0.00062	560
	300	0.349	0.00053	658
2.8	100	0.362	0.00086	421
	200	0.379	0.00062	611
	300	0.388	0.00029	1338
3.2	100	0.379	0.00110	345
	200	0.395	0.00054	731
	300	0.402	0.00028	1436

Therefore, using a combination of low pressure and high CFV gives the greatest benefits in terms of permeate flux and specific energy consumption. As shown in Table 4.4, a TMP of 100 kPa and CFV of 3.2 m s^{-1} resulted in the highest permeate volume and the most optimum specific energy consumption with respect to other operating conditions. The calculations for the specific energy consumptions are available in the accompany CD (Appendix 4.7).

4.3.5 Membrane resistances

Permeate flux behaviour during ceramic ultrafiltration of model wastewater containing CED paint particles can be analysed using the resistance-in-series model. The

resistance in series model describes the relationship between TMPs and permeate fluxes. The general equation of the resistance-in-series model can be written as [2]:

$$J = TMP / \eta_F (R_M + R_F + R_G) \quad (14)$$

where J is the permeate flux ($m^3\ m^{-2}\ s^{-1}$), TMP is the transmembrane pressure (Pa), η_F is the viscosity of feed water (0.001002 Pa s), R_M is the intrinsic membrane resistance (1.14E+12 m^{-1}), R_F is the adsorption resistance on inner pore fiber (m^{-1}) and R_G is the concentration polarization resistance (m^{-1}). The concentration polarization resistance (R_G) can be calculated using Eq. (15) [2]:

$$R_G = \Phi TMP \quad (15)$$

where Φ is the resistance index ($Pa^{-1}\ m^{-1}$). The adsorption and concentration polarization resistances were obtained by plotting permeate flux as a function of TMP and fitting the experimental data obtained into Eq. (14). Curve fitting was done in Microsoft Excel using the Solver add-in tool. Results obtained from the curve fitting are shown in Table 4.5. The adsorption resistance (R_F) was negligible during the first 2 minutes of the experiments but, as filtration time progresses, adsorption resistance significantly increased. This increase is very noticeable at a cross-flow velocity of 3.2 m s^{-1} due to high turbulence. High turbulence can cause the relatively smaller CED paint particles present in the feed stream to break down into even smaller or finer particles. The finer CED paint particles are then deposited either in membrane pore openings or into membrane pore channels.

As expected, the concentration polarization resistance (R_G) was the biggest resistance encountered during the ceramic ultrafiltration of model wastewater containing CED paint particles. The influence of concentration polarization has been reported to be severe in microfiltration and ultrafiltration due to high fluxes and low mass transfer coefficients [17]. The concentration polarization resistances obtained were directly proportional to TMP. As TMP increases, concentration polarization also increases. Although this was generally the case, the data also show that the effect of concentration polarization was minimized at a low TMP and high CFV.

The lowest concentration polarization resistances were obtained from the highest CFV of 3.2 m s^{-1} and the lowest TMP of 100 kPa – as highlighted in Table 4.5. At these operating conditions, the effect of concentration polarization weakens due to a high Reynolds number (*Re*) that is defined as

$$Re = \rho_F v \varnothing_{CM} / \eta_F \quad (16)$$

where v is the crossflow velocity in m s^{-1}.

All Reynolds number (*Re*) calculated at different CFVs used have turbulent flow characteristics (*Re* > 4000). An increase of CFV from 2.4 m s^{-1} to 2.8 m s^{-1} subsequently increased *Re* from 16736 to 19526 while increasing CFV further to 3.2 m s^{-1} resulted in a much higher *Re* of 22315. As reported in the literature [18], turbulent flow weakens the effect of concentration polarization due to high shear forces encountered by the cake formed. Therefore the more turbulent the flow regime is at low pressure, the greater its effect in weakening concentration polarization. Calculations for the membrane

resistances and Reynolds number are available in the accompanying CD (Appendices 4.8 and 4.9 respectively).

Table 4.5: Resistances obtained from the fitting of experimental data to the resistance-in-series model.

Parameters	R_M (x 10^{12} m^{-1})	R_F (x 10^{12} m^{-1})	R_G (x 10^{12} m^{-1})
2.4 m s^{-1}; 100 kPa			
2 mins.	1.14	0.99	3.43
60 mins.	1.14	6.54	12.90
120 mins.	1.14	10.6	24.20
2.4 m s^{-1}; 200 kPa			
2 mins.	1.14	0.99	6.86
60 mins.	1.14	6.54	25.80
120 mins.	1.14	10.6	48.40
2.4 m s^{-1}; 300 kPa			
2 mins.	1.14	0.99	10.30
60 mins.	1.14	6.54	38.80
120 mins.	1.14	10.6	72.60
2.8 m s^{-1}; 100 kPa			
2 mins.	1.14	0.98	2.60
60 mins.	1.14	13.40	17.60
120 mins.	1.14	14.00	21.90
2.8 m s^{-1}; 200 kPa			
2 mins.	1.14	0.98	5.20
60 mins.	1.14	13.40	35.20
120 mins.	1.14	14.00	43.90
2.8 m s^{-1}; 300 kPa			

2 mins.	1.14	0.98	7.80
60 mins.	1.14	13.40	52.80
120 mins.	1.14	14.00	65.80
3.2 m s^{-1}; 100 kPa			
2 mins.	1.14	0.98	**2.24**
60 mins.	1.14	13.00	**16.00**
120 mins.	1.14	37.00	**20.60**
3.2 m s^{-1}; 200 kPa			
2 mins.	1.14	0.98	4.48
60 mins.	1.14	13.00	32.00
120 mins.	1.14	37.00	79.10
3.2 m s^{-1}; 300 kPa			
2 mins.	1.14	0.98	6.73
60 mins.	1.14	13.00	48.10
120 mins.	1.14	37.00	119.00

4.4 Conclusions

The matching of CFV and TMP has been shown to be critical for the successful application of the 50 nm ceramic ultrafiltration membrane to wastewater containing CED paint particles. In this work, a CFV of 3.2 m s^{-1} and TMP of 100 kPa produced the highest steady-state permeate flux and the optimum energy consumption. It was also shown that under these operating conditions, the influence of concentration polarization was minimized and particle adhesion probability on membrane surface was at its lowest. Combining high TMPs with high CFVs is not recommended since, under these operating conditions, the steady-state permeate fluxes produced were relatively low and energy consumptions were high. Likewise, the concentration polarization

resistances obtained under these operating conditions were the highest. In general, a combination of high CFV and low TMP is suggested as the most beneficial operating condition for ceramic ultrafiltration of wastewater containing CED paint particles. Under such conditions, the larger particle sizes present in the wastewater are swept away from the surface of the membrane and the effect of particle compression due to pressure is minimized.

The work described in this chapter has since been published in the international literature [19].

4.5 References

[1] Streitberger, H. 2007. Electrodeposition coatings. *In:* Streitberger, H. & Dossel, K. (eds.) *Automotive paints and coatings.* 2nd ed. Weinheim: Wiley-VCH.

[2] Cheryan, M. 1998. *Ultrafiltration and microfiltration handbook,* Lancaster, Pennsylvania, Technomic Publishing Company, Inc.

[3] Siskens, C. A. M. 1996. Applications of ceramic membranes in liquid filtration. *In:* Burggraaf, A. J. & Cot, L. (eds.) *Fundamentals of Inorganic membrane science and technology.* Burlington: Elsevier Science B.V.

[4] Lee, S. & Cho, J. 2004. Comparison of ceramic and polymeric membranes for natural organic matter (NOM) removal. *Desalination,* 160**,** 223-232.

[5] Benfer, S., Popp, U., Richter, H., Siewert, C. & Tomandl, G. 2001. Development and characterization of ceramic nanofiltration membranes. *Separation and Purification Technology,* 22-23**,** 231-237.

[6] Crittenden, J. C., Trussell, R. R., Hand, D. W., Howe, K. J. & Tchobanoglous, G. 2005. *Water treatment: Principles and design,* Hoboken, NJ, John Wiley & Sons, Inc.

[7] Bowen, W. R. & Jenner, F. 1995. Theoretical descriptions of membrane filtration of colloids and fine particles: An assessment and review. *Advances in Colloid and Interface Science,* 56**,** 141-200.

[8] Stamatakis, K. & Chi, T. 1993. A simple model of cross-flow filtration based on particle adhesion. *AICHE Journal,* 39**,** 1292-1302.

[9] Randon, J., Crosnier De Bellaistre, M. & Rocca, J. L. 2003. Electrophoretic and electrochromatographic properties of zirconia based capillaries. *Chromatographia,* 57.

[10] O'Neill, M. E. 1968. A sphere in contact with a plane wall in a slow linear shear flow. *Chemical Engineering Science,* 23**,** 1293-1298.

[11] Holdich, R. G., Cumming, I. W. & Ismail, B. 1995. Variation of crossflow filtration rate with wall shear stress and the effect of deposit thickness. *Chemical Engineering Research and Design,* 73**,** 20-26.

[12] Altmann, J. & Ripperger, S. 1997. Particle deposition and layer formation at the crossflow microfiltration. *Journal of Membrane Science,* 124**,** 119-128.

[13] Israelachvili, J. N. 2010. Van der waals forces. *Intermolecular and surface forces.* 3 ed. Burlington: Elsevier Science.

[14] Krupp, H. 1967. Particle Adhesion Theory and Experiment. *Colloid Interface Sci.,* 11**,** 11-239.

[15] Bowen, W. R., Yousef, H. N. S. & Calvo, J. I. 2001. Dynamic crossflow ultrafiltration of colloids: A deposition probability cake filtration approach. *Separation and Purification Technology,* 24**,** 207-308.

[16] Waeger, F., Delhaye, T. & Fuchs, W. 2010. The use of ceramic microfiltration and ultrafiltration membranes for particle removal from anaerobic digester effluents. *Separation and Purification Technology,* 73**,** 271-278.

[17] Mulder, M. H. V. 1995. Polarization phenomena and fouling. *In:* Noble, R. D. & Stern, S. A. (eds.) *Membrane Separations Technology: Principles and Applications.* Burlington: Elsevier Science.

[18] Baker, R. J., Fane, A. G., Fell, C. J. D. & Yoo, B. H. 1985. Factors affecting flux in crossflow filtration. *Desalination,* 53**,** 81-93.

[19] Agana, B. A., Reeve, D. & Orbell, J. D. 2011. Optimization of the operational parameters for a 50 nm ZrO2 ceramic membrane as applied to the ultrafiltration of post-electrodeposition rinse wastewater. *Desalination,* 278**,** 325-332.

Chapter Five: Ceramic electro-ultrafiltration of post-electrodeposition rinse wastewater

5.1 Introduction

Crossflow ultrafiltration is one of the most successfully used treatment options for reclamation of wastewater containing ED paint particles. Although this is the case, suspended ED paint particles in wastewater still present a challenging problem during crossflow ultrafiltration. Utilizing an inappropriate crossflow velocity (CFV) and transmembrane pressure (TMP) usually leads to rapid cake formation on the membrane surface – significantly reducing filtration efficiency [1]. The use of high CFV and low TMP is the common solution to minimize particle deposition on a membrane surface but usually requires larger pump sizes that utilize substantial amounts of energy. The application of an electric field to enhance membrane filtration efficiency is another technique which can be employed in reclaiming wastewater containing charged particles [11].

Membrane electro-filtration, as it is commonly called, influences the movement and electrophoretic mobility of particles – minimizing concentration polarization and improving permeate flux [8, 16]. It is commonly carried out with the use of direct current (DC) - although an alternating current (AC) can also be used [22]. The method has been shown to increase permeate flux by factors ranging from 3 to 10 during experiments involving different types of solution [8, 15, 19]. Aside from increased permeate flux, filtrate obtained from the method has also been shown to have water of a quality suitable for reuse [11, 20, 21]. Experiments involving electro-ultrafiltration of CED paint particles were previously carried out by Radovich and Chao [16] using flat sheet polymeric membranes. Their work showed that the application of an electric field across the membrane can interrupt the formation of the concentration polarization layer. Radovich and Chao postulated that the electric field pulls the CED paint particles away

from the membrane surface resulting in the prevention of paint particle accumulation and cake layer formation.

The main objective of this chapter is to evaluate the influence of an applied electric field on the performance of a 50-nm ZrO_2 ceramic membrane during crossflow ultrafiltration of model wastewater containing CED paint particles. The different forces acting on the CED paint particles were calculated to determine their effects on particle deposition on the membrane surface. Likewise, different resistances were also calculated using a modified resistance-in-series [11] model in order to have a thorough understanding of permeate flux behaviour under the influence of an electric field. Filtration and energy consumption results obtained from this work were subsequently compared to results obtained from our previous work [1] in order to determine the benefits of applying an electric field in the ultrafiltration of this kind of wastewater.

5.2 Materials and methods

5.2.1 Actual wastewater

The acquisition and analysis of actual wastewater samples are similar to the ones described in Chapter 4.

5.2.2 Model wastewater

The preparation and analysis of the model wastewater samples are similar to the ones described in Chapter 4.

5.2.3 Ceramic membrane

The ceramic membrane used in the experiments was the same ZrO_2 membrane as used

in our previous work, Chapter 4, and subsequently published [1]. It has a nominal pore size of 50 nm and an effective membrane area of 0.005 m^2. Its dimensions are as follows: internal diameter, i.d. = 7 mm; outside diameter, o.d. = 10 mm; length, l = 250 mm. The isoelectric point of the active layer is approximately 7 [17] and therefore the membrane surface charge is positive or negative respectively below or above a pH of 7. This membrane was supplied by Pall Corporation Australia.

5.2.4 Ceramic ultrafiltration system

The schematic diagram of the ceramic electro-ultrafiltration system used in the experiments is shown in Figure 5.1. A variable speed pump (Hydracell CC Pump Model No. D/G-03-S) with ½ hp motor was used to deliver wastewater into the stainless steel ceramic module while DC supply equipment (BWD Instruments Model 246A; 0-70 V; 5 A) was used to deliver different magnitudes of voltages across the membrane. Since the CED paint particles are positively charged, the anode and cathode were positioned at the inlet and outlet ports of the membrane module respectively as shown in Figure 5.1. Both the anode and cathode were made of SS 316 material. For each experiment, the membrane filtrate was collected into a container and weighed while reject water was returned into the feed tank. Parameters such as pressures, temperatures, weights, and water qualities (pH and conductivity) were monitored at 2 minute intervals using probes and recorders connected to a computer. Each experiment run lasted for ~ 120 minutes.

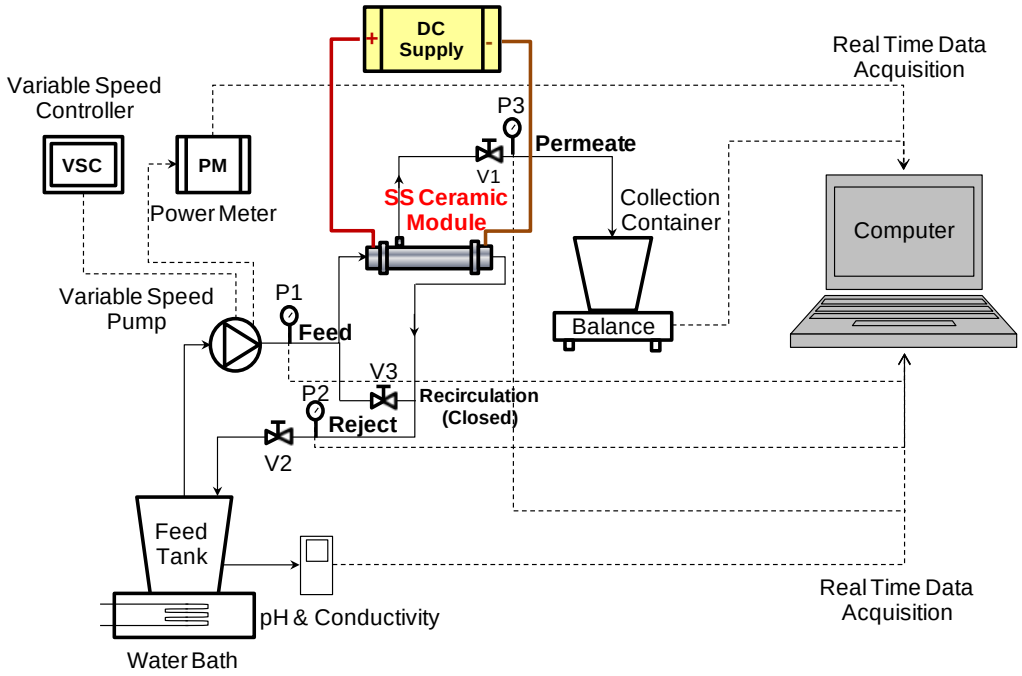

Figure 5.1: Schematic diagram of ceramic electro-ultrafiltration system used in the experiments – P1 – feed pressure; P2 – concentrate pressure; P3 – permeate pressure; V1 – permeate valve; V2 – concentrate valve; V3 – recirculation valve. The black solid lines represent water flow while the black broken lines represent real time data acquisition. Likewise, the red solid line represents the positive charge while the brown solid line represents the negative charge.

5.2.5 Operating parameters

Filtration experiments were performed at a constant CFV of 2.4 m s^{-1}. A CFV of 2.4 m s^{-1} was chosen because, at this velocity, concentration polarization resistances obtained in our previous work were the highest [1]. In order to produce an electric field, different magnitudes of voltages (20, 40 and 60 V) were applied across the ceramic membrane at a current of 0.5 A. The different magnitudes of the applied voltages used were evaluated at TMPs of 100, 200 and 300 kPa. Meanwhile, feedwater temperature was maintained within 19 – 24 °C by submerging the feed tank halfway into a water bath.

Likewise, conductivity and feedwater pH were also maintained within 100.0 – 120.0 µS cm^{-1} and 5.0 – 7.0, respectively by intermittent dilution of deionized water.

5.2.6 Analytical methods

The size distribution and zeta potential (ζ) of particles present in the model and actual wastewater samples were determined using a Malvern Zetasizer Nano Series (Nano-ZS). The results were then compared to each other to ascertain that the particle sizes present in the model wastewater reflected those in the actual wastewater [1]. Turbidity measurements were used to estimate total paint particle rejection rates. Feed and permeate water turbidity were measured using a La Motte 2020 Series Turbidity Meter. Turbidity rejection rates (R_{Turb}, %) were calculated using Eq. (1):

$$R_{Turb} = [(T_F - T_P) / T_F] \times 100\ \% \quad (1)$$

where T_F is the feed turbidity (NTU) and T_P is the permeate turbidity (NTU).

5.2.7 Membrane cleaning

The membrane cleaning protocol used in this work consists of tap water flushing, chemical cleaning and deionized water rinsing [1]. Tap water flushing was carried out for 15 minutes at a temperature of 45 °C. It was then followed by chemical cleaning using Ultrasil 10 – a commercially available cleaning chemical containing Sodium Hydroxide (NaOH) and Tetrasodium EDTA. Chemical cleaning parameters used were as follows: 1.5% v/v Ultrasil 10 solution, pH range of 11 – 12, temperature range of 45 – 50 °C, pressure of 100 kPa, cross flow velocity of 2.4 m s^{-1} and cleaning time of 45 – 60 minutes. After chemical cleaning, the membrane was rinsed with deionized water

for 15 minutes at a temperature of 21 °C. Chemical cleaning and deionized water rinsing were repeated when the pure water flux of the regenerated membrane was below its initial measured value. The cleaning chemical used was supplied by ECOLAB Australia.

5.3 Results and discussion

5.3.1 Wastewater characteristics

The average water qualities for both the model and actual wastewater samples are shown in Table 5.1.

Table 5.1: Average water qualities of model wastewater containing 5 % v/v CED paint and actual wastewater generated at the final rinsing stage of post-electrodeposition painting

pH		Conductivity (μS/cm)		TDS (mg/L)		Turbidity (NTU)	
Actual	Model	Actual	Model	Actual	Model	Actual	Model
6.7	6.2	56.2	102.0	44.0	79.9	262.0	4644.3

As shown in Table 5.1, the model wastewater has a worse water quality compared to the actual wastewater and hence represents a worst case scenario. Additionally, at higher TMPs, the CED paint particles present in the model wastewater deposit extensively on the membrane surface – even at higher CFVs [1]. Such behaviour results in rapid flux decline and relatively lower steady-state flux.

CED paint particle sizes present in the model and actual wastewater samples ranged from 78 to 342 nm and 91 to 531 nm respectively – with common particle sizes in the

range of 91 to 342 nm (as shown in Figure 5.2). The presence of larger particle sizes in the actual wastewater sample was due to particle agglomeration of non-adhered paint on car surfaces. Since majority of the particle sizes measured are present in both samples, it can be deduced that the model wastewater used in the experiments is representative of the actual wastewater generated at the final rinsing stage of the post-electrodeposition process.

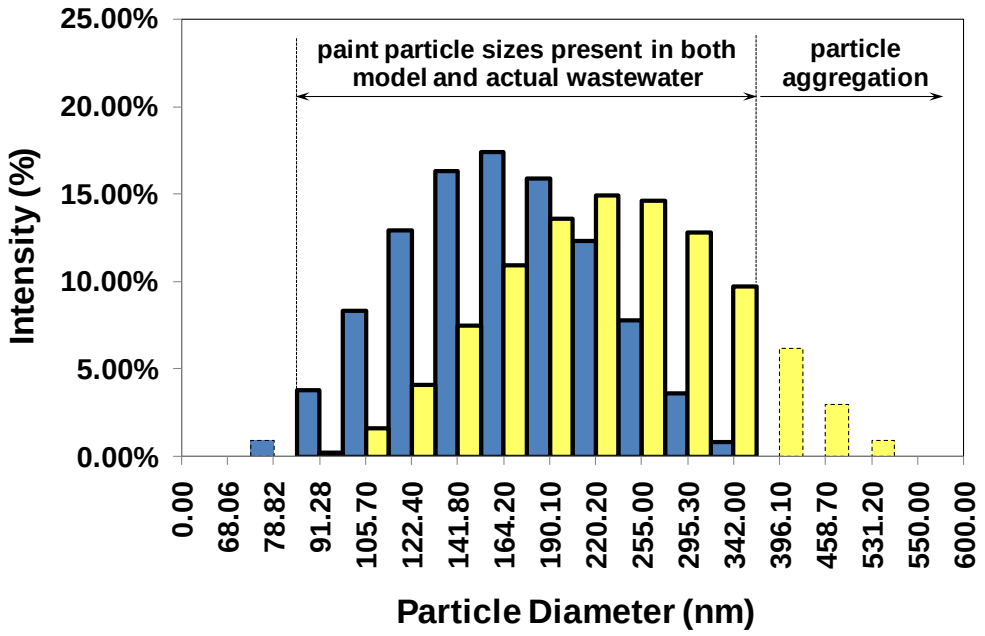

Figure 5.2: Particle size distribution for model and actual wastewater samples. Bars colored blue represent particle sizes in the model wastewater while bars colored yellow represent particle sizes in the actual wastewater generated at the final rinsing stage of post-electrodeposition process.

Particle stability in wastewater can be assessed based on the zeta potential (ζ). This parameter is an important measure of particle-particle and particle-surface interactions [10]. Such interactions influence membrane performance – especially in terms of fouling and permeate flux decline. The average zeta potential of the CED paint particles present in the model wastewater is 58 ± 2 mV at pH = 6.2. This value suggests

that the particles have good stability and are well dispersed in solution [4]. Since the paint particles are well dispersed in solution, particle aggregation is unlikely to happen. In this particular case, the particle sizes present in the model wastewater sample can be assumed to be the same throughout the experiments. The data used for plotting Figure 5.2 are available in the accompanying CD (Appendix 5.1).

5.3.2 Electric field (E) and critical electric field (E_{CR}) strengths

A schematic diagram of the ceramic ultrafiltration module with an applied voltage is shown in Figure 5.3. The diagram shown is similar to applying a charge into a conducting wire but in this specific case, the model wastewater acts as the electrical conductor. Upon the application of charge on the electrodes, an electrical field directly proportional to the applied voltage is produced on the module. The electric field (E, V/m) strength produced on the module can be estimated using Eq. (2) [9]:

$$E = V / L \qquad (2)$$

where V is the applied voltage (V) and L is the distance between the electrodes (m).

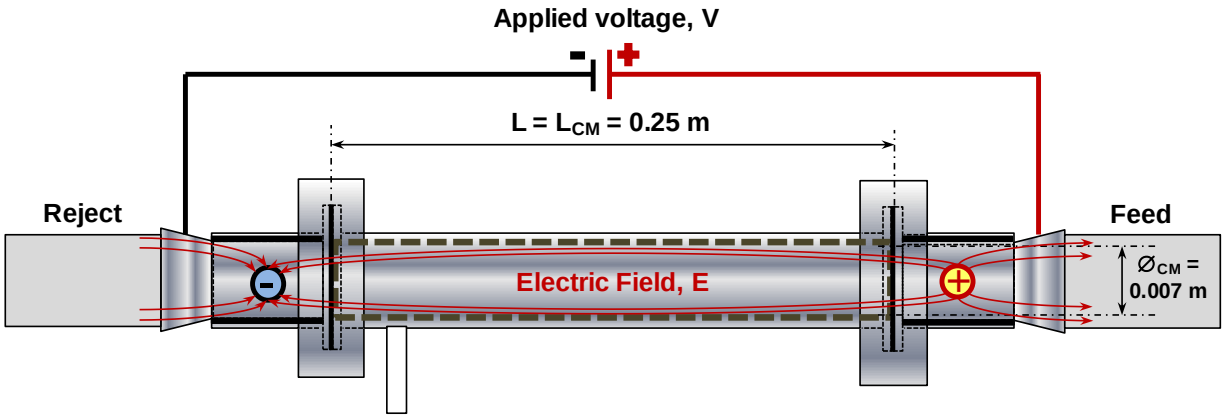

Figure 5.3: Schematic diagram of ceramic ultrafiltration module with an applied voltage.

In order to determine whether the magnitude of applied voltage will have any effect on filtration performance, the resultant electric field, E must be compared against the critical electric field, E_{CR}. The critical electric field (E_{CR},V/m) strength, defined as the electric field strength at which particle migration velocity into the membrane is zero, can be estimated using Eq. (3) [11]:

$$E_{CR} = J_{MAX} / \mu_P \quad (3)$$

where J_{MAX} is the maximum flux at a specified TMP and CFV ($m^3\ m^{-2}\ s^{-1}$) and μ_P is the electrophoretic mobility of the paint particles ($m^2\ V^{-1}\ s^{-1}$). The measured electrophoretic mobility (μ_P) of paint particles present in the model wastewater is 4.473E-08 $m^2\ V^{-1}\ s^{-1}$. As a general rule, when $E < E_{CR}$, filtration rate can still be improved by increasing the electric field (E). Alternatively, when $E \geq E_{CR}$, filtration rate is unlikely to improve even if the electric field (E) is increased [8, 11]. The results of the calculation for both the electric field and critical electric field strengths are summarized in Table 5.2. The calculations for the electric field and critical electric field strengths are shown in Appendix 5.2 – attached at the end of the thesis.

Table 5.2: Summary of the calculated electric field (E) and critical electric field (E_{CR}) strengths

Applied Voltage, V	E, V m^{-1}	TMP, kPa	E_{CR}, V m^{-1}
20	82	100	380
40	163	200	447
60	245	300	492

5.3.3 Forces acting on CED paint particles

Particle deposition on a membrane surface is commonly influenced by hydrodynamic

and surface interaction forces [18]. Hydrodynamic forces include drag, lift and gravitational forces while surface interaction forces include electrostatic double-layer and Van der Waals forces. The magnitudes of hydrodynamic and surface interaction forces depend on particles sizes present in the solution. In general, drag, lift, gravitational, and Van der Waals forces increase as particle sizes increase while electrostatic double-layer force decreases as particle sizes increase.

Drag forces experienced by CED paint particles during crossflow ultrafiltration can be estimated using Eqs. (4) and (5) [1, 14]:

$$F_{FD} = 3\pi\eta_F Ø_P J \quad (4)$$

where F_{FD} is the drag force due to filtrate flow (N); η_F is the viscosity of the model wastewater water at 20 °C (0.001002 Pa s); $Ø_P$ is the particle diameter (m); and J is the permeate flux ($m^3\ m^{-2}\ s^{-1}$).

$$F_{VD} = 0.638\ (\pi \Delta P Ø_{CM} Ø_P^{\,2} / L_{CM}) \quad (5)$$

where F_{VD} is the drag force due to feed velocity (N); ΔP is the pressure drop in the ceramic membrane during filtration (Pa); $Ø_{CM}$ is the internal diameter of the ceramic membrane (m); $Ø_P$ is the particle diameter (m); and L_{CM} is the length of the ceramic membrane (m).

The lift force (F_L, N) which is commonly due to shear flow can be estimated using Eq. (6) [3] while the gravitational force (F_G, N) can be estimated using Eq. (7) [18]:

$$F_L = 0.761 \left(\tau_W^{1.5} Ø_P^3 \rho_F / \eta_F \right) \quad (6)$$

where τ_W is the shear stress acting on the cake boundary (Pa); $Ø_P$ is the particle diameter (m); ρ_F is the density of the feed water at 20 °C (998.2 kg m^{-3}); and η_F is the viscosity of the feed water at 20 °C (0.001002 Pa s).

$$F_G = (\pi Ø_P^3 / 6) (\rho_P - \rho_F) g \quad (7)$$

where $Ø_P$ is the particle diameter (m); ρ_P is the particle density at 20 °C (1250 kg m^{-3}); ρ_F is the density of the feed water at 20 °C (998.2 kg m^{-3}); and g is the gravitational acceleration constant (9.81 m s^{-2}).

The Van der Waals and electrostatic double-layer forces between CED paint particles and membrane wall can be estimated using Eqs. (8) [3, 12] and (9) [5] respectively:

$$F_{VDW} = h\varpi Ø_P / 32\pi \bar{a}^2 \quad (8)$$

where F_{VDW} is the Van der Waals adhesive force (N); $Ø_P$ is the particle diameter (m); $h\varpi$ is the Lifschitz-van der Waals constant (1.0E-20 J); and $\bar{a}$ is the adhesive distance (4.0E-10 m) [13]. Since the analysis is focused on particle-membrane interaction, the adhesive distance $\bar{a}$ is considered a constant.

$$F_{EDL} = (4\pi R^* / \varepsilon\varepsilon_O \aleph) [\sigma_1\sigma_2 e^{-\aleph x} + 0.5 (\sigma_1^2 \sigma_2^2) e^{-2\aleph x}] \quad (9)$$

where F_{EDL} is the electrostatic double-layer force (N); $R^*=R_1$ ($R_2 = \infty$) is the particle radius interacting with a flat surface (m); ε is the dielectric permittivity of water at 20 °C (80.2); ε_O is the permittivity of vacuum (8.85E-12 C^2 N^{-1} m^{-2}); σ_1 is the surface charge density of particles (C m^{-2}); σ_2 is the surface charge density of the ceramic membrane's active layer (C m^{-2}); $\aleph$ is the inverse Debye length (m); and x is the distance between particles and membrane wall (m). The electrostatic double layer force (F_{EDL}) can either be repulsive or attractive depending on the net surface charge exhibited by both the particles and the membrane active surface.

The application of an electric field during ultrafiltration will add an additional force known as electrophoretic force (F_E). This force distracts particle migration onto the membrane surface resulting in reduced particle deposition. The electrophoretic force (F_E, N) can be estimated using Eq. (10) [19]:

$$F_E = 3\pi\eta_F \text{Ø}_P \lambda \mu_P E \quad (10)$$

where η_F is the viscosity of the feed water at 20 °C (0.001002 Pa s); Ø_P is the particle diameter (m); λ is the concentration correction factor, μ_P is the electrophoretic mobility of paint particles (4.473E-08 m^2 V^{-1} s^{-1}), and E is the electric field strength (V/m).

An analysis of the different forces acting on the CED paint particles during electro-ultrafiltration is shown in Figure 5.4.

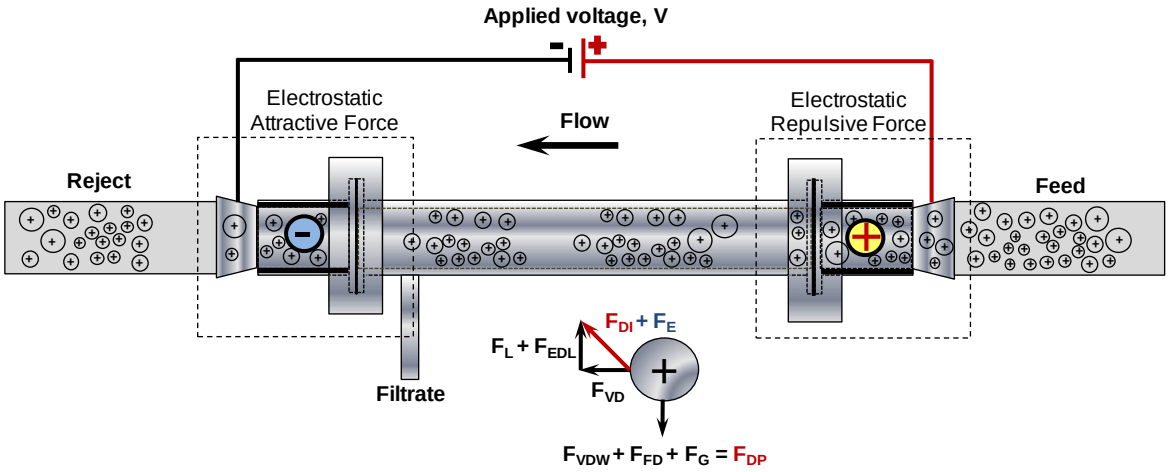

Figure 5.4: Forces acting on a suspended CED paint particle during crossflow electro-ultrafiltration of model wastewater – F_L is the lift force (N); F_{FD} is the drag force due to filtrate flow (N); F_{VD} is the drag force due to feed velocity (N); F_{VDW} is the Van der Waals adhesive force (N); F_{EDL} is the electrostatic double-layer force (N), F_G is the gravitational force (N), F_E is the electrophoretic force (N), F_{DI} is the deposition-inhibiting force (N), and F_{DP} is the deposition-promoting force.

The hydrodynamic and surface interaction forces mentioned above can generally be classified into two main categories namely, deposition-inhibiting and deposition-promoting forces. Components of the deposition-inhibiting force (F_{DI}) include velocity drag and lift forces while components of the deposition-promoting force (F_{DP}) include adhesive, filtrate drag, electrostatic double layer, and gravitational forces. Therefore, the deposition-inhibiting and deposition-promoting forces can be estimated using Eqs. (11) and (12) respectively:

$$F_{DI} = (F_{VD}^{\ 2} + (F_L + F_{EDL})^{\ 2})^{0.5} \quad (11)$$

$$F_{DP} = F_{VDW} + F_G + F_{FD} \quad (12)$$

Taking into account the electrophoretic force (F_E), Eq. (11) becomes:

$$F_{DI} = [(F_{VD}^2 + (F_L+F_{EDL})^2)^{0.5}] + F_E \quad (13)$$

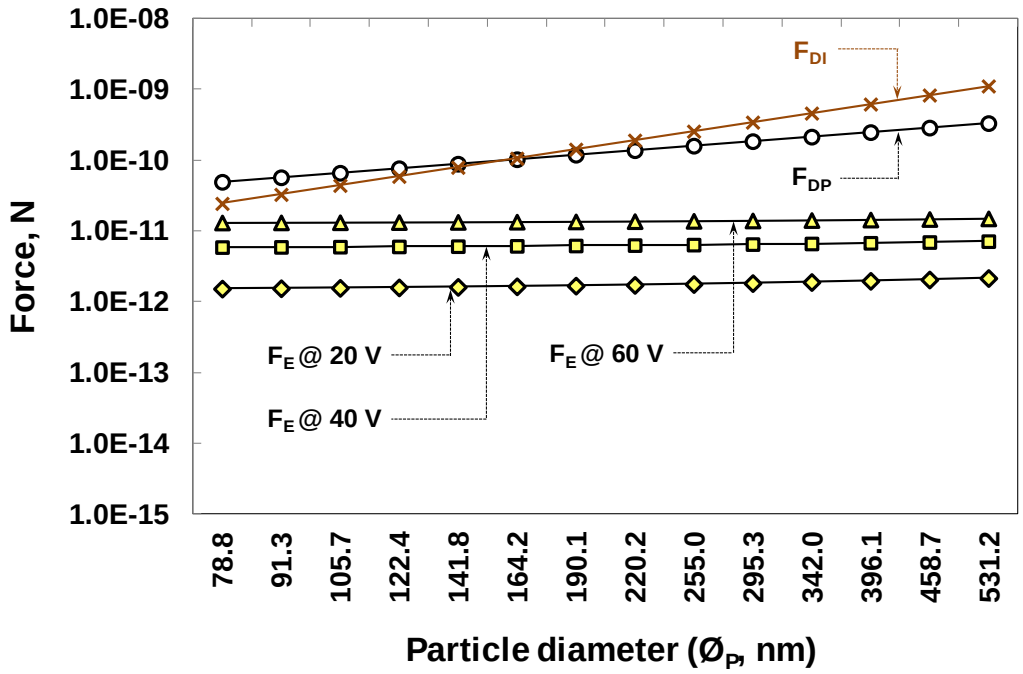

Figure 5.5: Magnitudes of forces acting on the CED paint particles during electro-ultrafiltration of model wastewater – F_E is the electrophoretic force (N), F_{DI} is the deposition-inhibiting force (N), and F_{DP} is the deposition-promoting force.

Based on the above equations, the magnitudes of the forces acting on the different sizes of CED paint particles present in the model wastewater have been calculated. These are represented in Figure 5.5. The calculations of these forces are shown in Appendix 5.3 – attached at the end of the thesis.

The deposition behaviour of paint particles during ultrafiltration of model wastewater can be explained based on the force balance between the deposition-inhibiting and

deposition-promoting forces. This force balance changes under the influence of an applied electric field. Without an applied electric field, paint particle sizes less than approximately 164 nm are likely to deposit on the membrane surface as shown in Figure 5.5. But with an applied electric field, the range of paint particle sizes likely to deposit on the membrane surface gets smaller (Figure 5.6). Likewise, as the electric field increases, the size of particles likely to deposit on the membrane surface also gets smaller. The smaller particle sizes on the membrane surface will create a thin cake layer resulting in better filtration rate.

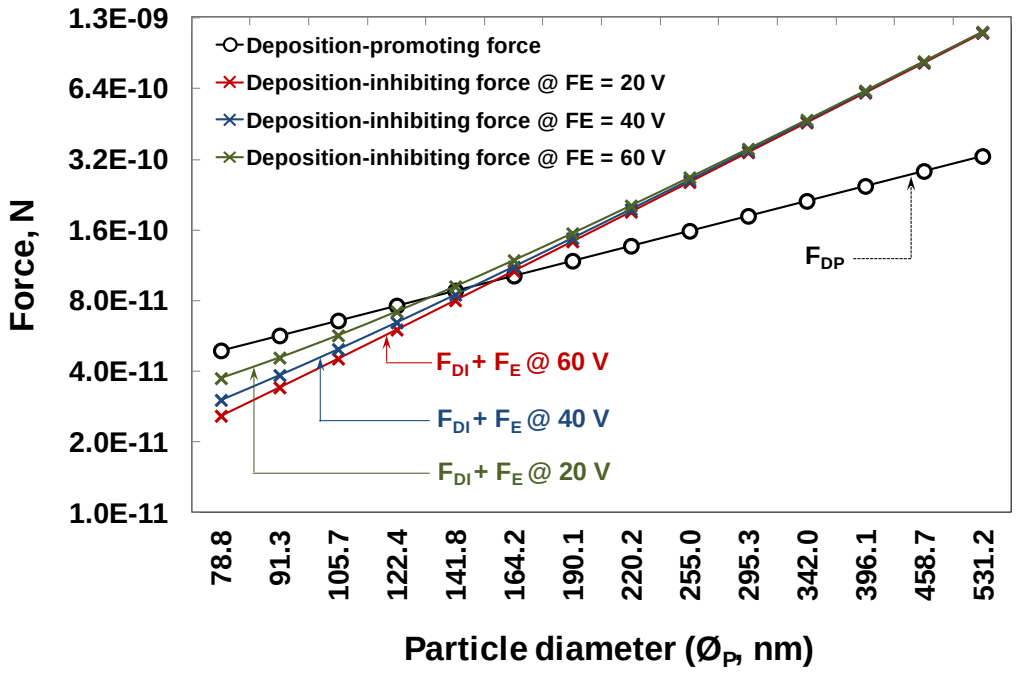

Figure 5.6: Influence of electrophoretic force (F_E) on paint particle deposition.

Prior to entering the membrane module, the CED paint particles experience charge repulsion near the anode (Figure 5.4). Since the velocity drag force (F_{VD}) is relatively larger than the charge repulsion force, majority of the paint particles are carried into the membrane and are repelled from the feed side into the reject side. Once the paint particles are near the reject side, they are attracted by the cathode. Although attraction

between the cathode and paint particles occurs, particle deposition into the cathode is inhibited due to a relatively larger F_{VD}. Therefore, the paint particles are carried by the bulk back into the feed tank.

5.3.4 Membrane flux

In order to determine the influence of an electric field on the filtration performance of the 50 nm ceramic membrane, filtration experiments (each of 120 minutes duration) involving the use of the model wastewater were carried out. Results of the experiments are shown in Figures 5.7a to c. The data used for plotting Figures 5.7a to c are available in the accompanying CD (Appendix 5.4).

a)

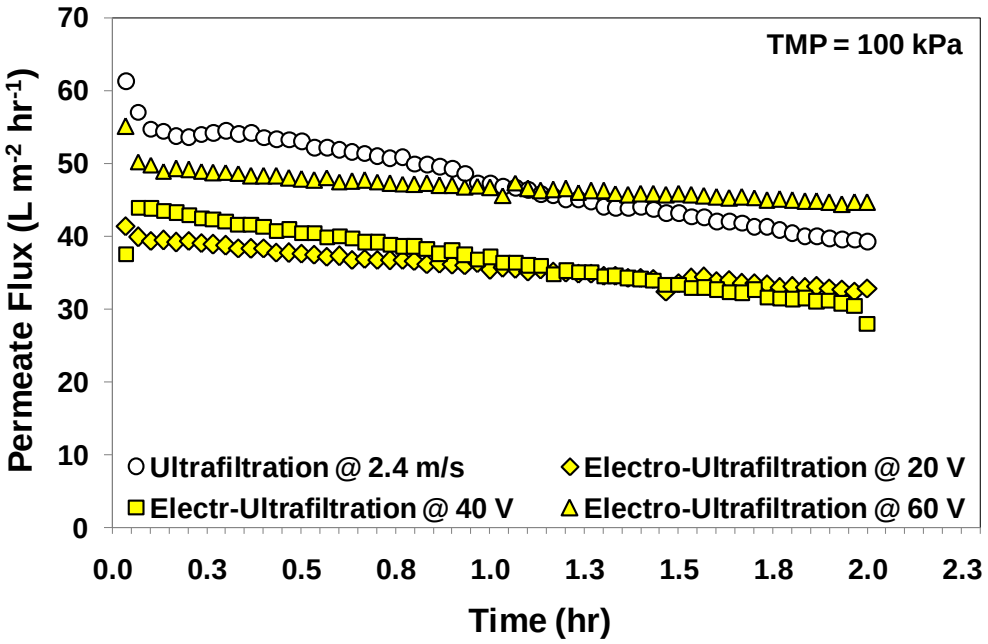

b)

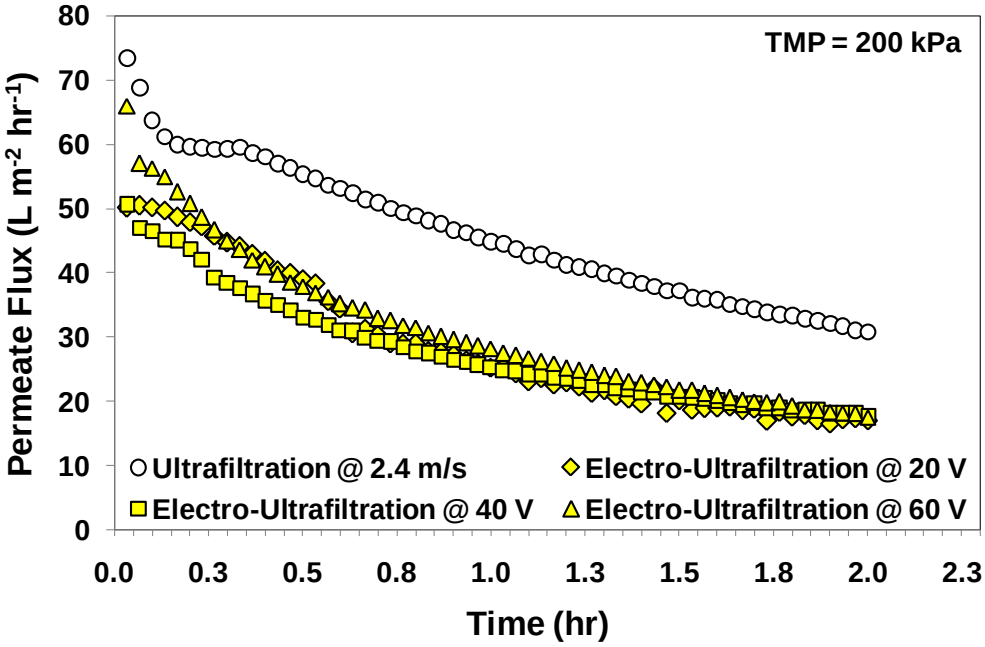

c)

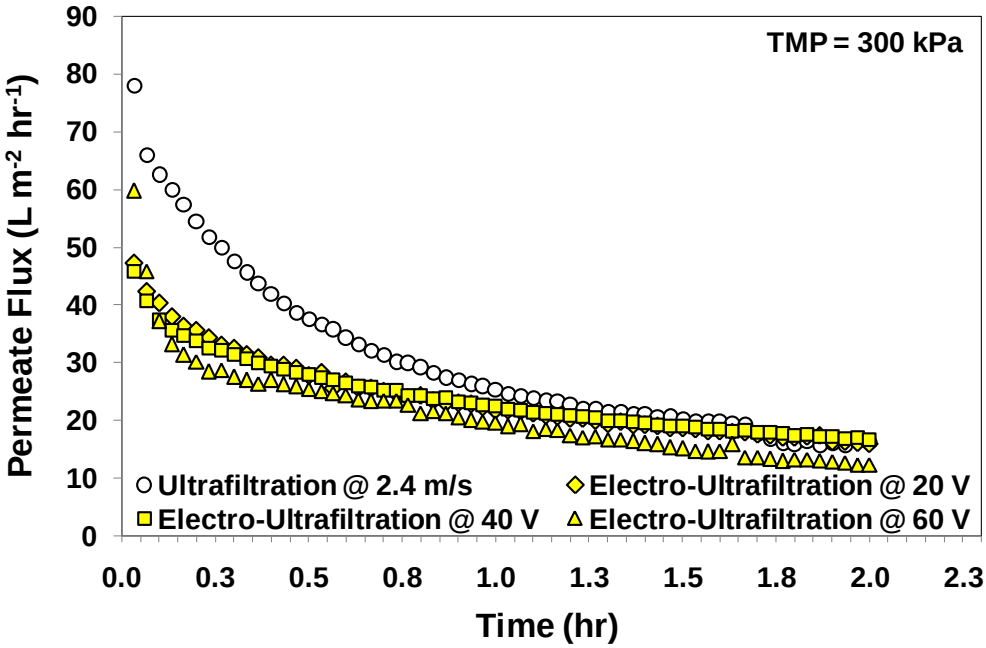

Figure 5.7: Permeate fluxes obtained during electro-ultrafiltration of model wastewater at TMPs of: a) 100 kPa, b) 200 kPa and c) 300 kPa; and CFV of 2.4 m s^{-1}. The permeate flux data for ultrafiltration at 2.4 m s^{-1} was lifted from the authors' previous work [1].

Permeate fluxes (J, $m^3\ m^{-2}\ s^{-1}$) were calculated using Eq. (14):

$$J = 0.001W / A_M\, t \qquad (14)$$

where W is the weight measured by the balance (kg), A_M is the effective membrane area (m^2), t is the sampling time (s).

To account for temperature variations, all permeate fluxes were standardized at a temperature of 20 °C using Eq. (15) [7]:

$$J_{20°C} = J\ (1.03)^{T_S - T_M} \qquad (15)$$

where $J_{20°C}$ is the flux at a standard temperature of 20 °C ($m^3\ m^{-2}\ s^{-1}$), T_S is the standard temperature (20 °C), T_M is the measured temperature (°C).

In general, the results show that permeate fluxes obtained during the electro-ultrafiltration of model wastewater is lower than ultrafiltration. The reason behind this is that charged paint particles undergo a drifting movement when passing through an electric field. The drifting velocity of the paint particles is directly proportional to the strength of the electric field. If the electric field produced by an applied voltage is weak, the drifting velocity will be small and the likelihood of deposition is high due to low particle mobility. But as electric field increases, the drifting velocity also increases and the likelihood for the particles to deposit on the membrane surface lessens due to higher particle mobility. The evidence for this can be clearly seen in Figure 5.7a. At a

TMP of 100 kPa, permeate fluxes increased as the applied voltages were increased to different magnitudes.

At the lowest TMP of 100 kPa, filtration decline rates for electro-ultrafiltration were better than ultrafiltration. This is because as the applied voltages were increased, the sizes of particles deposited on the membrane surface got smaller – as mentioned in Sec. 5.3.3. The smaller particle sizes form a thin cake layer and therefore filtration decline rates measured were slower. The improvement in the flux decline rate was magnified when applied voltage was set to 60 V. At an applied voltage of 60 V, the succeeding permeate fluxes obtained after 60 minutes were higher than ordinary ultrafiltration – as shown in Figure 5.7a.

On the other hand, the effects of the applied voltages at higher TMPs of 200 and 300 kPa were almost negligible as shown in Figures 5.7 b and c. In fact, particle depositions at these TMPs were enhanced as reflected on the filtration rates measured. The enhanced decline in filtration rates may be due to two reasons. Firstly, the electric fields produced by the applied voltages were not sufficient enough to overcome the influence of the TMPs considered (refer to Table 5.2). Secondly, particle deposition on the membrane surface happened very rapidly due to higher TMPs. As the smaller paint particles deposit on the membrane surface, they were continuously compressed leading to lower surface porosity and higher cake resistance – and eventually lower filtration rates. Additionally, it is also worth mentioning that one of the main characteristics of CED paint is that it sticks on the car surface when adequate force is applied (in car manufacturing, voltage will be the applied force). The application of higher TMPs during the electro-ultrafiltration of wastewater containing paint particles is similar to

applying high voltages. At higher TMPs the movement and electrophoretic mobility (μ_P) of the CED paint particles inside the membrane became more restricted. Because of this restriction, the paint particles have a tendency to migrate on the membrane surface due to a higher compressive force. Likewise, the applied electric fields (E) were also overwhelmed by higher TMPs resulting in rapid paint particle deposition on the membrane surface. Such scenario can be addressed by increasing the applied electric field (E) to counteract the effect of higher TMPs – as mentioned in Sec. 5.3.2.

5.3.5 Membrane resistances

The permeate flux behaviour shown in Figures 5.7a to c can be analysed using a modified resistance-in-series model [11]. The general equation for the resistance-in-series model can be written as [6]:

$$J = TMP / \eta_F (R_T) \quad (16)$$

where J is the permeate flux ($m^3\ m^{-2}\ s^{-1}$), TMP is the transmembrane pressure (Pa), η_F is the viscosity of feed water (0.001002 Pa s), and R_T is total membrane resistance (m^{-1}). Under the influence of an electric field, the total membrane resistance (R_T) can be calculated using Eq. (17):

$$R_T = R_{EF} + R_{EC} + R_{EM} \quad (17)$$

where R_{EF}, R_{EC} and R_{EM} are the adsorption, concentration polarization and membrane resistances respectively in the presence of an electric field (m^{-1}). Eq. (17) can be expanded further to yield Eq. (18):

$$R_T = [R_F / (1+ (\eta_F R_F/TMP)\ \mu_P E)] + [R_C / (1 + (\mu_C E/J_C))] + [R_M / (1 + (\mu_M E/J_M))] \quad (18)$$

where R_F is the adsorption resistance in the absence of an electric field (m^{-1}), μ_P is the electrophoretic mobility of the paint particles ($m^2\ V^{-1}\ s^{-1}$), E is the electric field (V/m), R_C is the concentration polarization resistance in the absence of an electric field (m^{-1}), μ_C is the cake electro-osmotic mobility ($m^2\ V^{-1}\ s^{-1}$), J_C is the flux through the cake in the absence of an electric field ($m^3\ m^{-2}\ s^{-1}$), R_M is the membrane resistance in the absence of an electric field (m^{-1}), μ_M is the membrane electro-osmotic mobility, and J_M is the membrane flux in the absence of an electric field. The total resistance (R_T) as well as its components were calculated using Eqs. (16) to (18). The results of the calculations are shown in Figure 5.8 and Table 5.3. Calculations for the membrane resistances are shown in Appendix 5.5 – attached at the end of the thesis.

Under the influence of an electric field, the total resistances (R_T) encountered during the ultrafiltration of model wastewater containing CED paint particles were dependent on both the applied voltage and pressure. At the lowest TMP of 100 kPa, the total resistance is a function of applied voltage. As the applied voltage is increased, the total resistance decreased. The decrease in total resistance can clearly be seen at an applied voltage of 60 V – as shown in Figure 5.8. It is also worth mentioning that the total resistances obtained at a TMP of 100 kPa were the lowest and their increase over time was minimal. The relatively low resistance encountered at 100 kPa explains the reason why permeate fluxes obtained in Figure 5.7a are generally better as compared to permeate fluxes obtained at much higher TMPs.

At higher TMPs of 200 and 300 kPa, the total resistance becomes a function of TMP, and the effect of the different magnitudes of applied voltages used is negated. Increasing the TMP from 100 to 200 kPa resulted in a medium rate of increase in the total resistance while increasing the TMP further to 300 kPa resulted in a rapid rate of increase in the total resistance. The total resistances obtained at TMPs of 200 and 300 kPa explains the permeate behaviours shown in Figures 5.7b and c. Permeate fluxes obtained at a TMP of 200 kPa were relatively lower compared to the permeate fluxes obtained at a TMP of 100 kPa but were better than the permeate fluxes obtained at a TMP of 300 kPa.

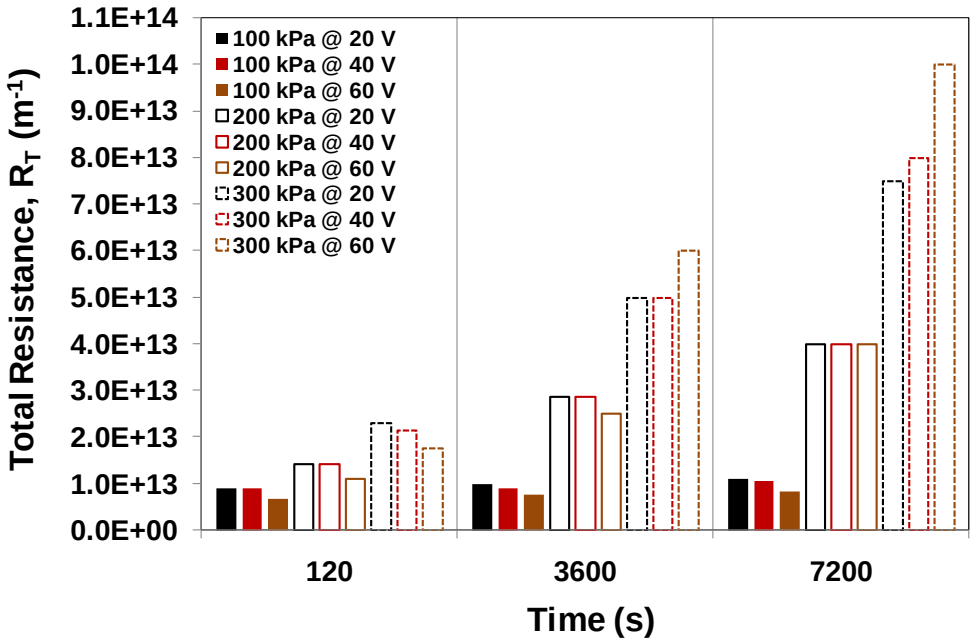

Figure 5.8: Total resistance (R_T) encountered during electro-ultrafiltration of model wastewater containing CED paint particles.

In general, the total resistances obtained during electro-ultrafiltration were similar to those obtained for ultrafiltration (Figure 5.9). The total resistances for both set-ups show an increasing trend over time. But during electro-ultrafiltration at 100 kPa, the total resistances obtained show gradual increases (Figure 5.8). In fact as the applied

voltage increases, the value of the total resistance decreases. Likewise, the total resistances obtained during electro-ultrafiltration at 100 kPa were generally lower compared to those obtained for ultrafiltration.

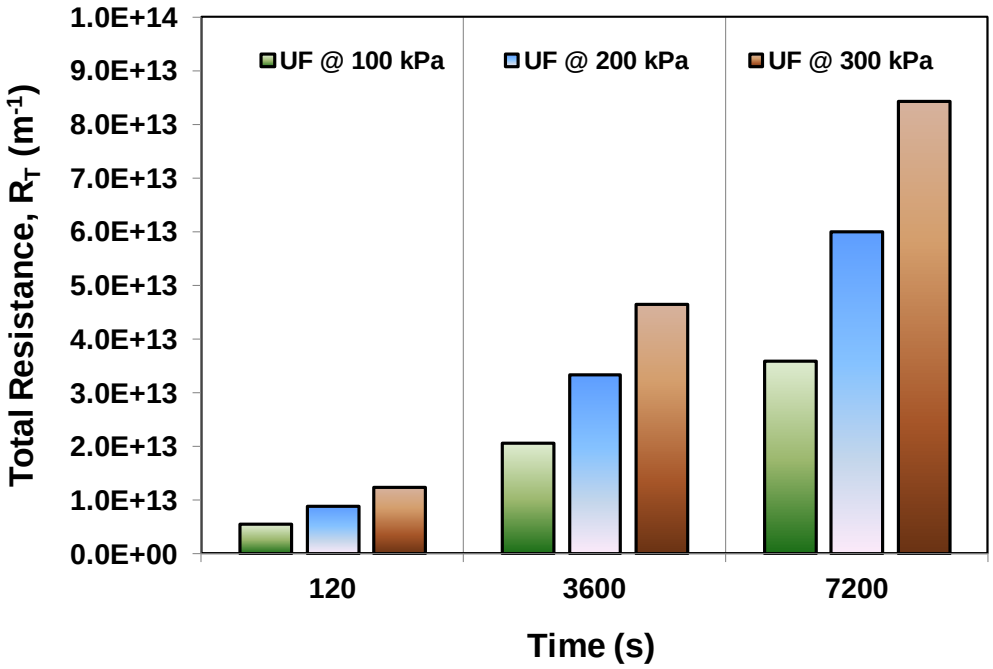

Figure 5.9: Total resistance (R_T) encountered during ultrafiltration of model wastewater containing CED paint particles. Data lifted from the authors' previous work [1].

The components of the total resistances (R_T) discussed above are shown in Table 5.3. At a TMP of 100 kPa, the adsorption resistances (R_{EF}) obtained showed an increasing trend but their values generally decreased when the magnitudes of the applied voltages were increased. Meanwhile, the concentration polarization resistances (R_{EC}) obtained showed a decreasing trend and similar to R_{EF}, their values decrease when the magnitudes of the applied voltages were increased. The trends shown by both R_{EF} and R_{EC} suggest that, at a TMP of 100 kPa, particle deposition on the membrane surface is a function of the applied voltages. As the magnitudes of the applied voltages are increased, the sizes of paint particles that are likely to deposit on the membrane surface get smaller. Although this is the case, the paint particles that are likely to deposit on the

membrane surface are generally larger than the membrane pores – as shown in Figure 5.2. Therefore, particle infiltration into the membrane pores is lessened. Likewise, the cake layer formed by these smaller paint particles will be thinner and will have better permeation rates over time.

On the other hand, at TMPs of 200 and 300 kPa, paint particle deposition onto the membrane surface becomes a function of pressure, and as mentioned previously, the effect of the applied voltages used is negligible. At these conditions, the rate of paint particle deposition on the membrane surface depends on the magnitude of the TMP – the higher the TMP, the faster the particles will deposit on the membrane surface. This scenario is clearly reflected in Table 5.3, with the concentration polarization resistance (R_{EC}) being the dominant resistance at higher TMPs.

Table 5.3: Different resistances obtained during electro-ultrafiltration of model wastewater containing CED paint particles

Parameters	R_{EM} (x 10^{12} m^{-1})	R_{EF} (x 10^{12} m^{-1})	R_{EC} (x 10^{12} m^{-1})
100 kPa; 20 V			
120 s	1.16	0.96	6.95
3600 s	1.17	5.28	3.53
7200 s	1.18	7.64	2.28
100 kPa; 40 V			
120 s	1.19	0.92	6.93
3600 s	1.20	4.42	3.44
7200 s	1.21	5.97	3.32
100 kPa; 60 V			
120 s	1.21	0.89	4.55
3600 s	1.23	3.81	2.64
7200 s	1.25	4.90	2.16
200 kPa; 20 V			
120 s	1.16	0.97	12.10

3600 s	1.17	5.84	21.50
7200 s	1.18	8.88	29.90
200 kPa; 40 V			
120 s	1.18	0.96	12.10
3600 s	1.21	5.28	22.00
7200 s	1.23	7.64	31.10
200 kPa; 60 V			
120 s	1.20	0.94	8.95
3600 s	1.24	4.81	18.90
7200 s	1.28	6.70	31.90
300 kPa; 20 V			
120 s	1.16	0.98	20.90
3600 s	1.20	6.06	42.60
7200 s	1.22	9.39	64.20
300 kPa; 40 V			
120 s	1.18	0.97	19.20
3600 s	1.26	5.64	43.00
7200 s	1.31	8.42	70.20
300 kPa; 60 V			
120 s	1.19	0.96	15.50
3600 s	1.33	5.28	53.50
7200 s	1.42	7.64	90.70

Because particle deposition is faster at higher TMPs, the cake layer formed on the surface of the membrane would increase in thickness rapidly and when compressed, will result in higher cake resistance over time – as shown in Table 5.3. The influence of the adsorption resistance (R_{EF}) at the TMPs considered was relatively small compared to concentration polarization resistance. Although the values obtained for adsorption resistances show a decreasing trend, this effect is not a result of the applied voltage but rather of the thickness of the cake layer formed. The cake layer formed on the surface of the membrane acts as another layer of resistance and therefore the thicker this layer gets, the lesser chance for the paint particles to infiltrate into the membrane pores.

The adsorption resistances obtained during electro-ultrafiltration of the model wastewater were relatively lower than those obtained for ultrafiltration (Table 5.4). This suggests that the electrophoretic force helped in inhibiting the infiltration of paint particles into the membrane pores. Likewise, the concentration polarization resistances obtained for electro-ultrafiltration were also generally lower than those obtained for ultrafiltration.

Table 5.4: Different resistances obtained during ultrafiltration of model wastewater containing CED paint particles. Data lifted from the authors' previous work [1]

Parameters	R_M (x 10^{12} m^{-1})	R_F (x 10^{12} m^{-1})	R_C (x 10^{12} m^{-1})
100 kPa			
120 s	1.14	0.99	3.43
3600 s	1.14	6.54	12.90
7200 s	1.14	10.6	24.20
200 kPa			
120 s	1.14	0.99	6.86
3600 s	1.14	6.54	25.80
7200 s	1.14	10.6	48.40
300 kPa			
120 s	1.14	0.99	10.30
3600 s	1.14	6.54	38.80
7200 s	1.14	10.6	72.60

5.3.6 Turbidity rejection rates

Turbidity rejection rates measured for all experiments were above 99.5% as shown in Figure 5.10. The results suggest that CED paint particle rejection in the model wastewater is mainly a function of the membrane pore size. This can be validated by the resistances shown in Table 5.3. For example, at TMPs of 200 and 300 kPa, the concentration polarization resistances were significantly higher than the adsorption

resistances – suggesting that majority of the CED paint particles just sit on the membrane surface. Meanwhile, the CED paint particles that find their way into the membrane pores get trapped inside the walls and majority of these particles never end up in the filtrate. Additionally, it can also be deduced that the chosen membrane pore size is suitable for wastewater containing suspended CED paint particles. It is also worth mentioning that the difference in turbidity rejection rates between electro-ultrafiltration and ultrafiltration is negligible as shown in Figure 5.10. The calculations for the turbidity rejection rates are available in the accompanying CD (Appendix 5.6).

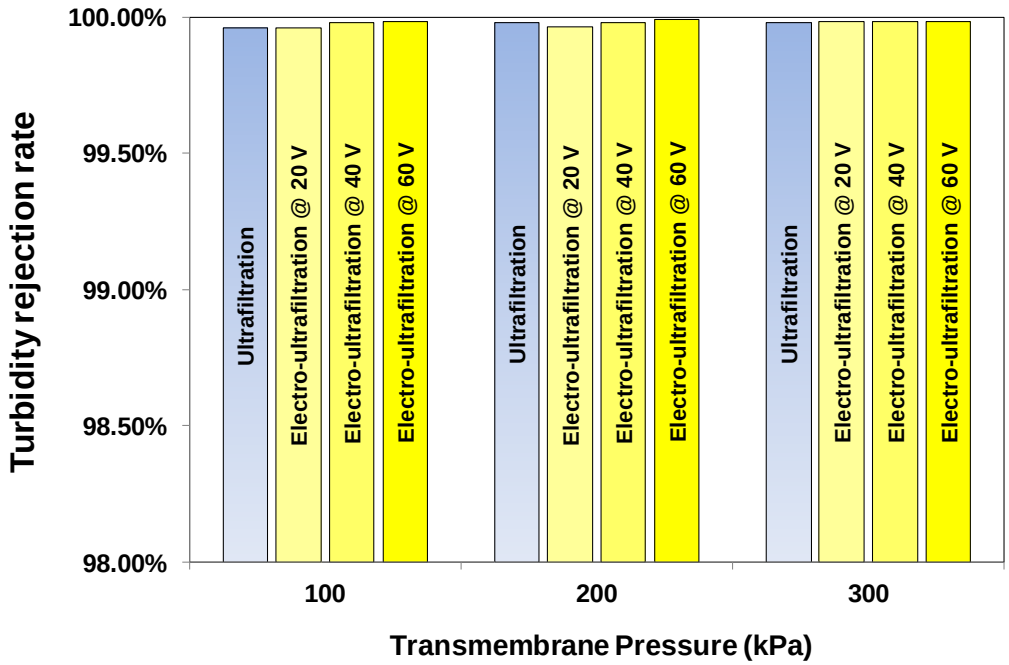

Figure 5.10: Turbidity rejection rates of the 50-nm ceramic membrane during electro-ultrafiltration and ultrafiltration of model wastewater containing CED paint particles. Data for ultrafiltration lifted from the authors' previous work [1]

5.3.7 Energy consumption

To determine the energy consumption of the electro-ultrafiltration set-up at different combinations of TMPs and applied voltages, the average power consumptions of the pump motor and the DC supply equipment were measured. The measured power

consumptions were subsequently used to calculate the total energy ($EC_{T,}$ kWh) consumptions using Eq. (19):

$$EC_T = EC_1 + EC_2 \quad (19)$$

where E_1 is the energy consumption of the DC supply equipment (kWh) and E_2 is the energy consumption of the pump motor (kWh). EC_1 and EC_2 can both be obtained by multiplying the measured power (kW) by time (h). Therefore Eq. (19) can be rewritten as:

$$EC_T = P_1t + P_2t \quad (20)$$

where P_1 is the power utilized by the DC supply equipment, P_2 is the power utilized by the pump motor and t is the length of experiment run considered (h). The specific energy consumption (kWh/m^3) was subsequently calculated using Eq. (21)

$$EC_{SP} = EC_T / V_P \quad (21)$$

where V_P is the volume of permeate produced per experiment run (m^3).

The specific energy consumption (kWh/m^3) data for electro-ultrafiltration were eventually compared to the specific energy consumption data previously obtained for ultrafiltration at a CFV of 2.4 m s^{-1}. Table 5.5 shows the specific energy consumption comparisons between electro-ultrafiltration and ultrafiltration with respect to treatment of model wastewater containing CED paint particles. The calculations for the specific

energy consumption of the electro-ultrafiltration system are available in the accompanying CD (Appendix 5.7).

The comparison between the specific energy consumption of electro-ultrafiltration and ultrafiltration was focused at a TMP of 100 kPa. At this TMP, specific energy consumptions were relatively lower and the flux decline rates measured were slower. On the other hand, at TMPs of 200 and 300 kPa, specific energy consumptions obtained were higher. Likewise, at TMPs of 200 and 300 kPa, filtration decline rates were rapid and the steady – state permeate flow rates (Table 5.6) obtained were very low.

Table 5.5: Comparison of energy consumptions between electro ultrafiltration and ultrafiltration with respect to treatment of model wastewater containing CED paint particles. Energy consumption data for ultrafiltration was lifted from Chapter 4.

CFV (m/s)	Pressure (kPa)	Voltage (Volts)	Energy Consump. (kWh)	Volume (m^3)	Specific Energy Consump. (kWh/m^3)
2.4	100	20	0.305	0.0003	1017
		40	0.325	0.0003	1083
		60	0.345	0.0004	863
2.4	200	20	0.318	0.0002	1590
		40	0.338	0.0002	1690
		60	0.358	0.0002	1790
2.4	300	20	0.319	0.0002	1595
		40	0.339	0.0002	1695
		60	0.359	0.0001	3590
2.4	100	0	0.285	0.0004	713
	200	0	0.298	0.0003	993
	300	0	0.299	0.0002	1495

At a TMP of 100 kPa and CFV of 2.4 m s^{-1}, the specific energy consumption decreases as the applied voltage is increased. In contrast, at higher pressures of 200 & 300 kPa (w/ CFV the same), specific energy consumption increases as applied voltage is increased. Similarly, for ultrafiltration, specific energy consumptions increase as TMP is increased.

The addition of an applied voltage resulted in the improvement of permeate fluxes. . This improvement was magnified at an applied voltage of 60 V. At an applied voltage of 60 V, permeate fluxes obtained after 60 minutes were higher than the permeate fluxes obtained from ultrafiltration without an applied voltage. Likewise, the steady-state permeate flow rate obtained at a TMP of 100 kPa and applied voltage of 60 V was relatively higher as compared to ultrafiltration at 100 kPa – as shown in Table 5.6.

Table 5.6: Comparison of permeate flow based on different operating parameters. Data for ultrafiltration lifted from the authors' previous work [1]. CFV used is 2.4 m s^{-1}

Operating Parameters	Steady-state permeate flow rate, kg hr^{-1}
Ultrafiltration @ 100 kPa	0.197
Ultrafiltration @ 200 kPa	0.154
Ultrafiltration @ 300 kPa	0.081
Electro-ultrafiltration @ 20 V; 100 kPa	0.164
Electro-ultrafiltration @ 40V; 100 kPa	0.140
Electro-ultrafiltration @ 60 V; 100 kPa	0.224
Electro-ultrafiltration @ 20 V; 200 kPa	0.086
Electro-ultrafiltration @ 40 V; 200 kPa	0.089
Electro-ultrafiltration @ 60 V; 200 kPa	0.088
Electro-ultrafiltration @ 20 V; 300 kPa	0.080
Electro-ultrafiltration @ 40 V; 300 kPa	0.083
Electro-ultrafiltration @ 60 V; 300 kPa	0.062

5.4 Conclusions

The usefulness of applying an electric field during electro-ultrafiltration of model wastewater containing CED paint particles is dependent on the correct combination of applied voltage and pressure. At a TMP of 100 kPa, the application of voltage on the ceramic ultrafiltration system improved flux rates. The most significant improvement in flux rates was obtained at an applied voltage of 60 V. At this voltage, flux rates obtained after 60 minutes were higher than the flux rates obtained from ultrafiltration without an applied voltage. Increasing further the TMP to 200 and 300 kPa did not yield any improvement in flux rates at all magnitudes of applied voltages. In fact at these TMPs, energy consumptions were high and flux decline rates were rapid. Likewise, the steady state permeate fluxes obtained at these TMPs were relatively very low compared to steady state permeate fluxes obtained at a TMP of 100 kPa. This permeate flux behaviour can be attributed to the higher compressive force encountered by the paint particles and the insufficient electric fields used. Relative to ordinary ultrafiltration, the use of an additional 20 V increased the energy consumption of the electro-ultrafiltration system by 7 %. Such increase is doubled and tripled when 40 and 60 V were utilized respectively.

In general, results showed that the application of electro-ultrafiltration in the recovery of post-electrodeposition rinse wastewater was successful at bench scale level. It has been shown in this work that such a set-up will work successfully on wastewater containing a worst case scenario of CED paint contamination – provided that the correct operating parameters are used. Although results were obtained in lab-scale trials, these can be applied in an actual membrane plant installation but may involve some modifications.

For example, higher applied voltages may be used to maintain the electric field strength across a relatively bigger and longer ceramic membrane.

The work described in this chapter has since been published in the international literature [2].

5.5 References

[1] Agana, B. A., Reeve, D. & Orbell, J. D. 2011. Optimization of the operational parameters for a 50 nm ZrO2 ceramic membrane as applied to the ultrafiltration of post-electrodeposition rinse wastewater. *Desalination,* 278**,** 325-332.

[2] Agana, B. A., Reeve, D. & Orbell, J. D. 2012. The influence of an applied electric field during ceramic ultrafiltration of post-electrodeposition rinse wastewater. *Water Research,* 46**,** 3574-3584.

[3] Altmann, J. & Ripperger, S. 1997. Particle deposition and layer formation at the crossflow microfiltration. *Journal of Membrane Science,* 124**,** 119-128.

[4] ASTM 1985. Zeta Potential of Colloids in Water and Waste Water. *ASTM Standard D 4187-82.*

[5] Butt, H.-J. & Kappl, M. 2009. *Surface and Interfacial Forces,* Hoboken, Wiley-VCH.

[6] Cheryan, M. 1998. *Ultrafiltration and microfiltration handbook*, Lancaster, Pennsylvania, Technomic Publishing Company, Inc.

[7] Crittenden, J. C., Trussell, R. R., Hand, D. W., Howe, K. J. & Tchobanoglous, G. 2005. *Water treatment: Principles and design,* Hoboken, NJ, John Wiley & Sons, Inc.

[8] Enevoldsen, A. D., Hansen, E. B. & Jonsson, G. 2007. Electro-ultrafiltration of industrial enzyme solutions. *Journal of Membrane Science,* 299**,** 28-37.

[9] Glisson, T. H. & Glisson, T. H. 2011. Current, Voltage, and Resistance. *Introduction to Circuit Analysis and Design.* Springer Netherlands.

[10] Huisman, I. H., Trägårdh, G., Trägårdh, C. & Pihlajamäki, A. 1998. Determining the zeta-potential of ceramic microfiltration membranes using the electroviscous effect. *Journal of Membrane Science,* 147**,** 187-194.

[11] Huotari, H. M., Trägårdh, G. & Huisman, I. H. 1999. Crossflow Membrane Filtration Enhanced by an External DC Electric Field: A Review. *Chemical Engineering Research and Design,* 77**,** 461-468.

[12] Israelachvili, J. N. 2010. Van der waals forces. *Intermolecular and surface forces.* 3 ed. Burlington: Elsevier Science.

[13] Krupp, H. 1967. Particle Adhesion Theory and Experiment. *Colloid Interface Sci.,* 11**,** 11-239.

[14] O'Neill, M. E. 1968. A sphere in contact with a plane wall in a slow linear shear flow. *Chemical Engineering Science,* 23**,** 1293-1298.

[15] Oussedik, S., Belhocine, D., Grib, H., Lounici, H., Piron, D. L. & Mameri, N. 2000. Enhanced ultrafiltration of bovine serum albumin with pulsed electric field and fluidized activated alumina. *Desalination,* 127**,** 59-68.

[16] Radovich, J. M. & Chao, I. M. 1982. ELECTROULTRAFILTRATION OF A CATIONIC ELECTRODEPOSITION PAINT. *Journal of Coatings Technology,* 54**,** 33-40.

[17] Randon, J., Crosnier De Bellaistre, M. & Rocca, J. L. 2003. Electrophoretic and electrochromatographic properties of zirconia based capillaries. *Chromatographia,* 57.

[18] Stamatakis, K. & Chi, T. 1993. A simple model of cross-flow filtration based on particle adhesion. *AICHE Journal,* 39**,** 1292-1302.

[19] Weigert, T., Altmann, J. & Ripperger, S. 1999. Crossflow electrofiltration in pilot scale. *Journal of Membrane Science,* 159**,** 253-262.

[20] Yang, G. C. C. & Li, C.-J. 2007. Electrofiltration of silica nanoparticle-containing wastewater using tubular ceramic membranes. *Separation and Purification Technology,* 58**,** 159-165.

[21] Yang, G. C. C. & Yang, T.-Y. 2004. Reclamation of high quality water from treating CMP wastewater by a novel crossflow electrofiltration/electrodialysis process. *Journal of Membrane Science,* 233**,** 151-159.

[22] Zumbusch, P. v., Kulcke, W. & Brunner, G. 1998. Use of alternating electrical fields as anti-fouling strategy in ultrafiltration of biological suspensions - Introduction of a new experimental procedure for crossflow filtration. *Journal of Membrane Science,* 142**,** 75-86.

Chapter Six: The application of a 5 nm TiO_2 ceramic membrane for the ultrafiltration of beverage production wastewater

6.1 Introduction

Beverage production wastewater originates from processes such as bottle rinsing, product filling, cooling or heating and "clean-in-place" (CIP). Contaminants found in this type of wastewater include cleaning chemicals, product mixes and concentrates, and dirt and sugars. Due to the nature of the contaminants present in beverage production wastewater, critical water quality parameters such as conductivity, chemical oxygen demand (COD), total dissolved solids (TDS) and total suspended solids (TSS) are expected to be elevated. For example, in the work of Amuda and Amoo [1], the average conductivity, COD and TSS of the beverage wastewater used in their experiments were 2995 μS/cm, 1750 mg/L and 1620 mg/L respectively. Similarly, in the work of Matosic *et al.* [2], the average conductivity, COD and chloride of the beverage wastewater used in their experiments were 2600 μS/cm, 722 mg/L and 760 mg/L respectively.

The removal of suspended solids present in beverage production wastewater is an important pretreatment step during water reclamation. This ensures that the effect of fouling on a main treatment system such as high-pressure membrane filtration (i.e. reverse osmosis (RO) and nanofiltration (NF)) is minimized. Commonly used processes for pretreatment of beverage production wastewater include coagulation/flocculation [1, 3] and low-pressure membrane filtration (i.e. microfiltration (MF) and ultrafiltration (UF)) [4, 5]. Coagulation is a process of destabilizing colloidal materials by particle charge neutralization and initial aggregation of solids present in the wastewater, while flocculation is a process which facilitates particle agglomeration of coagulated colloidal and finely divided suspended materials either through physical mixing or through the aid of coagulants such as ferric chloride and polymers [1, 6]. Although coagulation/flocculation is a simple process, it usually involves the use of physical separation

equipment such as floatation and settling tanks – making it less desirable in terms of footprint and operating costs. Likewise, the addition of chemicals into the wastewater may present additional complications during water reclamation. For example, an increase in TDS was observed when inorganic and polymeric coagulants were used for treatment of dairy wastewater [7].

Wastewater pretreatment in recent years has shifted towards the use of low-pressure membrane processes such as microfiltration (MF) and ultrafiltration (UF) [8]. This shift can be attributed to some of the known advantages of low-pressure membrane filtration over conventional treatment systems. These advantages include: a) consistent permeate water qualities despite variations in quality of feed water; b) efficient separation process even without a change of phase; c) continuous operation under steady-state conditions; and d) compact modular construction [9, 10]. The decision on whether to use MF or UF as pretreatment for a specific wastewater will usually depend on the types and particle sizes of contaminants present. In general, microfiltration rejects suspended solids in the 0.1 to 1 μm size range, including microorganisms such as bacteria and protozoa, while ultrafiltration rejects large dissolved molecules and colloidal particles in the 0.01 to 0. 1 μm size range [10]. Although both types of membranes can generally be used for pretreatment of wastewater, a UF membrane is generally preferred in an industrial setting [11]. A UF membrane can effectively remove suspended solids and emulsified oils present in industrial wastewater [12-14] and UF filtrate water quality has been shown to be superior to MF – especially in terms of the silt density index (SDI) [15].

Other types of beverage wastewater treatment have also been presented in literature. For example, Sekine *et al.* [16] used a solar photo-fenton process for the treatment of

colored softdrink wastewater. The process showed a COD removal efficiency of 99.3 % after 75 min during a fine day condition (i.e. not cloudy). Although this was the case, they suggested that the solar photo-fenton process should be designed and operated based on accumulated energy rather than reaction time. Tawfik and El-Kamah [17] used a two-stage anaerobic hybrid (AH) reactor system followed by a sequencing batch reactor (SBR) to treat wastewater generated by the fruit juice industry. Results showed that the contaminant removal efficiencies of the two AH reactors connected in series is higher compared to a single AH reactor. The single AH reactor achieved COD and TSS removal efficiencies of 42.0 % and 56.4 % respectively while the two AH reactors connected in series achieved COD and TSS removal efficiencies of 67.4 % and 71.5 % respectively. The effluents from the two AH reactors connected in series were subsequently fed in to the SBR unit for further treatment. Because of this, further reductions in COD concentrations were achieved. On the other hand, Manyele *et al.* [18] used a three-phase fluidised bed biological reactor to treat beverage wastewater. Results showed that the COD removal efficiency of the reactor was dependent on the initial pH level of the beverage wastewater. At initial pH values of 9.0 and 11.5, COD removal efficiencies obtained were 98.0 % and 50.0 % respectively.

Membrane bioreactors (MBRs) have also been shown to be effective in the treatment of beverage wastewater. For example, Ng *et al.* [19] showed that a novel bio-entrapped membrane reactor (BEMR) can effectively remove organics from food and beverage wastewater and at the same time limit the occurrence of membrane fouling. Matosic *et al.* [2] also showed in their work that an MBR can successfully remove COD, BOD and TOC at a 90.0 % efficiency rate.

Polymeric membranes are the most commonly used membranes for wastewater treatment in the food and beverage industry [5, 20-22]. However, these types of membranes have issues with material instability and their operating life is affected by the nature and frequency of cleaning. For instance, exposure to strong doses of chlorine can cause significant degradation of membrane material [23]. Currently, the availability of commercially manufactured polymeric membranes able to withstand extreme operating conditions (e.g. low pH, high temperatures, etc.) is limited [24].

Ceramic membranes are possible alternatives to polymeric membranes for the pretreatment of highly contaminated industrial wastewater due to their chemical and thermal stability [25, 26]. They work well within a pH range of 1 to 14 and can be operated at temperatures as high as 500°C [27]. One of the distinctive characteristics of ceramic membranes is their ability to endure strong doses of chlorine – an extremely effective cleansing agent at alkaline pH [23]. Other advantages of ceramic membranes include longer lifespan, higher average flux and lower cleaning frequency [25]. Although ceramic membranes may offer some advantages compared to polymeric membranes, their use in industrial wastewater treatment has been limited to date by their higher initial cost and by their intrinsic brittleness. In regard to the latter, sudden pressure surges and temperature changes can cause physical and thermal shocks respectively which may crack damage the membrane [23].

This chapter investigates the performance of a 5 nm TiO_2 ceramic ultrafiltration membrane with respect to beverage production wastewater. This specific membrane was chosen for the following reasons. Firstly, different cleaning chemicals and detergents are present in the actual wastewater streams and therefore a ceramic membrane is more

suitable than a polymeric membrane with respect to chemical stability considerations. Secondly, the active layer of the chosen ceramic membrane (TiO_2) is a good inhibitor of biofilm growth and fouling [28]. This characteristics of the active layer are well suited for wastewater containing a high level of organic contamination – such as the beverage production wastewater that is the subject of this investigation. Lastly, the measured particle sizes present in the actual beverage production wastewater samples ranged from 24 – 5560 nm; making an ultrafiltration membrane more appropriate than a microfiltration membrane. The performance of the 5 nm ceramic ultrafiltration membrane was evaluated based on different combinations of transmembrane pressures (TMPs) and cross-flow velocities (CFVs). Forces acting on suspended particles were calculated to determine their effect on particle deposition onto the membrane surface. Likewise, different resistances and fouling mechanisms were assessed based on the resistance-in-series (RIS) and Hermia's fouling models, respectively, to ensure a thorough understanding of the permeate flux behaviour. The majority of the data obtained from the experiments were analysed in a similar manner to a previous published work [29].

6.2 Materials and methods

6.2.1 Wastewater sample

Actual wastewater samples generated from a beverage production facility were used in all the experiments. The collection point of these wastewater samples is shown in Figure 6.1.

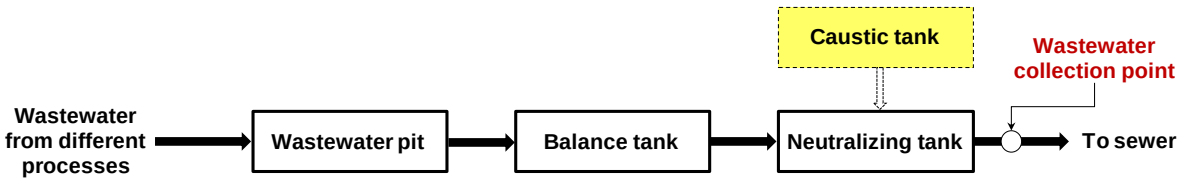

Figure 6.1: Wastewater collection point at the beverage production facility.

Wastewater streams generated from different processes within the production facility are collected in a wastewater pit and subsequently transferred to a balance tank (holding tank). From the balance tank, it is then transferred into a neutralizing tank where pH adjustment is carried out through the addition of caustic soda (NaOH). Wastewater pH is adjusted in order to meet pH discharge levels set out in the facility's Tradewaste Agreement with the local water retailer. The average wastewater quality measured at the wastewater collection point (after the neutralizing tank) is shown in Table 6.1. Water quality parameters such as TDS, suspended solid (SS) and COD were tested by a NATA (National Association of Testing Authorities) accredited testing laboratory. While water quality parameters such as pH, turbidity and conductivity were tested on-site. Turbidity tests were performed using a La Motte 2020 Series Turbidity Meter, while pH and conductivity tests were performed using a Hach Multimeter (Model IM6700). Testing for turbidity was based on USEPA method 180.1, while testing for pH and conductivity were based on USEPA electrode and direct measurement methods respectively.

Table 6.1: Average water quality of wastewater samples collected from the beverage production facility. Sampling was conducted for a period of one month.

Parameter	No. of Samples	Ave.	Min.	Max.	Standard deviation
pH	14	8.3	6.3	10.9	1.6
TDS, mg/L	14	2369	1430	3480	674
SS, mg/L	14	52	29	72	14
Zeta Potential (ζ), mV	14	-23.1	-17.2	-27.4	2.2
Turbidity, NTU	14	58	49.6	65.7	5
Conductivity, μS/cm	14	2337	850	3800	1301
COD, mg/L	14	3750	1800	5200	1430

Wastewater samples were collected in 20 L plastic containers and kept in a cold room at a temperature of 4 °C. Prior to every experiment, a specified volume (6 L) of wastewater sample is transferred into a stainless steel container. The stainless steel container is then left for a couple of hours inside the laboratory to bring up the wastewater temperature to ambient level. All wastewater samples were used within 48 hours of collection. Unused wastewater samples are diluted with tap water and subsequently discharged to sewer.

6.2.2 Ceramic membrane

A Membralox T1-70 single channel ceramic membrane with a titanium dioxide (TiO_2) active layer was used in all the experiments. The membrane has a nominal pore size of 5 nm and an effective membrane area of 0.005 m^2. Its dimensions are as follows – internal diameter, i.d. = 7 mm; outside diameter, o.d. = 10 mm; length, l = 250 mm. The isoelectric point of the active layer is approximately 6.2 [30] and therefore the membrane surface charge is positive or negative respectively below or above a pH of 6.2. This membrane was supplied by Pall Corporation Australia.

6.2.3 Ceramic ultrafiltration system

The ceramic ultrafiltration system used in this Chapter is similar to the one used in Chapter 4.

6.2.4 Analytical methods

The analytical methods used are similar to the one used in Chapter 4. Contaminant rejection rates ($\%R_C$) were calculated using Eq. (1):

$$\%R_C = [(C_F - C_P) / C_F] \times 100\ \% \quad (1)$$

where C_F is the feed contaminant concentration and C_P is the filtrate contaminant concentration.

6.2.5 Membrane cleaning

The membrane cleaning protocol used is similar to the one used in Chapter 4.

6.3 Results and discussions

6.3.1 Pure water flux (PWF)

Experiments aimed at establishing the relationship between pure water flux (PWF) and TMP were carried out prior to commencing actual wastewater experiments (1 hr per TMP). The experiments for these were performed using only one module. Distilled water having a conductivity of 2 μS/cm was used as feed to ensure that no form of fouling will occur during filtration. Results showed that PWF of the ceramic membrane was highly correlated ($R^2 = 0.999$) with TMP as shown in Figure 6.2. A high correlation between PWF and TMP is expected since the only resistance present during the experiments is the intrinsic membrane resistance (R_M). Furthermore, the slope of the line shown in Figure 6.2 gives the pure water permeability (PWP) of the ceramic membrane. The data used for plotting Figure 6.2 are available in the accompanying CD (Appendix 6.1).

Since the relationship between PWF and TMP had been established, the intrinsic membrane resistance can now be calculated using Eq. (2) [23]:

$$R_M = TMP / \eta_F PWF \quad (2)$$

where η_F is the dynamic viscosity of the feed water at 20°C (0.001002 Pa s). The calculated intrinsic membrane resistance (R_M) for the 5 nm ceramic membrane is equal to 1.36E+13 m^{-1}.

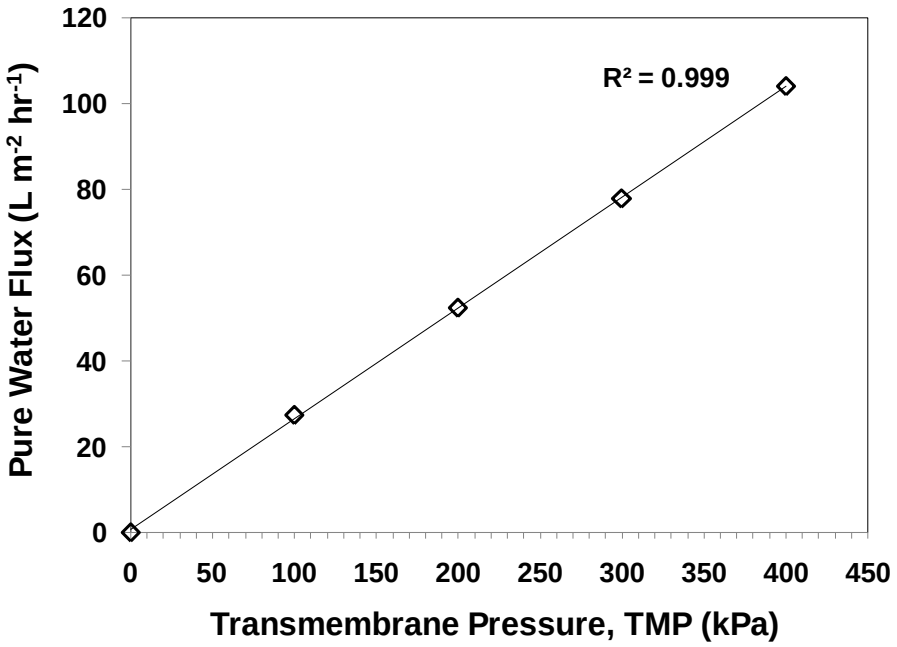

Figure 6.2: Pure water flux of 5 nm ceramic membrane as a function of TMP at a CFV of 2.5 m s^{-1} and temperature of 20 °C. The pure water permeability (J_{PWP}, $m^3 m^{-2} s^{-1} kPa^{-1}$) of the membrane is given by the slope of the line.

6.3.2 Particle size distribution

Particle sizes present in the actual wastewater samples ranged from 24 nm to 5560 nm as shown in Figure 6.3. These particles have an average zeta potential (ζ) of - 23.1 ± 2.2 mV (at pH = 8.3) – suggesting incipient instability [32]. Because particles present in the actual wastewater are likely to exhibit instability, particle aggregation may occur.

Particle aggregation is not considered to be a problem during ultrafiltration because the more the particles aggregate, the better. Larger particles have higher hydrodynamic forces acting on them and therefore are more likely to be swept away from the membrane surface. The data used for plotting Figure 6.3 are available in the accompanying CD (Appendix 6.2).

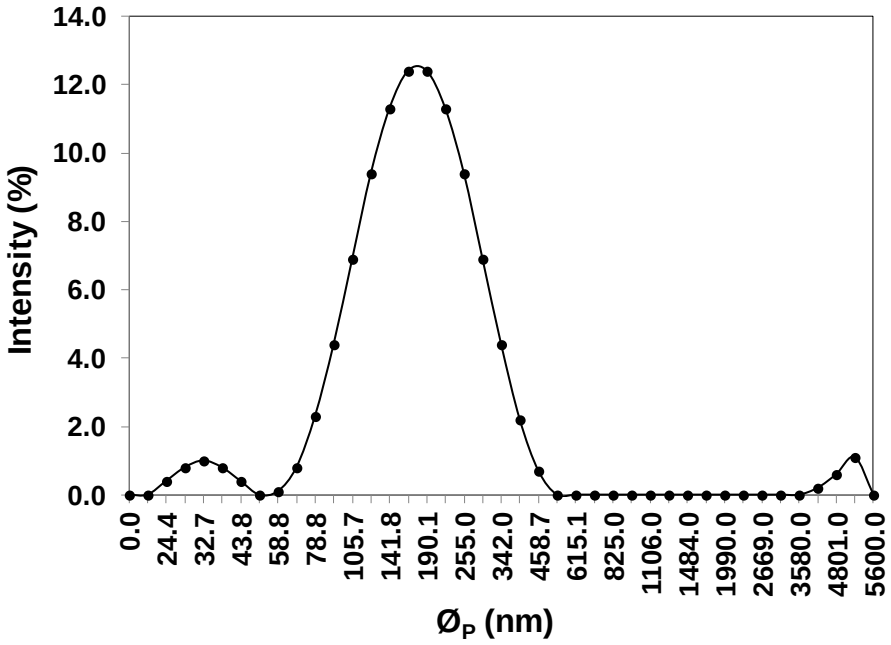

Figure 6.3: Particle size distribution for beverage production wastewater ($Ø_{Pmean}$ = 161.4 nm).

6.3.3 An analysis of the forces on the particles

The deposition of particles onto a membrane surface is influenced by hydrodynamic and surface interaction forces [33]. Hydrodynamic forces include drag, lift and gravitational forces while surface interaction forces include electrostatic double-layer and Van der Waals forces. The magnitudes for both hydrodynamic and surface interaction forces depend on particle size. In general, drag, lift, gravitational, and Van der Waals forces increase as particle sizes increases while the electrostatic double-layer force decreases as particle size increases.

Figure 6.4 depicts the different forces that are postulated to act on suspended particles during crossflow ultrafiltration of the beverage production wastewater.

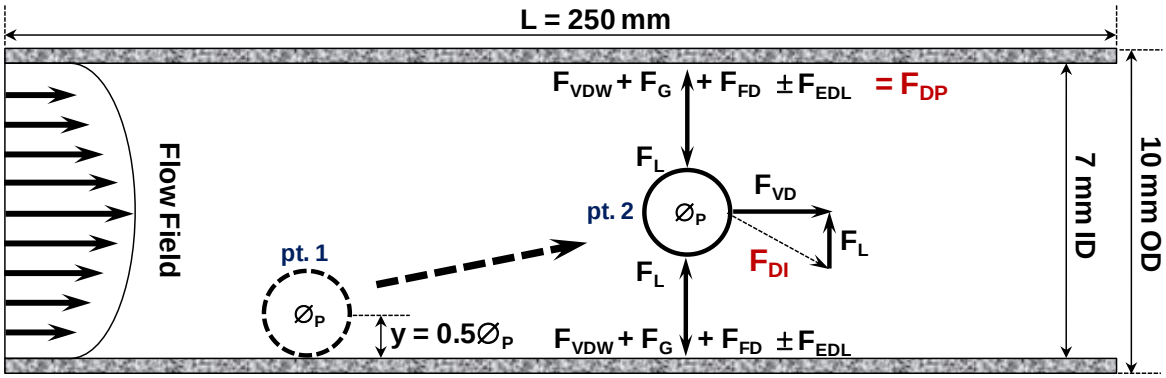

Figure 6.4: Forces acting on suspended particles during crossflow ultrafiltration of beverage production wastewater – $Ø_P$ is the particle diameter (m); F_L is the lift force (N); F_{FD} is the drag force due to filtrate flow (N); F_{VD} is the drag force due to feed velocity (N); F_{VDW} is the Van der Waals adhesive force (N); F_{EDL} is the electrostatic double-layer force (N); F_G is the gravitational force; F_{DP} is the deposition-promoting force; and F_{DI} is the deposition-inhibiting force.

Drag forces experienced by particles during crossflow ultrafiltration can be estimated using Eqs. (3) and (4) [29, 34]:

$$F_{FD} = 3\pi\eta_F Ø_P J \quad (3)$$

where F_{FD} is the drag force due to filtrate flow (N); η_F is the viscosity of the feed water at 20 °C (0.001002 Pa s); $Ø_P$ is the particle diameter (m); and J is the permeate flux (m^3 m^{-2} s^{-1}).

$$F_{VD} = 0.638\ (\pi \Delta P Ø_{CM} Ø_P^{\,2} / L_{CM}) \quad (4)$$

where F_{VD} is the drag force due to feed velocity (N); ΔP is the pressure drop in the ceramic membrane during filtration (Pa); $Ø_{CM}$ is the internal diameter of the ceramic membrane (m); $Ø_P$ is the particle diameter (m); and L_{CM} is the length of the ceramic membrane (m). The velocity drag force, F_{VD} was derived based on pt. 1 as shown in Figure 6.4.

The lift force which is commonly due to shear flow can be estimated using Eq. (5) [35] while the gravitational (buoyant) force can be estimated using Eq. 6 [33]:

$$F_L = 0.761 (\tau_W^{1.5} Ø_P^3 \rho_F / \eta_F) \quad (5)$$

where F_L is the lift force (N); τ_W is the shear stress acting on the cake boundary (Pa); $Ø_P$ is the particle diameter (m); ρ_F is the density of the feed water at 20°C (998.2 kg m^{-3}); and η_F is the viscosity of the feed water at 20 °C (0.001002 Pa s).

$$F_G = (\pi Ø_P^3 / 6) (\rho_P - \rho_F) g \quad (6)$$

where F_G is the gravitational force (N); $Ø_P$ is the particle diameter (m); ρ_P is the particle density (1250 kg m^{-3}, average density of standard soil and dry loam soil [36]); ρ_F is the density of the feed water at 20 °C (998.2 kg m^{-3}); and g is the gravitational acceleration constant (9.81 m s^{-2}).

Van der Waals and electrostatic double-layer forces between particles and membrane wall can be estimated using Eqs. (7) [35, 37] and (8) [38] respectively:

$$F_{VDW} = h\varpi Ø_P / 32\pi\bar{a}^2 \quad (7)$$

where F_{VDW} is the Van der Waals adhesive force (N); $Ø_P$ is the particle diameter (m); $h\varpi$ is the Lifschitz-van der Waals constant (1.0E-20 J); and ā is the adhesive distance (4.0E-10 m) [39]. Since the analysis is focused on particle-membrane interaction, the adhesive distance ā is considered a constant.

$$F_{EDL} = (4\pi R^* / \varepsilon\varepsilon_O \aleph) [\sigma_1\sigma_2 e^{-\aleph x} + 0.5 (\sigma_1^2\sigma_2^2) e^{-2\aleph x}] \quad (8)$$

where F_{EDL} is the electrostatic double-layer force (N); $R^*=R_1$ ($R_2 = \infty$) is the particle radius interacting with a flat surface (m); ε is the dielectric permittivity of water at 20 °C (80.2); ε_O is the permittivity of vacuum (8.85E-12 C^2 N^{-1} m^{-2}); σ_1 is the surface charge density of particles (C m^{-2}); σ_2 is the surface charge density of the ceramic membrane's active layer (C m^{-2}); ℵ is the inverse Debye length (m^{-1}); and x is the distance between particles and membrane wall (m). The electrical double-layer force was calculated based on distances (x) ranging from 4.0E-9 to 1.0E-8 m. The electrostatic double-layer force can either be attractive or repulsive depending on the net surface charge exhibited by both the particles and membrane active layer. In this instance, the electrostatic double-layer force was repulsive because both the particles and membrane active layer are negatively charged at a feedwater pH of 8.3.

The different forces acting on particles can be further categorized into two main classifications namely, deposition-promoting force (F_{DP}) and deposition-inhibiting force (F_{DI}). Based on Figure 6.5 (pt.2), F_{DP} and F_{DI} can be calculated using Eqs. (9) and (10) respectively:

$$F_{DP} = F_{VDW} + F_G + F_{FD} - F_{EDL} \quad (9)$$

$$F_{DI} = (F_{VD}^2 + F_L^2)^{0.5} \quad (10)$$

The magnitudes of F_{DP} and F_{DI} acting on different particle sizes present in the beverage production wastewater are shown in Figure 6.5. The calculations of these forces are shown in Appendix 6.3 – attached at the end of the thesis.

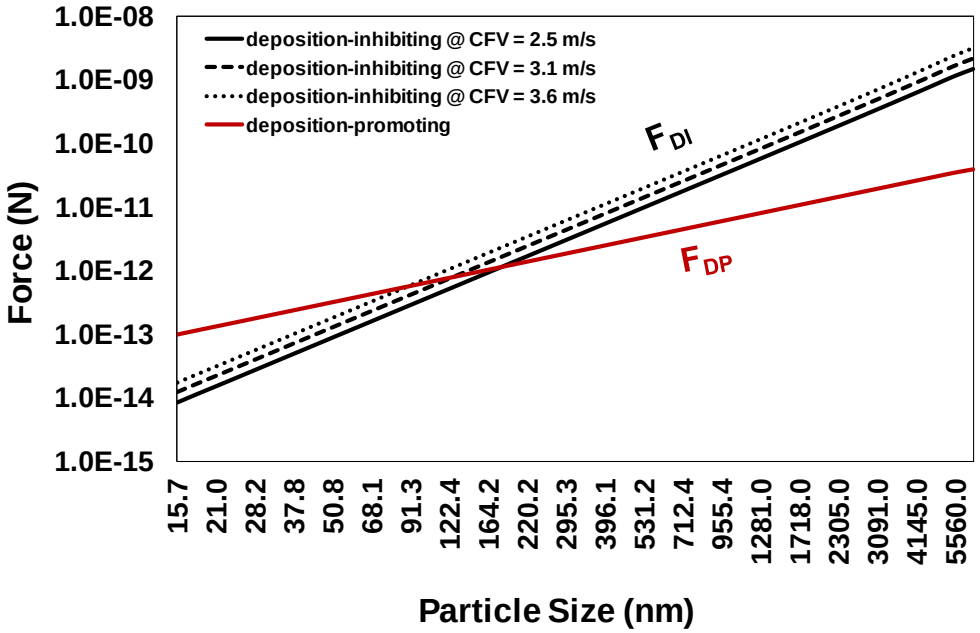

Figure 6.5: Deposition-promoting and deposition-inhibiting forces acting on particles during crossflow ultrafiltration of beverage production wastewater.

Based on the magnitudes of F_{DP} and F_{DI} shown in Figure 6.5, the following conclusions may be made: a) at a CFV of 2.5 m s^{-1}, particle sizes less than 200 nm are likely to be deposited on the membrane surface; b) at a CFV of 3.1 m s^{-1}, particle sizes less than 150 nm are likely to be deposited on the membrane surface; c) at a CFV of 3.6 m s^{-1}, particle sizes less than 100 nm are likely to be deposited on the membrane surface; and d) particle sizes greater than 200 nm are likely to be swept away from the membrane surface at

all CFVs used. In general, as CFV increases, the range of particle sizes that are likely to be deposited on the membrane surface gets smaller.

6.3.4 Influence of CFV and TMP on filtration performance

The influence of different CFVs on particle deposition has been established in Section 6.3.3 but the influence of different combinations of TMPs and CFVs on filtration performance has not yet been determined. In order to determine the influence of different combinations of TMPs and CFVs on the performance of the 5 nm ceramic membrane, duplicate filtration experiments (each of 185 minutes duration) involving the use of the actual beverage production wastewater were carried out. Results of the experiments are shown in Figures 6.6a to c. The data used for plotting Figures 6.6a to c are available in the accompanying CD (Appendix 6.4).

Permeate fluxes (J, $m^3\ m^{-2}\ s^{-1}$) were calculated using Eq. (11):

$$J = 0.001W / A_M\, t \qquad (11)$$

where W is the weight measured by the balance (kg), A_M is the effective membrane area (m^2), t is the sampling time (s).

To account for temperature variations, all permeate fluxes were standardized at a temperature of 20°C using Eq. (12) [40]:

$$J_{20°C} = J\ (1.03)^{T_S - T_M} \qquad (12)$$

where $J_{20°C}$ is the flux at a standard temperature of 20°C ($m^3\ m^{-2}\ s^{-1}$), T_S is the standard temperature (20 °C), T_M is the measured temperature (°C).

a)

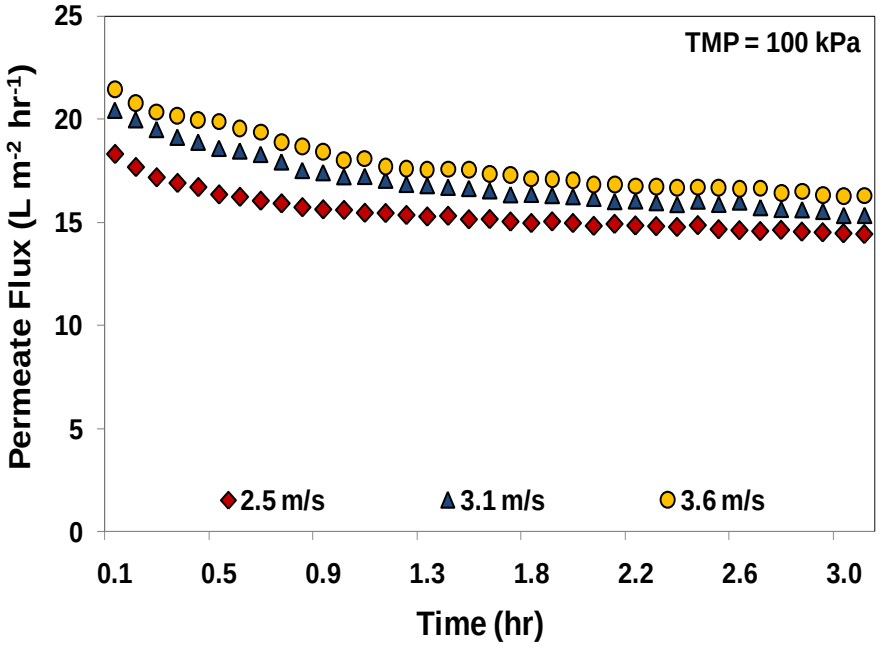

b)

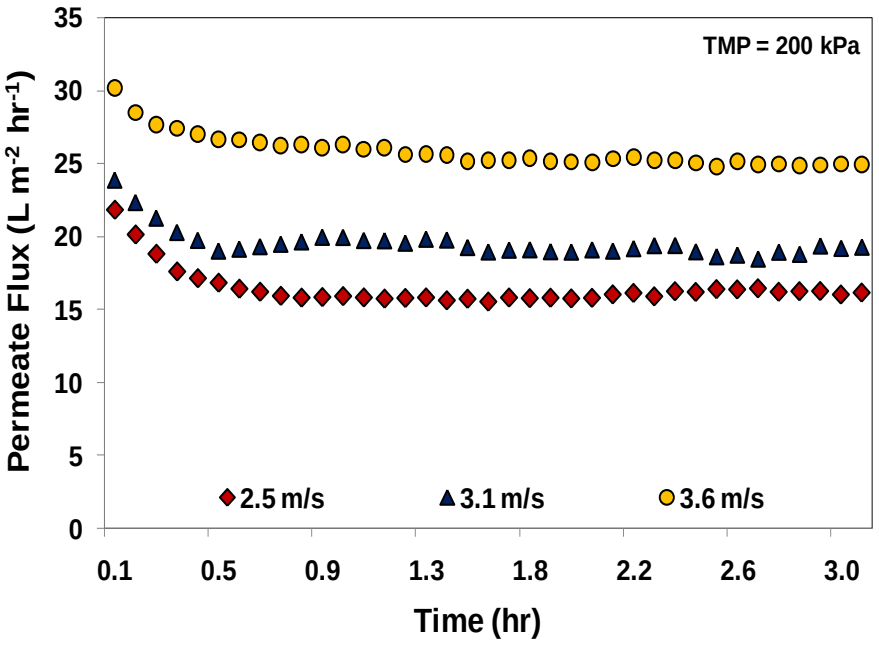

c)

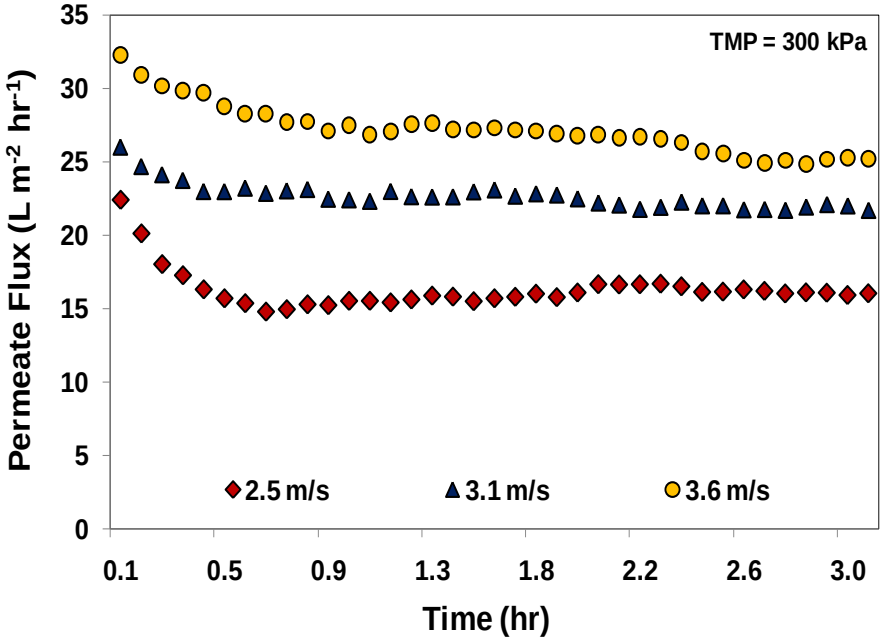

Figure 6.6: Permeate flux as a function of time at TMPs of: a) 100 kPa, b) 200 kPa and c) 300 kPa; and CFVs of 2.5, 3.1 and 3.6 m s^{-1}. All permeate fluxes were standardized at a temperature of 20 °C. Steady-state conditions were observed after approximately 2700 s. After this period, gradual increases or decreases in permeate fluxes were measured.

Results from the experiments show that flux improvement during ultrafiltration of beverage production wastewater is dependent on both CFV and TMP. At the lowest CFV of 2.5 m s^{-1}, the permeate fluxes measured showed minor improvement when TMP was increased to 200 and 300 kPa. At higher TMPs of 200 and 300 kPa, the permeate fluxes measured had high initial values but subsequently went down and reached steady-state conditions after approximately 45 minutes. The steady-state fluxes measured for all TMPs at a CFV of 2.5 m s^{-1} were almost identical to each other. On the contrary, at higher CFVs of 3.1 and 3.6 m s^{-1}, permeate fluxes improved when TMP was increased to 200 and 300 kPa (as shown in Figures 6.6b to c). The steady-state permeate fluxes

measured at CFVs of 3.1 and 3.6 m s^{-1} increased by 22 % and 53 % respectively when TMP was increased to 200 kPa. Further increasing the TMP to 300 kPa resulted in a 16 % and 4 % increase in steady-state permeate fluxes at CFVs of 3.1 and 3.6 m s^{-1} respectively. This permeate flux behaviour can be attributed to the instability of the particles present in the beverage production wastewater samples. Since the particles have a tendency to aggregate, the larger masses formed are likely to be swept away from the membrane surface due to higher hydrodynamic forces – as mentioned in Section 6.3.2. When the majority of the particles are swept away from the membrane surface, the resistance encountered during filtration becomes less - resulting in increased permeate flux.

6.3.5 Membrane resistances

Resistances encountered during ceramic ultrafiltration of the beverage production wastewater can be analysed using the resistance-in-series (RIS) model. The general form of the RIS model can be written as [23]:

$$J = TMP / \eta_F (R_M + R_F + R_G) \quad (13)$$

where J is the permeate flux (m^3 m^{-2} s^{-1}), TMP is the transmembrane pressure (Pa), η_F is the viscosity of feed water (0.001002 Pa s), R_M is the intrinsic membrane resistance (1.36E+13 m^{-1}), R_F is the adsorption resistance on inner pore fiber (m^{-1}) and R_G is the concentration polarization resistance (m^{-1}). The concentration polarization resistance (R_G) can be calculated using Eq. (14) [23]:

$$R_G = \Phi \, TMP \quad (14)$$

where Φ is the resistance index (Pa^{-1} m^{-1}). The adsorption resistances and resistance indices were obtained by plotting permeate flux as a function of TMP and fitting the experimental data obtained into Eq. (13). Curve fitting using the least-squares method was done in Microsoft Excel. Results obtained from the curve fitting are shown in Figures 6.7a to c.

The adsorption resistance (R_F) had negligible effects on permeate flux during the ultrafiltration of beverage production wastewater. The values obtained for R_F were very low compared to R_M – suggesting that few particles deposited onto the ceramic membrane's inner pores. The concentration polarization resistance (R_G) was the main resistance encountered during the experiments. This was expected since concentration polarization has been reported to be severe in microfiltration and ultrafiltration due to high fluxes and low mass transfer coefficients [41]. The concentration polarization resistances obtained were directly proportional to TMP as shown in Figures 6.7a to c. As TMP increases, the concentration polarization resistance also increases. Although this was generally the case, results also show that the concentration polarization resistances obtained at a CFV of 3.6 m s^{-1} were the lowest.

The lowest concentration polarization resistances were obtained at a CFV of 3.6 m s^{-1} due to a high Reynolds number (*Re*). A high Reynolds number (*Re* > 4000) will exhibit turbulent flow. Turbulent flow weakens the effect of concentration polarization due to high shear forces encountered by the cake formed [42]. Therefore, the more turbulent the flow regime is, the greater its effect in weakening concentration polarization. *Re* for the different CFVs used was calculated using Eq. (15):

$$Re = \rho_F v \emptyset_{CM} / \eta_F \quad (15)$$

where v is the crossflow velocity in m s^{-1} and ØCM is the internal diameter of the ceramic membrane (m). Based on Eq. (15), an increase of CFV from 2.5 m s^{-1} to 3.1 m s^{-1} subsequently increased *Re* from 17434 to 21618 while increasing CFV further to 3.6 m s^{-1} resulted in a much higher *Re* of 25104.

It should be noted that the adsorption resistances (R_F) obtained at all CFVs show decreasing trends. These trends can be attributed to the formation of a cake layer on the membrane surface with respect to filtration time. As filtration time lengthens, the thickness of the cake layer formed on the membrane surface increases. Such an increase inhibits the deposition of particles into the membrane pores resulting in relatively lower R_F values – as shown in Figures 6.7a to c.

a)

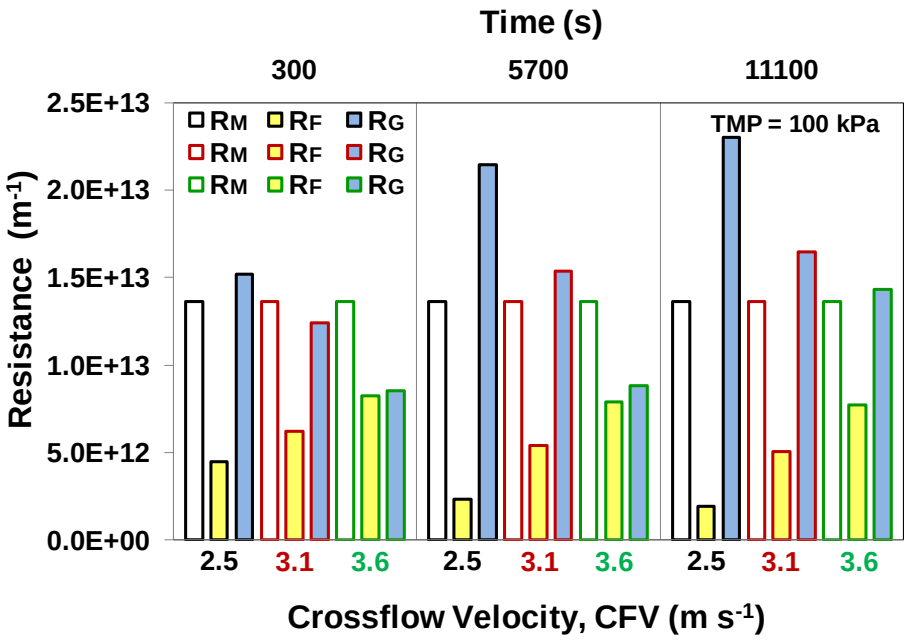

b)

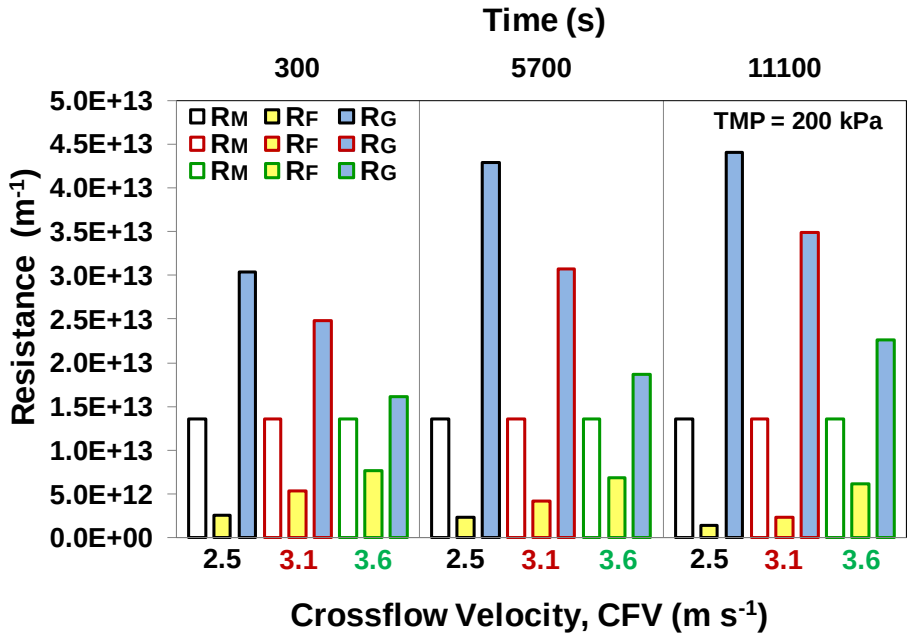

c)

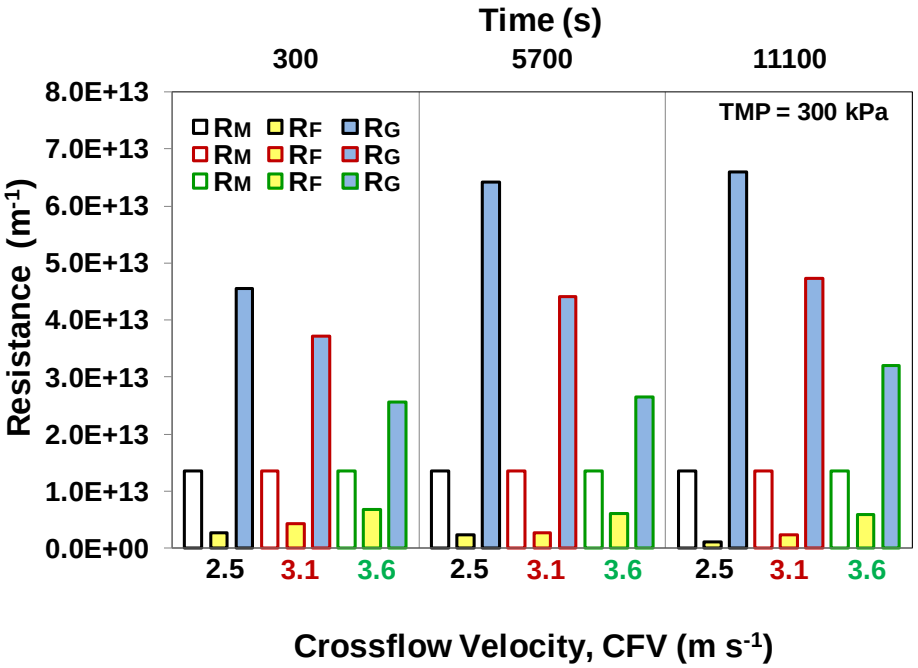

Figures 6.7: Membrane resistances at: a) 100 kPa; b) 200 kPa and c) 300 kPa.

Additionally, the adsorption resistances obtained at CFVs of 3.1 and 3.6 m s^{-1} were generally higher than those obtained at a CFV of 2.5 m s^{-1}. This behaviour may be due to

the relative severity of cake layer formation on the membrane surface with respect to different CFVs. At a CFV of 2.5 m s^{-1}, the cake layer formed on the membrane surface was more severe than that formed at CFVs of 3.1 and 3.6 m s^{-1} – as shown by the relative concentration polarization resistances obtained (Figures 6.7a to c). Therefore, at a CFV of 2.5 m s^{-1}, lesser particles were adsorbed into the membrane pores due to relatively thicker cake layer formation. On the other hand, at CFVs of 3.1 and 3.6 m s^{-1}, more particles were adsorbed into the membrane pores due to relatively thinner cake layer formation. Calculations for the membrane resistances and Reynolds number are available in the accompanying CD (Appendices 6.5 and 6.6 respectively)

6.3.6 Fouling mechanism

Fouling mechanisms during the ultrafiltration of beverage production wastewater can be analysed using Hermia's fouling models [43]. Hermia's fouling models were primarily developed to identify the different fouling mechanisms involved during dead-end filtration at constant pressure. Although this is the case, several researchers have successfully applied the models to analyse experimental data obtained from crossflow filtration [44-47]. Here, Hermia's models will be used specifically to establish the most appropriate fouling mechanism (based on the R^2 value) involved during the ultrafiltration of beverage production wastewater at different combinations of TMP and CFV.

The general equation used to describe different fouling mechanisms at constant pressure filtration is given by Eq. (16):

$$d^2t/dV^2 = K\,(dt/dV)^n \qquad (16)$$

where K is a constant and n is the blocking index. The different values of n are the following: n = 0 for cake filtration; n = 1.5 for standard blocking; n = 1 for intermediate blocking; and n = 2 for complete blocking.

The integrated forms of Hermia's fouling models are given by Eqs. (17) to (20) [48]:

$$t/V = 1/Q_O + K_C V/2 \qquad \text{(cake filtration)} \qquad (17)$$

$$t/V = 1/Q_O + K_S t/2 \qquad \text{(standard blocking)} \qquad (18)$$

$$1/Q = 1/Q_O + K_i t \qquad \text{(intermediate blocking)} \qquad (19)$$

$$Q = Q_O + K_b V \qquad \text{(complete blocking)} \qquad (20)$$

where t is the time (s); V is the accumulated filtrate volume (m^3); Q is the experimental flow rate ($m^3\ s^{-1}$); Q_O is the initial flow rate ($m^3\ s^{-1}$); and K is a constant. The subscripts in the constant K refer to the blocking mechanisms (i.e. c for cake filtration, s for standard blocking, i for intermediate blocking, and b for complete blocking).

Since the integrated forms of Hermia's models presented above are all linear equations, plotting the left side of Eqs. (17) and (20) and Eqs. (18) and (19) as a function of volume and time respectively should yield a straight line. The results of the model fitting to the experimental data (i.e. permeate fluxes obtained) are shown in Figures 6.8a to l.

The fitting of Hermia's models to the experimental data shows that cake filtration was

the dominant fouling mechanism at a TMP of 100 kPa. At higher pressures of 200 and 300 kPa, the fouling mechanism could not be established clearly due to low correlation values obtained. Although this was the case, correlation values obtained for cake filtration and standard blocking at TMPs of 200 and 300 kPa were the highest among the different types of fouling mechanisms considered. But in Section 6.3.5, it was shown that the adsorption resistances (R_F) obtained were negligible all throughout the duration of the experiments because of their relatively smaller values compared to the intrinsic membrane resistance (R_M). Therefore at TMPs of 200 and 300 kPa, the fouling mechanism appears to be inclined towards cake filtration.

The low correlation values obtained at higher TMPs may be due to the inability of Hermia's models to take into consideration the interaction between TMP and CFV since they were primarily developed for dead-end filtration. The rate of particle deposition during dead-end filtration differs from crossflow filtration [23]. In dead-end filtration, particles present in the feedwater continuously build up on the membrane surface throughout the filtration period. The rate of particle deposition at this mode is directly proportional to the TMP. The higher the TMP, the faster the particles deposit on the membrane surface. Likewise, in this mode, particles already deposited on the membrane surface have the tendency to be compressed leading to higher cake resistance and low permeate flux. In contrast, only a portion of the particles present in the feedwater get deposited on the membrane surface during crossflow filtration. Particle deposition rate at this mode is influenced by CFV and TMP. When flow becomes more turbulent due to high CFVs and TMPs, particles already deposited have the tendency to be swept away from the membrane surface resulting in reduced cake resistance and permeate flux improvement. Specifically, for the wastewater used in the experiments, it was shown

that higher CFVs and TMPs limited the rate of particle deposition resulting in higher permeate fluxes. Calculations for the model fitting are shown in Appendix 6.7 – attached at the end of the thesis.

a)

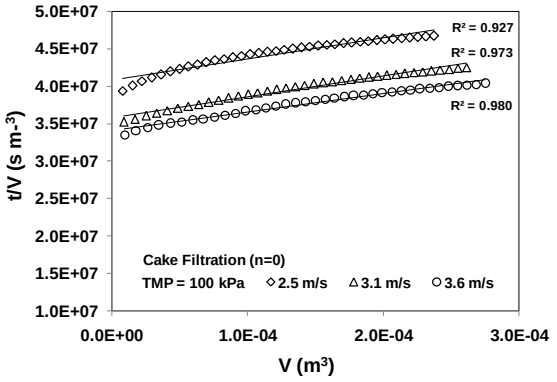

b)

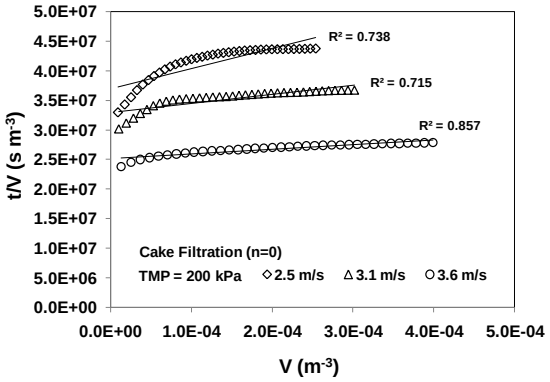

c)

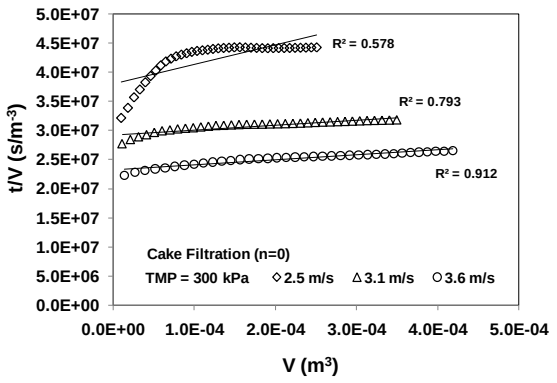

d)

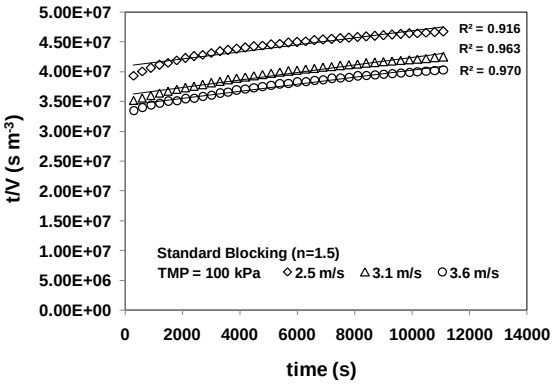

e)

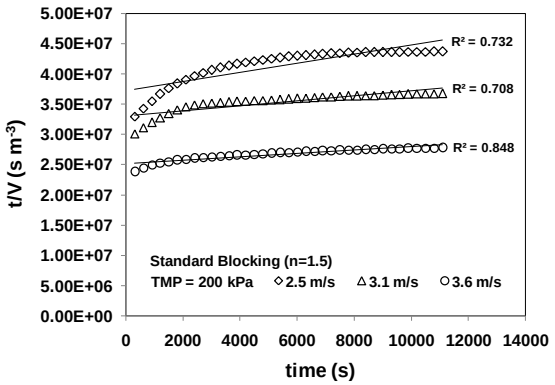

f)

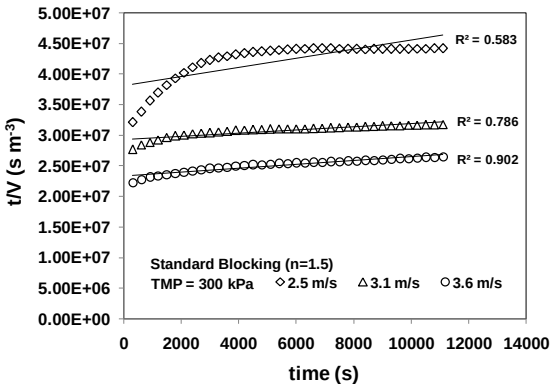

g)

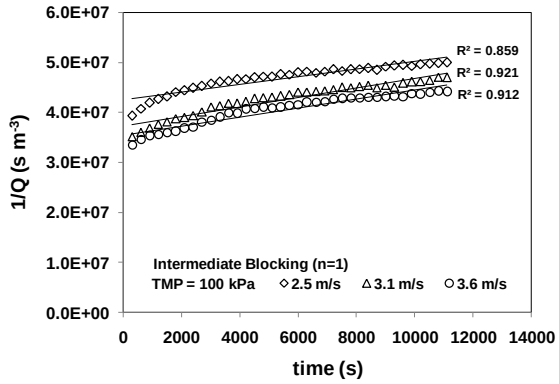

h)

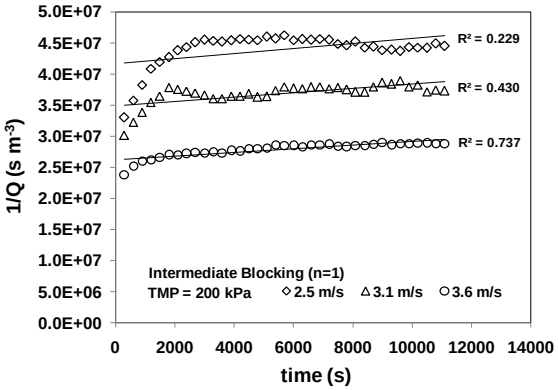

i)

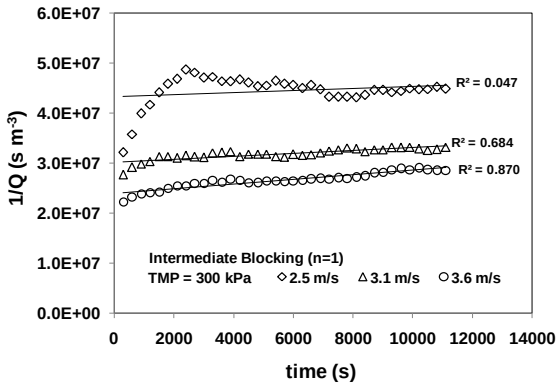

j)

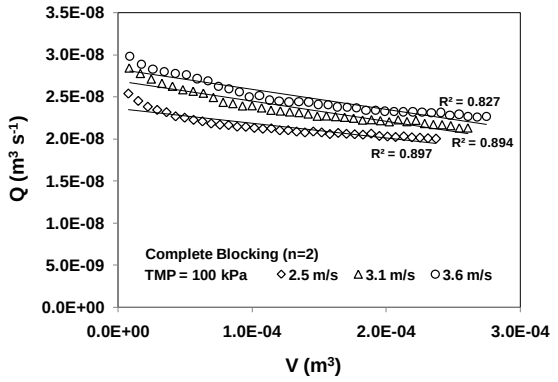

k)

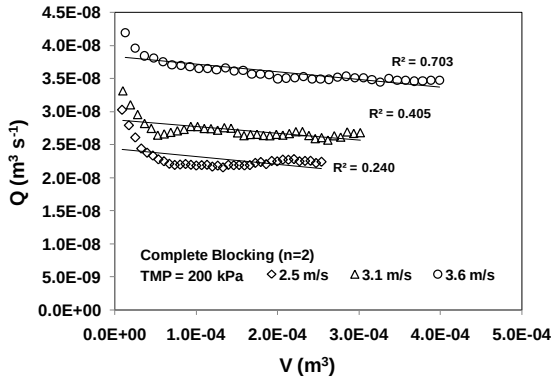

l)

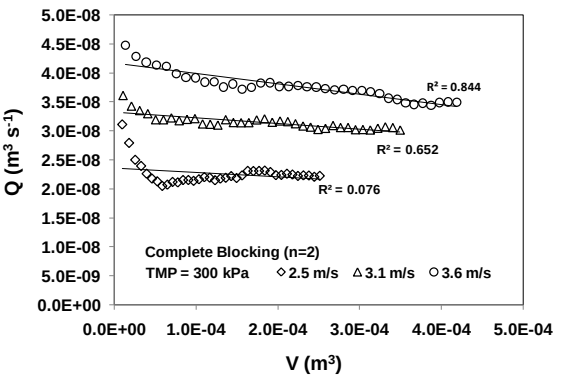

Figure 6.8: Model fitting to the experimental data. Cake filtration at a) 100 kPa, b) 200 kPa and c) 300 kPa; standard blocking at d) 100 kPa, e) 200 kPa and f) 300 kPa; intermediate blocking at g) 100 kPa, h) 200 kPa and i) 300 kPa; and complete blocking at j) 100 kPa, k) 200 kPa and l) 300 kPa.

6.3.7 Influence of CFV and TMP on contaminant rejection

The influences of TMP and CFV on turbidity and COD rejection rates are shown in Figures 6.9a and b.

a)

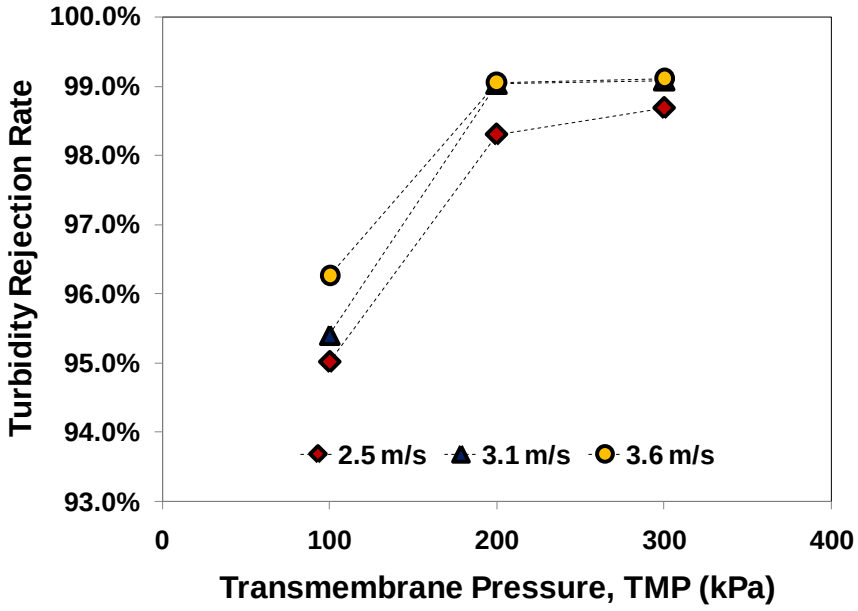

b)

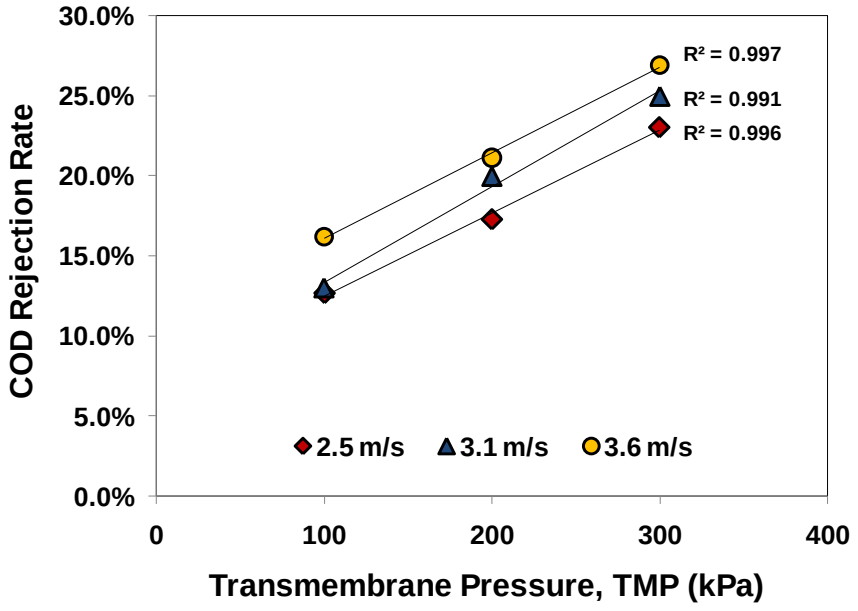

Figure 6.9: Influence of different combinations of TMPs and CFVs on: a) turbidity rejection rate and b) COD rejection rate.

For turbidity, a big increase in rejection rate was obtained at all CFVs when TMP was increased from 100 to 200 kPa. Increasing the TMP further to 300 kPa yielded a slight increase in turbidity rejection rate at all CFVs. Meanwhile, COD rejection rates obtained at all CFVs showed a linear correlation ($R^2 > 0.99$) with TMP. The COD rejection rate of the ceramic membrane may be associated with the suspended particles present in the wastewater samples since an increase in turbidity rejection correlates with an increased COD rejection.

In general, both turbidity and COD rejection rates increase as TMP and CFV increase. The increase in TMP and CFV makes the flow more turbulent and thus particles are swept away from the membrane surface. Once particles are swept away from the membrane surface, concentration polarization is reduced – resulting in better filtrate quality. Calculations for the turbidity and COD rejection rates are available in the accompanying CD (Appendix 6.8).

6.3.8 Influence of CFV and TMP on energy consumption

Improvements in permeate fluxes and contaminant rejection rates during the experiments were achieved at higher TMPs and CFVs. However, maintaining high TMPs and CFVs usually involve the consumption of substantial amounts of energy [29, 49], especially for systems requiring larger pumps. To investigate this further, the average power consumption of the pump motor for each experiment run was recorded. The recorded power consumptions were subsequently used to calculate energy consumptions using Eqs. (21) and (22):

$$EC_T = Pt \quad (21)$$

$$EC_{SP} = E_{CT} / V_P \quad (22)$$

where EC_T is the energy consumption (kWh), P is the average recorded power (kW), t is the experiment duration (hr), EC_{SP} is the specific energy consumption (kWh/m^3), and V_P is the volume of the permeate per experiment run (m^3). Table 6.2 shows the specific energy consumption of the 5 nm ceramic ultrafiltration system as a function of different CFVs and TMPs. The calculations on specific energy consumptions are available in the accompany CD (Appendix 6.9).

Table 6.2: Energy consumption of the ceramic ultrafiltration system as a function of different CFVs and TMPs

CFV (m/s)	Pressure (kPa)	Energy Consumption (kWh)	Volume (m^3)	Specific Energy Consumption (kWh/m^3)
2.5	100	0.183	0.00023	796
	200	0.204	0.00025	816
	300	0.216	0.00024	900
3.1	100	0.216	0.00025	864
	200	0.234	0.00029	807
	300	0.243	0.00034	715
3.6	100	0.264	0.00027	978
	200	0.282	0.00035	806
	300	0.297	0.00040	743

The results show that both CFV and TMP influence the energy consumption of the ceramic ultrafiltration system. At a lower CFV of 2.5 m s^{-1}, specific energy consumption increases as TMP is increased. On the other hand, at CFVs of 3.1 & 3.6 m s^{-1}, specific energy consumptions decrease as TMP is increased. Therefore, based on Table 6.2, a CFV of 3.1 m s^{-1} and TMP of 300 kPa show the most beneficial operating condition in

terms of specific energy consumption and permeate volume. Although further increasing the CFV to 3.6 m s^{-1} leads to a slight increase in permeate flow, the specific energy consumption is relatively higher.

6.4 Conclusions

A judicious combination of CFV and TMP has been shown to be critical for the successful application of a 5 nm ceramic ultrafiltration membrane to beverage production wastewater. In general, at higher CFVs of 3.1 and 3.6 m s^{-1}, permeate fluxes and contaminant rejection rates show significant improvements when TMP is increased to 200 and 300 kPa. This filtration behaviour can be attributed to the decrease of particle deposition on the membrane surface due to turbulent flow. At the CFVs mentioned, the majority of the particles present in the beverage production wastewater are swept away from the membrane surface resulting in lower concentration polarization (cake layer) resistance and increased permeate flux. Likewise, once the majority of particles are swept away from the membrane surface, their infiltration into the membrane pores is also reduced resulting in lesser suspended solids in the filtrate. The results also show that at CFVs of 3.1 & 3.6 m s^{-1}, specific energy consumptions decrease at an increasing TMP. Likewise, a CFV of 3.1 m s^{-1} and TMP of 300 kPa has been identified to be the most optimum combination in terms of specific energy consumption and permeate flow rate.

The work described in this chapter has since been published in the international literature [50].

6.5 References

[1] Amuda, O. S. & Amoo, I. A. 2007. Coagulation/flocculation process and sludge conditioning in beverage industrial wastewater treatment. *Journal of Hazardous Materials,* 141**,** 778-783.

[2] Matošić, M., Prstec, I., Jakopović, H. K. & Mijatović, I. 2009. Treatment of beverage production wastewater by membrane bioreactor. *Desalination,* 246**,** 285-293.

[3] Amuda, O. S., Amoo, I. A. & Ajayi, O. O. 2006. Performance optimization of coagulant/flocculant in the treatment of wastewater from a beverage industry. *Journal of Hazardous Materials,* 129**,** 69-72.

[4] Chmiel, H., Kaschek, M., Blöcher, C., Noronha, M. & Mavrov, V. 2003. Concepts for the treatment of spent process water in the food and beverage industries. *Desalination,* 152**,** 307-314.

[5] Tay, J.-H. & Jeyaseelan, S. 1995. Membrane filtration for reuse of wastewater from beverage industry. *Resources, Conservation and Recycling,* 15**,** 33-40.

[6] Russell, D. L. 2006. *Practical Wastewater Treatment,* Hoboken, Wiley-Interscience.

[7] Sarkar, B., Chakrabarti, P. P., Vijaykumar, A. & Kale, V. 2006. Wastewater treatment in dairy industries -- possibility of reuse. *Desalination,* 195**,** 141-152.

[8] Kim, J., DiGiano, F. A. & Reardon, R. D. 2008. Autopsy of high-pressure membranes to compare effectiveness of MF and UF pretreatment in water reclamation. *Water Research,* 42**,** 697-706.

[9] Chen, J. P., Mou, H., Wang, L. K. & Matsuura, T. 2006. Membrane filtration. *In:* Wang, L. K., Hung, Y. & Shammas, N. K. (eds.) *Handbook of environmental*

engineering, volume 4: Advanced physicochemical treatment processes. Totowa, NJ: The Humana Press Inc.

[10] Bennett, A. 2005. Membranes in industry: facilitating reuse of wastewater. *Filtration & Separation,* 42**,** 28-30.

[11] Vedavyasan, C. V. 2007. Pretreatment trends - an overview. *Desalination,* 203**,** 296-299.

[12] Karakulski, K. & Morawski, W. A. 2000. Purification of copper wire drawing emulsion by application of UF and RO. *Desalination,* 131**,** 87-95.

[13] Norouzbahari, S., Roostaazad, R. & Hesampour, M. 2009. Crude oil desalter effluent treatment by a hybrid UF/RO membrane separation process. *Desalination,* 238**,** 174-182.

[14] Zhang, J., Zeng, H., Ye, C., Chen, L. & Yan, X. 2008. Pilot test of UF pretreatment prior to RO for cooling tower blowdown reuse of power plant. *Desalination,* 222**,** 9-16.

[15] Teng, C. K., Hawlader, M. N. A. & Malek, A. 2003. An experiment with different pretreatment methods. *Desalination,* 156**,** 51-58.

[16] Sekine, M., Salehi, Z., Tokumura, M. & Kawase, Y. 2012. Solar photo-Fenton process for the treatment of colored soft drink wastewater: Decolorization, mineralization and COD removal of oolong tea effluent. *Journal of Environmental Science and Health - Part A Toxic/Hazardous Substances and Environmental Engineering,* 47**,** 2181-2189.

[17] Tawfik, A. & El-Kamah, H. 2012. Treatment of fruit-juice industry wastewater in a two-stage anaerobic hybrid (AH) reactor system followed by a sequencing batch reactor (SBR). *Environmental Technology,* 33**,** 429-436.

[18] Manyele, S. V., Peay, M. & Halfani, M. R. 2008. Treatment of beverage-processing wastewater in a three-phase fluidised bed biological reactor. *International Journal of Food Science and Technology,* 43**,** 1058-1065.

[19] Ng, K. K., Lin, C. F., Panchangam, S. C., Andy Hong, P. K. & Yang, P. Y. 2011. Reduced membrane fouling in a novel bio-entrapped membrane reactor for treatment of food and beverage processing wastewater. *Water Research,* 45**,** 4269-4278.

[20] Avula, R. Y., Nelson, H. M. & Singh, R. K. 2009. Recycling of poultry process wastewater by ultrafiltration. *Innovative Food Science & Emerging Technologies,* 10**,** 1-8.

[21] Mohammadi, T. & Esmaeelifar, A. 2004. Wastewater treatment using ultrafiltration at a vegetable oil factory. *Desalination,* 166**,** 329-337.

[22] Noronha, M., Britz, T., Mavrov, V., Janke, H. D. & Chmiel, H. 2002. Treatment of spent process water from a fruit juice company for purposes of reuse: hybrid process concept and on-site test operation of a pilot plant. *Desalination,* 143**,** 183-196.

[23] Cheryan, M. 1998. *Ultrafiltration and microfiltration handbook,* Lancaster, Pennsylvania, Technomic Publishing Company, Inc.

[24] Zavastin, D., Cretescu, I., Bezdadea, M., Bourceanu, M., Dragan, M., Lisa, G., Mangalagiu, I., Vasic, V. & Savic, J. 2010. Preparation, characterization and applicability of cellulose acetate-polyurethane blend membrane in separation techniques. *Colloids and Surfaces A: Physicochemical and Engineering Aspects,* 370**,** 120-128.

[25] Siskens, C. A. M. 1996. Applications of ceramic membranes in liquid filtration. *In:* Burggraaf, A. J. & Cot, L. (eds.) *Fundamentals of Inorganic membrane science and technology*. Burlington: Elsevier Science B.V.

[26] Lee, S. & Cho, J. 2004. Comparison of ceramic and polymeric membranes for natural organic matter (NOM) removal. *Desalination,* 160**,** 223-232.

[27] Benfer, S., Popp, U., Richter, H., Siewert, C. & Tomandl, G. 2001. Development and characterization of ceramic nanofiltration membranes. *Separation and Purification Technology,* 22-23**,** 231-237.

[28] Ciston, S., Lueptow, R. M. & Gray, K. A. 2008. Bacterial attachment on reactive ceramic ultrafiltration membranes. *Journal of Membrane Science,* 320**,** 101-107.

[29] Agana, B. A., Reeve, D. & Orbell, J. D. 2011. Optimization of the operational parameters for a 50 nm ZrO2 ceramic membrane as applied to the ultrafiltration of post-electrodeposition rinse wastewater. *Desalination,* 278**,** 325-332.

[30] Suttiponparnit, K., Jiang, J., Sahu, M., Suvachittanont, S., Charinpanitkul, T. & Biswas, P. 2011. Role of Surface Area, Primary Particle Size, and Crystal Phase on Titanium Dioxide Nanoparticle Dispersion Properties. *Nanoscale Research Letters,* 6**,** 1-8.

[31] Agana, B. A., Reeve, D. & Orbell, J. D. 2012. The influence of an applied electric field during ceramic ultrafiltration of post-electrodeposition rinse wastewater. *Water Research,* 46**,** 3574-3584.

[32] ASTM 1985. Zeta Potential of Colloids in Water and Waste Water. *ASTM Standard D 4187-82.*

[33] Stamatakis, K. & Chi, T. 1993. A simple model of cross-flow filtration based on particle adhesion. *AICHE Journal,* 39**,** 1292-1302.

[34] O'Neill, M. E. 1968. A sphere in contact with a plane wall in a slow linear shear flow. *Chemical Engineering Science,* 23**,** 1293-1298.

[35] Altmann, J. & Ripperger, S. 1997. Particle deposition and layer formation at the crossflow microfiltration. *Journal of Membrane Science,* 124**,** 119-128.

[36] Cardarelli, F. 2008. Soils and Fertilizers. *Materials Handbook.* 2nd ed.: Springer London.

[37] Israelachvili, J. N. 2010. Van der waals forces. *Intermolecular and surface forces.* 3 ed. Burlington: Elsevier Science.

[38] Butt, H.-J. & Kappl, M. 2009. *Surface and Interfacial Forces,* Hoboken, Wiley-VCH.

[39] Krupp, H. 1967. Particle Adhesion Theory and Experiment. *Colloid Interface Sci.,* 11**,** 11-239.

[40] Crittenden, J. C., Trussell, R. R., Hand, D. W., Howe, K. J. & Tchobanoglous, G. 2005. *Water treatment: Principles and design,* Hoboken, NJ, John Wiley & Sons, Inc.

[41] Mulder, M. H. V. 1995. Polarization phenomena and fouling. *In:* Noble, R. D. & Stern, S. A. (eds.) *Membrane Separations Technology: Principles and Applications.* Burlington: Elsevier Science.

[42] Baker, R. J., Fane, A. G., Fell, C. J. D. & Yoo, B. H. 1985. Factors affecting flux in crossflow filtration. *Desalination,* 53**,** 81-93.

[43] Hermia, J. 1982. CONSTANT PRESSURE BLOCKING FILTRATION LAWS - APPLICATION TOPOWER-LAW NON-NEWTONIAN FLUIDS. *TRANS INST CHEM ENG,* V 60**,** 183-187.

[44] Vela, M. C. V., Blanco, S. A., García, J. L. & Rodríguez, E. B. 2008. Analysis of membrane pore blocking models applied to the ultrafiltration of PEG. *Separation and Purification Technology,* 62**,** 489-498.

[45] Lim, A. L. & Bai, R. 2003. Membrane fouling and cleaning in microfiltration of activated sludge wastewater. *Journal of Membrane Science,* 216**,** 279-290.

[46] Hwang, K. J. & Lin, T. T. 2002. Effect of morphology of polymeric membrane on the performance of cross-flow microfiltration. *Journal of Membrane Science,* 199**,** 41-52.

[47] Mohammadi, T. & Esmaeelifar, A. 2005. Wastewater treatment of a vegetable oil factory by a hybrid ultrafiltration-activated carbon process. *Journal of Membrane Science,* 254**,** 129-137.

[48] Wang, F. & Tarabara, V. V. 2008. Pore blocking mechanisms during early stages of membrane fouling by colloids. *Journal of Colloid and Interface Science,* 328**,** 464-469.

[49] Waeger, F., Delhaye, T. & Fuchs, W. 2010. The use of ceramic microfiltration and ultrafiltration membranes for particle removal from anaerobic digester effluents. *Separation and Purification Technology,* 73**,** 271-278.

[50] Agana, B. A., Reeve, D. & Orbell, J. D. 2013. Performance optimization of a 5 nm TiO2 ceramic membrane with respect to beverage production wastewater. *Desalination,* 311**,** 162-172.

Chapter Seven: Recommendations and Conclusions

7.1 Overview

An in-series integrated water management strategy has been devised and deployed for the systematic identification of possible water conservation opportunities for two large Australian manufacturing companies.

A water audit characterized all water streams for both companies' production sites, leading to the development of comprehensive water flow diagrams. This also served to identify some operational issues that could impinge on water management. Such operational issues emanate from employee work practices performed during operations such as the manual addition of freshwater into processes, equipment cleaning and general plant cleaning. If such issues can be addressed by management, substantial amounts of freshwater can be saved, as outlined in Chapter 2. The water flow diagrams, as well as concomitant water test results obtained via the audit, served as the basis for subsequent strategies.

Thus, a process integration strategy, which utilized commercially available water pinch software, has successfully identified possible water reuse opportunities. These reuse opportunities were evaluated in consultation with management and some were implemented on site - with significant savings. For example, the implementation of directly reusing wastewater generated by the Air Handling Units (AHUs) and the RO system reduced Citywater consumption of processes such as sludge pools and car parts pretreatment, as discussed in Chapter 2. Likewise, implementing the recommended reclamation of the post-electrodeposition rinse wastewater via an ultrafiltration process will result to an additional savings in Citywater consumption. Meanwhile, for Company B, the implementation of the recommended direct reuse of wastewater generated by

process utilities such as boilers, vacuum pumps and washer/rinsers will result to a substantial reduction of Citywater consumption. Aside from reductions in Citywater consumptions, both companies will also benefit from reduced wastewater discharges if the streams mentioned are reused back into processes.

Finally, the delineation of a water recycling strategy allowed the suitability of different membranes for treating specific wastewater streams to be considered. Thus, a laboratory-scale membrane test rig, constructed and used as an integral part of this study, has provided valuable information in relation to the applicability of different membranes for the reclamation of specific wastewater streams generated at both companies. By using the test rig, different operating parameters essential to the successful operation of such membranes used were identified – as described in Chapters 3 - 6. Likewise, the use of the test rig made it possible to effectively evaluate different membrane candidates prior to doing pilot-scale evaluations. General results for these membrane experiments are summarized as follows:

1. Polymeric UF membranes cannot be used directly as pretreatment for Company A's oily wastewater stream due to the presence of suspended CED paint particles. The CED paint particles - made up of paint pigment, unstable resins and polymers, rapidly deposit on the membrane surface, creating a cake layer similar to a paint coating. Although such particle deposition may be minimized by increasing the velocity of the feed water, membrane cleaning remains a critical issue. The nature and frequency of cleaning to remove the CED paint particles on the membrane surface is likely to significantly degrade the membrane material – leading to a reduced lifespan. For this specific

wastewater stream, a ceramic membrane has been evaluated and is suggested as being more appropriate in terms of chemical and thermal stability.

2. Ceramic UF membranes are also recommended as being more appropriate for pretreatment of Company A's oily wastewater stream – the bulk of which comes from the final rinsing stages of car bodies. Specifically, a 50 nm ZrO_2 ceramic UF membrane was tested on a model wastewater containing 5 % v/v suspension of CED paint. The model wastewater prepared for the experiments was similar in composition to the actual wastewater generated at the final rinsing stages. Likewise, the model wastewater has been prepared to have a worse water quality as compared to the actual wastewater mentioned. In general, it was deduced that a combination of high CFV and low TMP is the most beneficial operating condition for ceramic ultrafiltration of wastewater containing CED paint particles [1]. A CFV of 3.2 m s^{-1} and TMP of 100 kPa produced the highest permeate flux and optimum energy consumption.

3. The use of an applied electric field across a 50 nm ZrO_2 ceramic UF membrane also proved to be beneficial during ultrafiltration (at low CFV) of wastewater containing CED paint. An electric field produced by the applied voltage influenced the movement and electrophoretic mobility of the CED paint particles. Results showed that the influence of an electric field during electro-ultrafiltration of the model wastewater containing 5 % v/v suspension of CED paint was dependent on both the applied voltage and transmembrane pressure (TMP) [2]. At an applied voltage of 60 V and TMP of 100 kPa, flux rates obtained after 60 minutes were higher than the flux rates obtained from ultrafiltration alone. Such set-up can also be applied for company A's oily wastewater because the bulk of the volume that constitute this stream comes from the final rinsing

stages of car bodies. Wastewater generated at the final rinsing stages is similar in composition to the model wastewater used – as previously mentioned in Item 2. Therefore, the use of electro-ultrafiltration for the treatment of Company A's oily wastewater stream will possibly yield similar results with electro-ultrafiltration experiments involving the model wastewater.

4. A polyvinylidine-difluoride (PVDF) UF membrane was identified as being suitable for pretreatment of beverage production wastewater (Company B). Flux decline rates for the PVDF-UF membrane were relatively lower as compared to the polyacrylonitrile (PAN) UF membrane tested. Likewise, for this specific wastewater stream, the PVDF-UF membrane showed higher reduction rates with respect to critical water parameters such as turbidity and TOC. Although the PVDF-UF membrane has been shown to be suitable for the beverage production wastewater, in the long run, the use of such a membrane for this specific stream is not advisable. The beverage production wastewater evaluated in this study contains different types of chemicals and has high levels of organic contamination. The chemicals present in the beverage production wastewater may cause premature degradation of membrane material – resulting to a shorter lifespan. Meanwhile, high levels of organic contamination may severely foul the membrane. Such fouling may require the use of aggressive cleaning chemicals and a longer cleaning period to completely regenerate the membrane. This scenario may also lead to premature membrane material degradation. Again for this type of wastewater, a ceramic membrane is recommended as being more suitable.

5. Since it was determined that a polymeric membrane was not suitable for pretreatment of beverage production wastewater, a ceramic UF membrane was also

evaluated. This ceramic membrane has a 5 nm nominal pore size with a TiO_2 active layer. It was used for the following reasons: 1) different cleaning chemicals and detergents are present in the wastewater stream and therefore a membrane material able to withstand such harsh conditions should be used; 2) the active layer of the chosen ceramic membrane (TiO_2) is a good inhibitor of biofilm growth and fouling; and 3) the particles sizes ranged from 24 – 5560 nm. Results showed that a CFV of 3.1 m s^{-1} and TMP of 300 kPa was the most optimum operating condition in terms of energy consumption and permeate flow rate.

6. A polyvinylidine-difluoride (PVDF) UF membrane was suggested for the pretreatment of Company A's metals wastewater stream. This specific type of membrane has a MWCO of 30 kD, and is hydrophobic with a 4° contact angle. The PVDF-UF membrane used showed slow flux decline rates, and high turbidity and TOC reduction rates.

7. A thin film low-pressure RO membrane was suggested as being suitable for the reclamation of oily and beverage production wastewater streams. This type of RO membrane has a high flux and a NaCl rejection rate of approximately 99.0 %. Permeate flux decline rates for the RO membrane with respect to the two wastewaters mentioned were slow. Likewise, reduction rates of water quality parameters such as conductivity and COD were high.

8. The data obtained for RO and NF membranes with respect to the treatment of the metals wastewater stream are not consistent with the literature since RO membranes are known to have greater capacity to remove dissolved salts as compared to an NF

membrane. Therefore, before a conclusion on whether an RO or NF membrane is suitable for the reclamation of the metals wastewater stream, a comprehensive study should be conducted.

9. The specific energy consumptions (kWh/m^3) for all the membranes used in the experiments were dependent on TMP, permeate flow rate and system efficiency Additionally, UF membranes operate according to the pore flow model and therefore the proper combination of CFV and TMP is particularly important in order to inhibit particle deposition and slow down flux decline rate. On the other hand, NF and RO membranes operate according to the solution-diffusion model and therefore the intensity of TMP dictate permeate flux and rejection rates.

7.2 Recommendations

7.2.1 Automation of pretreatment and post treatment processes at Company A's Paint Shop

Water use at the pretreatment and post treatment processes found at Company A's paint shop account for approximately 32.0 % of the total water consumption. In these processes, a number of irregularities in water use related to employee work practices were identified. Although the provision of training and seminars aimed at changing employees' perceptions on water use can be effective in reducing water consumption at the above-mentioned processes, such a strategy might only work for the short term. Unless continuously reinforced, employees remember training and seminars only for a short period of time and are likely to revert to old established work habits – usually unknowingly, but sometimes deliberately. Therefore for a long-term solution, automation of pretreatment and post treatment processes is the best option. Automating

water use at these processes will not involve major changes since the system of pipes needed for such a venture is already in place – i.e. overflow and diversion pipes to other process. At most, this will involve the installation of various instrumentations such as controllers, timers and valves.

7.2.2 Seminars and trainings on water use for Company B's production employees

Since the majority of the water-using processes at Company B's production site are already automated (i.e. CIP systems, water supply systems, etc.), the initial focus of water conservation should be aimed at employees' work practices. For this company, water-using activities during the production period are commonly cleaning related. For example, it was observed during the water audit that floor cleaning was either done after every change in employees' work shift or in the product produced. Such activity, depending on the employee performing the cleaning, can lead to a substantial amount of freshwater use. This type of practice, having been identified, can easily be corrected by changing the employees' perception on water use through constant seminars and trainings. Once the perception on water use improves, the company can subsequently introduce a Standard Operating Procedure (SOP) for water use. Such seminars and trainings may not work effectively for Company A since majority of the water uses on-site are process related. Most of the employees' mindset on water use is always based on the quality of the final product. For example, to prevent impurities from clinging to car bodies, the operator would set the rinses at high flow. Likewise, to prevent painting defects, the operator may continuously overflow a car dipping bath to maintain conductivity levels on the safest side.

7.2.3 Cost of reclaiming specific wastewater streams through membrane processes

As mentioned in Chapter 2, the biggest opportunity for water reuse comes from the contaminated wastewater streams. The suitability of specific membrane processes were tested for these streams and discussed in detail in Chapters 3 to 6. The estimated costs of the membrane processes that are suitable for specific wastewater streams are shown in Tables 7.1 to 7.4. The formulas used in the cost calculations are given in Eqs. (1) to (8).

The wastewater recycling rate was calculated using Eq. (1):

$$\% R_{WW} = W_R / WW_T \times 100\ \% \quad (1)$$

where $\% R_{WW}$ is the wastewater recycling rate; W_R is the volume of treated water for reuse per day, m^3; and WW_T is the total volume of wastewater generated per day, m^3. The initial cost of equipment installation was calculated using Eq. (2):

$$C_I = C_E + C_M \quad (2)$$

where C_I is the total initial cost of equipment installation, \$AUD; C_E is the equipment cost, \$AUD; and C_M is the miscellaneous cost, \$AUD. Miscellaneous cost includes civil works, connection set-up and freight. This cost was estimated using Eq. (3):

$$C_M = 0.05\ C_E \quad (3)$$

The total savings from wastewater recycling was calculated using Eq. (4):

$$S_T = FW_S + WW_S \quad (4)$$

where S_T is the total savings per year, \$AUD; FW_S is the freshwater savings per year, \$AUD; and WW_S is the actual wastewater savings per year, \$AUD. Freshwater and actual wastewater savings per year were calculated using Eqs. (5) and (6) respectively:

$$FW_S = W_R \times C_W \times N_D \quad (5)$$

where C_W is the cost of freshwater per m^3, \$AUD; and N_D is the number of days the manufacturing facility operates (N~240 days).

$$WW_S = WW_{SI} - 0.2\ (WW_{SI}) \quad (6)$$

where WW_{SI} is the initial wastewater savings per year, \$AUD. The initial wastewater savings per year was calculated using Eq. (7):

$$WW_{SI} = W_R \times C_{WW} \times N_D \quad (7)$$

where C_{WW} is the cost of wastewater discharge per m^3, and N_D is the number of days the manufacturing facility operates (N~240 days). The term $0.2 \times WW_{SI}$ in Eq. (9) is a cost provision that accounts for any increase in water quality parameters such as TDS, COD and BOD.

Finally, the payback period was calculated using Eq. (8):

$$P_P = C_I / S_T \quad (8)$$

Table 7.1: Estimated cost of UF membrane system for reclamation of post-electrodeposition rinse wastewater (WW_T = 253 m^3/day), Company A

% R_{WW}	C_I, \$AUD ($C_E + C_M$)	S_T, \$AUD/yr ($FW_S + WW_S$)	P_P, yrs – months
10.0 %	105,000.00	680.63	154 – 4
30.0 %	210,000.00	32,870.91	6 – 5
50.0 %	315,000.00	65,061.18	4 – 10
70.0 %	420,000.00	89,274.05	4 – 9
90.0 %	525,000.00	114,178.21	4 – 8

Table 7.2: Estimated cost of ceramic UF and polymeric RO membrane systems for reclamation of oily wastewater stream (WW_T = 578 m^3/day; RO recovery = 75 %), Company A

% R_{WW}	C_I, \$AUD ($C_E + C_M$)	S_T, \$AUD/yr ($FW_S + WW_S$)	P_P, yrs – months
7.5 %	257,250.00	4,457.52	57 – 9
22.5 %	467,250.00	44,263.53	10 – 8
37.5 %	813,750.00	76,255.81	10 – 8
52.5 %	1,128,750.00	115,759.85	9 – 10
67.5 %	1,338,750.00	170,829.38	7 – 10

Table 7.3: Estimated cost of polymeric UF and NF membrane systems for reclamation of metals wastewater stream (WW_T = 144 m^3/day; NF recovery = 75 %), Company A

% R_{WW}	C_I, \$AUD ($C_E + C_M$)	S_T, \$AUD/yr ($FW_S + WW_S$)	P_P, yrs – months
67.5 %	94,500.00	47,392.41	2 – 0

Table 7.4: Estimated cost of ceramic UF and polymeric RO membrane systems for reclamation of beverage production wastewater (WWT = 942 m^3/day; RO recovery = 75 %), Company B

% R_{WW}	C_I, \$AUD ($C_E + C_M$)	S_T, \$AUD/yr ($FW_S + WW_S$)	P_P, yrs – months
7.5 %	362,250.00	20,215.69	17 – 11
22.5 %	813,750.00	68,762.78	11 – 10
37.5 %	1,233,750.00	140,085.14	8 – 10
52.5 %	1,774,500.00	205,152.05	8 – 8
67.5 %	2,194,500.00	264,330.89	8 – 4

As expected, the payback period for the proposed membrane systems generally shortens as the wastewater recycling rate is increased. Although this is the case, majority of the payback periods for the installation of specific membrane systems were above 4 years. The costs reveal that it is basically cheaper to discharge the highly contaminated wastewater streams as Tradewaste rather than installing wastewater treatment equipment such as membrane systems. This is because the current water tariffs in Australia are low – making on-site treatment of wastewater uneconomic. However, it is worth noting that this may not always be the case.

Tables 7.1 to 7.4 show the costs of single and dual membrane treatment systems. The wastewater recycling rates for each type of system are explained as follows. For a single treatment system (i.e. the UF system, Table 7.1), the wastewater recycling rate is a straightforward calculation. For example a 30 % wastewater recycling rate would mean a volume of 76 m^3/day (30 % of 253 m^3/day). But for a dual treatment system (i.e. UF and RO/NF systems, Tables 7.2 to 7.4, the wastewater recycling rate would mean a combination of the rates for both UF and RO/NF systems. For example, Table

7.2 shows a wastewater recycling rate of 67.5 %. This percentage is equivalent to a volume of approximately 390 m^3/day (67.5 % of 578 m^3/day). In order to obtain this volume, around 90 % (520 m^3/day) of the total wastewater generated is reclaimed by the UF system. The filtrate obtained from the UF system is subsequently passed through an RO system at a recovery rate of 75 %. The volume of the pure water after the RO system is 390 m^3/day.

The equipment cost estimates used in this section were obtained directly from the membrane manufacturers. Since costs were merely estimates, there's a possibility that they may either increase or decrease depending on the final equipment design. The calculations on the membrane costs are shown in Appendix 7.1 – attached at the end of the thesis.

7.2.4 Membrane concentrate management

The management of membrane concentrate at the two manufacturing sites will slightly differ from each other since they generate contrasting wastewater qualities. Likewise, other factors such as existing wastewater treatment facilities and wastewater tariffs can also influence the final decision on concentrate management.

7.2.4.1 Company A

The use of ceramic UF membranes for the pretreatment of the oily wastewater stream will generate reject water containing highly concentrated oil & grease and cathodic electrodeposition (CED) paint particles. This concentrate can be fed into the existing oily wastewater treatment system to eliminate the suspended particles present. The existing wastewater treatment system consists of a series of treatment processes such as

coagulation, pH adjustment, flocculation, and dissolved air flotation. Subsequently, the treated UF concentrate can be mixed with the RO concentrate and treated further. The concentrate management method mentioned above is also applicable during reclamation of post-electrodeposition rinse wastewater.

The use of polymeric UF membranes to pretreat the metals wastewater stream will generate reject water containing highly concentrated suspended particles. Such reject water can be mixed with the reject water generated by the NF membrane that contains high levels of metals. The mixed UF and NF concentrate can be fed into the existing metals wastewater treatment system to eliminate suspended particles and specific metals such as Ni, Zn and Mn. The existing metals wastewater treatment system is composed of processes such as pH adjustment, flocculation and dissolved air flotation. The treated concentrates can be mixed together and treated further.

There are many commercially available technologies for the treatment of membrane concentrate. Some of the more appropriate technologies for company A's membrane concentrate include Wind Aided Intensified eVaporation (WAIV) and membrane distillation. WAIV technology is an enhancement of the natural evaporation technology. Compared to natural evaporation, WAIV requires smaller land area and utilizes the drying power of the wind [3]. This technology increases the evaporation rates by 50 – 90 %. On the other hand, membrane distillation is also a promising technology that is not fully commercialized yet. It is quite different from other membrane technologies because it uses the difference in vapour pressure rather than total pressure to extract pure water from a membrane concentrate stream. Its major energy requirement is low-grade thermal energy which is readily available in industrial

sites in the form of cooling tower feed, excess steam, generator exhaust, etc [4]. Different types of membrane distillation include Direct Contact Membrane Distillation (DCMD), Air Gap Membrane Distillation (AGMD), Sweep Gas Membrane Distillation (SGMD), and Vacuum Membrane Distillation (VMD). Typical operating temperature for membrane distillation ranges from 60 – 80 °C.

The choice of concentrate treatment will depend on the company's goal. If Company A aims for zero liquid discharge, WAIV technology will be more suitable for membrane concentrate treatment. Alternatively, membrane distillation will be more suitable if Company A aims to recover pure water from the membrane concentrate. The sludge generated from the treatment of the membrane concentrate can be sent off-site through a waste collection and treatment company. Such practice of sending sludge off-site for disposal and treatment already exists at Company A.

7.2.4.2 Company B

As with Company A, the concentrate from the UF and RO membranes can be mixed together and subsequently treated using either WAIV or membrane distillation technology. The sludge generated from the treatment of the membrane concentrate can also be sent off-site through a waste collection and treatment company. After appropriate treatment (i.e. dewatering), the sludge can be dumped directly in landfills.

7.3 Conclusions

The in-series integrated water management strategy deployed in the study has been effective in systematically identifying possible water conservation opportunities at two large Australian manufacturing companies. The water audit completely characterized

all water streams found at both companies' production sites leading to the development of water flow diagrams - and also identified some operational issues that could impinge on water management. The water flow diagram, as well as comprehensive water test results obtained during the course of the audit, served as the basis for succeeding strategies. The process integration strategy, which utilized commercially available water pinch software, successfully identified possible water reuse opportunities. These reuse opportunities were further evaluated and some were implemented on site with significant savings. Finally, the water recycling strategy showed the suitability of different membranes for treating specific wastewater streams. Results showed that the membranes tested have generally good contaminant rejection rates, slow flux decline rates and low energy usage.

The synergy of the different water management strategies deployed in this study can bring about substantial reduction of Citywater consumption and wastewater discharge. For example, it was shown at Company A that 33 tonnes/day (2.2 % of total input) of Citywater consumption was saved by directly reusing wastewater generated from other processes. Likewise, it was also shown at Company A that a further 80.8 tonnes/day (5.7 % of total input) of freshwater consumption can be saved through treatment of the post-electrodeposition rinse wastewater using an ultrafiltration process. The combined value of the Citywater savings for Company A translates to a wastewater reduction of approximately 16.1 %. For Company B, approximately 83.2 tonnes/day (5.7 % of total input) of Citywater can be saved just by reclaiming wastewater generated from different identified processes. The reclaimed wastewater will be treated by the conventional treatment system currently in operation at the production site and reused back into

different water-using processes. This translates into a wastewater reduction of approximately 8.6 % for Company B.

The above water savings identified for both companies is, in fact, just the tip of the iceberg. The bulk of water savings will most likely come from wastewater treatment of the highly contaminated streams, using appropriate low-pressure membranes. In this regard, the use of the laboratory-scale membrane test rig, in conjunction with the other strategies employed, has provided valuable information into the applicability of different low-pressure membranes for the reclamation of specific wastewater streams generated at both companies. As demonstrated herein, employing such a test rig allows different operating parameters essential to the successful operation of candidate membranes to be characterized. Notably, the use of the test rig made it possible to effectively evaluate different low-pressure membrane candidates at much lower costs as compared to doing pilot-scale evaluations.

Although the results obtained so far are very promising, other issues such as applicability, membrane concentrate management and cost of commercial membrane equipment should also be researched further to completely assess the viability of their implementation. Results obtained from the process integration strategy are based on steady state assumptions and therefore implementation should always be checked against actual process operating conditions. It should be noted that the management of concentrate disposal is a long-standing problem for users of membrane technologies [5, 6]. Therefore the proper disposal of membrane concentrate should be a primary concern for both companies since they have to satisfy the Tradewaste discharge limits imposed on them by the local water retailer. Likewise, the commercial cost of the membrane

equipment should also be reliably known since the installation of such equipment will greatly depend on such monetary values.

In general, the results of the study revealed that total water recycling for both companies is achievable provided they make significant process changes to increase water use efficiency and are prepared to invest in appropriate water reclamation technologies. With the current production set-ups, it is estimated that both companies could reclaim approximately 75% of the wastewater generated through process integration and the use of membrane processes. The remaining 25 % of the wastewater generated at both companies can be eliminated through significant process changes. At the present time, there is little financial incentive for these companies to embark on such a venture since the current water tariffs in Australia is cheaper than the cost of investing in process changes and water reclamation technologies. Although this is currently the case, both companies could achieve a sustainable future in terms of a steady supply of water for use in different production processes should the current situation change.

7.4 Areas for further research

A number of areas for further research were identified from this work. These areas are as follows:

1) Current commercially available water pinch software is usually based on steady-state assumptions. Such assumptions don't take into consideration changes in operating parameters – i.e. changes in temperature, pressure, etc. Changes in operating parameters have a big effect on water use. For example, a 1 °C change in temperature can significantly alter the volume of feedwater supply to boilers, cooling towers and air

handling units. Therefore, in order to capture such changes, the development of water pinch software based on artificial intelligence is proposed. This software should be designed in such a way that it will directly interact with the existing process controls installed at both companies. The software will automatically adjust water use of processes when critical operating parameters change. For example, when the temperature changes from 1 °C to 2 °C, the feedwater supply to a boiler increases. Likewise, when temperature changes from 2 °C to 1 °C, the feedwater supply to a boiler decreases. Considering the process operating parameters (e.g. temperature, pressure, etc.) during a water pinch analysis will facilitate dynamic changes in feedwater supply to processes. Data on these changes can subsequently be captured by the proposed software and used as a basis for increasing process water use efficiency even in the absence of an actual plant trial.

2) In this work, a 75 % wastewater recycling rate can be achieved at the two companies studied. This is based on a combination of process integration and the use of membrane processes to reclaim wastewater. To achieve total water recycling, the remaining 25 % of wastewater generated should either be reused or eliminated completely. Therefore, to bridge the gap to achieving total water recycling, a study on significant process improvements aimed at improving water use efficiency is proposed. The study would deal directly with water-using processes. For example, if the current cooling tower is an open circuit type, it can be changed to a dry type in order to reduce water consumption.

3) The passage of iron (Fe) through the selected NF and RO membranes has not been fully investigated in this study. Assuming that this is not an experimental artifact, understanding the mechanisms behind the passage of Fe through these membranes will

lead to better understanding of membrane material suitability. Likewise, it is also worth identifying why the iron has been present as a neutral species.

4) Water reclamation of different wastewater streams is very dependent on the pretreatment process to be used – as discussed in Chapters 3 to 6. Since the majority of the membrane lab-scale experiments conducted as part of this project has been shown to be successful, it is proposed that a membrane pilot scale model should be deployed on the actual manufacturing sites of both companies. The pilot scale model will validate the results obtained from the lab-scale experiments. Likewise, the necessary adjustments on operating parameters can be done prior to actual plant installation.

5) The installation of membrane treatment equipment will involve costs throughout its operating lifetime. It is recommended that a study involving a full whole life cost analysis be carried out, with the possibility of considering the role of subsidies that cover the installation of equipment.

7.5 References

[1] Agana, B. A., Reeve, D. & Orbell, J. D. 2011. Optimization of the operational parameters for a 50 nm ZrO2 ceramic membrane as applied to the ultrafiltration of post-electrodeposition rinse wastewater. *Desalination,* 278**,** 325-332.

[2] Agana, B. A., Reeve, D. & Orbell, J. D. 2012. The influence of an applied electric field during ceramic ultrafiltration of post-electrodeposition rinse wastewater. *Water Research,* 46**,** 3574-3584.

[3] Pérez-González, A., Urtiaga, A. M., Ibáñez, R. & Ortiz, I. 2012. State of the art and review on the treatment technologies of water reverse osmosis concentrates. *Water Research,* 46**,** 267-283.

[4] Meindersma, G. W., Guijt, C. M. & De Haan, A. B. 2005. Water recycling and desalination by air gap membrane distillation. *Environmental Progress,* 24**,** 434-441.

[5] Arnal, J. M., Sancho, M., Iborra, I., Gozálvez, J. M., Santafé, A. & Lora, J. 2005. Concentration of brines from RO desalination plants by natural evaporation. *Desalination,* 182**,** 435-439.

[6] Sperlich, A., Warschke, D., Wegmann, C., Ernst, M. & Jekel, M. 2010. Treatment of membrane concentrates: Phosphate removal and reduction of scaling potential. *Water Science and Technology,* 61**,** 301-306.

Appendices

Appendix 2.1: Specifications of GE TransPort PT878 ultrasonic flowmeter. All data were supplied by General Electric (GE).

Parameter	Operational limits
Fluid types	Acoustically conductive fluids, including most clean liquids, and many liquids with entrained solids or gas bubbles. Maximum void fraction depends on transducer, interrogation carrier frequency, path length and pipe configuration.
Pipe sizes	0.5 in to 300 in (12.7 mm to 7.6 m) and larger
Pipe wall thickness	Up to 3 in (76.2 mm)
Pipe materials	All metals and most plastics. Consult GE for concrete, composite materials, and highly corroded or lined pipes.
Clamp-on flow accuracy (Velocity)	• Pipe ID>6 in (150 mm): ±1% to 2% of reading typical • Pipe ID<6 in (150 mm): ±2% to 5% of reading typical
Repeatability	±0.1% to 0.3% of reading
Range (Bidirectional)	Range (Bidirectional) –40 to 40 ft/s (–12.2 to 12.2 m/s)
Rangeability (Overall)	400:1
Measurement	Volumetric flow, totalized flow and flow velocity
Flow measurement method	Patented Correlation Transit-Time mode
Enclosure	Submersible IP67
Dimensions	Weight 3 lb (1.36 kg), Size (h x w x d) 9.4 in x 5.5 in x 1.5 in (238 mm x 138 mm x 38 mm)
Display	240 x 200 pixel backlit LCD graphic display
Keypad	25-key rubberized tactile membrane keypad
Internal battery	Rechargeable battery: 9 to 11 hr of continuous operation
Battery charger input	100 to 250 VAC, 50/60 Hz, 0.38 A
Memory	FLASH memory, field-upgradable
Operating temperature	–4°F to 131°F (–20°C to 55°C)
Storage temperature	–40°F to 158°F (–40°C to 70°C)

Parameter	Operational limits
Standard inputs/outputs	• One 0/4 to 20 mA current output, 550 Ω maximum load • One user-selectable pulse (solid state, 5 V maximum) or frequency (5 V square wave, 100 to 10,000 Hz) • Two 4 to 20 mA analog inputs with switchable power supply for loop-powered temperature transmitters
Digital interface	Infrared communication port for printer or PC interface
Site-parameter programming	• Menu-driven operator interface using keypad and "soft" function keys • Online help functions including pipe tables • Storage for saving site parameters
Data logging	• Memory capacity to log over 100,000 flow data points • Keypad programmable for log units, update times, and start and stop time
Display functions	• Graphic display shows flow in numerical or graphic format • Displays logged data • Extensive diagnostic parameters • Supports multiple languages: Dutch, English, French, German, Italian, Japanese, Portuguese, Russian, Spanish, Swedish and others
Transducer temperature ranges	• Standard: -40°F to 302°F (-40°C to 150°C) • Optional: -328°F to 752°F (-200°C to 400°C)
Transducer mountings	Stainless steel chain or strap, welded or magnetic clamping fixtures
Transducer cables	• Standard: One pair of LEMO® coaxial transducer connectors with 25-ft (8-m) cables • Optional: 1,000-ft (305-m) extension cables available for most transducers
PC-interface software	The TransPort PT878 communicates with a PC through the infrared interface and Windows® operating systems. Consult the manual for details on sites, logs and other operations with a PC.
RS232-to-infrared	Infrared adapter plugs into any available serial port to give desktop PCs infrared capability.

Appendix 2.7: Comprehensive water flow diagram for Company A

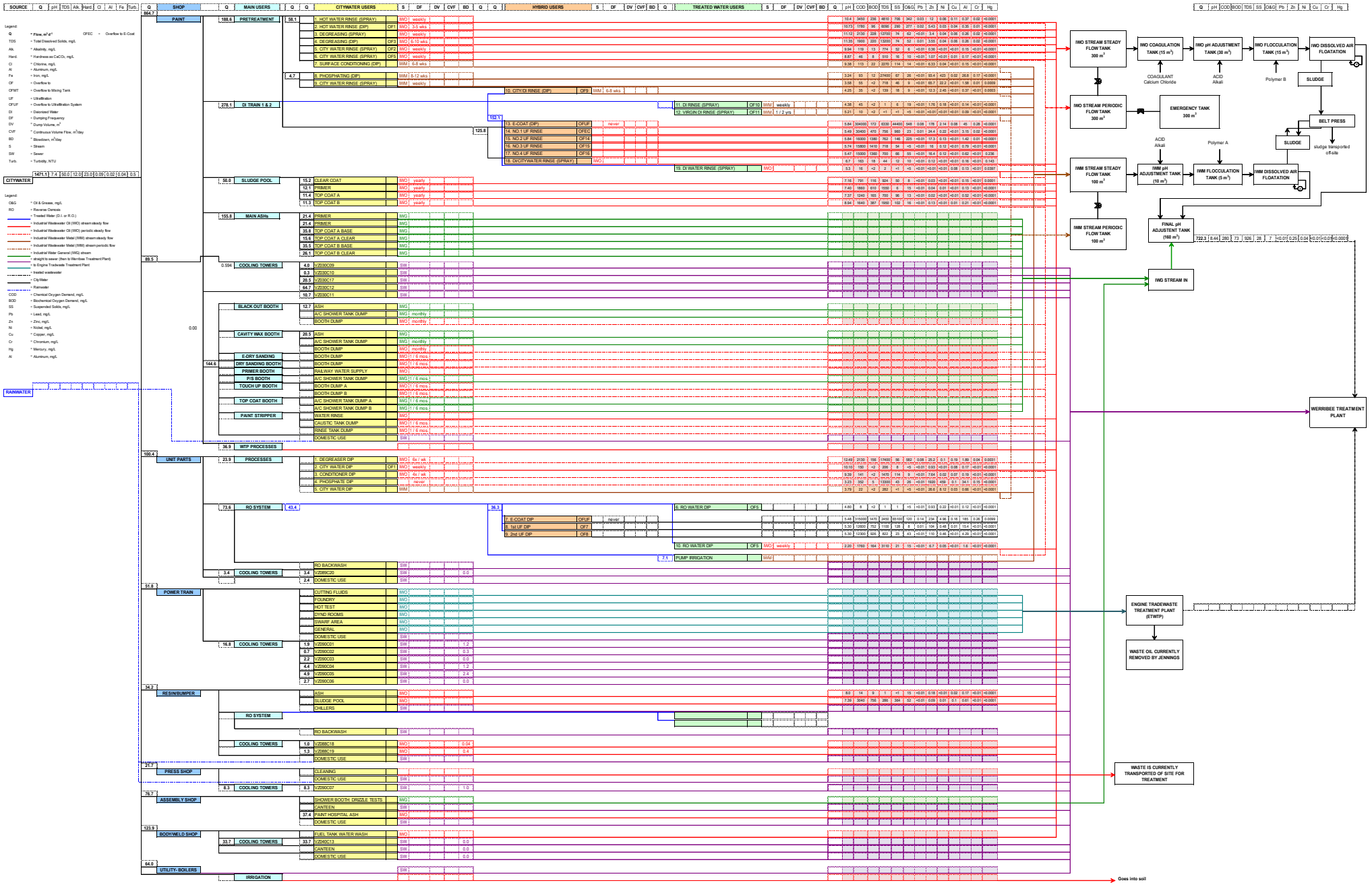

Appendix 2.8: Comprehensive water flow diagram for Company B

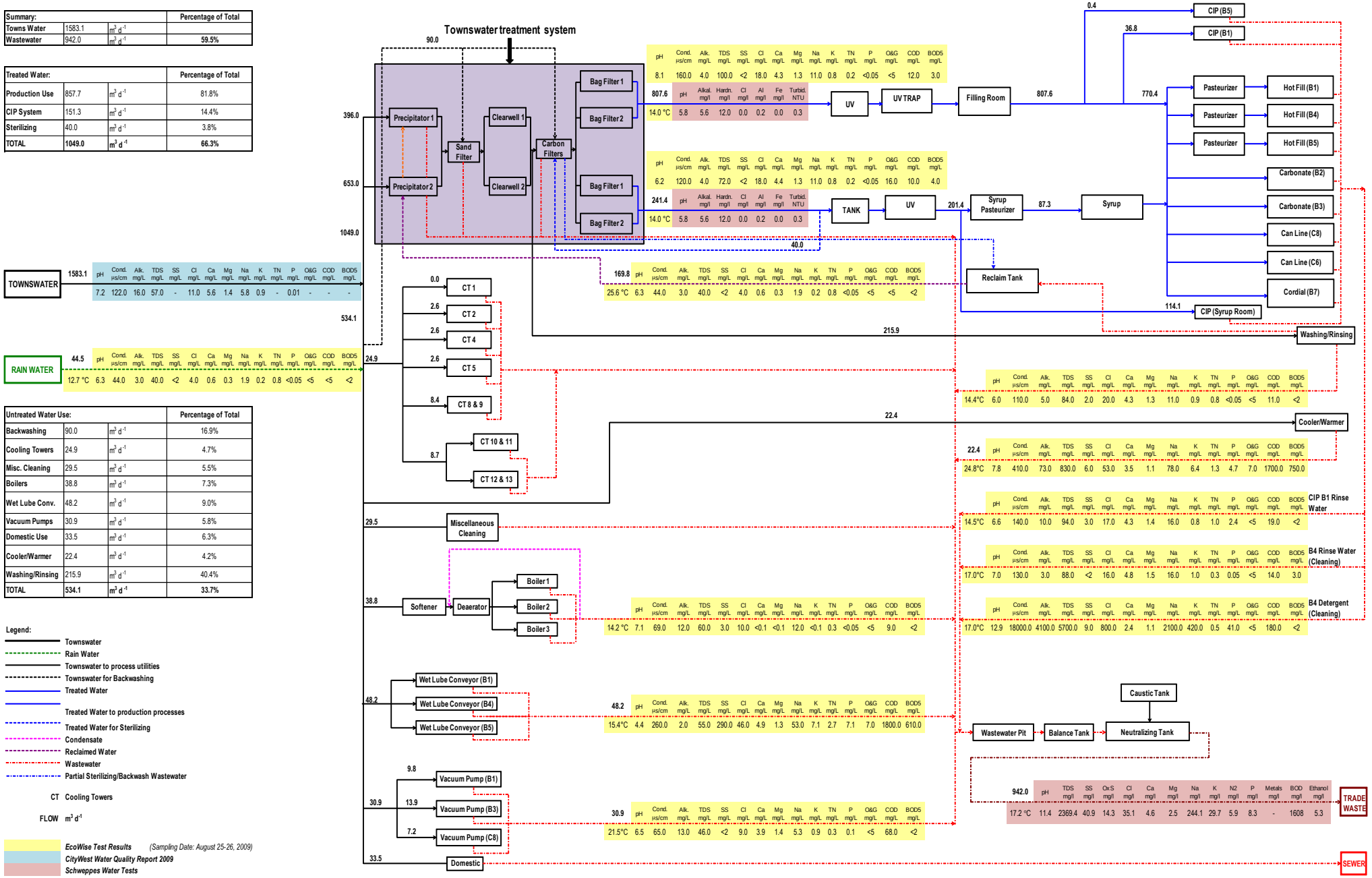

Appendix 2.9: Wastewater test results for representative streams identified at Company A

Parameter		pH	Conductivity		TDS	TDS (IO)	SS	Al	Sb	As	Ba	B	Ca	Cr	Co	Cu	Fe	Pb	Mg	Mn	Mo	Ni	P	K	Se	Ag	Na	Sr	Sn	Ti	V	Zn	S	Hg	O&G	COD	BOD
Units		-	-		mg/L	mg/L	mg/L	mg/L	mg/L	mg/L	mg/L	mg/L	mg/L	mg/L	mg/L	mg/L	mg/L	mg/L	mg/L	mg/L	mg/L	mg/L	mg/L	mg/L	mg/L	mg/L	mg/L	mg/L	mg/L	mg/L	mg/L	mg/L	mg/L	mg/L	mg/L	mg/L	mg/L
CITYWEST WATER RESULTS 2008		7.00	137.00		60.00			0.02		0.001			6.70	0.01		0.01	0.05	0.01	1.40	0.003			0.01	0.90			5.90					0.01		0.001			
Limit of Reporting		-	-		1	1	1	0.01	0.01	0.01	0.1	0.1	1	0.01	0.01	0.01	0.01	0.01	1	0.01	0.01	0.01	1	1	0.01	0.01	1	0.1	0.01	0.01	0.01	0.01	1	0.0001	5	5	2
ID	PAINT SHOP																																				
1	Clear Coat	7.16	834.00	µs/cm	924	636	50	0.15	<0.01	<0.01	0.7	0.3	18	<0.01	<0.01	<0.01	0.56	<0.01	7	0.02	<0.01	<0.01	<1	11	<0.01	<0.01	105	<0.1	<0.01	<0.01	<0.01	0.03	3	0.0001	8	791	116
2	Primer	7.40	1447.00	µs/cm	1550	690	6	0.13	<0.01	<0.01	3.5	0.4	23	<0.01	<0.01	<0.01	0.36	<0.01	10	0.06	<0.01	0.01	<1	19	<0.01	<0.01	251	0.1	<0.01	<0.01	<0.01	0.04	4	<0.0001	15	1860	610
3	Top Coat A	7.37	703.00	µs/cm	700	336	96	0.52	<0.01	<0.01	0.8	0.4	14	<0.01	<0.01	<0.01	0.38	<0.01	5	0.03	0.02	<0.01	<1	7	<0.01	<0.01	97	<0.1	<0.01	<0.01	<0.01	0.02	5	<0.0001	13	1240	165
4	Top Coat B	8.94	2.27	ms/cm	1950	1200	102	0.21	<0.01	<0.01	0.4	0.3	10	<0.01	<0.01	0.01	0.29	<0.01	9	0.01	0.02	<0.01	<1	17	<0.01	<0.01	433	<0.1	<0.01	<0.01	<0.01	0.13	8	<0.0001	16	1640	387
5	IWO Inlet	8.99	545.00	µs/cm	480	228	130	0.31	<0.01	<0.01	0.3	0.4	8	0.03	<0.01	0.05	1.13	<0.01	3	0.06	<0.01	0.02	5	54	<0.01	<0.01	44	<0.1	0.06	0.47	<0.01	1.23	3	<0.0001	45	575	125
6	IWM Inlet	5.93	834.00	µs/cm	626	426	188	0.92	<0.01	<0.01	0.1	0.3	7	0.01	<0.01	0.07	5.5	0.01	2	5.56	<0.01	8.3	71	12	<0.01	<0.01	113	<0.1	0.03	0.14	<0.01	27.9	2	<0.0001	21	250	<2
7	IWG Inlet	6.67	186.90	µs/cm	130	8	7	0.18	<0.01	<0.01	<0.1	0.2	8	<0.01	<0.01	0.03	0.35	<0.01	3	<0.01	<0.01	<0.01	<1	1	<0.01	<0.01	8	<0.1	<0.01	<0.01	<0.01	0.31	4	<0.0001	<5	14	<2
8	TWTP Outlet	8.44	1555.00	µs/cm	926	734	28	0.18	<0.01	<0.01	<0.1	0.4	7	<0.01	<0.01	<0.01	0.02	<0.01	3	0.02	<0.01	0.04	14	59	<0.01	<0.01	224	<0.1	0.02	0.01	<0.01	0.25	6	<0.0001	7	280	73
9	Degrease Stage 1	10.40	6.16	ms/cm	4810	3710	706	0.37	<0.01	<0.01	3.1	0.6	4	0.02	<0.01	0.11	2.88	0.03	7	0.25	0.02	0.06	18	1350	<0.01	<0.01	264	<0.1	0.1	0.28	<0.01	12	16	<0.0001	342	3450	236
10	Degrease Stage 2	10.73	6.79	ms/cm	6090	3800	290	0.35	<0.01	<0.01	1.2	0.4	4	0.01	<0.01	0.04	1	0.02	4	0.12	0.01	0.03	22	1480	<0.01	<0.01	292	<0.1	0.08	0.41	<0.01	5.43	16	<0.0001	277	1780	96
11	Degrease Stage 3	11.12	16.41	ms/cm	12700	9490	74	0.26	<0.01	<0.01	0.6	0.3	3	0.02	<0.01	0.06	0.51	<0.01	2	0.08	0.02	0.04	23	6700	<0.01	<0.01	437	<0.1	0.18	0.14	<0.01	3.4	8	<0.0001	62	2130	228
12	Degrease Stage 4	11.35	16.43	ms/cm	13200	10400	74	0.26	<0.01	<0.01	0.5	0.4	4	0.02	<0.01	0.06	0.53	0.01	2	0.08	0.02	0.04	23	7000	<0.01	<0.01	549	<0.1	0.14	0.13	<0.01	3.55	9	<0.0001	52	1900	220
13	Degrease Drain	10.33	1844.00	µs/cm	1120	732	116	0.23	0.02	<0.01	0.6	0.6	7	0.01	<0.01	0.04	0.74	0.01	4	0.08	<0.01	0.02	44	314	<0.01	<0.01	161	<0.1	0.05	1.05	<0.01	3.46	9	<0.0001	42	566	20
14	Phosphate Stage 5	9.94	849.00	µs/cm	774	478	52	0.15	<0.01	<0.01	<0.1	0.3	4	<0.01	<0.01	<0.01	0.06	<0.01	3	0.02	<0.01	<0.01	30	84	<0.01	<0.01	97	<0.1	<0.01	0.22	<0.01	0.36	5	<0.0001	6	119	13
15	Phosphate Stage 6	8.87	464.00	µs/cm	510	264	16	0.17	<0.01	<0.01	<0.1	0.4	5	<0.01	<0.01	0.01	0.17	<0.01	3	0.03	<0.01	<0.01	28	9	<0.01	<0.01	69	<0.1	<0.01	0.89	<0.01	1.07	5	<0.0001	10	46	8
16	Phosphate Stage 7	9.38	2.77	ms/cm	2270	1700	114	0.15	<0.01	<0.01	<0.1	0.3	4	<0.01	<0.01	<0.01	0.4	<0.01	14	0.17	<0.01	0.04	232	24	<0.01	<0.01	587	<0.1	0.49	3.06	<0.01	6.33	24	<0.0001	14	113	22
17	Phosphate Stage 8	3.24	26.50	ms/cm	27400	22000	67	26.8	0.22	0.08	<0.1	4.2	13	0.17	0.26	0.02	6.28	<0.01	17	323	<0.01	423	3740	43	<0.01	0.01	592	<0.1	0.02	0.05	0.01	93.4	24	<0.0001	26	93	12
18	Phosphate Drain	3.63	1219.00	µs/cm	748	646	39	1.48	0.03	<0.01	<0.1	0.9	1	0.01	<0.01	<0.01	6.6	<0.01	<1	10.6	<0.01	20.2	167	2	<0.01	<0.01	176	<0.1	0.03	0.02	<0.01	60.7	12	0.0034	<5	45	<2
19	Stage 9	3.58	1280.00	µs/cm	718	452	46	1.58	0.02	<0.01	<0.1	0.9	1	0.01	0.01	<0.01	4.86	<0.01	<1	11.7	<0.01	22.2	187	2	<0.01	<0.01	198	<0.1	0.04	0.01	<0.01	65.7	2	0.0009	9	55	<2
20	Stage 10	4.25	189.40	µs/cm	139	138	18	0.37	0.01	<0.01	<0.1	0.5	<1	<0.01	<0.01	<0.01	1.45	<0.01	<1	1.39	<0.01	2.45	20	<1	<0.01	<0.01	26	<0.1	<0.01	<0.01	<0.01	12.3	<1	0.0003	9	35	<2
21	Stage 11	4.38	23.20	µs/cm	1	<1	6	0.14	0.01	<0.01	<0.1	0.4	<1	<0.01	<0.01	<0.01	0.27	<0.01	<1	0.12	<0.01	0.18	1	<1	<0.01	<0.01	2	<0.1	<0.01	<0.01	<0.01	1.76	<1	<0.0001	19	45	<2
22	Stage 12	5.21	1.49	µs/cm	<1	<1	<1	0.09	<0.01	<0.01	<0.1	0.4	<1	<0.01	<0.01	<0.01	0.01	<0.01	<1	<0.01	<0.01	<0.01	<1	<1	<0.01	<0.01	<1	<0.1	<0.01	<0.01	<0.01	<0.01	26	<0.0001	<5	10	<2
23	ED Tank	5.84	1282.00	µs/cm	6330	4700	44400	45	<0.01	0.02	1	0.8	3	0.28	<0.01	0.08	11	0.08	<1	0.33	0.72	2.14	24	<1	<0.01	0.02	5	<0.1	178	2.03	0.56	178	24	<0.0001	548	304000	172
24	UF 1	5.49	771.00	µs/cm	756	330	960	3.15	0.02	<0.01	0.1	0.7	2	0.02	<0.01	<0.01	1.2	0.01	<1	0.29	0.04	0.22	2	<1	0.01	<0.01	6	<0.1	13.2	0.2	0.04	24.4	160	<0.0001	23	30400	470
25	UF 2	5.84	770.00	µs/cm	762	360	146	1.42	0.02	<0.01	0.1	0.8	2	0.01	<0.01	<0.01	0.53	<0.01	<1	0.3	0.01	0.13	<1	<1	0.02	<0.01	6	<0.1	3.63	0.16	<0.01	17.3	32	<0.0001	225	16000	1380
26	UF 3	5.74	733.00	µs/cm	718	340	54	0.79	0.01	<0.01	0.1	0.7	2	<0.01	<0.01	<0.01	0.44	<0.01	<1	0.28	<0.01	0.12	<1	<1	0.01	<0.01	6	<0.1	1.53	0.09	<0.01	16	17	<0.0001	<5	15800	1410
27	UF 4	5.47	752.00	µs/cm	700	454	66	0.62	0.02	<0.01	0.1	0.8	3	<0.01	<0.01	<0.01	0.4	<0.01	<1	0.29	<0.01	0.12	<1	<1	0.01	<0.01	6	<0.1	0.78	0.12	<0.01	16.4	18	0.236	55	15000	1360
28	~~CW Rinse~~	sample not taken																																			
29	DI/CW Rinse	6.70	56.20	µs/cm	44	26	12	0.16	<0.01	<0.01	<0.1	0.4	4	<0.01	<0.01	<0.01	0.06	<0.01	<1	<0.01	<0.01	<0.01	<1	<1	<0.01	<0.01	5	<0.1	0.06	0.16	<0.01	0.12	2	0.143	10	163	18
30	DI Rinse	5.30	1.85	µs/cm	2	<1	<1	0.13	<0.01	<0.01	<0.1	0.4	<1	<0.01	<0.01	0.08	0.02	<0.01	<1	<0.01	<0.01	<0.01	<1	<1	<0.01	<0.01	<1	<0.1	0.03	<0.01	<0.01	<0.01	<1	0.0397	<5	16	<2
31	ED Drain	6.70	59.50	µs/cm	46	32	17	0.2	<0.01	<0.01	<0.1	0.4	4	<0.01	<0.01	<0.01	0.06	<0.01	<1	<0.01	<0.01	<0.01	<1	<1	<0.01	<0.01	5	<0.1	0.06	0.15	<0.01	0.17	30	0.0139	<5	214	18
	UNIT PARTS																																				
32	Degrease Stage 1	12.49	26.40	ms/cm	17400	11000	56	1.89	0.02	0.01	0.6	0.5	4	0.04	<0.01	0.19	2.32	0.08	<1	0.6	0.02	0.1	8	5260	<0.01	<0.01	811	0.1	1.26	0.08	<0.01	25.2	7	0.0031	582	2130	156
33	Degrease Stage 2	10.10	389.00	µs/cm	206	76	8	0.17	<0.01	<0.01	<0.1	0.4	14	<0.01	<0.01	0.08	0.14	<0.01	4	0.02	<0.01	<0.01	<1	46	<0.01	<0.01	24	<0.1	0.02	<0.01	<0.01	0.93	7	<0.0001	<5	150	<2
34	Degrease Stage 3	9.39	2.03	ms/cm	1470	794	114	0.19	<0.01	<0.01	0.3	0.6	13	<0.01	<0.01	0.07	0.82	<0.01	13	0.2	<0.01	0.02	248	56	<0.01	<0.01	544	<0.1	0.05	8.3	<0.01	7.64	24	<0.0001	9	141	<2
35	Degrease Drain to TWTP	11.50	26.00	ms/cm	1250	932	52	0.28	<0.01	<0.01	0.1	0.4	15	<0.01	<0.01	0.09	0.49	<0.01	4	0.07	<0.01	0.01	<1	272	<0.01	<0.01	67	<0.1	0.11	0.02	<0.01	2.46	8	<0.0001	8	259	21
36	Phosphate Stage 4	3.23	18.34	ms/cm	13300	5030	43	34.1	0.15	0.17	0.1	1.4	12	0.15	0.54	0.1	8.34	<0.01	23	370	<0.01	459	3920	114	<0.01	0.02	3650	<0.1	0.04	0.09	0.02	1920	26	<0.0001	26	352	5
37	Phosphate Stage 5	3.79	429.00	µs/cm	282	56	<1	0.66	0.01	<0.01	<0.1	0.6	<1	<0.01	<0.01	0.03	1.1	<0.01	<1	5.09	<0.01	8.12	62	3	<0.01	<0.01	48	<0.1	<0.01	0.01	<0.01	26.6	17	<0.0001	<5	22	<2
38	Phosphate Stage 6	4.80	415.00	µs/cm	1	<1	1	0.12	<0.01	<0.01	<0.1	0.4	<1	<0.01	<0.01	<0.01	0.13	<0.01	<1	0.13	<0.01	0.22	2	<1	<0.01	<0.01	3	<0.1	<0.01	<0.01	<0.01	0.93	<1	<0.0001	<5	8	<2
39	Phosphate Drain to TWTP	3.78	418.00	µs/cm	310	34	6	0.6	<0.01	<0.01	<0.1	0.5	<1	<0.01	<0.01	<0.01	2	<0.01	<1	4.84	<0.01	7.7	60	2	<0.01	<0.01	46	<0.1	0.02	0.02	<0.01	25.5	<1	0.059	237	12	<2
40	ED Stage 7	5.48	1459.00	µs/cm	2450	1700	65100	185	0.15	0.02	1.6	1	7	0.26	<0.01	0.18	39.6	0.14	1	1.84	1.2	4.96	44	11	<0.01	0.06	18	<0.1	136	1.24	0.33	234	23	0.0099	120	315000	1470
41	ED Stage 8	5.30	1019.00	µs/cm	1100	110	128	15.4	0.04	<0.01	0.4	0.9	6	<0.01	<0.01	0.01	0.86	0.01	1	1.87	0.03	0.48	1	15	0.01	<0.01	23	<0.1	6.04	0.07	<0.01	104	10	<0.0001	8	12600	752
42	ED Stage 9	5.30	976.00	µs/cm	822	546	23	4.29	0.04	<0.01	0.4	1	6	<0.01	<0.01	<0.01	0.2	<0.01	1	1.9	<0.01	0.46	<1	16	0.01	<0.01	25	<0.1	0.83	<0.01	<0.01	110	21	<0.0001	43	12300	926
43	ED Stage 10	2.20	3.49	ms/cm	3110	1190	21	1.6	<0.01	<0.01	<0.1	0.5	<1	<0.01	<0.01	<0.01	0.11	<0.01	<1	0.11	<0.01	0.05	<1	1	<0.01	<0.01	3	<0.1	0.32	<0.01	<0.01	6.7	<1	<0.0001	15	1760	164
44	ED Drain to TWTP	3.33	231.00	µs/cm	320	270	64	2.82	0.02	<0.01	<0.1	0.5	<1	0.3	<0.01	0.01	1.56	<0.01	<1	0.11	0.05	0.17	<1	<1	<0.01	<0.01	2	<0.1	0.88	0.02	<0.01	5.97	3	<0.0001	40	4640	702
45	RO Concentrate	6.80	345.00	µs/cm	224	22	1	0.17	<0.01	<0.01	<0.1	0.5	26	<0.01	<0.01	0.12	0.04	<0.01	7	<0.01	<0.01	<0.01	<1	4	<0.01	<0.01	28	<0.1	0.03	<0.01	<0.01	0.01	13	<0.0001	5	21	<2
	RESIN																																				
46	Sludge Pool	7.39	414.00	µs/cm	286	120	364	0.61	<0.01	<0.01	0.8	0.5	14	<0.01	<0.01	0.1	2.41	<0.01	4	0.05	<0.01	0.01	3	2	<0.01	<0.01	71	<0.1	0.02	0.25	<0.01	0.09	4	<0.0001	52	3040	756
47	ASH blowdown	8.00	7.51	µs/cm	1	<1	<1	0.17	<0.01	<0.01	<0.1	0.5	<1	<0.01	<0.01	0.02	0.05	<0.01	<1	<0.01	<0.01	<0.01	<1	<1	<0.01	<0.01	1	<0.1	0.02	<0.01	<0.01	0.18	<1	<0.0001	15	14	9
48	RO Concentrate	8.00	135.50	µs/cm	102	50	1	0.15	<0.01	<0.01	<0.1	0.5	<1	<0.01	<0.01	0.02	0.04	<0.01	<1	<0.01	<0.01	<0.01	<1	2	<0.01	<0.01	28	<0.1	0.01	<0.01	<0.01	<0.01	5	<0.0001	<5	14	<2

Appendix 2.10: Wastewater test results for representative streams identified at Company B

Parameter		Temp. (on-site)	pH (on-site)	Conductivity (on-site)	pH	Conductivity @25°C	Alkalinity as $CaCO_3$	TDS @180°C	TDS (IO) @550°C	SS	Cl	Ca	Mg	Na	K	TN	P	O&G	COD	BOD_5	REMARKS
Units		(°C)	-	μs/cm	-	μs/cm	mg/L	mg/L	mg/L	mg/L	mg/L	mg/L	mg/L	mg/L	mg/L	mg/L	mg/L	mg/L	mg/L	mg/L	
ID	**PRODUCTION ROOM**																				
1	Hot Fill (B1) Wastewater																				
2	Hot Fill (B4) Wastewater (Detergent)	17.0	13.2	18000.0	12.9	18000.0	4100.0	5700.0	5400.0	9.0	800.0	2.4	1.1	2100.0	420.0	0.5	41.0	<5	180.0	<2	using CIP (Syrup Room) for cleaning
	Hot Fill (B4) Wastewater (Rinse Water)	17.0	11.1	130.0	7.0	130.0	3.0	88.0	58.0	<2	16.0	4.8	1.5	16.0	1.0	0.3	0.05	<5	14.0	3.0	
3	Carbonate (B3) Wastewater																				
4	Can Line (C6) Wastewater																				
5	Cordial (B7) Wastewater																				
6	CIP (B1) Wastewater	14.5	7.9	172.2	6.6	140.0	10.0	94.0	70.0	3.0	17.0	4.3	1.4	16.0	0.8	1.0	2.4	<5	19.0	<2	sample taken at recovered water tank
7	CIP (Syrup Room) Wastewater																				
8	Bottle Washing/Rinsing Wastewater	14.4	6.7	110.1	6.0	110.0	5.0	84.0	58.0	2.0	20.0	4.3	1.3	11.0	0.9	0.8	<0.05	<5	11.0	<2	sample taken at B3
9	Cooler/Warmer Wastewater	24.8	6.5	392.0	7.8	410.0	73.0	830.0	200.0	6.0	53.0	3.5	1.1	78.0	6.4	1.3	4.7	7.0	1700.0	750.0	sample taken at B1
ID	**UTILITIES**																				
10	Reclaim Tank	25.6	6.8	111.8	6.4	110.0	6.0	92.0	58.0	120.0	17.0	4.7	1.4	11.0	0.9	0.3	0.1	7.0	81.0	<2	
11	Boiler Condensate	14.2	6.4	127.5	7.1	69.0	12.0	60.0	50.0	3.0	10.0	<0.1	<0.1	12.0	<0.1	0.3	<0.05	<5	9.0	<2	sample taken after deaerator
12 13	Wet Lube Conveyor Wastewater (for B1 & B4)	15.4	4.3	206.0	4.4	260.0	2.0	550.0	160.0	290.0	46.0	4.9	1.3	53.0	7.1	2.7	7.1	7.0	1800.0	610.0	sample taken at B1 conveyor
14 15 16	Vacuum Pumps Wastewater (for B1, B3 & C8)	21.5	7.8	66.0	6.5	65.0	13.0	46.0	32.0	<2	9.0	3.9	1.4	5.3	0.9	0.3	0.06	<5	68.0	<2	sample taken at B3
17	Rainwater Tank	12.7	8.9	76.7	6.3	44.0	3.0	40.0	16.0	<2	4.0	0.6	0.3	1.9	0.2	0.8	<0.05	<5	<5	<2	
ID	**OTHERS**																				
18	Water to Filling Room	14.0	7.2	133.5	8.1	160.0	4.0	100.0	34.0	<2	18.0	4.3	1.3	11.0	0.8	0.2	<0.05	<5	12.0	3.0	
19	Water to Syrup Room	14.0	7.1	113.4	6.2	120.0	4.0	72.0	56.0	<2	18.0	4.4	1.3	11.0	0.8	0.2	<0.05	16.0	10.0	4.0	

Appendix 4.3: Calculations of the forces acting on CED paint particles suspended in the model wastewater

Particle Sizes (nm) $\varnothing_P$	Particle Sizes (m) $\varnothing_P$	Viscosity of Feed (Pa s) η_F	Pressure Drop (Pa) ΔP			Internal Diameter of ceramic membrane (m) $\varnothing_{CM}$	Length of ceramic membrane (m), L_{CM}
			2.4 m s^{-1}	2.8 m s^{-1}	3.2 m s^{-1}		
78.82	7.882E-08	1.002E-03	69826.7	95511.6	119357.9	0.007	0.25
91.28	9.128E-08	1.002E-03	69826.7	95511.6	119357.9	0.007	0.25
105.70	1.057E-07	1.002E-03	69826.7	95511.6	119357.9	0.007	0.25
122.40	1.224E-07	1.002E-03	69826.7	95511.6	119357.9	0.007	0.25
141.80	1.418E-07	1.002E-03	69826.7	95511.6	119357.9	0.007	0.25
164.20	1.642E-07	1.002E-03	69826.7	95511.6	119357.9	0.007	0.25
190.10	1.901E-07	1.002E-03	69826.7	95511.6	119357.9	0.007	0.25
220.20	2.202E-07	1.002E-03	69826.7	95511.6	119357.9	0.007	0.25
255.00	2.550E-07	1.002E-03	69826.7	95511.6	119357.9	0.007	0.25
295.30	2.953E-07	1.002E-03	69826.7	95511.6	119357.9	0.007	0.25
342.00	3.420E-07	1.002E-03	69826.7	95511.6	119357.9	0.007	0.25
396.10	3.961E-07	1.002E-03	69826.7	95511.6	119357.9	0.007	0.25
458.70	4.587E-07	1.002E-03	69826.7	95511.6	119357.9	0.007	0.25
531.20	5.312E-07	1.002E-03	69826.7	95511.6	119357.9	0.007	0.25

F_{VD} (Newtons) $= (2.55\pi\Delta P\varnothing_{CM}\varnothing_P^2)/4L_{CM}$			Permeation Flux or permeate velocity (m s^{-1}) J			F_{FD} (Newtons) $= 3\pi\eta_F\varnothing_P J$		
2.4 m s^{-1}	2.8 m s^{-1}	3.2 m s^{-1}	100 kPa	200 kPa	300 kPa	100 kPa	200 kPa	300 kPa
2.43267E-11	3.3275E-11	4.15827E-11	1.0178E-04	1.8434E-04	2.5135E-04	7.576E-14	1.372E-13	1.871E-13
3.26258E-11	4.46269E-11	5.57688E-11	1.0178E-04	1.8434E-04	2.5135E-04	8.774E-14	1.589E-13	2.167E-13
4.37482E-11	5.98405E-11	7.47808E-11	1.0178E-04	1.8434E-04	2.5135E-04	1.016E-13	1.840E-13	2.509E-13
5.86642E-11	8.02431E-11	1.00277E-10	1.0178E-04	1.8434E-04	2.5135E-04	1.176E-13	2.131E-13	2.905E-13
7.87341E-11	1.07696E-10	1.34584E-10	1.0178E-04	1.8434E-04	2.5135E-04	1.363E-13	2.469E-13	3.366E-13
1.05574E-10	1.44408E-10	1.80462E-10	1.0178E-04	1.8434E-04	2.5135E-04	1.578E-13	2.858E-13	3.898E-13
1.41506E-10	1.93557E-10	2.41882E-10	1.0178E-04	1.8434E-04	2.5135E-04	1.827E-13	3.309E-13	4.512E-13
1.89865E-10	2.59705E-10	3.24545E-10	1.0178E-04	1.8434E-04	2.5135E-04	2.117E-13	3.833E-13	5.227E-13
2.54619E-10	3.48278E-10	4.35232E-10	1.0178E-04	1.8434E-04	2.5135E-04	2.451E-13	4.439E-13	6.053E-13
3.41458E-10	4.67059E-10	5.8367E-10	1.0178E-04	1.8434E-04	2.5135E-04	2.838E-13	5.141E-13	7.010E-13
4.57997E-10	6.26466E-10	7.82875E-10	1.0178E-04	1.8434E-04	2.5135E-04	3.287E-13	5.954E-13	8.118E-13
6.14356E-10	8.4034E-10	1.05015E-09	1.0178E-04	1.8434E-04	2.5135E-04	3.807E-13	6.895E-13	9.402E-13
8.23888E-10	1.12694E-09	1.40831E-09	1.0178E-04	1.8434E-04	2.5135E-04	4.409E-13	7.985E-13	1.089E-12
1.10491E-09	1.51134E-09	1.88867E-09	1.0178E-04	1.8434E-04	2.5135E-04	5.106E-13	9.247E-13	1.261E-12

Fluid Density (kg m^{-3}) ρ_F	F_L (Newtons) $= 0.216\pi\varnothing_P^4\rho_F V_{av}^2 / r^2$			τ_W $= \Delta P\,\varnothing_{CM} / 4L$			F_L (Newtons) $= 0.761\,\tau_w^{1.5}\varnothing_P^3\rho_F^{0.5} / \eta_F$		
	2.4 m s^{-1}	2.8 m s^{-1}	3.2 m s^{-1}	2.4 m s^{-1}	2.8 m s^{-1}	3.2 m s^{-1}	2.4 m s^{-1}	2.8 m s^{-1}	3.2 m s^{-1}
998.2	1.2293E-20	1.6732E-20	2.1854E-20	488.787	668.581	835.505	1.270E-13	2.031E-13	2.838E-13
998.2	2.2111E-20	3.0096E-20	3.9309E-20	488.787	668.581	835.505	1.972E-13	3.155E-13	4.407E-13
998.2	3.9757E-20	5.4113E-20	7.0679E-20	488.787	668.581	835.505	3.062E-13	4.899E-13	6.843E-13
998.2	7.1489E-20	9.7304E-20	1.2709E-19	488.787	668.581	835.505	4.755E-13	7.607E-13	1.063E-12
998.2	1.2877E-19	1.7527E-19	2.2893E-19	488.787	668.581	835.505	7.393E-13	1.183E-12	1.652E-12
998.2	2.3153E-19	3.1514E-19	4.1161E-19	488.787	668.581	835.505	1.148E-12	1.836E-12	2.565E-12
998.2	4.1595E-19	5.6615E-19	7.3947E-19	488.787	668.581	835.505	1.781E-12	2.850E-12	3.981E-12
998.2	7.4883E-19	1.0192E-18	1.3312E-18	488.787	668.581	835.505	2.769E-12	4.429E-12	6.187E-12
998.2	1.3467E-18	1.8330E-18	2.3941E-18	488.787	668.581	835.505	4.300E-12	6.878E-12	9.609E-12
998.2	2.4220E-18	3.2965E-18	4.3057E-18	488.787	668.581	835.505	6.677E-12	1.068E-11	1.492E-11
998.2	4.3573E-18	5.9308E-18	7.7463E-18	488.787	668.581	835.505	1.037E-11	1.659E-11	2.318E-11
998.2	7.8403E-18	1.0671E-17	1.3938E-17	488.787	668.581	835.505	1.611E-11	2.578E-11	3.601E-11
998.2	1.4100E-17	1.9192E-17	2.5067E-17	488.787	668.581	835.505	2.503E-11	4.004E-11	5.593E-11
998.2	2.5360E-17	3.4517E-17	4.5084E-17	488.787	668.581	835.505	3.887E-11	6.218E-11	8.686E-11

a	$h\varpi$	F_{VDW} (Newtons) $= h\varpi\, d_P / 32\pi a^2$	Particle Density (kg m^{-3}) ρ_P	Fluid Density (kg m^{-3}) ρ_F	Gravitational Acceleration (m s^{-2}) g	F_G (Newtons) $= 1/6\pi\varnothing_p^3(\rho_P - \rho_F)g$
4E-10	1.00E-20	4.90022E-11	1098.0	998.2071	9.81	2.51002E-19
4E-10	1.00E-20	5.67486E-11	1098.0	998.2071	9.81	3.89848E-19
4E-10	1.00E-20	6.57134E-11	1098.0	998.2071	9.81	6.05331E-19
4E-10	1.00E-20	7.60958E-11	1098.0	998.2071	9.81	9.39967E-19
4E-10	1.00E-20	8.81567E-11	1098.0	998.2071	9.81	1.46149E-18
4E-10	1.00E-20	1.02083E-10	1098.0	998.2071	9.81	2.26928E-18
4E-10	1.00E-20	1.18185E-10	1098.0	998.2071	9.81	3.52139E-18
4E-10	1.00E-20	1.36898E-10	1098.0	998.2071	9.81	5.47293E-18
4E-10	1.00E-20	1.58533E-10	1098.0	998.2071	9.81	8.49941E-18
4E-10	1.00E-20	1.83587E-10	1098.0	998.2071	9.81	1.31995E-17
4E-10	1.00E-20	2.12621E-10	1098.0	998.2071	9.81	2.05044E-17
4E-10	1.00E-20	2.46254E-10	1098.0	998.2071	9.81	3.18554E-17
4E-10	1.00E-20	2.85173E-10	1098.0	998.2071	9.81	4.94714E-17
4E-10	1.00E-20	3.30246E-10	1098.0	998.2071	9.81	7.68321E-17

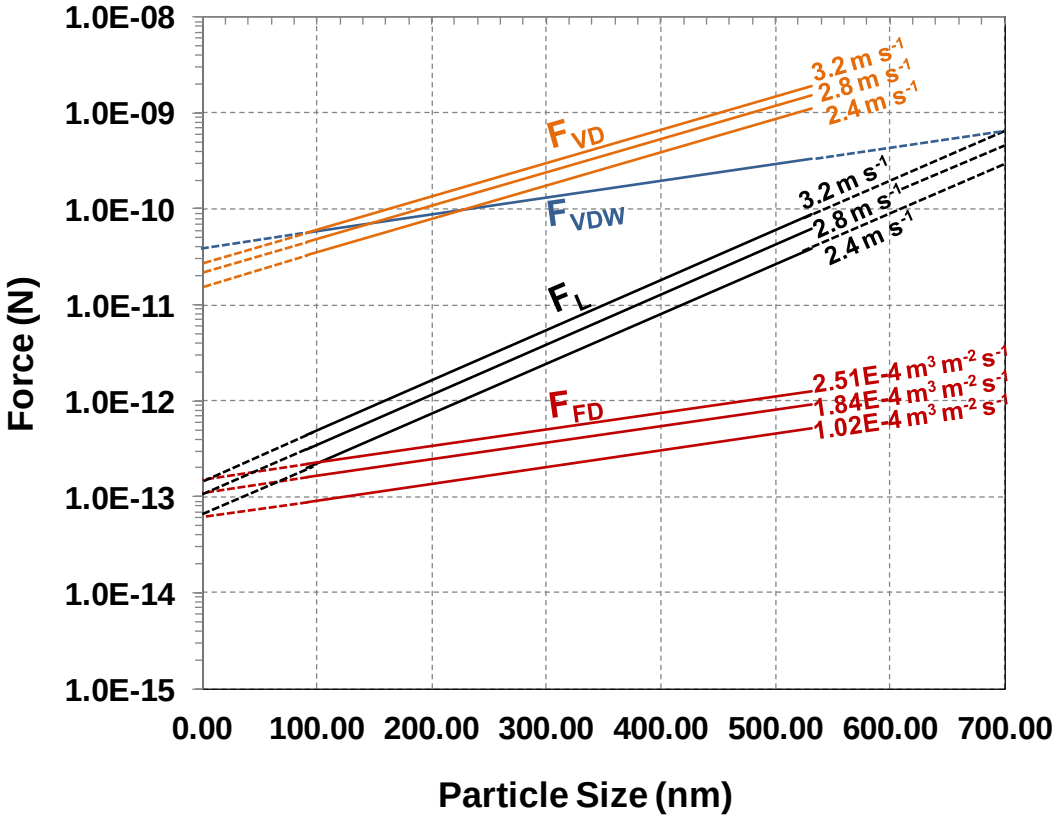
1.0E-08
1.0E-09
1.0E-10
1.0E-11
1.0E-12
1.0E-13
1.0E-14
1.0E-15
Force (N)
0.00
100.00
200.00
300.00
400.00
500.00
600.00
700.00
Particle Size (nm)
F VD
F VDW
F L
F FD
3.2 m s-1
2.8 m s-1
2.4 m s-1
3.2 m s-1
2.8 m s-1
2.4 m s-1
2.51E-4 m3 m-2 s-1
1.84E-4 m3 m-2 s-1
1.02E-4 m3 m-2 s-1

Appendix 4.4: Calculations for the particle adhesion probability based on particle size diameter

F_{VD} (Newtons) $= (2.55p\Delta Pd_{CM}d_P^2)/4L_{CM}$			F_{FD} (Newtons) $= 3p\eta_F d_P J$		
2.4 m s^{-1}	2.8 m s^{-1}	3.2 m s^{-1}	1.39E-04	1.84E-04	2.01E-04
2.37E-11	3.20E-11	4.02E-11	1.04E-13	1.37E-13	1.50E-13
3.17E-11	4.30E-11	5.40E-11	1.20E-13	1.59E-13	1.73E-13
4.25E-11	5.76E-11	7.23E-11	1.39E-13	1.84E-13	2.01E-13
5.70E-11	7.73E-11	9.70E-11	1.61E-13	2.13E-13	2.32E-13
7.66E-11	1.04E-10	1.30E-10	1.86E-13	2.47E-13	2.69E-13
1.03E-10	1.39E-10	1.75E-10	2.16E-13	2.86E-13	3.12E-13
1.38E-10	1.86E-10	2.34E-10	2.50E-13	3.31E-13	3.61E-13
1.85E-10	2.50E-10	3.14E-10	2.89E-13	3.84E-13	4.18E-13
2.48E-10	3.35E-10	4.21E-10	3.35E-13	4.44E-13	4.84E-13
3.32E-10	4.50E-10	5.65E-10	3.88E-13	5.14E-13	5.61E-13
4.45E-10	6.03E-10	7.57E-10	4.49E-13	5.96E-13	6.49E-13

F_L (Newtons) $= 0.761\ t_w^{1.5}d_P^3\ \rho_F^{0.5}/\ \eta_F$			F_{VDW} (Newtons) $= hv\ d_P / 32pa^2$	F_G (Newtons) $= 1/6pd_p^3(\rho_P - \rho_F)g$
2.4 m s^{-1}	2.8 m s^{-1}	3.2 m s^{-1}		
1.22E-13	1.92E-13	2.70E-13	4.90E-11	2.51E-19
1.89E-13	2.98E-13	4.19E-13	5.67E-11	3.90E-19
2.94E-13	4.63E-13	6.51E-13	6.57E-11	6.05E-19
4.56E-13	7.19E-13	1.01E-12	7.61E-11	9.40E-19
7.09E-13	1.12E-12	1.57E-12	8.82E-11	1.46E-18
1.10E-12	1.74E-12	2.44E-12	1.02E-10	2.27E-18
1.71E-12	2.69E-12	3.79E-12	1.18E-10	3.52E-18
2.65E-12	4.19E-12	5.89E-12	1.37E-10	5.47E-18
4.12E-12	6.50E-12	9.14E-12	1.59E-10	8.50E-18
6.40E-12	1.01E-11	1.42E-11	1.84E-10	1.32E-17
9.95E-12	1.57E-11	2.21E-11	2.13E-10	2.05E-17

TMP = 100 kPa; CFV = 2.4m/s

$F_X = F_{VD}$	$F_Y = F_{FD} + F_{VDW} + F_G - F_L$	$\gamma = (F_Y) / ((F_X^2 + F_Y^2)^{0.5})$
2.365E-11	4.898E-11	0.901
3.172E-11	5.668E-11	0.873
4.254E-11	6.556E-11	0.839
5.704E-11	7.580E-11	0.799
7.656E-11	8.763E-11	0.753
1.027E-10	1.012E-10	0.702
1.376E-10	1.167E-10	0.647
1.846E-10	1.345E-10	0.589
2.476E-10	1.547E-10	0.530
3.320E-10	1.776E-10	0.472
4.453E-10	2.031E-10	0.415

TMP = 100 kPa; CFV = 2.8 m/s

$F_X = F_{VD}$	$F_Y = F_{FD} + F_{VDW} + F_G - F_L$	$\gamma = (F_Y) / ((F_X^2 + F_Y^2)^{0.5})$
3.204E-11	4.891E-11	0.836
4.297E-11	5.657E-11	0.796
5.763E-11	6.539E-11	0.750
7.727E-11	7.554E-11	0.699
1.037E-10	8.723E-11	0.644
1.391E-10	1.006E-10	0.586
1.864E-10	1.157E-10	0.528
2.501E-10	1.330E-10	0.470
3.354E-10	1.524E-10	0.414
4.498E-10	1.739E-10	0.361
6.033E-10	1.974E-10	0.311

TMP = 100 kPa; CFV = 3.2 m/s

$F_X = F_{VD}$	$F_Y = F_{FD} + F_{VDW} + F_G - F_L$	$\gamma = (F_Y) / ((F_X^2 + F_Y^2)^{0.5})$
4.023E-11	4.884E-11	0.772
5.395E-11	5.645E-11	0.723
7.234E-11	6.520E-11	0.669
9.701E-11	7.525E-11	0.613
1.302E-10	8.677E-11	0.555
1.746E-10	9.986E-11	0.496
2.340E-10	1.146E-10	0.440
3.140E-10	1.313E-10	0.386
4.211E-10	1.497E-10	0.335
5.647E-10	1.698E-10	0.288
7.574E-10	1.910E-10	0.245

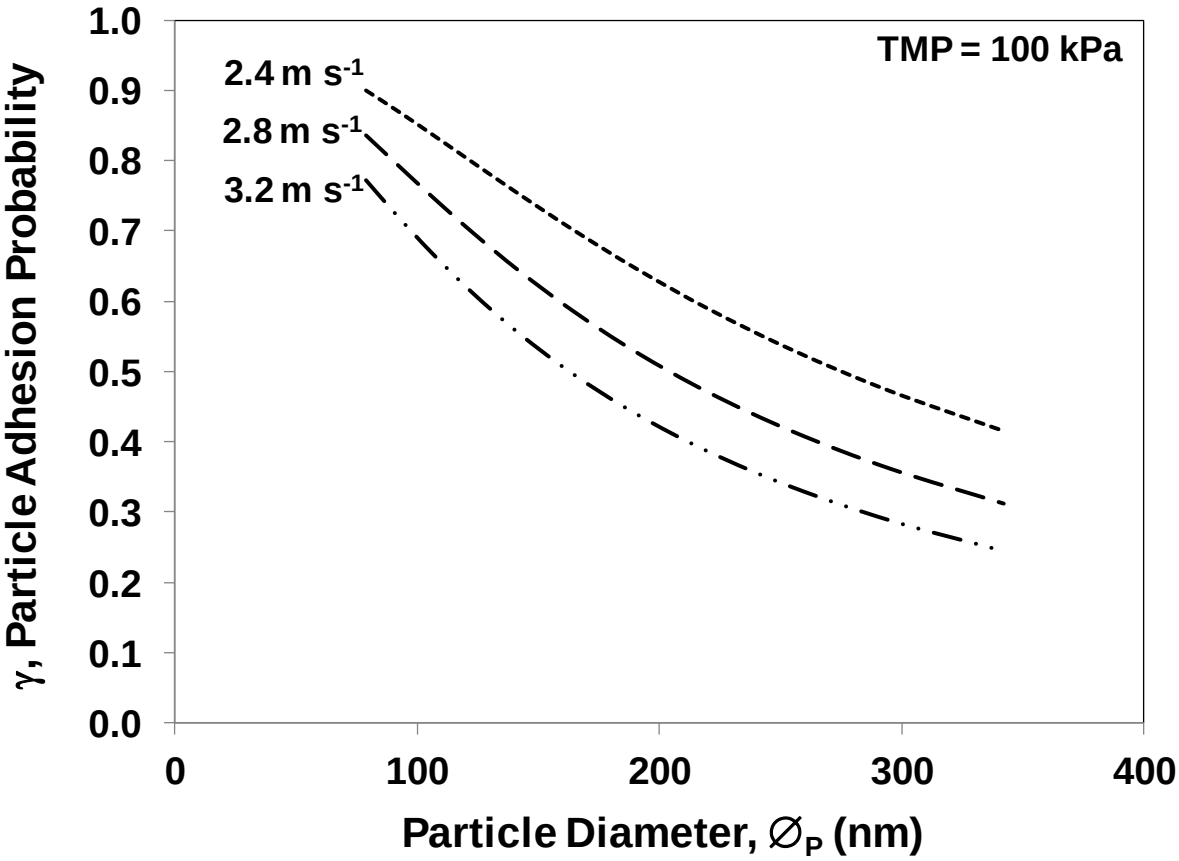

Appendix 5.2: Calculations for the electric field and critical electric field strengths

@ CFV 2.4 m s^{-1}

TMP (kPa) :

100	0.000017
200	0.000020
300	0.000022

Critical Electric Field Strength @ 20 V; 0.5 A $E_C = J_{max} / \mu_P$

μ_P = **4.473E-08** $m^2 V^{-1} s^{-1}$

@ 100 kPa	@ 200 kPa	@ 300 kPa
380 V/m	447 V/m	492 V/m
3.8 V/cm	4.5 V/cm	4.9 V/cm

Electric Field Strength $E = \Phi / L$

L = 2.450E-01 m

20	40	60
@ 20 V	@ 40 V	@ 60 V
82 V/m	163 V/m	245 V/m
0.82 V/cm	1.63 V/cm	2.45 V/cm

80	100
@ 80 V	@ 100 V
326.53 V/m	4.082E+02 V/m
3.27 V/cm	4.08 V/cm

Appendix 5.3: Calculations of the forces acting on CED paint particles under the influence of an electric field

Particle Sizes (nm)	Particle Sizes (m) $Ø_P$	Viscosity of Feed (Pa s) η_F	Pressure Drop (Pa) ΔP 2.4 m s^{-1}	Internal Diameter of ceramic membrane (m) $Ø_{CM}$	Length of ceramic membrane (m), L_{CM}	F_{VD} (Newtons) $= (2.55\pi\Delta P Ø_{CM} Ø_P^2)/4L_{CM}$ 2.4 m s^{-1}
10.0	1.0E-08	1.0E-03	7.0E+04	7.0E-03	2.5E-01	3.9E-13
25.0	2.5E-08	1.0E-03	7.0E+04	7.0E-03	2.5E-01	2.4E-12
50.0	5.0E-08	1.0E-03	7.0E+04	7.0E-03	2.5E-01	9.8E-12
78.8	**7.9E-08**	**1.0E-03**	**7.0E+04**	**7.0E-03**	**2.5E-01**	**2.4E-11**
91.3	**9.1E-08**	**1.0E-03**	**7.0E+04**	**7.0E-03**	**2.5E-01**	**3.3E-11**
105.7	**1.1E-07**	**1.0E-03**	**7.0E+04**	**7.0E-03**	**2.5E-01**	**4.4E-11**
122.4	**1.2E-07**	**1.0E-03**	**7.0E+04**	**7.0E-03**	**2.5E-01**	**5.9E-11**
141.8	**1.4E-07**	**1.0E-03**	**7.0E+04**	**7.0E-03**	**2.5E-01**	**7.9E-11**
164.2	**1.6E-07**	**1.0E-03**	**7.0E+04**	**7.0E-03**	**2.5E-01**	**1.1E-10**
190.1	**1.9E-07**	**1.0E-03**	**7.0E+04**	**7.0E-03**	**2.5E-01**	**1.4E-10**
220.2	**2.2E-07**	**1.0E-03**	**7.0E+04**	**7.0E-03**	**2.5E-01**	**1.9E-10**
255.0	**2.6E-07**	**1.0E-03**	**7.0E+04**	**7.0E-03**	**2.5E-01**	**2.5E-10**
295.3	**3.0E-07**	**1.0E-03**	**7.0E+04**	**7.0E-03**	**2.5E-01**	**3.4E-10**
342.0	**3.4E-07**	**1.0E-03**	**7.0E+04**	**7.0E-03**	**2.5E-01**	**4.6E-10**
396.1	**4.0E-07**	**1.0E-03**	**7.0E+04**	**7.0E-03**	**2.5E-01**	**6.1E-10**
458.7	**4.6E-07**	**1.0E-03**	**7.0E+04**	**7.0E-03**	**2.5E-01**	**8.2E-10**
531.2	**5.3E-07**	**1.0E-03**	**7.0E+04**	**7.0E-03**	**2.5E-01**	**1.1E-09**
550.0	5.5E-07	1.0E-03	7.0E+04	7.0E-03	2.5E-01	1.2E-09
575.0	5.8E-07	1.0E-03	7.0E+04	7.0E-03	2.5E-01	1.3E-09
600.0	6.0E-07	1.0E-03	7.0E+04	7.0E-03	2.5E-01	1.4E-09

Permeation Flux or permeate velocity (m s^{-1}) J				F_{FD} (Newtons) $= 3\pi\eta_F Ø_P \lambda J$			Fluid Density (kg m^{-3}) ρ_F	F_L (Newtons) $= 0.216\pi Ø_P^4 \rho_F V_{av}^2 / r^2$
100 kPa	200 kPa	300 kPa	λ	100 kPa	200 kPa	300 kPa		2.4 m s^{-1}
1.4E-04	1.8E-04	2.0E-04	1.0E+00	1.3E-14	1.7E-14	1.9E-14	1.0E+03	3.2E-24
1.4E-04	1.8E-04	2.0E-04	1.0E+00	3.3E-14	4.4E-14	4.7E-14	1.0E+03	1.2E-22
1.4E-04	1.8E-04	2.0E-04	1.0E+00	6.6E-14	8.7E-14	9.5E-14	1.0E+03	2.0E-21
1.4E-04	**1.8E-04**	**2.0E-04**	**1.0E+00**	**1.0E-13**	**1.4E-13**	**1.5E-13**	**1.0E+03**	**1.2E-20**
1.4E-04	**1.8E-04**	**2.0E-04**	**1.0E+00**	**1.2E-13**	**1.6E-13**	**1.7E-13**	**1.0E+03**	**2.2E-20**
1.4E-04	**1.8E-04**	**2.0E-04**	**1.0E+00**	**1.4E-13**	**1.8E-13**	**2.0E-13**	**1.0E+03**	**4.0E-20**
1.4E-04	**1.8E-04**	**2.0E-04**	**1.0E+00**	**1.6E-13**	**2.1E-13**	**2.3E-13**	**1.0E+03**	**7.1E-20**
1.4E-04	**1.8E-04**	**2.0E-04**	**1.0E+00**	**1.9E-13**	**2.5E-13**	**2.7E-13**	**1.0E+03**	**1.3E-19**
1.4E-04	**1.8E-04**	**2.0E-04**	**1.0E+00**	**2.2E-13**	**2.9E-13**	**3.1E-13**	**1.0E+03**	**2.3E-19**
1.4E-04	**1.8E-04**	**2.0E-04**	**1.0E+00**	**2.5E-13**	**3.3E-13**	**3.6E-13**	**1.0E+03**	**4.2E-19**
1.4E-04	**1.8E-04**	**2.0E-04**	**1.0E+00**	**2.9E-13**	**3.8E-13**	**4.2E-13**	**1.0E+03**	**7.5E-19**
1.4E-04	**1.8E-04**	**2.0E-04**	**1.0E+00**	**3.4E-13**	**4.4E-13**	**4.8E-13**	**1.0E+03**	**1.3E-18**
1.4E-04	**1.8E-04**	**2.0E-04**	**1.0E+00**	**3.9E-13**	**5.1E-13**	**5.6E-13**	**1.0E+03**	**2.4E-18**
1.4E-04	**1.8E-04**	**2.0E-04**	**1.0E+00**	**4.5E-13**	**6.0E-13**	**6.5E-13**	**1.0E+03**	**4.4E-18**
1.4E-04	**1.8E-04**	**2.0E-04**	**1.0E+00**	**5.2E-13**	**6.9E-13**	**7.5E-13**	**1.0E+03**	**7.8E-18**
1.4E-04	**1.8E-04**	**2.0E-04**	**1.0E+00**	**6.0E-13**	**8.0E-13**	**8.7E-13**	**1.0E+03**	**1.4E-17**
1.4E-04	**1.8E-04**	**2.0E-04**	**1.0E+00**	**7.0E-13**	**9.3E-13**	**1.0E-12**	**1.0E+03**	**2.5E-17**
1.4E-04	1.8E-04	2.0E-04	1.0E+00	7.2E-13	9.6E-13	1.0E-12	1.0E+03	2.9E-17
1.4E-04	1.8E-04	2.0E-04	1.0E+00	7.6E-13	1.0E-12	1.1E-12	1.0E+03	3.5E-17
1.4E-04	1.8E-04	2.0E-04	1.0E+00	7.9E-13	1.0E-12	1.1E-12	1.0E+03	4.1E-17

τ_W = $\Delta P\ \phi_{CM}$ / 4L	F_L (Newtons) = $0.761\ \tau_w^{1.5} \phi_P^3\ \rho_F^{0.5} / \eta_F$ 2.4 m s^{-1}	a	$h\varpi$	F_{VDW} (Newtons) = $h\varpi\ \phi_P / 32\pi a^2$	Particle Density (kg m^{-3}) ρ_P	Fluid Density (kg m^{-3}) ρ_F	Gravitational Acceleration (m s^{-1}) g
4.9E+02	2.6E-16	4.0E-10	1.0E-20	6.2E-12	1.1E+03	1.0E+03	9.8E+00
4.9E+02	4.1E-15	4.0E-10	1.0E-20	1.6E-11	1.1E+03	1.0E+03	9.8E+00
4.9E+02	3.2E-14	4.0E-10	1.0E-20	3.1E-11	1.1E+03	1.0E+03	9.8E+00
4.9E+02	**1.3E-13**	**4.0E-10**	**1.0E-20**	**4.9E-11**	**1.1E+03**	**1.0E+03**	**9.8E+00**
4.9E+02	**2.0E-13**	**4.0E-10**	**1.0E-20**	**5.7E-11**	**1.1E+03**	**1.0E+03**	**9.8E+00**
4.9E+02	**3.1E-13**	**4.0E-10**	**1.0E-20**	**6.6E-11**	**1.1E+03**	**1.0E+03**	**9.8E+00**
4.9E+02	**4.8E-13**	**4.0E-10**	**1.0E-20**	**7.6E-11**	**1.1E+03**	**1.0E+03**	**9.8E+00**
4.9E+02	**7.4E-13**	**4.0E-10**	**1.0E-20**	**8.8E-11**	**1.1E+03**	**1.0E+03**	**9.8E+00**
4.9E+02	**1.1E-12**	**4.0E-10**	**1.0E-20**	**1.0E-10**	**1.1E+03**	**1.0E+03**	**9.8E+00**
4.9E+02	**1.8E-12**	**4.0E-10**	**1.0E-20**	**1.2E-10**	**1.1E+03**	**1.0E+03**	**9.8E+00**
4.9E+02	**2.8E-12**	**4.0E-10**	**1.0E-20**	**1.4E-10**	**1.1E+03**	**1.0E+03**	**9.8E+00**
4.9E+02	**4.3E-12**	**4.0E-10**	**1.0E-20**	**1.6E-10**	**1.1E+03**	**1.0E+03**	**9.8E+00**
4.9E+02	**6.7E-12**	**4.0E-10**	**1.0E-20**	**1.8E-10**	**1.1E+03**	**1.0E+03**	**9.8E+00**
4.9E+02	**1.0E-11**	**4.0E-10**	**1.0E-20**	**2.1E-10**	**1.1E+03**	**1.0E+03**	**9.8E+00**
4.9E+02	**1.6E-11**	**4.0E-10**	**1.0E-20**	**2.5E-10**	**1.1E+03**	**1.0E+03**	**9.8E+00**
4.9E+02	**2.5E-11**	**4.0E-10**	**1.0E-20**	**2.9E-10**	**1.1E+03**	**1.0E+03**	**9.8E+00**
4.9E+02	**3.9E-11**	**4.0E-10**	**1.0E-20**	**3.3E-10**	**1.1E+03**	**1.0E+03**	**9.8E+00**
4.9E+02	4.3E-11	4.0E-10	1.0E-20	3.4E-10	1.1E+03	1.0E+03	9.8E+00
4.9E+02	4.9E-11	4.0E-10	1.0E-20	3.6E-10	1.1E+03	1.0E+03	9.8E+00
4.9E+02	5.6E-11	4.0E-10	1.0E-20	3.7E-10	1.1E+03	1.0E+03	9.8E+00

F_G (Newtons) = $1/6\pi\phi_p^3(\rho_P - \rho_F)g$	π	ϕ_P (m)	η (Pa s)	$\lambda = 1$	μ ($m^2\ V^{-1}\ s^{-1}$)	L (m)	λ_C (S/m)	A_{wire} (m^2)
5.1E-22	3.1E+00	1.0E-08	1.0E-03	4.0E+01	4.5E-08	2.5E-01	1.1E-02	3.9E-05
8.0E-21	3.1E+00	2.5E-08	1.0E-03	4.0E+01	4.5E-08	2.5E-01	1.1E-02	3.9E-05
6.4E-20	3.1E+00	5.0E-08	1.0E-03	4.0E+01	4.5E-08	2.5E-01	1.1E-02	3.9E-05
2.5E-19	**3.1E+00**	**7.9E-08**	**1.0E-03**	**4.0E+01**	**4.5E-08**	**2.5E-01**	**1.1E-02**	**3.9E-05**
3.9E-19	**3.1E+00**	**9.1E-08**	**1.0E-03**	**4.0E+01**	**4.5E-08**	**2.5E-01**	**1.1E-02**	**3.9E-05**
6.1E-19	**3.1E+00**	**1.1E-07**	**1.0E-03**	**4.0E+01**	**4.5E-08**	**2.5E-01**	**1.1E-02**	**3.9E-05**
9.4E-19	**3.1E+00**	**1.2E-07**	**1.0E-03**	**4.0E+01**	**4.5E-08**	**2.5E-01**	**1.1E-02**	**3.9E-05**
1.5E-18	**3.1E+00**	**1.4E-07**	**1.0E-03**	**4.0E+01**	**4.5E-08**	**2.5E-01**	**1.1E-02**	**3.9E-05**
2.3E-18	**3.1E+00**	**1.6E-07**	**1.0E-03**	**4.0E+01**	**4.5E-08**	**2.5E-01**	**1.1E-02**	**3.9E-05**
3.5E-18	**3.1E+00**	**1.9E-07**	**1.0E-03**	**4.0E+01**	**4.5E-08**	**2.5E-01**	**1.1E-02**	**3.9E-05**
5.5E-18	**3.1E+00**	**2.2E-07**	**1.0E-03**	**4.0E+01**	**4.5E-08**	**2.5E-01**	**1.1E-02**	**3.9E-05**
8.5E-18	**3.1E+00**	**2.6E-07**	**1.0E-03**	**4.0E+01**	**4.5E-08**	**2.5E-01**	**1.1E-02**	**3.9E-05**
1.3E-17	**3.1E+00**	**3.0E-07**	**1.0E-03**	**4.0E+01**	**4.5E-08**	**2.5E-01**	**1.1E-02**	**3.9E-05**
2.1E-17	**3.1E+00**	**3.4E-07**	**1.0E-03**	**4.0E+01**	**4.5E-08**	**2.5E-01**	**1.1E-02**	**3.9E-05**
3.2E-17	**3.1E+00**	**4.0E-07**	**1.0E-03**	**4.0E+01**	**4.5E-08**	**2.5E-01**	**1.1E-02**	**3.9E-05**
4.9E-17	**3.1E+00**	**4.6E-07**	**1.0E-03**	**4.0E+01**	**4.5E-08**	**2.5E-01**	**1.1E-02**	**3.9E-05**
7.7E-17	**3.1E+00**	**5.3E-07**	**1.0E-03**	**4.0E+01**	**4.5E-08**	**2.5E-01**	**1.1E-02**	**3.9E-05**
8.5E-17	3.1E+00	5.5E-07	1.0E-03	4.0E+01	4.5E-08	2.5E-01	1.1E-02	3.9E-05
9.7E-17	3.1E+00	5.8E-07	1.0E-03	4.0E+01	4.5E-08	2.5E-01	1.1E-02	3.9E-05
1.1E-16	3.1E+00	6.0E-07	1.0E-03	4.0E+01	4.5E-08	2.5E-01	1.1E-02	3.9E-05

$R = L / \lambda_C A$	$I = V/R$				$E = V / L$			E (V/m)		
Ω (ohm)	20 V	40 V	60 V	λ_C (Siemens/m)	20 V	40 V	60 V	20 V	40 V	60 V
5.9E+05	3.4E-05	6.8E-05	1.0E-04	1.1E-02	8.2E+01	1.6E+02	2.4E+02	8.2E+01	1.6E+02	2.4E+02
5.9E+05	3.4E-05	6.8E-05	1.0E-04	1.1E-02	8.2E+01	1.6E+02	2.4E+02	8.2E+01	1.6E+02	2.4E+02
5.9E+05	3.4E-05	6.8E-05	1.0E-04	1.1E-02	8.2E+01	1.6E+02	2.4E+02	8.2E+01	1.6E+02	2.4E+02
5.9E+05	**3.4E-05**	**6.8E-05**	**1.0E-04**	**1.1E-02**	**8.2E+01**	**1.6E+02**	**2.4E+02**	**8.2E+01**	**1.6E+02**	**2.4E+02**
5.9E+05	**3.4E-05**	**6.8E-05**	**1.0E-04**	**1.1E-02**	**8.2E+01**	**1.6E+02**	**2.4E+02**	**8.2E+01**	**1.6E+02**	**2.4E+02**
5.9E+05	**3.4E-05**	**6.8E-05**	**1.0E-04**	**1.1E-02**	**8.2E+01**	**1.6E+02**	**2.4E+02**	**8.2E+01**	**1.6E+02**	**2.4E+02**
5.9E+05	**3.4E-05**	**6.8E-05**	**1.0E-04**	**1.1E-02**	**8.2E+01**	**1.6E+02**	**2.4E+02**	**8.2E+01**	**1.6E+02**	**2.4E+02**
5.9E+05	**3.4E-05**	**6.8E-05**	**1.0E-04**	**1.1E-02**	**8.2E+01**	**1.6E+02**	**2.4E+02**	**8.2E+01**	**1.6E+02**	**2.4E+02**
5.9E+05	**3.4E-05**	**6.8E-05**	**1.0E-04**	**1.1E-02**	**8.2E+01**	**1.6E+02**	**2.4E+02**	**8.2E+01**	**1.6E+02**	**2.4E+02**
5.9E+05	**3.4E-05**	**6.8E-05**	**1.0E-04**	**1.1E-02**	**8.2E+01**	**1.6E+02**	**2.4E+02**	**8.2E+01**	**1.6E+02**	**2.4E+02**
5.9E+05	**3.4E-05**	**6.8E-05**	**1.0E-04**	**1.1E-02**	**8.2E+01**	**1.6E+02**	**2.4E+02**	**8.2E+01**	**1.6E+02**	**2.4E+02**
5.9E+05	**3.4E-05**	**6.8E-05**	**1.0E-04**	**1.1E-02**	**8.2E+01**	**1.6E+02**	**2.4E+02**	**8.2E+01**	**1.6E+02**	**2.4E+02**
5.9E+05	**3.4E-05**	**6.8E-05**	**1.0E-04**	**1.1E-02**	**8.2E+01**	**1.6E+02**	**2.4E+02**	**8.2E+01**	**1.6E+02**	**2.4E+02**
5.9E+05	**3.4E-05**	**6.8E-05**	**1.0E-04**	**1.1E-02**	**8.2E+01**	**1.6E+02**	**2.4E+02**	**8.2E+01**	**1.6E+02**	**2.4E+02**
5.9E+05	**3.4E-05**	**6.8E-05**	**1.0E-04**	**1.1E-02**	**8.2E+01**	**1.6E+02**	**2.4E+02**	**8.2E+01**	**1.6E+02**	**2.4E+02**
5.9E+05	3.4E-05	6.8E-05	1.0E-04	1.1E-02	8.2E+01	1.6E+02	2.4E+02	8.2E+01	1.6E+02	2.4E+02
5.9E+05	3.4E-05	6.8E-05	1.0E-04	1.1E-02	8.2E+01	1.6E+02	2.4E+02	8.2E+01	1.6E+02	2.4E+02
5.9E+05	3.4E-05	6.8E-05	1.0E-04	1.1E-02	8.2E+01	1.6E+02	2.4E+02	8.2E+01	1.6E+02	2.4E+02

Electrophoretic Force (N), $F_E = 3\pi\emptyset_P\eta_F\lambda\mu E$			π	$R^* = R_1$ (m)	ε, dielectric permittivity of water @ 20°C	ε_O, permittivity of vacuum (C^2/N-m^2)	$\aleph$, inverse Debye Length (960 nm)	$4\pi R^* / \varepsilon\varepsilon_O\aleph$	ζ_{Paint}	ζ_{ZrO2}	Debye Length λ_D
20 V	40 V	60 V							58 mV	20 mV	
1.4E-14	2.8E-14	4.1E-14	3.1E+00	1.0E-08	8.0E+01	8.9E-12	**1.0E+06**	**1.4E-14**	5.8E-02	2.0E-02	**9.6E-07**
3.4E-14	6.9E-14	1.0E-13	3.1E+00	2.5E-08	8.0E+01	8.9E-12	**1.0E+06**	**3.6E-14**	5.8E-02	2.0E-02	**9.6E-07**
6.9E-14	1.4E-13	2.1E-13	3.1E+00	5.0E-08	8.0E+01	8.9E-12	**1.0E+06**	**7.2E-14**	5.8E-02	2.0E-02	**9.6E-07**
1.1E-13	**2.2E-13**	**3.3E-13**	**3.1E+00**	**7.9E-08**	**8.0E+01**	**8.9E-12**	**1.0E+06**	**1.1E-13**	**5.8E-02**	**2.0E-02**	**9.6E-07**
1.3E-13	**2.5E-13**	**3.8E-13**	**3.1E+00**	**9.1E-08**	**8.0E+01**	**8.9E-12**	**1.0E+06**	**1.3E-13**	**5.8E-02**	**2.0E-02**	**9.6E-07**
1.5E-13	**2.9E-13**	**4.4E-13**	**3.1E+00**	**1.1E-07**	**8.0E+01**	**8.9E-12**	**1.0E+06**	**1.5E-13**	**5.8E-02**	**2.0E-02**	**9.6E-07**
1.7E-13	**3.4E-13**	**5.1E-13**	**3.1E+00**	**1.2E-07**	**8.0E+01**	**8.9E-12**	**1.0E+06**	**1.8E-13**	**5.8E-02**	**2.0E-02**	**9.6E-07**
2.0E-13	**3.9E-13**	**5.9E-13**	**3.1E+00**	**1.4E-07**	**8.0E+01**	**8.9E-12**	**1.0E+06**	**2.0E-13**	**5.8E-02**	**2.0E-02**	**9.6E-07**
2.3E-13	**4.5E-13**	**6.8E-13**	**3.1E+00**	**1.6E-07**	**8.0E+01**	**8.9E-12**	**1.0E+06**	**2.4E-13**	**5.8E-02**	**2.0E-02**	**9.6E-07**
2.6E-13	**5.2E-13**	**7.9E-13**	**3.1E+00**	**1.9E-07**	**8.0E+01**	**8.9E-12**	**1.0E+06**	**2.7E-13**	**5.8E-02**	**2.0E-02**	**9.6E-07**
3.0E-13	**6.1E-13**	**9.1E-13**	**3.1E+00**	**2.2E-07**	**8.0E+01**	**8.9E-12**	**1.0E+06**	**3.2E-13**	**5.8E-02**	**2.0E-02**	**9.6E-07**
3.5E-13	**7.0E-13**	**1.1E-12**	**3.1E+00**	**2.6E-07**	**8.0E+01**	**8.9E-12**	**1.0E+06**	**3.7E-13**	**5.8E-02**	**2.0E-02**	**9.6E-07**
4.1E-13	**8.1E-13**	**1.2E-12**	**3.1E+00**	**3.0E-07**	**8.0E+01**	**8.9E-12**	**1.0E+06**	**4.3E-13**	**5.8E-02**	**2.0E-02**	**9.6E-07**
4.7E-13	**9.4E-13**	**1.4E-12**	**3.1E+00**	**3.4E-07**	**8.0E+01**	**8.9E-12**	**1.0E+06**	**4.9E-13**	**5.8E-02**	**2.0E-02**	**9.6E-07**
5.5E-13	**1.1E-12**	**1.6E-12**	**3.1E+00**	**4.0E-07**	**8.0E+01**	**8.9E-12**	**1.0E+06**	**5.7E-13**	**5.8E-02**	**2.0E-02**	**9.6E-07**
6.3E-13	**1.3E-12**	**1.9E-12**	**3.1E+00**	**4.6E-07**	**8.0E+01**	**8.9E-12**	**1.0E+06**	**6.6E-13**	**5.8E-02**	**2.0E-02**	**9.6E-07**
7.3E-13	**1.5E-12**	**2.2E-12**	**3.1E+00**	**5.3E-07**	**8.0E+01**	**8.9E-12**	**1.0E+06**	**7.7E-13**	**5.8E-02**	**2.0E-02**	**9.6E-07**
7.6E-13	1.5E-12	2.3E-12	3.1E+00	5.5E-07	8.0E+01	8.9E-12	**1.0E+06**	**7.9E-13**	5.8E-02	2.0E-02	**9.6E-07**
7.9E-13	1.6E-12	2.4E-12	3.1E+00	5.8E-07	8.0E+01	8.9E-12	**1.0E+06**	**8.3E-13**	5.8E-02	2.0E-02	**9.6E-07**
8.3E-13	1.7E-12	2.5E-12	3.1E+00	6.0E-07	8.0E+01	8.9E-12	**1.0E+06**	**8.7E-13**	5.8E-02	2.0E-02	**9.6E-07**

σ_1 (C/m^2), $\varepsilon\varepsilon_0\zeta$ / λ_D	σ_2 (C/m^2), $\varepsilon\varepsilon_0\zeta$ / λ_D	$\sigma_1\sigma_2$	$0.5*(\sigma_1^2+\sigma_2^2)$	χ, Distance between sphere & membrane wall						
				4 nm	5 nm	6 nm	7 nm	8 nm	9 nm	10 nm
4.3E-05	1.5E-05	6.3E-10	1.0E-09	4.0E-09	5.0E-09	6.0E-09	7.0E-09	8.0E-09	9.0E-09	1.0E-08
4.3E-05	1.5E-05	6.3E-10	1.0E-09	4.0E-09	5.0E-09	6.0E-09	7.0E-09	8.0E-09	9.0E-09	1.0E-08
4.3E-05	1.5E-05	6.3E-10	1.0E-09	4.0E-09	5.0E-09	6.0E-09	7.0E-09	8.0E-09	9.0E-09	1.0E-08
4.3E-05	**1.5E-05**	**6.3E-10**	**1.0E-09**	**4.0E-09**	**5.0E-09**	**6.0E-09**	**7.0E-09**	**8.0E-09**	**9.0E-09**	**1.0E-08**
4.3E-05	**1.5E-05**	**6.3E-10**	**1.0E-09**	**4.0E-09**	**5.0E-09**	**6.0E-09**	**7.0E-09**	**8.0E-09**	**9.0E-09**	**1.0E-08**
4.3E-05	**1.5E-05**	**6.3E-10**	**1.0E-09**	**4.0E-09**	**5.0E-09**	**6.0E-09**	**7.0E-09**	**8.0E-09**	**9.0E-09**	**1.0E-08**
4.3E-05	**1.5E-05**	**6.3E-10**	**1.0E-09**	**4.0E-09**	**5.0E-09**	**6.0E-09**	**7.0E-09**	**8.0E-09**	**9.0E-09**	**1.0E-08**
4.3E-05	**1.5E-05**	**6.3E-10**	**1.0E-09**	**4.0E-09**	**5.0E-09**	**6.0E-09**	**7.0E-09**	**8.0E-09**	**9.0E-09**	**1.0E-08**
4.3E-05	**1.5E-05**	**6.3E-10**	**1.0E-09**	**4.0E-09**	**5.0E-09**	**6.0E-09**	**7.0E-09**	**8.0E-09**	**9.0E-09**	**1.0E-08**
4.3E-05	**1.5E-05**	**6.3E-10**	**1.0E-09**	**4.0E-09**	**5.0E-09**	**6.0E-09**	**7.0E-09**	**8.0E-09**	**9.0E-09**	**1.0E-08**
4.3E-05	**1.5E-05**	**6.3E-10**	**1.0E-09**	**4.0E-09**	**5.0E-09**	**6.0E-09**	**7.0E-09**	**8.0E-09**	**9.0E-09**	**1.0E-08**
4.3E-05	**1.5E-05**	**6.3E-10**	**1.0E-09**	**4.0E-09**	**5.0E-09**	**6.0E-09**	**7.0E-09**	**8.0E-09**	**9.0E-09**	**1.0E-08**
4.3E-05	**1.5E-05**	**6.3E-10**	**1.0E-09**	**4.0E-09**	**5.0E-09**	**6.0E-09**	**7.0E-09**	**8.0E-09**	**9.0E-09**	**1.0E-08**
4.3E-05	**1.5E-05**	**6.3E-10**	**1.0E-09**	**4.0E-09**	**5.0E-09**	**6.0E-09**	**7.0E-09**	**8.0E-09**	**9.0E-09**	**1.0E-08**
4.3E-05	**1.5E-05**	**6.3E-10**	**1.0E-09**	**4.0E-09**	**5.0E-09**	**6.0E-09**	**7.0E-09**	**8.0E-09**	**9.0E-09**	**1.0E-08**
4.3E-05	**1.5E-05**	**6.3E-10**	**1.0E-09**	**4.0E-09**	**5.0E-09**	**6.0E-09**	**7.0E-09**	**8.0E-09**	**9.0E-09**	**1.0E-08**
4.3E-05	**1.5E-05**	**6.3E-10**	**1.0E-09**	**4.0E-09**	**5.0E-09**	**6.0E-09**	**7.0E-09**	**8.0E-09**	**9.0E-09**	**1.0E-08**
4.3E-05	1.5E-05	6.3E-10	1.0E-09	4.0E-09	5.0E-09	6.0E-09	7.0E-09	8.0E-09	9.0E-09	1.0E-08
4.3E-05	1.5E-05	6.3E-10	1.0E-09	4.0E-09	5.0E-09	6.0E-09	7.0E-09	8.0E-09	9.0E-09	1.0E-08
4.3E-05	1.5E-05	6.3E-10	1.0E-09	4.0E-09	5.0E-09	6.0E-09	7.0E-09	8.0E-09	9.0E-09	1.0E-08

$\aleph\chi$							$2\aleph\chi$						
4 nm	5 nm	6 nm	7 nm	8 nm	9 nm	10 nm	4 nm	5 nm	6 nm	7 nm	8 nm	9 nm	10 nm
4.2E-03	5.2E-03	6.3E-03	7.3E-03	8.3E-03	9.4E-03	1.0E-02	8.3E-03	1.0E-02	1.3E-02	1.5E-02	1.7E-02	1.9E-02	2.1E-02
4.2E-03	5.2E-03	6.3E-03	7.3E-03	8.3E-03	9.4E-03	1.0E-02	8.3E-03	1.0E-02	1.3E-02	1.5E-02	1.7E-02	1.9E-02	2.1E-02
4.2E-03	5.2E-03	6.3E-03	7.3E-03	8.3E-03	9.4E-03	1.0E-02	8.3E-03	1.0E-02	1.3E-02	1.5E-02	1.7E-02	1.9E-02	2.1E-02
4.2E-03	**5.2E-03**	**6.3E-03**	**7.3E-03**	**8.3E-03**	**9.4E-03**	**1.0E-02**	**8.3E-03**	**1.0E-02**	**1.3E-02**	**1.5E-02**	**1.7E-02**	**1.9E-02**	**2.1E-02**
4.2E-03	**5.2E-03**	**6.3E-03**	**7.3E-03**	**8.3E-03**	**9.4E-03**	**1.0E-02**	**8.3E-03**	**1.0E-02**	**1.3E-02**	**1.5E-02**	**1.7E-02**	**1.9E-02**	**2.1E-02**
4.2E-03	**5.2E-03**	**6.3E-03**	**7.3E-03**	**8.3E-03**	**9.4E-03**	**1.0E-02**	**8.3E-03**	**1.0E-02**	**1.3E-02**	**1.5E-02**	**1.7E-02**	**1.9E-02**	**2.1E-02**
4.2E-03	**5.2E-03**	**6.3E-03**	**7.3E-03**	**8.3E-03**	**9.4E-03**	**1.0E-02**	**8.3E-03**	**1.0E-02**	**1.3E-02**	**1.5E-02**	**1.7E-02**	**1.9E-02**	**2.1E-02**
4.2E-03	**5.2E-03**	**6.3E-03**	**7.3E-03**	**8.3E-03**	**9.4E-03**	**1.0E-02**	**8.3E-03**	**1.0E-02**	**1.3E-02**	**1.5E-02**	**1.7E-02**	**1.9E-02**	**2.1E-02**
4.2E-03	**5.2E-03**	**6.3E-03**	**7.3E-03**	**8.3E-03**	**9.4E-03**	**1.0E-02**	**8.3E-03**	**1.0E-02**	**1.3E-02**	**1.5E-02**	**1.7E-02**	**1.9E-02**	**2.1E-02**
4.2E-03	**5.2E-03**	**6.3E-03**	**7.3E-03**	**8.3E-03**	**9.4E-03**	**1.0E-02**	**8.3E-03**	**1.0E-02**	**1.3E-02**	**1.5E-02**	**1.7E-02**	**1.9E-02**	**2.1E-02**
4.2E-03	**5.2E-03**	**6.3E-03**	**7.3E-03**	**8.3E-03**	**9.4E-03**	**1.0E-02**	**8.3E-03**	**1.0E-02**	**1.3E-02**	**1.5E-02**	**1.7E-02**	**1.9E-02**	**2.1E-02**
4.2E-03	**5.2E-03**	**6.3E-03**	**7.3E-03**	**8.3E-03**	**9.4E-03**	**1.0E-02**	**8.3E-03**	**1.0E-02**	**1.3E-02**	**1.5E-02**	**1.7E-02**	**1.9E-02**	**2.1E-02**
4.2E-03	**5.2E-03**	**6.3E-03**	**7.3E-03**	**8.3E-03**	**9.4E-03**	**1.0E-02**	**8.3E-03**	**1.0E-02**	**1.3E-02**	**1.5E-02**	**1.7E-02**	**1.9E-02**	**2.1E-02**
4.2E-03	**5.2E-03**	**6.3E-03**	**7.3E-03**	**8.3E-03**	**9.4E-03**	**1.0E-02**	**8.3E-03**	**1.0E-02**	**1.3E-02**	**1.5E-02**	**1.7E-02**	**1.9E-02**	**2.1E-02**
4.2E-03	**5.2E-03**	**6.3E-03**	**7.3E-03**	**8.3E-03**	**9.4E-03**	**1.0E-02**	**8.3E-03**	**1.0E-02**	**1.3E-02**	**1.5E-02**	**1.7E-02**	**1.9E-02**	**2.1E-02**
4.2E-03	**5.2E-03**	**6.3E-03**	**7.3E-03**	**8.3E-03**	**9.4E-03**	**1.0E-02**	**8.3E-03**	**1.0E-02**	**1.3E-02**	**1.5E-02**	**1.7E-02**	**1.9E-02**	**2.1E-02**
4.2E-03	**5.2E-03**	**6.3E-03**	**7.3E-03**	**8.3E-03**	**9.4E-03**	**1.0E-02**	**8.3E-03**	**1.0E-02**	**1.3E-02**	**1.5E-02**	**1.7E-02**	**1.9E-02**	**2.1E-02**
4.2E-03	5.2E-03	6.3E-03	7.3E-03	8.3E-03	9.4E-03	1.0E-02	8.3E-03	1.0E-02	1.3E-02	1.5E-02	1.7E-02	1.9E-02	2.1E-02
4.2E-03	5.2E-03	6.3E-03	7.3E-03	8.3E-03	9.4E-03	1.0E-02	8.3E-03	1.0E-02	1.3E-02	1.5E-02	1.7E-02	1.9E-02	2.1E-02
4.2E-03	5.2E-03	6.3E-03	7.3E-03	8.3E-03	9.4E-03	1.0E-02	8.3E-03	1.0E-02	1.3E-02	1.5E-02	1.7E-02	1.9E-02	2.1E-02

$e^{\kappa\chi}$							$e^{2\kappa\chi}$						
4 nm	5 nm	6 nm	7 nm	8 nm	9 nm	10 nm	4 nm	5 nm	6 nm	7 nm	8 nm	9 nm	10 nm
1.0E+00	1.0E+00	1.0E+00	1.0E+00	1.0E+00	1.0E+00	1.0E+00	1.0E+00	1.0E+00	1.0E+00	1.0E+00	1.0E+00	1.0E+00	1.0E+00
1.0E+00	1.0E+00	1.0E+00	1.0E+00	1.0E+00	1.0E+00	1.0E+00	1.0E+00	1.0E+00	1.0E+00	1.0E+00	1.0E+00	1.0E+00	1.0E+00
1.0E+00	1.0E+00	1.0E+00	1.0E+00	1.0E+00	1.0E+00	1.0E+00	1.0E+00	1.0E+00	1.0E+00	1.0E+00	1.0E+00	1.0E+00	1.0E+00
1.0E+00	1.0E+00	1.0E+00	1.0E+00	1.0E+00	1.0E+00	1.0E+00	1.0E+00	1.0E+00	1.0E+00	1.0E+00	1.0E+00	1.0E+00	1.0E+00
1.0E+00	1.0E+00	1.0E+00	1.0E+00	1.0E+00	1.0E+00	1.0E+00	1.0E+00	1.0E+00	1.0E+00	1.0E+00	1.0E+00	1.0E+00	1.0E+00
1.0E+00	1.0E+00	1.0E+00	1.0E+00	1.0E+00	1.0E+00	1.0E+00	1.0E+00	1.0E+00	1.0E+00	1.0E+00	1.0E+00	1.0E+00	1.0E+00
1.0E+00	1.0E+00	1.0E+00	1.0E+00	1.0E+00	1.0E+00	1.0E+00	1.0E+00	1.0E+00	1.0E+00	1.0E+00	1.0E+00	1.0E+00	1.0E+00
1.0E+00	1.0E+00	1.0E+00	1.0E+00	1.0E+00	1.0E+00	1.0E+00	1.0E+00	1.0E+00	1.0E+00	1.0E+00	1.0E+00	1.0E+00	1.0E+00
1.0E+00	1.0E+00	1.0E+00	1.0E+00	1.0E+00	1.0E+00	1.0E+00	1.0E+00	1.0E+00	1.0E+00	1.0E+00	1.0E+00	1.0E+00	1.0E+00
1.0E+00	1.0E+00	1.0E+00	1.0E+00	1.0E+00	1.0E+00	1.0E+00	1.0E+00	1.0E+00	1.0E+00	1.0E+00	1.0E+00	1.0E+00	1.0E+00
1.0E+00	1.0E+00	1.0E+00	1.0E+00	1.0E+00	1.0E+00	1.0E+00	1.0E+00	1.0E+00	1.0E+00	1.0E+00	1.0E+00	1.0E+00	1.0E+00
1.0E+00	1.0E+00	1.0E+00	1.0E+00	1.0E+00	1.0E+00	1.0E+00	1.0E+00	1.0E+00	1.0E+00	1.0E+00	1.0E+00	1.0E+00	1.0E+00
1.0E+00	1.0E+00	1.0E+00	1.0E+00	1.0E+00	1.0E+00	1.0E+00	1.0E+00	1.0E+00	1.0E+00	1.0E+00	1.0E+00	1.0E+00	1.0E+00
1.0E+00	1.0E+00	1.0E+00	1.0E+00	1.0E+00	1.0E+00	1.0E+00	1.0E+00	1.0E+00	1.0E+00	1.0E+00	1.0E+00	1.0E+00	1.0E+00
1.0E+00	1.0E+00	1.0E+00	1.0E+00	1.0E+00	1.0E+00	1.0E+00	1.0E+00	1.0E+00	1.0E+00	1.0E+00	1.0E+00	1.0E+00	1.0E+00
1.0E+00	1.0E+00	1.0E+00	1.0E+00	1.0E+00	1.0E+00	1.0E+00	1.0E+00	1.0E+00	1.0E+00	1.0E+00	1.0E+00	1.0E+00	1.0E+00
1.0E+00	1.0E+00	1.0E+00	1.0E+00	1.0E+00	1.0E+00	1.0E+00	1.0E+00	1.0E+00	1.0E+00	1.0E+00	1.0E+00	1.0E+00	1.0E+00
1.0E+00	1.0E+00	1.0E+00	1.0E+00	1.0E+00	1.0E+00	1.0E+00	1.0E+00	1.0E+00	1.0E+00	1.0E+00	1.0E+00	1.0E+00	1.0E+00
1.0E+00	1.0E+00	1.0E+00	1.0E+00	1.0E+00	1.0E+00	1.0E+00	1.0E+00	1.0E+00	1.0E+00	1.0E+00	1.0E+00	1.0E+00	1.0E+00

F_{EDL} (Newtons) = $4\pi R^* / \varepsilon\varepsilon_0\kappa\ [\ \sigma_1\sigma_2 / e^{-\kappa\chi} + 0.5\ (\sigma_1^2+\sigma_2^2) / e^{-2\kappa\chi})$							μ_P	E, V/m		
4 nm	5 nm	6 nm	7 nm	8 nm	9 nm	10 nm	$m^2\ V^{-1}\ s^{-1}$	20 V	40 V	60 V
2.4E-23	2.4E-23	2.4E-23	2.4E-23	2.4E-23	2.4E-23	2.4E-23	4.5E-08	8.2E+01	1.6E+02	2.4E+02
6.0E-23	6.0E-23	5.9E-23	5.9E-23	5.9E-23	5.9E-23	5.9E-23	4.5E-08	8.2E+01	1.6E+02	2.4E+02
1.2E-22	1.2E-22	1.2E-22	1.2E-22	1.2E-22	1.2E-22	1.2E-22	4.5E-08	8.2E+01	1.6E+02	2.4E+02
1.9E-22	1.9E-22	1.9E-22	1.9E-22	1.9E-22	1.9E-22	1.9E-22	4.5E-08	8.2E+01	1.6E+02	2.4E+02
2.2E-22	2.2E-22	2.2E-22	2.2E-22	2.2E-22	2.2E-22	2.2E-22	4.5E-08	8.2E+01	1.6E+02	2.4E+02
2.5E-22	2.5E-22	2.5E-22	2.5E-22	2.5E-22	2.5E-22	2.5E-22	4.5E-08	8.2E+01	1.6E+02	2.4E+02
2.9E-22	2.9E-22	2.9E-22	2.9E-22	2.9E-22	2.9E-22	2.9E-22	4.5E-08	8.2E+01	1.6E+02	2.4E+02
3.4E-22	3.4E-22	3.4E-22	3.4E-22	3.4E-22	3.4E-22	3.3E-22	4.5E-08	8.2E+01	1.6E+02	2.4E+02
3.9E-22	3.9E-22	3.9E-22	3.9E-22	3.9E-22	3.9E-22	3.9E-22	4.5E-08	8.2E+01	1.6E+02	2.4E+02
4.5E-22	4.5E-22	4.5E-22	4.5E-22	4.5E-22	4.5E-22	4.5E-22	4.5E-08	8.2E+01	1.6E+02	2.4E+02
5.3E-22	5.2E-22	5.2E-22	5.2E-22	5.2E-22	5.2E-22	5.2E-22	4.5E-08	8.2E+01	1.6E+02	2.4E+02
6.1E-22	6.1E-22	6.1E-22	6.1E-22	6.0E-22	6.0E-22	6.0E-22	4.5E-08	8.2E+01	1.6E+02	2.4E+02
7.0E-22	7.0E-22	7.0E-22	7.0E-22	7.0E-22	7.0E-22	7.0E-22	4.5E-08	8.2E+01	1.6E+02	2.4E+02
8.2E-22	8.1E-22	8.1E-22	8.1E-22	8.1E-22	8.1E-22	8.1E-22	4.5E-08	8.2E+01	1.6E+02	2.4E+02
9.5E-22	9.4E-22	9.4E-22	9.4E-22	9.4E-22	9.4E-22	9.4E-22	4.5E-08	8.2E+01	1.6E+02	2.4E+02
1.1E-21	1.1E-21	1.1E-21	1.1E-21	1.1E-21	1.1E-21	1.1E-21	4.5E-08	8.2E+01	1.6E+02	2.4E+02
1.3E-21	1.3E-21	1.3E-21	1.3E-21	1.3E-21	1.3E-21	1.3E-21	4.5E-08	8.2E+01	1.6E+02	2.4E+02
1.3E-21	1.3E-21	1.3E-21	1.3E-21	1.3E-21	1.3E-21	1.3E-21	4.5E-08	8.2E+01	1.6E+02	2.4E+02
1.4E-21	1.4E-21	1.4E-21	1.4E-21	1.4E-21	1.4E-21	1.4E-21	4.5E-08	8.2E+01	1.6E+02	2.4E+02
1.4E-21	1.4E-21	1.4E-21	1.4E-21	1.4E-21	1.4E-21	1.4E-21	4.5E-08	8.2E+01	1.6E+02	2.4E+02

V_P (m/s)			I (A)			t (s)	**q = It (C)**		
20 V	**40 V**	**60 V**	**20 V**	**40 V**	**60 V**		**20 V**	**40 V**	**60 V**
2.4E+00	2.4E+00	2.4E+00	3.4E-05	6.8E-05	1.0E-04	9.0	3.0E-04	6.1E-04	9.1E-04
2.4E+00	2.4E+00	2.4E+00	3.4E-05	6.8E-05	1.0E-04	9.0	3.0E-04	6.1E-04	9.1E-04
2.4E+00	2.4E+00	2.4E+00	3.4E-05	6.8E-05	1.0E-04	9.0	3.0E-04	6.1E-04	9.1E-04
2.4E+00	**2.4E+00**	**2.4E+00**	**3.4E-05**	**6.8E-05**	**1.0E-04**	**9.0**	**3.0E-04**	**6.1E-04**	**9.1E-04**
2.4E+00	**2.4E+00**	**2.4E+00**	**3.4E-05**	**6.8E-05**	**1.0E-04**	**9.0**	**3.0E-04**	**6.1E-04**	**9.1E-04**
2.4E+00	**2.4E+00**	**2.4E+00**	**3.4E-05**	**6.8E-05**	**1.0E-04**	**9.0**	**3.0E-04**	**6.1E-04**	**9.1E-04**
2.4E+00	**2.4E+00**	**2.4E+00**	**3.4E-05**	**6.8E-05**	**1.0E-04**	**9.0**	**3.0E-04**	**6.1E-04**	**9.1E-04**
2.4E+00	**2.4E+00**	**2.4E+00**	**3.4E-05**	**6.8E-05**	**1.0E-04**	**9.0**	**3.0E-04**	**6.1E-04**	**9.1E-04**
2.4E+00	**2.4E+00**	**2.4E+00**	**3.4E-05**	**6.8E-05**	**1.0E-04**	**9.0**	**3.0E-04**	**6.1E-04**	**9.1E-04**
2.4E+00	**2.4E+00**	**2.4E+00**	**3.4E-05**	**6.8E-05**	**1.0E-04**	**9.0**	**3.0E-04**	**6.1E-04**	**9.1E-04**
2.4E+00	**2.4E+00**	**2.4E+00**	**3.4E-05**	**6.8E-05**	**1.0E-04**	**9.0**	**3.0E-04**	**6.1E-04**	**9.1E-04**
2.4E+00	**2.4E+00**	**2.4E+00**	**3.4E-05**	**6.8E-05**	**1.0E-04**	**9.0**	**3.0E-04**	**6.1E-04**	**9.1E-04**
2.4E+00	**2.4E+00**	**2.4E+00**	**3.4E-05**	**6.8E-05**	**1.0E-04**	**9.0**	**3.0E-04**	**6.1E-04**	**9.1E-04**
2.4E+00	**2.4E+00**	**2.4E+00**	**3.4E-05**	**6.8E-05**	**1.0E-04**	**9.0**	**3.0E-04**	**6.1E-04**	**9.1E-04**
2.4E+00	**2.4E+00**	**2.4E+00**	**3.4E-05**	**6.8E-05**	**1.0E-04**	**9.0**	**3.0E-04**	**6.1E-04**	**9.1E-04**
2.4E+00	**2.4E+00**	**2.4E+00**	**3.4E-05**	**6.8E-05**	**1.0E-04**	**9.0**	**3.0E-04**	**6.1E-04**	**9.1E-04**
2.4E+00	**2.4E+00**	**2.4E+00**	**3.4E-05**	**6.8E-05**	**1.0E-04**	**9.0**	**3.0E-04**	**6.1E-04**	**9.1E-04**
2.4E+00	**2.4E+00**	**2.4E+00**	**3.4E-05**	**6.8E-05**	**1.0E-04**	**9.0**	**3.0E-04**	**6.1E-04**	**9.1E-04**
2.4E+00	2.4E+00	2.4E+00	3.4E-05	6.8E-05	1.0E-04	9.0	3.0E-04	6.1E-04	9.1E-04
2.4E+00	2.4E+00	2.4E+00	3.4E-05	6.8E-05	1.0E-04	9.0	3.0E-04	6.1E-04	9.1E-04
2.4E+00	2.4E+00	2.4E+00	3.4E-05	6.8E-05	1.0E-04	9.0	3.0E-04	6.1E-04	9.1E-04

μ_O , Tm / A	**r, m**	**B = μ_O I / 2π r (Teslas)**			**$F_M = qV_PB$ (Magnetic Force or Lorentz Force, N)**			**F_E**		
		20 V	**40 V**	**60 V**				**20 V**	**40 V**	**60 V**
					20 V	**40 V**	**60 V**			
1.3E-06	3.5E-03	1.9E-09	3.9E-09	5.8E-09	1.4E-12	5.7E-12	1.3E-11	1.4E-12	5.7E-12	1.3E-11
1.3E-06	3.5E-03	1.9E-09	3.9E-09	5.8E-09	1.4E-12	5.7E-12	1.3E-11	1.5E-12	5.7E-12	1.3E-11
1.3E-06	3.5E-03	1.9E-09	3.9E-09	5.8E-09	1.4E-12	5.7E-12	1.3E-11	1.5E-12	5.8E-12	1.3E-11
1.3E-06	**3.5E-03**	**1.9E-09**	**3.9E-09**	**5.8E-09**	**1.4E-12**	**5.7E-12**	**1.3E-11**	1.5E-12	5.9E-12	1.3E-11
1.3E-06	**3.5E-03**	**1.9E-09**	**3.9E-09**	**5.8E-09**	**1.4E-12**	**5.7E-12**	**1.3E-11**	1.5E-12	5.9E-12	1.3E-11
1.3E-06	**3.5E-03**	**1.9E-09**	**3.9E-09**	**5.8E-09**	**1.4E-12**	**5.7E-12**	**1.3E-11**	1.6E-12	6.0E-12	1.3E-11
1.3E-06	**3.5E-03**	**1.9E-09**	**3.9E-09**	**5.8E-09**	**1.4E-12**	**5.7E-12**	**1.3E-11**	1.6E-12	6.0E-12	1.3E-11
1.3E-06	**3.5E-03**	**1.9E-09**	**3.9E-09**	**5.8E-09**	**1.4E-12**	**5.7E-12**	**1.3E-11**	1.6E-12	6.1E-12	1.3E-11
1.3E-06	**3.5E-03**	**1.9E-09**	**3.9E-09**	**5.8E-09**	**1.4E-12**	**5.7E-12**	**1.3E-11**	1.6E-12	6.1E-12	1.3E-11
1.3E-06	**3.5E-03**	**1.9E-09**	**3.9E-09**	**5.8E-09**	**1.4E-12**	**5.7E-12**	**1.3E-11**	1.7E-12	6.2E-12	1.4E-11
1.3E-06	**3.5E-03**	**1.9E-09**	**3.9E-09**	**5.8E-09**	**1.4E-12**	**5.7E-12**	**1.3E-11**	1.7E-12	6.3E-12	1.4E-11
1.3E-06	**3.5E-03**	**1.9E-09**	**3.9E-09**	**5.8E-09**	**1.4E-12**	**5.7E-12**	**1.3E-11**	1.8E-12	6.4E-12	1.4E-11
1.3E-06	**3.5E-03**	**1.9E-09**	**3.9E-09**	**5.8E-09**	**1.4E-12**	**5.7E-12**	**1.3E-11**	1.8E-12	6.5E-12	1.4E-11
1.3E-06	**3.5E-03**	**1.9E-09**	**3.9E-09**	**5.8E-09**	**1.4E-12**	**5.7E-12**	**1.3E-11**	1.9E-12	6.6E-12	1.4E-11
1.3E-06	**3.5E-03**	**1.9E-09**	**3.9E-09**	**5.8E-09**	**1.4E-12**	**5.7E-12**	**1.3E-11**	2.0E-12	6.8E-12	1.4E-11
1.3E-06	**3.5E-03**	**1.9E-09**	**3.9E-09**	**5.8E-09**	**1.4E-12**	**5.7E-12**	**1.3E-11**	2.0E-12	6.9E-12	1.5E-11
1.3E-06	**3.5E-03**	**1.9E-09**	**3.9E-09**	**5.8E-09**	**1.4E-12**	**5.7E-12**	**1.3E-11**	2.1E-12	7.1E-12	1.5E-11
1.3E-06	3.5E-03	1.9E-09	3.9E-09	5.8E-09	1.4E-12	5.7E-12	1.3E-11	2.2E-12	7.2E-12	1.5E-11
1.3E-06	3.5E-03	1.9E-09	3.9E-09	5.8E-09	1.4E-12	5.7E-12	1.3E-11	2.2E-12	7.3E-12	1.5E-11
1.3E-06	3.5E-03	1.9E-09	3.9E-09	5.8E-09	1.4E-12	5.7E-12	1.3E-11	2.2E-12	7.3E-12	1.5E-11

$F_L + F_{EDL}$	F_{VD}	Shear force F_{VD}	$F_{DP} = F_{FD} + F_G + F_{VDW}$			F_{DI}	$F_{DI} + F_E$		
			100 kPa	200 kPa	300 kPa		20 V	40 V	60 V
2.6E-16	3.9E-13	3.9E-13	6.2E-12	6.2E-12	6.2E-12	3.9E-13	1.82E-12	6.09E-12	1.32E-11
4.1E-15	2.4E-12	2.4E-12	1.6E-11	1.6E-11	1.6E-11	2.4E-12	3.90E-12	8.19E-12	1.53E-11
3.2E-14	9.8E-12	9.8E-12	3.1E-11	3.1E-11	3.1E-11	9.8E-12	1.13E-11	1.56E-11	2.28E-11
1.3E-13	2.4E-11	2.4E-11	4.9E-11	4.9E-11	4.9E-11	2.4E-11	2.59E-11	3.02E-11	3.74E-11
2.0E-13	3.3E-11	3.3E-11	5.7E-11	5.7E-11	5.7E-11	3.3E-11	3.42E-11	3.85E-11	4.58E-11
3.1E-13	4.4E-11	4.4E-11	6.6E-11	6.6E-11	6.6E-11	4.4E-11	4.53E-11	4.97E-11	5.69E-11
4.8E-13	5.9E-11	5.9E-11	7.6E-11	7.6E-11	7.6E-11	5.9E-11	6.03E-11	6.47E-11	7.19E-11
7.4E-13	7.9E-11	7.9E-11	8.8E-11	8.8E-11	8.8E-11	7.9E-11	8.04E-11	8.48E-11	9.21E-11
1.1E-12	1.1E-10	1.1E-10	1.0E-10	1.0E-10	1.0E-10	1.1E-10	1.07E-10	1.12E-10	1.19E-10
1.8E-12	1.4E-10	1.4E-10	1.2E-10	1.2E-10	1.2E-10	1.4E-10	1.43E-10	1.48E-10	1.55E-10
2.8E-12	1.9E-10	1.9E-10	1.4E-10	1.4E-10	1.4E-10	1.9E-10	1.92E-10	1.96E-10	2.04E-10
4.3E-12	2.5E-10	2.5E-10	1.6E-10	1.6E-10	1.6E-10	2.5E-10	2.56E-10	2.61E-10	2.68E-10
6.7E-12	3.4E-10	3.4E-10	1.8E-10	1.8E-10	1.8E-10	3.4E-10	3.43E-10	3.48E-10	3.55E-10
1.0E-11	4.6E-10	4.6E-10	2.1E-10	2.1E-10	2.1E-10	4.6E-10	4.60E-10	4.65E-10	4.72E-10
1.6E-11	6.1E-10	6.1E-10	2.5E-10	2.5E-10	2.5E-10	6.1E-10	6.17E-10	6.21E-10	6.29E-10
2.5E-11	8.2E-10	8.2E-10	2.9E-10	2.9E-10	2.9E-10	8.2E-10	8.26E-10	8.31E-10	8.39E-10
3.9E-11	1.1E-09	1.1E-09	3.3E-10	3.3E-10	3.3E-10	1.1E-09	1.11E-09	1.11E-09	1.12E-09
4.3E-11	1.2E-09	1.2E-09	3.4E-10	3.4E-10	3.4E-10	1.2E-09	1.19E-09	1.19E-09	1.20E-09
4.9E-11	1.3E-09	1.3E-09	3.6E-10	3.6E-10	3.6E-10	1.3E-09	1.30E-09	1.30E-09	1.31E-09
5.6E-11	1.4E-09	1.4E-09	3.7E-10	3.7E-10	3.7E-10	1.4E-09	1.41E-09	1.42E-09	1.43E-09

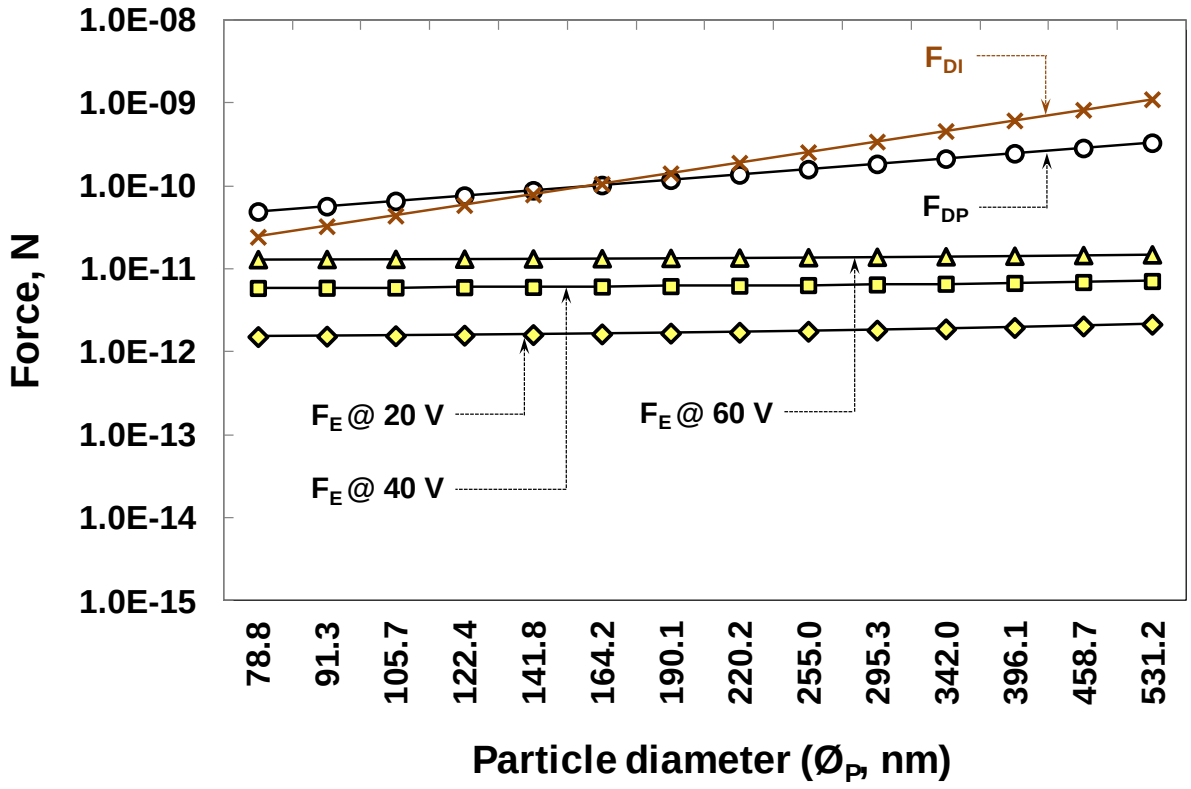

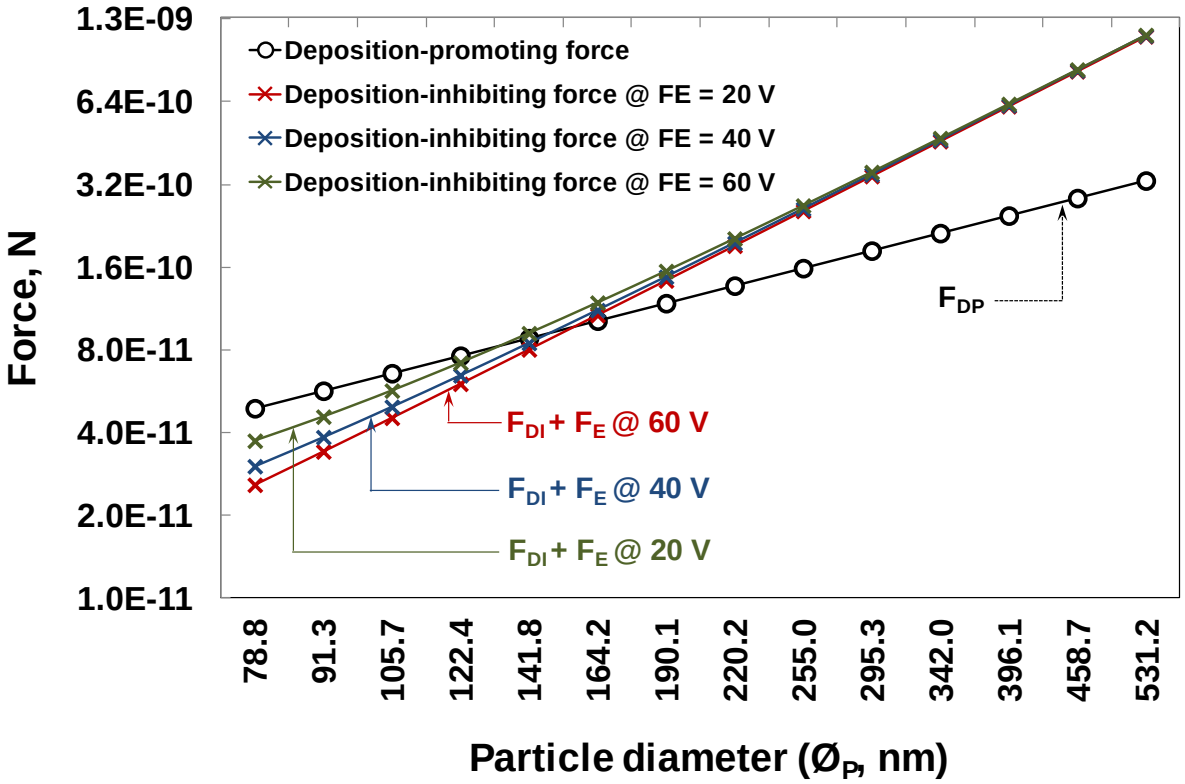
1.3E-09
6.4E-10
3.2E-10
1.6E-10
8.0E-11
4.0E-11
2.0E-11
1.0E-11
Force, N
Deposition-promoting force
Deposition-inhibiting force @ FE = 20 V
Deposition-inhibiting force @ FE = 40 V
Deposition-inhibiting force @ FE = 60 V
F_DP
F_DI + F_E @ 60 V
F_DI + F_E @ 40 V
F_DI + F_E @ 20 V
78.8
91.3
105.7
122.4
141.8
164.2
190.1
220.2
255.0
295.3
342.0
396.1
458.7
531.2
Particle diameter (Ø_P, nm)

Appendix 5.5: Calculations for the membrane resistances encountered during electro-ultrafiltration of model wastewater containing CED paint

$$R_{EM} = (R_M) / (1+ [\mu_M E/J_M])$$

R_M is membrane resistance in the absence of electric field (m^{-1})
μ_M is the membrane electro-osmotic mobility ($m^2 V^{-1} s^{-1}$)
E is the electric field strength (V/m)
J_M is the flux in the absence of an electric field ($m^3 m^{-2} s^{-1}$)

20 V	TMP	Time (min)	R_M	μ_M	E	J_M	$\mu_M E/J_M$	C	R_{EM}
	100	2	1.14E+12	-4.06E-09	8.16E+01	0.000017	-1.95E-02	1	1.16E+12
		60	1.14E+12	-4.06E-09	8.16E+01	0.000013	-2.55E-02	1	1.17E+12
		120	1.14E+12	-4.06E-09	8.16E+01	0.000011	-3.02E-02	1	1.18E+12
	200	2	1.14E+12	-4.06E-09	8.16E+01	0.000020	-1.66E-02	1	1.16E+12
		60	1.14E+12	-4.06E-09	8.16E+01	0.000012	-2.76E-02	1	1.17E+12
		120	1.14E+12	-4.06E-09	8.16E+01	0.000009	-3.69E-02	1	1.18E+12
	300	2	1.14E+12	-4.06E-09	8.16E+01	0.000022	-0.015076	1	1.16E+12
		60	1.14E+12	-4.06E-09	8.16E+01	0.000007	-0.04738	1	1.20E+12
		120	1.14E+12	-4.06E-09	8.16E+01	0.000005	-0.066333	1	1.22E+12
40 V	100	2	1.14E+12	-4.06E-09	1.63E+02	0.000017	-3.90E-02	1	1.19E+12
		60	1.14E+12	-4.06E-09	1.63E+02	0.000013	-5.10E-02	1	1.20E+12
		120	1.14E+12	-4.06E-09	1.63E+02	0.000011	-6.03E-02	1	1.21E+12
	200	2	1.14E+12	-4.06E-09	1.63E+02	0.000020	-3.32E-02	1	1.18E+12
		60	1.14E+12	-4.06E-09	1.63E+02	0.000012	-5.53E-02	1	1.21E+12
		120	1.14E+12	-4.06E-09	1.63E+02	0.000009	-7.37E-02	1	1.23E+12
	300	2	1.14E+12	-4.06E-09	1.63E+02	0.000022	-0.030151	1	1.18E+12
		60	1.14E+12	-4.06E-09	1.63E+02	0.000007	-0.094761	1	1.26E+12
		120	1.14E+12	-4.06E-09	1.63E+02	0.000005	-0.132665	1	1.31E+12
60 V	100	2	1.14E+12	-4.06E-09	2.45E+02	0.000017	-5.85E-02	1	1.21E+12
		60	1.14E+12	-4.06E-09	2.45E+02	0.000013	-7.65E-02	1	1.23E+12
		120	1.14E+12	-4.06E-09	2.45E+02	0.000011	-9.05E-02	1	1.25E+12
	200	2	1.14E+12	-4.06E-09	2.45E+02	0.000020	-4.97E-02	1	1.20E+12
		60	1.14E+12	-4.06E-09	2.45E+02	0.000012	-8.29E-02	1	1.24E+12
		120	1.14E+12	-4.06E-09	2.45E+02	0.000009	-1.11E-01	1	1.28E+12
	300	2	1.14E+12	-4.06E-09	2.45E+02	0.000022	-0.045227	1	1.19E+12
		60	1.14E+12	-4.06E-09	2.45E+02	0.000007	-0.142141	1	1.33E+12
		120	1.14E+12	-4.06E-09	2.45E+02	0.000005	-0.198998	1	1.42E+12

$R_{EF} = (R_F) / (1+ (\eta_F R_F/TMP)\ \mu_P E)$

R_M is membrane resistance in the absence of electric field (m^{-1})

μ_M is the membrane electro-osmotic mobility ($m^2\ V^{-1}\ s^{-1}$)

E is the electric field strength (V/m)

J_M is the flux in the absence of an electric field ($m^3\ m^{-2}\ s^{-1}$)

	TMP	Time (min)	R_F	η_F	μ_P	E	$\eta_F R_F$ / TMP	C	R_{EF}
20 V	100000	2	9.90E+11	1.00E-03	4.47E-08	8.16E+01	9.92E+03	1	9.55E+11
	100000	60	6.54E+12	1.00E-03	4.47E-08	8.16E+01	6.55E+04	1	5.28E+12
	100000	120	1.06E+13	1.00E-03	4.47E-08	8.16E+01	1.06E+05	1	7.64E+12
	200000	2	9.90E+11	1.00E-03	4.47E-08	8.16E+01	4.96E+03	1	9.72E+11
	200000	60	6.54E+12	1.00E-03	4.47E-08	8.16E+01	3.28E+04	1	5.84E+12
	200000	120	1.06E+13	1.00E-03	4.47E-08	8.16E+01	5.31E+04	1	8.88E+12
	300000	2	9.90E+11	1.00E-03	4.47E-08	8.16E+01	3.31E+03	1	9.78E+11
	300000	60	6.54E+12	1.00E-03	4.47E-08	8.16E+01	2.18E+04	1	6.06E+12
	300000	120	1.06E+13	1.00E-03	4.47E-08	8.16E+01	3.54E+04	1	9.39E+12
40 V	100000	2	9.90E+11	1.00E-03	4.47E-08	1.63E+02	9.92E+03	1	9.23E+11
	100000	60	6.54E+12	1.00E-03	4.47E-08	1.63E+02	6.55E+04	1	4.42E+12
	100000	120	1.06E+13	1.00E-03	4.47E-08	1.63E+02	1.06E+05	1	5.97E+12
	200000	2	9.90E+11	1.00E-03	4.47E-08	1.63E+02	4.96E+03	1	9.55E+11
	200000	60	6.54E+12	1.00E-03	4.47E-08	1.63E+02	3.28E+04	1	5.28E+12
	200000	120	1.06E+13	1.00E-03	4.47E-08	1.63E+02	5.31E+04	1	7.64E+12
	300000	2	9.90E+11	1.00E-03	4.47E-08	1.63E+02	3.31E+03	1	9.67E+11
	300000	60	6.54E+12	1.00E-03	4.47E-08	1.63E+02	2.18E+04	1	5.64E+12
	300000	120	1.06E+13	1.00E-03	4.47E-08	1.63E+02	3.54E+04	1	8.42E+12
60 V	100000	2	9.90E+11	1.00E-03	4.47E-08	2.45E+02	9.92E+03	1	8.93E+11
	100000	60	6.54E+12	1.00E-03	4.47E-08	2.45E+02	6.55E+04	1	3.81E+12
	100000	120	1.06E+13	1.00E-03	4.47E-08	2.45E+02	1.06E+05	1	4.90E+12
	200000	2	9.90E+11	1.00E-03	4.47E-08	2.45E+02	4.96E+03	1	9.39E+11
	200000	60	6.54E+12	1.00E-03	4.47E-08	2.45E+02	3.28E+04	1	4.81E+12
	200000	120	1.06E+13	1.00E-03	4.47E-08	2.45E+02	5.31E+04	1	6.70E+12
	300000	2	9.90E+11	1.00E-03	4.47E-08	2.45E+02	3.31E+03	1	9.55E+11
	300000	60	6.54E+12	1.00E-03	4.47E-08	2.45E+02	2.18E+04	1	5.28E+12
	300000	120	1.06E+13	1.00E-03	4.47E-08	2.45E+02	3.54E+04	1	7.64E+12

$R_{EC} = R_T - R_{EM} - R_{EF}$

20 Volts

Time (min)	100 kPa				200 kPa				300 kPa			
	R_T	R_{EM}	R_{EF}	R_{EC}	R_T	R_{EM}	R_{EF}	R_{EC}	R_T	R_{EM}	R_{EF}	R_{EC}
2	9.07E+12	1.16E+12	9.55E+11	6.95E+12	1.43E+13	1.16E+12	9.72E+11	1.21E+13	2.30E+13	1.16E+12	9.78E+11	2.09E+13
60	9.98E+12	1.17E+12	5.28E+12	3.53E+12	2.85E+13	1.17E+12	5.84E+12	2.15E+13	4.99E+13	1.20E+12	6.06E+12	4.26E+13
120	1.11E+13	1.18E+12	7.64E+12	2.28E+12	3.99E+13	1.18E+12	8.88E+12	2.99E+13	7.49E+13	1.22E+12	9.39E+12	6.42E+13

40 Volts

Time (min)	100 kPa				200 kPa				300 kPa			
	R_T	R_{EM}	R_{EF}	R_{EC}	R_T	R_{EM}	R_{EF}	R_{EC}	R_T	R_{EM}	R_{EF}	R_{EC}
2	9.04E+12	1.19E+12	9.23E+11	6.93E+12	1.43E+13	1.18E+12	9.55E+11	1.21E+13	2.14E+13	1.18E+12	9.67E+11	1.92E+13
60	9.06E+12	1.20E+12	4.42E+12	3.44E+12	2.85E+13	1.21E+12	5.28E+12	2.20E+13	4.99E+13	1.26E+12	5.64E+12	4.30E+13
120	1.05E+13	1.21E+12	5.97E+12	3.32E+12	3.99E+13	1.23E+12	7.64E+12	3.11E+13	7.99E+13	1.31E+12	8.42E+12	7.02E+13

60 Volts

Time (min)	100 kPa				200 kPa				300 kPa			
	R_T	R_{EM}	R_{EF}	R_{EC}	R_T	R_{EM}	R_{EF}	R_{EC}	R_T	R_{EM}	R_{EF}	R_{EC}
2	6.65E+12	1.21E+12	8.93E+11	4.55E+12	1.11E+13	1.20E+12	9.39E+11	8.95E+12	1.76E+13	1.19E+12	9.55E+11	1.55E+13
60	7.68E+12	1.23E+12	3.81E+12	2.64E+12	2.50E+13	1.24E+12	4.81E+12	1.89E+13	5.99E+13	1.33E+12	5.28E+12	5.33E+13
120	8.32E+12	1.25E+12	4.90E+12	2.16E+12	3.99E+13	1.28E+12	6.70E+12	3.19E+13	9.98E+13	1.42E+12	7.64E+12	9.07E+13

$R_T = TMP / J\eta_F$ $\eta_F =$ **0.001002 Pa s**

I = 0.5 A

								Ultrafiltration
Voltage	=			20	volts	Time (min)	R_T (m^{-1})	
TMP	**=**	**TMP**	**η_F**	**100000**	**Pascal**			
J	=	100000	0.001002	0.000011	$m^3m^{-2}s^{-1}$	120	9.1E+12	5.6E+12
		100000	0.001002	0.000010	$m^3m^{-2}s^{-1}$	3600	1.0E+13	2.1E+13
		100000	0.001002	0.000009	$m^3m^{-2}s^{-1}$	7200	1.1E+13	3.6E+13
TMP	**=**			**200000**	**Pascal**			
J	=	200000	0.001002	0.000014	$m^3m^{-2}s^{-1}$	120	1.4E+13	9.0E+12
		200000	0.001002	0.000007	$m^3m^{-2}s^{-1}$	3600	2.9E+13	3.3E+13
		200000	0.001002	0.000005	$m^3m^{-2}s^{-1}$	7200	4.0E+13	6.0E+13
TMP	**=**			**300000**	**Pascal**			
J	=	300000	0.001002	0.000013	$m^3m^{-2}s^{-1}$	120	2.3E+13	1.2E+13
		300000	0.001002	0.000006	$m^3m^{-2}s^{-1}$	3600	5.0E+13	4.6E+13
		300000	0.001002	0.000004	$m^3m^{-2}s^{-1}$	7200	7.5E+13	8.4E+13
Voltage	=			40	volts	Time (min)		
TMP	**=**			**100000**	**Pascal**			
J	=	100000	0.001002	0.000010	$m^3m^{-2}s^{-1}$	120	9.0E+12	
		100000	0.001002	0.000010	$m^3m^{-2}s^{-1}$	3600	9.1E+12	
		100000	0.001002	0.000008	$m^3m^{-2}s^{-1}$	7200	1.1E+13	
TMP	**=**			**200000**	**Pascal**			
J	=	200000	0.001002	0.000014	$m^3m^{-2}s^{-1}$	120	1.4E+13	
		200000	0.001002	0.000007	$m^3m^{-2}s^{-1}$	3600	2.9E+13	
		200000	0.001002	0.000005	$m^3m^{-2}s^{-1}$	7200	4.0E+13	
TMP	**=**			**300000**	**Pascal**			
J	=	300000	0.001002	0.000014	$m^3m^{-2}s^{-1}$	120	2.1E+13	
		300000	0.001002	0.000006	$m^3m^{-2}s^{-1}$	3600	5.0E+13	
		300000	0.001002	0.000005	$m^3m^{-2}s^{-1}$	7200	8.0E+13	
Voltage	=			60	volts	Time (min)		
TMP	**=**			**100000**	**Pascal**			
J	=	100000	0.001002	0.000015	$m^3m^{-2}s^{-1}$	120	6.7E+12	
		100000	0.001002	0.000013	$m^3m^{-2}s^{-1}$	3600	7.7E+12	
		100000	0.001002	0.000012	$m^3m^{-2}s^{-1}$	7200	8.3E+12	
TMP	**=**			**200000**	**Pascal**			
J	=	200000	0.001002	0.000018	$m^3m^{-2}s^{-1}$	120	1.1E+13	
		200000	0.001002	0.000008	$m^3m^{-2}s^{-1}$	3600	2.5E+13	
		200000	0.001002	0.000005	$m^3m^{-2}s^{-1}$	7200	4.0E+13	
TMP	**=**			**300000**	**Pascal**			
J	=	300000	0.001002	0.000017	$m^3m^{-2}s^{-1}$	120	1.8E+13	
		300000	0.001002	0.000005	$m^3m^{-2}s^{-1}$	3600	6.0E+13	
		300000	0.001002	0.000003	$m^3m^{-2}s^{-1}$	7200	1.0E+14	

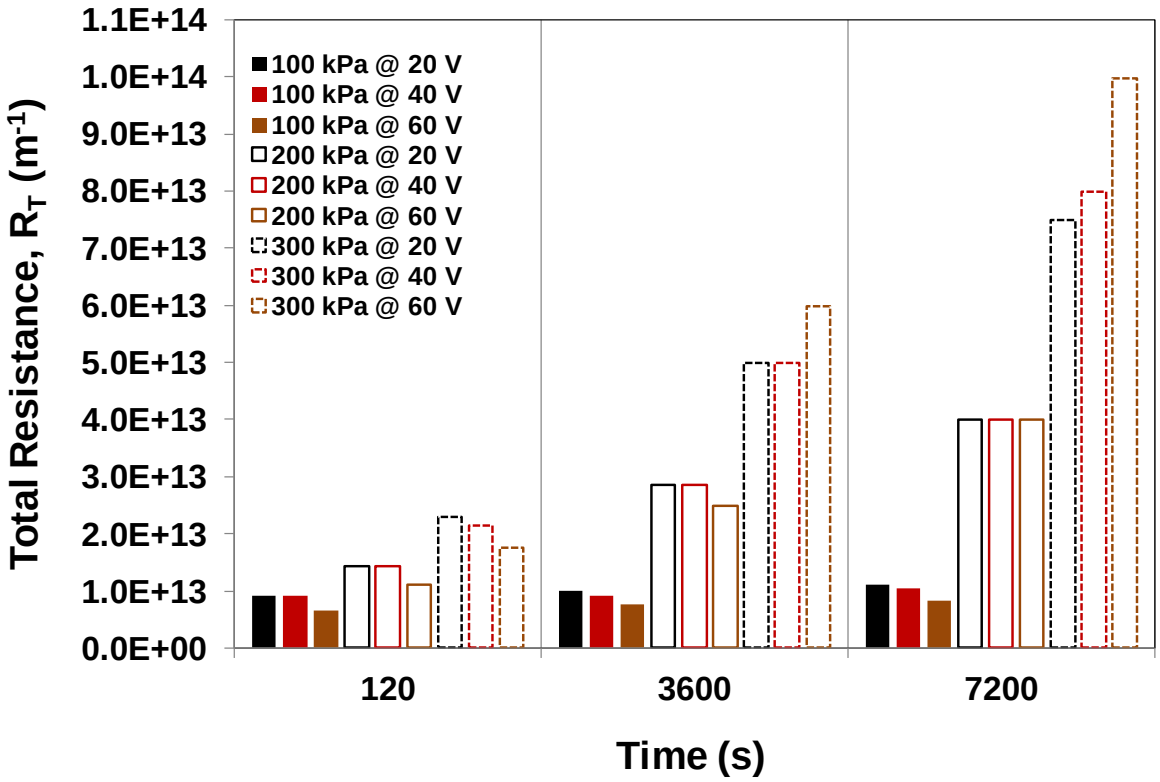
Total Resistance, R_T (m^{-1})
1.1E+14
1.0E+14
9.0E+13
8.0E+13
7.0E+13
6.0E+13
5.0E+13
4.0E+13
3.0E+13
2.0E+13
1.0E+13
0.0E+00
100 kPa @ 20 V
100 kPa @ 40 V
100 kPa @ 60 V
200 kPa @ 20 V
200 kPa @ 40 V
200 kPa @ 60 V
300 kPa @ 20 V
300 kPa @ 40 V
300 kPa @ 60 V
120
3600
7200
Time (s)

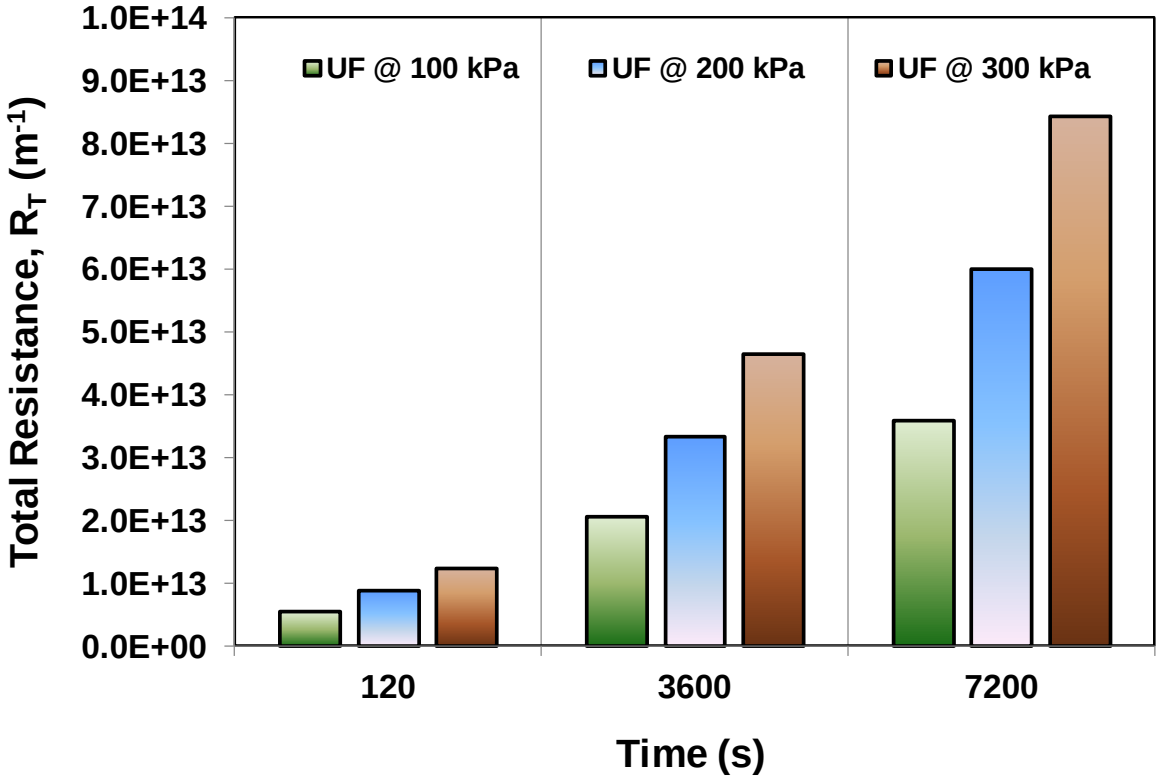
Total Resistance, R_T (m^{-1})
1.0E+14
9.0E+13
8.0E+13
7.0E+13
6.0E+13
5.0E+13
4.0E+13
3.0E+13
2.0E+13
1.0E+13
0.0E+00
UF @ 100 kPa
UF @ 200 kPa
UF @ 300 kPa
120
3600
7200
Time (s)

Appendix 6.3: Calculations of the forces acting on particles suspended in the beverage production wastewater

Particle Sizes (nm)	Particle Sizes (m) $Ø_P$	Viscosity of Feed (Pa s) η_F	Pressure Drop (Pa) ΔP			Internal Diameter of ceramic membrane (m) $Ø_{CM}$	Length of ceramic membrane (m), L_{CM}
			2.5 m s^{-1}	3.1 m s^{-1}	3.6 m s^{-1}		
15.7	1.6E-08	1.002E-03	61720.8	87851.4	122524.2	0.007	0.25
18.2	1.8E-08	1.002E-03	61720.8	87851.4	122524.2	0.007	0.25
21.0	2.1E-08	1.002E-03	61720.8	87851.4	122524.2	0.007	0.25
24.4	2.4E-08	1.002E-03	61720.8	87851.4	122524.2	0.007	0.25
28.2	2.8E-08	1.002E-03	61720.8	87851.4	122524.2	0.007	0.25
32.7	3.3E-08	1.002E-03	61720.8	87851.4	122524.2	0.007	0.25
37.8	3.8E-08	1.002E-03	61720.8	87851.4	122524.2	0.007	0.25
43.8	4.4E-08	1.002E-03	61720.8	87851.4	122524.2	0.007	0.25
50.8	5.1E-08	1.002E-03	61720.8	87851.4	122524.2	0.007	0.25
58.8	5.9E-08	1.002E-03	61720.8	87851.4	122524.2	0.007	0.25
68.1	6.8E-08	1.002E-03	61720.8	87851.4	122524.2	0.007	0.25
78.8	7.9E-08	1.002E-03	61720.8	87851.4	122524.2	0.007	0.25
91.3	9.1E-08	1.002E-03	61720.8	87851.4	122524.2	0.007	0.25
105.7	1.1E-07	1.002E-03	61720.8	87851.4	122524.2	0.007	0.25
122.4	1.2E-07	1.002E-03	61720.8	87851.4	122524.2	0.007	0.25
141.8	1.4E-07	1.002E-03	61720.8	87851.4	122524.2	0.007	0.25
164.2	1.6E-07	1.002E-03	61720.8	87851.4	122524.2	0.007	0.25
190.1	1.9E-07	1.002E-03	61720.8	87851.4	122524.2	0.007	0.25
220.2	2.2E-07	1.002E-03	61720.8	87851.4	122524.2	0.007	0.25
255.0	2.6E-07	1.002E-03	61720.8	87851.4	122524.2	0.007	0.25
295.3	3.0E-07	1.002E-03	61720.8	87851.4	122524.2	0.007	0.25
342.0	3.4E-07	1.002E-03	61720.8	87851.4	122524.2	0.007	0.25
396.1	4.0E-07	1.002E-03	61720.8	87851.4	122524.2	0.007	0.25
458.7	4.6E-07	1.002E-03	61720.8	87851.4	122524.2	0.007	0.25
531.2	5.3E-07	1.002E-03	61720.8	87851.4	122524.2	0.007	0.25
615.1	6.2E-07	1.002E-03	61720.8	87851.4	122524.2	0.007	0.25
712.4	7.1E-07	1.002E-03	61720.8	87851.4	122524.2	0.007	0.25
825.0	8.3E-07	1.002E-03	61720.8	87851.4	122524.2	0.007	0.25
955.4	9.6E-07	1.002E-03	61720.8	87851.4	122524.2	0.007	0.25
1106.0	1.1E-06	1.002E-03	61720.8	87851.4	122524.2	0.007	0.25
1281.0	1.3E-06	1.002E-03	61720.8	87851.4	122524.2	0.007	0.25
1484.0	1.5E-06	1.002E-03	61720.8	87851.4	122524.2	0.007	0.25
1718.0	1.7E-06	1.002E-03	61720.8	87851.4	122524.2	0.007	0.25
1990.0	2.0E-06	1.002E-03	61720.8	87851.4	122524.2	0.007	0.25
2305.0	2.3E-06	1.002E-03	61720.8	87851.4	122524.2	0.007	0.25
2669.0	2.7E-06	1.002E-03	61720.8	87851.4	122524.2	0.007	0.25
3091.0	3.1E-06	1.002E-03	61720.8	87851.4	122524.2	0.007	0.25
3580.0	3.6E-06	1.002E-03	61720.8	87851.4	122524.2	0.007	0.25
4145.0	4.1E-06	1.002E-03	61720.8	87851.4	122524.2	0.007	0.25
4801.0	4.8E-06	1.002E-03	61720.8	87851.4	122524.2	0.007	0.25
5560.0	5.6E-06	1.002E-03	61720.8	87851.4	122524.2	0.007	0.25
6310.0	6.3E-06	1.002E-03	61720.8	87851.4	122524.2	0.007	0.25

F_{VD} (Newtons) $= (2.55p\Delta P\emptyset_{CM}\emptyset_P^2)/4L_{CM}$			Permeation Flux or permeate velocity ($m\ s^{-1}$) J			F_{FD} (Newtons) $= 3p\eta_F\emptyset_P J$			Fluid Density ($kg\ m^{-3}$) ρ_F
2.5 m s^{-1}	3.1 m s^{-1}	3.6 m s^{-1}	100 kPa	200 kPa	300 kPa	100 kPa	200 kPa	300 kPa	
8.5E-13	1.2E-12	1.7E-12	7.631E-06	1.456E-05	2.166E-05	1.1E-15	2.2E-15	3.2E-15	9.982E+02
1.1E-12	1.6E-12	2.3E-12	7.631E-06	1.456E-05	2.166E-05	1.3E-15	2.5E-15	3.7E-15	9.982E+02
1.5E-12	2.2E-12	3.0E-12	7.631E-06	1.456E-05	2.166E-05	1.5E-15	2.9E-15	4.3E-15	9.982E+02
2.1E-12	2.9E-12	4.1E-12	7.631E-06	1.456E-05	2.166E-05	1.8E-15	3.3E-15	5.0E-15	9.982E+02
2.8E-12	3.9E-12	5.5E-12	7.631E-06	1.456E-05	2.166E-05	2.0E-15	3.9E-15	5.8E-15	9.982E+02
3.7E-12	5.3E-12	7.3E-12	7.631E-06	1.456E-05	2.166E-05	2.4E-15	4.5E-15	6.7E-15	9.982E+02
5.0E-12	7.1E-12	9.8E-12	7.631E-06	1.456E-05	2.166E-05	2.7E-15	5.2E-15	7.7E-15	9.982E+02
6.6E-12	9.5E-12	1.3E-11	7.631E-06	1.456E-05	2.166E-05	3.2E-15	6.0E-15	9.0E-15	9.982E+02
8.9E-12	1.3E-11	1.8E-11	7.631E-06	1.456E-05	2.166E-05	3.7E-15	7.0E-15	1.0E-14	9.982E+02
1.2E-11	1.7E-11	2.4E-11	7.631E-06	1.456E-05	2.166E-05	4.2E-15	8.1E-15	1.2E-14	9.982E+02
1.6E-11	2.3E-11	3.2E-11	7.631E-06	1.456E-05	2.166E-05	4.9E-15	9.4E-15	1.4E-14	9.982E+02
2.2E-11	3.1E-11	4.3E-11	7.631E-06	1.456E-05	2.166E-05	5.7E-15	1.1E-14	1.6E-14	9.982E+02
2.9E-11	4.1E-11	5.7E-11	7.631E-06	1.456E-05	2.166E-05	6.6E-15	1.3E-14	1.9E-14	9.982E+02
3.9E-11	5.5E-11	7.7E-11	7.631E-06	1.456E-05	2.166E-05	7.6E-15	1.5E-14	2.2E-14	9.982E+02
5.2E-11	7.4E-11	1.0E-10	7.631E-06	1.456E-05	2.166E-05	8.8E-15	1.7E-14	2.5E-14	9.982E+02
7.0E-11	9.9E-11	1.4E-10	7.631E-06	1.456E-05	2.166E-05	1.0E-14	1.9E-14	2.9E-14	9.982E+02
9.3E-11	1.3E-10	1.9E-10	7.631E-06	1.456E-05	2.166E-05	1.2E-14	2.3E-14	3.4E-14	9.982E+02
1.3E-10	1.8E-10	2.5E-10	7.631E-06	1.456E-05	2.166E-05	1.4E-14	2.6E-14	3.9E-14	9.982E+02
1.7E-10	2.4E-10	3.3E-10	7.631E-06	1.456E-05	2.166E-05	1.6E-14	3.0E-14	4.5E-14	9.982E+02
2.3E-10	3.2E-10	4.5E-10	7.631E-06	1.456E-05	2.166E-05	1.8E-14	3.5E-14	5.2E-14	9.982E+02
3.0E-10	4.3E-10	6.0E-10	7.631E-06	1.456E-05	2.166E-05	2.1E-14	4.1E-14	6.0E-14	9.982E+02
4.0E-10	5.8E-10	8.0E-10	7.631E-06	1.456E-05	2.166E-05	2.5E-14	4.7E-14	7.0E-14	9.982E+02
5.4E-10	7.7E-10	1.1E-09	7.631E-06	1.456E-05	2.166E-05	2.9E-14	5.4E-14	8.1E-14	9.982E+02
7.3E-10	1.0E-09	1.4E-09	7.631E-06	1.456E-05	2.166E-05	3.3E-14	6.3E-14	9.4E-14	9.982E+02
9.8E-10	1.4E-09	1.9E-09	7.631E-06	1.456E-05	2.166E-05	3.8E-14	7.3E-14	1.1E-13	9.982E+02
1.3E-09	1.9E-09	2.6E-09	7.631E-06	1.456E-05	2.166E-05	4.4E-14	8.5E-14	1.3E-13	9.982E+02
1.8E-09	2.5E-09	3.5E-09	7.631E-06	1.456E-05	2.166E-05	5.1E-14	9.8E-14	1.5E-13	9.982E+02
2.4E-09	3.4E-09	4.7E-09	7.631E-06	1.456E-05	2.166E-05	5.9E-14	1.1E-13	1.7E-13	9.982E+02
3.2E-09	4.5E-09	6.3E-09	7.631E-06	1.456E-05	2.166E-05	6.9E-14	1.3E-13	2.0E-13	9.982E+02
4.2E-09	6.0E-09	8.4E-09	7.631E-06	1.456E-05	2.166E-05	8.0E-14	1.5E-13	2.3E-13	9.982E+02
5.7E-09	8.1E-09	1.1E-08	7.631E-06	1.456E-05	2.166E-05	9.2E-14	1.8E-13	2.6E-13	9.982E+02
7.6E-09	1.1E-08	1.5E-08	7.631E-06	1.456E-05	2.166E-05	1.1E-13	2.0E-13	3.0E-13	9.982E+02
1.0E-08	1.5E-08	2.0E-08	7.631E-06	1.456E-05	2.166E-05	1.2E-13	2.4E-13	3.5E-13	9.982E+02
1.4E-08	2.0E-08	2.7E-08	7.631E-06	1.456E-05	2.166E-05	1.4E-13	2.7E-13	4.1E-13	9.982E+02
1.8E-08	2.6E-08	3.7E-08	7.631E-06	1.456E-05	2.166E-05	1.7E-13	3.2E-13	4.7E-13	9.982E+02
2.5E-08	3.5E-08	4.9E-08	7.631E-06	1.456E-05	2.166E-05	1.9E-13	3.7E-13	5.5E-13	9.982E+02
3.3E-08	4.7E-08	6.6E-08	7.631E-06	1.456E-05	2.166E-05	2.2E-13	4.2E-13	6.3E-13	9.982E+02
4.4E-08	6.3E-08	8.8E-08	7.631E-06	1.456E-05	2.166E-05	2.6E-13	4.9E-13	7.3E-13	9.982E+02
5.9E-08	8.5E-08	1.2E-07	7.631E-06	1.456E-05	2.166E-05	3.0E-13	5.7E-13	8.5E-13	9.982E+02
8.0E-08	1.1E-07	1.6E-07	7.631E-06	1.456E-05	2.166E-05	3.5E-13	6.6E-13	9.8E-13	9.982E+02
1.1E-07	1.5E-07	2.1E-07	7.631E-06	1.456E-05	2.166E-05	4.0E-13	7.6E-13	1.1E-12	9.982E+02
1.4E-07	2.0E-07	2.7E-07	7.631E-06	1.456E-05	2.166E-05	4.5E-13	8.7E-13	1.3E-12	9.982E+02

F_L (Newtons) $= 0.216 p Ø_P^4 \rho_F V_{av}^2 / r^2$			t_W $= \Delta P \, Ø_{CM} / 4L$			F_L (Newtons) $= 0.761 \, t_w^{1.5} Ø_P^3 \, \rho_F^{0.5} / \eta_F$		
2.4 m s^{-1}	2.8 m s^{-1}	3.2 m s^{-1}				2.5 m s^{-1}	3.1 m s^{-1}	3.6 m s^{-1}
1.930E-23	2.627E-23	3.431E-23	4.320E+02	6.150E+02	8.577E+02	8.3E-16	1.4E-15	2.3E-15
3.495E-23	4.757E-23	6.213E-23	4.320E+02	6.150E+02	8.577E+02	1.3E-15	2.2E-15	3.6E-15
6.242E-23	8.495E-23	1.110E-22	4.320E+02	6.150E+02	8.577E+02	2.0E-15	3.4E-15	5.6E-15
1.122E-22	1.527E-22	1.994E-22	4.320E+02	6.150E+02	8.577E+02	3.1E-15	5.3E-15	8.7E-15
2.017E-22	2.745E-22	3.586E-22	4.320E+02	6.150E+02	8.577E+02	4.8E-15	8.2E-15	1.4E-14
3.628E-22	4.939E-22	6.450E-22	4.320E+02	6.150E+02	8.577E+02	7.5E-15	1.3E-14	2.1E-14
6.530E-22	8.888E-22	1.161E-21	4.320E+02	6.150E+02	8.577E+02	1.2E-14	2.0E-14	3.3E-14
1.174E-21	1.598E-21	2.088E-21	4.320E+02	6.150E+02	8.577E+02	1.8E-14	3.1E-14	5.1E-14
2.113E-21	2.876E-21	3.756E-21	4.320E+02	6.150E+02	8.577E+02	2.8E-14	4.8E-14	7.9E-14
3.800E-21	5.172E-21	6.755E-21	4.320E+02	6.150E+02	8.577E+02	4.4E-14	7.4E-14	1.2E-13
6.834E-21	9.302E-21	1.215E-20	4.320E+02	6.150E+02	8.577E+02	6.8E-14	1.2E-13	1.9E-13
1.229E-20	1.673E-20	2.185E-20	4.320E+02	6.150E+02	8.577E+02	1.1E-13	1.8E-13	3.0E-13
2.211E-20	3.010E-20	3.931E-20	4.320E+02	6.150E+02	8.577E+02	1.6E-13	2.8E-13	4.6E-13
3.976E-20	5.411E-20	7.068E-20	4.320E+02	6.150E+02	8.577E+02	2.5E-13	4.3E-13	7.1E-13
7.149E-20	9.730E-20	1.271E-19	4.320E+02	6.150E+02	8.577E+02	4.0E-13	6.7E-13	1.1E-12
1.288E-19	1.753E-19	2.289E-19	4.320E+02	6.150E+02	8.577E+02	6.1E-13	1.0E-12	1.7E-12
2.315E-19	3.151E-19	4.116E-19	4.320E+02	6.150E+02	8.577E+02	9.5E-13	1.6E-12	2.7E-12
4.159E-19	5.662E-19	7.395E-19	4.320E+02	6.150E+02	8.577E+02	1.5E-12	2.5E-12	4.1E-12
7.488E-19	1.019E-18	1.331E-18	4.320E+02	6.150E+02	8.577E+02	2.3E-12	3.9E-12	6.4E-12
1.347E-18	1.833E-18	2.394E-18	4.320E+02	6.150E+02	8.577E+02	3.6E-12	6.1E-12	1.0E-11
2.422E-18	3.297E-18	4.306E-18	4.320E+02	6.150E+02	8.577E+02	5.5E-12	9.4E-12	1.6E-11
4.357E-18	5.931E-18	7.746E-18	4.320E+02	6.150E+02	8.577E+02	8.6E-12	1.5E-11	2.4E-11
7.840E-18	1.067E-17	1.394E-17	4.320E+02	6.150E+02	8.577E+02	1.3E-11	2.3E-11	3.7E-11
1.410E-17	1.919E-17	2.507E-17	4.320E+02	6.150E+02	8.577E+02	2.1E-11	3.5E-11	5.8E-11
2.536E-17	3.452E-17	4.508E-17	4.320E+02	6.150E+02	8.577E+02	3.2E-11	5.5E-11	9.0E-11
4.559E-17	6.206E-17	8.105E-17	4.320E+02	6.150E+02	8.577E+02	5.0E-11	8.5E-11	1.4E-10
8.204E-17	1.117E-16	1.458E-16	4.320E+02	6.150E+02	8.577E+02	7.8E-11	1.3E-10	2.2E-10
1.475E-16	2.008E-16	2.623E-16	4.320E+02	6.150E+02	8.577E+02	1.2E-10	2.1E-10	3.4E-10
2.654E-16	3.612E-16	4.718E-16	4.320E+02	6.150E+02	8.577E+02	1.9E-10	3.2E-10	5.3E-10
4.766E-16	6.487E-16	8.472E-16	4.320E+02	6.150E+02	8.577E+02	2.9E-10	5.0E-10	8.2E-10
8.576E-16	1.167E-15	1.525E-15	4.320E+02	6.150E+02	8.577E+02	4.5E-10	7.7E-10	1.3E-09
1.545E-15	2.103E-15	2.746E-15	4.320E+02	6.150E+02	8.577E+02	7.0E-10	1.2E-09	2.0E-09
2.775E-15	3.777E-15	4.933E-15	4.320E+02	6.150E+02	8.577E+02	1.1E-09	1.9E-09	3.1E-09
4.995E-15	6.799E-15	8.880E-15	4.320E+02	6.150E+02	8.577E+02	1.7E-09	2.9E-09	4.7E-09
8.991E-15	1.224E-14	1.598E-14	4.320E+02	6.150E+02	8.577E+02	2.6E-09	4.5E-09	7.4E-09
1.616E-14	2.200E-14	2.873E-14	4.320E+02	6.150E+02	8.577E+02	4.1E-09	7.0E-09	1.1E-08
2.907E-14	3.957E-14	5.169E-14	4.320E+02	6.150E+02	8.577E+02	6.4E-09	1.1E-08	1.8E-08
5.232E-14	7.121E-14	9.301E-14	4.320E+02	6.150E+02	8.577E+02	9.9E-09	1.7E-08	2.8E-08
9.402E-14	1.280E-13	1.671E-13	4.320E+02	6.150E+02	8.577E+02	1.5E-08	2.6E-08	4.3E-08
1.692E-13	2.303E-13	3.008E-13	4.320E+02	6.150E+02	8.577E+02	2.4E-08	4.0E-08	6.7E-08
3.044E-13	4.143E-13	5.411E-13	4.320E+02	6.150E+02	8.577E+02	3.7E-08	6.3E-08	1.0E-07
5.049E-13	6.873E-13	8.976E-13	4.320E+02	6.150E+02	8.577E+02	5.4E-08	9.2E-08	1.5E-07

a	*hv*	F_{VDW} (Newtons) = hv $Ø_P$ / 32pa^2	p	R* = R_1 (m)	e, dielectric permittivity of water @ 20°C	e_O, permittivity of vacuum (C^2/N-m^2)	À, inverse Debye Length (960 nm)	4pR* / ee_OÀ
4.000E-10	1.000E-20	9.8E-12	3.142E+00	7.8E-09	8.02E+01	8.85E-12	**1.04E+06**	**1.13E-14**
4.000E-10	1.000E-20	1.1E-11	3.142E+00	9.1E-09	8.02E+01	8.85E-12	**1.04E+06**	**1.31E-14**
4.000E-10	1.000E-20	1.3E-11	3.142E+00	1.1E-08	8.02E+01	8.85E-12	**1.04E+06**	**1.52E-14**
4.000E-10	1.000E-20	1.5E-11	3.142E+00	1.2E-08	8.02E+01	8.85E-12	**1.04E+06**	**1.76E-14**
4.000E-10	1.000E-20	1.8E-11	3.142E+00	1.4E-08	8.02E+01	8.85E-12	**1.04E+06**	**2.04E-14**
4.000E-10	1.000E-20	2.0E-11	3.142E+00	1.6E-08	8.02E+01	8.85E-12	**1.04E+06**	**2.36E-14**
4.000E-10	1.000E-20	2.4E-11	3.142E+00	1.9E-08	8.02E+01	8.85E-12	**1.04E+06**	**2.73E-14**
4.000E-10	1.000E-20	2.7E-11	3.142E+00	2.2E-08	8.02E+01	8.85E-12	**1.04E+06**	**3.16E-14**
4.000E-10	1.000E-20	3.2E-11	3.142E+00	2.5E-08	8.02E+01	8.85E-12	**1.04E+06**	**3.67E-14**
4.000E-10	1.000E-20	3.7E-11	3.142E+00	2.9E-08	8.02E+01	8.85E-12	**1.04E+06**	**4.24E-14**
4.000E-10	1.000E-20	4.2E-11	3.142E+00	3.4E-08	8.02E+01	8.85E-12	**1.04E+06**	**4.92E-14**
4.000E-10	1.000E-20	4.9E-11	3.142E+00	3.9E-08	8.02E+01	8.85E-12	**1.04E+06**	**5.69E-14**
4.000E-10	1.000E-20	5.7E-11	3.142E+00	4.6E-08	8.02E+01	8.85E-12	**1.04E+06**	**6.59E-14**
4.000E-10	1.000E-20	6.6E-11	3.142E+00	5.3E-08	8.02E+01	8.85E-12	**1.04E+06**	**7.63E-14**
4.000E-10	1.000E-20	7.6E-11	3.142E+00	6.1E-08	8.02E+01	8.85E-12	**1.04E+06**	**8.84E-14**
4.000E-10	1.000E-20	8.8E-11	3.142E+00	7.1E-08	8.02E+01	8.85E-12	**1.04E+06**	**1.02E-13**
4.000E-10	1.000E-20	1.0E-10	3.142E+00	8.2E-08	8.02E+01	8.85E-12	**1.04E+06**	**1.19E-13**
4.000E-10	1.000E-20	1.2E-10	3.142E+00	9.5E-08	8.02E+01	8.85E-12	**1.04E+06**	**1.37E-13**
4.000E-10	1.000E-20	1.4E-10	3.142E+00	1.1E-07	8.02E+01	8.85E-12	**1.04E+06**	**1.59E-13**
4.000E-10	1.000E-20	1.6E-10	3.142E+00	1.3E-07	8.02E+01	8.85E-12	**1.04E+06**	**1.84E-13**
4.000E-10	1.000E-20	1.8E-10	3.142E+00	1.5E-07	8.02E+01	8.85E-12	**1.04E+06**	**2.13E-13**
4.000E-10	1.000E-20	2.1E-10	3.142E+00	1.7E-07	8.02E+01	8.85E-12	**1.04E+06**	**2.47E-13**
4.000E-10	1.000E-20	2.5E-10	3.142E+00	2.0E-07	8.02E+01	8.85E-12	**1.04E+06**	**2.86E-13**
4.000E-10	1.000E-20	2.9E-10	3.142E+00	2.3E-07	8.02E+01	8.85E-12	**1.04E+06**	**3.31E-13**
4.000E-10	1.000E-20	3.3E-10	3.142E+00	2.7E-07	8.02E+01	8.85E-12	**1.04E+06**	**3.84E-13**
4.000E-10	1.000E-20	3.8E-10	3.142E+00	3.1E-07	8.02E+01	8.85E-12	**1.04E+06**	**4.44E-13**
4.000E-10	1.000E-20	4.4E-10	3.142E+00	3.6E-07	8.02E+01	8.85E-12	**1.04E+06**	**5.15E-13**
4.000E-10	1.000E-20	5.1E-10	3.142E+00	4.1E-07	8.02E+01	8.85E-12	**1.04E+06**	**5.96E-13**
4.000E-10	1.000E-20	5.9E-10	3.142E+00	4.8E-07	8.02E+01	8.85E-12	**1.04E+06**	**6.90E-13**
4.000E-10	1.000E-20	6.9E-10	3.142E+00	5.5E-07	8.02E+01	8.85E-12	**1.04E+06**	**7.99E-13**
4.000E-10	1.000E-20	8.0E-10	3.142E+00	6.4E-07	8.02E+01	8.85E-12	**1.04E+06**	**9.25E-13**
4.000E-10	1.000E-20	9.2E-10	3.142E+00	7.4E-07	8.02E+01	8.85E-12	**1.04E+06**	**1.07E-12**
4.000E-10	1.000E-20	1.1E-09	3.142E+00	8.6E-07	8.02E+01	8.85E-12	**1.04E+06**	**1.24E-12**
4.000E-10	1.000E-20	1.2E-09	3.142E+00	1.0E-06	8.02E+01	8.85E-12	**1.04E+06**	**1.44E-12**
4.000E-10	1.000E-20	1.4E-09	3.142E+00	1.2E-06	8.02E+01	8.85E-12	**1.04E+06**	**1.66E-12**
4.000E-10	1.000E-20	1.7E-09	3.142E+00	1.3E-06	8.02E+01	8.85E-12	**1.04E+06**	**1.93E-12**
4.000E-10	1.000E-20	1.9E-09	3.142E+00	1.5E-06	8.02E+01	8.85E-12	**1.04E+06**	**2.23E-12**
4.000E-10	1.000E-20	2.2E-09	3.142E+00	1.8E-06	8.02E+01	8.85E-12	**1.04E+06**	**2.59E-12**
4.000E-10	1.000E-20	2.6E-09	3.142E+00	2.1E-06	8.02E+01	8.85E-12	**1.04E+06**	**2.99E-12**
4.000E-10	1.000E-20	3.0E-09	3.142E+00	2.4E-06	8.02E+01	8.85E-12	**1.04E+06**	**3.47E-12**
4.000E-10	1.000E-20	3.5E-09	3.142E+00	2.8E-06	8.02E+01	8.85E-12	**1.04E+06**	**4.02E-12**
4.000E-10	1.000E-20	3.9E-09	3.142E+00	3.2E-06	8.02E+01	8.85E-12	**1.04E+06**	**4.56E-12**

$h_{membrane}$ (m)	I.R.$_{membrane}$ (m)	A_{sphere} (m^2), $4pr^2$	$A_{inside\ cyl}$ (m^2), 2prh	Charge (Coulumb) 1e = 1.602E-19 C	s_1 (C/m^2), q/A_{sphere}	s_2 (C/m^2), $q/A_{inside\ cyl}$	$s_1 s_2$	$0.5*(s_1^2 + s_2^2)$
2.50E-01	7.00E-03	7.73E-16	1.10E-02	1.60E-19	2.07E-04	1.46E-17	3.02E-21	2.15E-08
2.50E-01	7.00E-03	1.04E-15	1.10E-02	1.60E-19	1.54E-04	1.46E-17	2.24E-21	1.18E-08
2.50E-01	7.00E-03	1.39E-15	1.10E-02	1.60E-19	1.15E-04	1.46E-17	1.68E-21	6.63E-09
2.50E-01	7.00E-03	1.86E-15	1.10E-02	1.60E-19	8.59E-05	1.46E-17	1.25E-21	3.69E-09
2.50E-01	7.00E-03	2.50E-15	1.10E-02	1.60E-19	6.41E-05	1.46E-17	9.34E-22	2.05E-09
2.50E-01	7.00E-03	3.35E-15	1.10E-02	1.60E-19	4.78E-05	1.46E-17	6.96E-22	1.14E-09
2.50E-01	7.00E-03	4.50E-15	1.10E-02	1.60E-19	3.56E-05	1.46E-17	5.19E-22	6.34E-10
2.50E-01	7.00E-03	6.03E-15	1.10E-02	1.60E-19	2.66E-05	1.46E-17	3.87E-22	3.53E-10
2.50E-01	7.00E-03	8.09E-15	1.10E-02	1.60E-19	1.98E-05	1.46E-17	2.88E-22	1.96E-10
2.50E-01	7.00E-03	1.09E-14	1.10E-02	1.60E-19	1.48E-05	1.46E-17	2.15E-22	1.09E-10
2.50E-01	7.00E-03	1.46E-14	1.10E-02	1.60E-19	1.10E-05	1.46E-17	1.60E-22	6.06E-11
2.50E-01	7.00E-03	1.95E-14	1.10E-02	1.60E-19	8.21E-06	1.46E-17	1.20E-22	3.37E-11
2.50E-01	7.00E-03	2.62E-14	1.10E-02	1.60E-19	6.12E-06	1.46E-17	8.92E-23	1.87E-11
2.50E-01	7.00E-03	3.51E-14	1.10E-02	1.60E-19	4.56E-06	1.46E-17	6.65E-23	1.04E-11
2.50E-01	7.00E-03	4.71E-14	1.10E-02	1.60E-19	3.40E-06	1.46E-17	4.96E-23	5.79E-12
2.50E-01	7.00E-03	6.32E-14	1.10E-02	1.60E-19	2.54E-06	1.46E-17	3.69E-23	3.22E-12
2.50E-01	7.00E-03	8.47E-14	1.10E-02	1.60E-19	1.89E-06	1.46E-17	2.76E-23	1.79E-12
2.50E-01	7.00E-03	1.14E-13	1.10E-02	1.60E-19	1.41E-06	1.46E-17	2.06E-23	9.96E-13
2.50E-01	7.00E-03	1.52E-13	1.10E-02	1.60E-19	1.05E-06	1.46E-17	1.53E-23	5.53E-13
2.50E-01	7.00E-03	2.04E-13	1.10E-02	1.60E-19	7.84E-07	1.46E-17	1.14E-23	3.07E-13
2.50E-01	7.00E-03	2.74E-13	1.10E-02	1.60E-19	5.85E-07	1.46E-17	8.52E-24	1.71E-13
2.50E-01	7.00E-03	3.67E-13	1.10E-02	1.60E-19	4.36E-07	1.46E-17	6.35E-24	9.50E-14
2.50E-01	7.00E-03	4.93E-13	1.10E-02	1.60E-19	3.25E-07	1.46E-17	4.74E-24	5.28E-14
2.50E-01	7.00E-03	6.61E-13	1.10E-02	1.60E-19	2.42E-07	1.46E-17	3.53E-24	2.94E-14
2.50E-01	7.00E-03	8.86E-13	1.10E-02	1.60E-19	1.81E-07	1.46E-17	2.63E-24	1.63E-14
2.50E-01	7.00E-03	1.19E-12	1.10E-02	1.60E-19	1.35E-07	1.46E-17	1.96E-24	9.08E-15
2.50E-01	7.00E-03	1.59E-12	1.10E-02	1.60E-19	1.00E-07	1.46E-17	1.46E-24	5.05E-15
2.50E-01	7.00E-03	2.14E-12	1.10E-02	1.60E-19	7.49E-08	1.46E-17	1.09E-24	2.81E-15
2.50E-01	7.00E-03	2.87E-12	1.10E-02	1.60E-19	5.59E-08	1.46E-17	8.14E-25	1.56E-15
2.50E-01	7.00E-03	3.84E-12	1.10E-02	1.60E-19	4.17E-08	1.46E-17	6.07E-25	8.69E-16
2.50E-01	7.00E-03	5.16E-12	1.10E-02	1.60E-19	3.11E-08	1.46E-17	4.53E-25	4.83E-16
2.50E-01	7.00E-03	6.92E-12	1.10E-02	1.60E-19	2.32E-08	1.46E-17	3.37E-25	2.68E-16
2.50E-01	7.00E-03	9.27E-12	1.10E-02	1.60E-19	1.73E-08	1.46E-17	2.52E-25	1.49E-16
2.50E-01	7.00E-03	1.24E-11	1.10E-02	1.60E-19	1.29E-08	1.46E-17	1.88E-25	8.29E-17
2.50E-01	7.00E-03	1.67E-11	1.10E-02	1.60E-19	9.60E-09	1.46E-17	1.40E-25	4.61E-17
2.50E-01	7.00E-03	2.24E-11	1.10E-02	1.60E-19	7.16E-09	1.46E-17	1.04E-25	2.56E-17
2.50E-01	7.00E-03	3.00E-11	1.10E-02	1.60E-19	5.34E-09	1.46E-17	7.78E-26	1.42E-17
2.50E-01	7.00E-03	4.03E-11	1.10E-02	1.60E-19	3.98E-09	1.46E-17	5.80E-26	7.92E-18
2.50E-01	7.00E-03	5.40E-11	1.10E-02	1.60E-19	2.97E-09	1.46E-17	4.32E-26	4.40E-18
2.50E-01	7.00E-03	7.24E-11	1.10E-02	1.60E-19	2.21E-09	1.46E-17	3.22E-26	2.45E-18
2.50E-01	7.00E-03	9.71E-11	1.10E-02	1.60E-19	1.65E-09	1.46E-17	2.40E-26	1.36E-18
2.50E-01	7.00E-03	1.25E-10	1.10E-02	1.60E-19	1.28E-09	1.46E-17	1.87E-26	8.20E-19

c, Distance between sphere & membrane wall **Àc**

4 nm	5 nm	6 nm	7 nm	8 nm	9 nm	10 nm	4 nm	5 nm	6 nm	7 nm	8 nm	9 nm	10 nm
4.0E-09	5.0E-09	6.0E-09	7.0E-09	8.0E-09	9.0E-09	1.0E-08	4E-03	5E-03	6E-03	7E-03	8E-03	9E-03	1E-02
4.0E-09	5.0E-09	6.0E-09	7.0E-09	8.0E-09	9.0E-09	1.0E-08	4E-03	5E-03	6E-03	7E-03	8E-03	9E-03	1E-02
4.0E-09	5.0E-09	6.0E-09	7.0E-09	8.0E-09	9.0E-09	1.0E-08	4E-03	5E-03	6E-03	7E-03	8E-03	9E-03	1E-02
4.0E-09	5.0E-09	6.0E-09	7.0E-09	8.0E-09	9.0E-09	1.0E-08	4E-03	5E-03	6E-03	7E-03	8E-03	9E-03	1E-02
4.0E-09	5.0E-09	6.0E-09	7.0E-09	8.0E-09	9.0E-09	1.0E-08	4E-03	5E-03	6E-03	7E-03	8E-03	9E-03	1E-02
4.0E-09	5.0E-09	6.0E-09	7.0E-09	8.0E-09	9.0E-09	1.0E-08	4E-03	5E-03	6E-03	7E-03	8E-03	9E-03	1E-02
4.0E-09	5.0E-09	6.0E-09	7.0E-09	8.0E-09	9.0E-09	1.0E-08	4E-03	5E-03	6E-03	7E-03	8E-03	9E-03	1E-02
4.0E-09	5.0E-09	6.0E-09	7.0E-09	8.0E-09	9.0E-09	1.0E-08	4E-03	5E-03	6E-03	7E-03	8E-03	9E-03	1E-02
4.0E-09	5.0E-09	6.0E-09	7.0E-09	8.0E-09	9.0E-09	1.0E-08	4E-03	5E-03	6E-03	7E-03	8E-03	9E-03	1E-02
4.0E-09	5.0E-09	6.0E-09	7.0E-09	8.0E-09	9.0E-09	1.0E-08	4E-03	5E-03	6E-03	7E-03	8E-03	9E-03	1E-02
4.0E-09	5.0E-09	6.0E-09	7.0E-09	8.0E-09	9.0E-09	1.0E-08	4E-03	5E-03	6E-03	7E-03	8E-03	9E-03	1E-02
4.0E-09	5.0E-09	6.0E-09	7.0E-09	8.0E-09	9.0E-09	1.0E-08	4E-03	5E-03	6E-03	7E-03	8E-03	9E-03	1E-02
4.0E-09	5.0E-09	6.0E-09	7.0E-09	8.0E-09	9.0E-09	1.0E-08	4E-03	5E-03	6E-03	7E-03	8E-03	9E-03	1E-02
4.0E-09	5.0E-09	6.0E-09	7.0E-09	8.0E-09	9.0E-09	1.0E-08	4E-03	5E-03	6E-03	7E-03	8E-03	9E-03	1E-02
4.0E-09	5.0E-09	6.0E-09	7.0E-09	8.0E-09	9.0E-09	1.0E-08	4E-03	5E-03	6E-03	7E-03	8E-03	9E-03	1E-02
4.0E-09	5.0E-09	6.0E-09	7.0E-09	8.0E-09	9.0E-09	1.0E-08	4E-03	5E-03	6E-03	7E-03	8E-03	9E-03	1E-02
4.0E-09	5.0E-09	6.0E-09	7.0E-09	8.0E-09	9.0E-09	1.0E-08	4E-03	5E-03	6E-03	7E-03	8E-03	9E-03	1E-02
4.0E-09	5.0E-09	6.0E-09	7.0E-09	8.0E-09	9.0E-09	1.0E-08	4E-03	5E-03	6E-03	7E-03	8E-03	9E-03	1E-02
4.0E-09	5.0E-09	6.0E-09	7.0E-09	8.0E-09	9.0E-09	1.0E-08	4E-03	5E-03	6E-03	7E-03	8E-03	9E-03	1E-02
4.0E-09	5.0E-09	6.0E-09	7.0E-09	8.0E-09	9.0E-09	1.0E-08	4E-03	5E-03	6E-03	7E-03	8E-03	9E-03	1E-02
4.0E-09	5.0E-09	6.0E-09	7.0E-09	8.0E-09	9.0E-09	1.0E-08	4E-03	5E-03	6E-03	7E-03	8E-03	9E-03	1E-02
4.0E-09	5.0E-09	6.0E-09	7.0E-09	8.0E-09	9.0E-09	1.0E-08	4E-03	5E-03	6E-03	7E-03	8E-03	9E-03	1E-02
4.0E-09	5.0E-09	6.0E-09	7.0E-09	8.0E-09	9.0E-09	1.0E-08	4E-03	5E-03	6E-03	7E-03	8E-03	9E-03	1E-02
4.0E-09	5.0E-09	6.0E-09	7.0E-09	8.0E-09	9.0E-09	1.0E-08	4E-03	5E-03	6E-03	7E-03	8E-03	9E-03	1E-02
4.0E-09	5.0E-09	6.0E-09	7.0E-09	8.0E-09	9.0E-09	1.0E-08	4E-03	5E-03	6E-03	7E-03	8E-03	9E-03	1E-02
4.0E-09	5.0E-09	6.0E-09	7.0E-09	8.0E-09	9.0E-09	1.0E-08	4E-03	5E-03	6E-03	7E-03	8E-03	9E-03	1E-02
4.0E-09	5.0E-09	6.0E-09	7.0E-09	8.0E-09	9.0E-09	1.0E-08	4E-03	5E-03	6E-03	7E-03	8E-03	9E-03	1E-02
4.0E-09	5.0E-09	6.0E-09	7.0E-09	8.0E-09	9.0E-09	1.0E-08	4E-03	5E-03	6E-03	7E-03	8E-03	9E-03	1E-02
4.0E-09	5.0E-09	6.0E-09	7.0E-09	8.0E-09	9.0E-09	1.0E-08	4E-03	5E-03	6E-03	7E-03	8E-03	9E-03	1E-02
4.0E-09	5.0E-09	6.0E-09	7.0E-09	8.0E-09	9.0E-09	1.0E-08	4E-03	5E-03	6E-03	7E-03	8E-03	9E-03	1E-02
4.0E-09	5.0E-09	6.0E-09	7.0E-09	8.0E-09	9.0E-09	1.0E-08	4E-03	5E-03	6E-03	7E-03	8E-03	9E-03	1E-02
4.0E-09	5.0E-09	6.0E-09	7.0E-09	8.0E-09	9.0E-09	1.0E-08	4E-03	5E-03	6E-03	7E-03	8E-03	9E-03	1E-02
4.0E-09	5.0E-09	6.0E-09	7.0E-09	8.0E-09	9.0E-09	1.0E-08	4E-03	5E-03	6E-03	7E-03	8E-03	9E-03	1E-02
4.0E-09	5.0E-09	6.0E-09	7.0E-09	8.0E-09	9.0E-09	1.0E-08	4E-03	5E-03	6E-03	7E-03	8E-03	9E-03	1E-02
4.0E-09	5.0E-09	6.0E-09	7.0E-09	8.0E-09	9.0E-09	1.0E-08	4E-03	5E-03	6E-03	7E-03	8E-03	9E-03	1E-02
4.0E-09	5.0E-09	6.0E-09	7.0E-09	8.0E-09	9.0E-09	1.0E-08	4E-03	5E-03	6E-03	7E-03	8E-03	9E-03	1E-02
4.0E-09	5.0E-09	6.0E-09	7.0E-09	8.0E-09	9.0E-09	1.0E-08	4E-03	5E-03	6E-03	7E-03	8E-03	9E-03	1E-02
4.0E-09	5.0E-09	6.0E-09	7.0E-09	8.0E-09	9.0E-09	1.0E-08	4E-03	5E-03	6E-03	7E-03	8E-03	9E-03	1E-02
4.0E-09	5.0E-09	6.0E-09	7.0E-09	8.0E-09	9.0E-09	1.0E-08	4E-03	5E-03	6E-03	7E-03	8E-03	9E-03	1E-02
4.0E-09	5.0E-09	6.0E-09	7.0E-09	8.0E-09	9.0E-09	1.0E-08	4E-03	5E-03	6E-03	7E-03	8E-03	9E-03	1E-02
4.0E-09	5.0E-09	6.0E-09	7.0E-09	8.0E-09	9.0E-09	1.0E-08	4E-03	5E-03	6E-03	7E-03	8E-03	9E-03	1E-02
4.0E-09	5.0E-09	6.0E-09	7.0E-09	8.0E-09	9.0E-09	1.0E-08	4E-03	5E-03	6E-03	7E-03	8E-03	9E-03	1E-02

2Àc							$e^{Àc}$						
4 nm	5 nm	6 nm	7 nm	8 nm	9 nm	10 nm	4 nm	5 nm	6 nm	7 nm	8 nm	9 nm	10 nm
8E-03	1E-02	1E-02	1E-02	2E-02	2E-02	2E-02	1.00	1.01	1.01	1.01	1.01	1.01	1.01
8E-03	1E-02	1E-02	1E-02	2E-02	2E-02	2E-02	1.00	1.01	1.01	1.01	1.01	1.01	1.01
8E-03	1E-02	1E-02	1E-02	2E-02	2E-02	2E-02	1.00	1.01	1.01	1.01	1.01	1.01	1.01
8E-03	1E-02	1E-02	1E-02	2E-02	2E-02	2E-02	1.00	1.01	1.01	1.01	1.01	1.01	1.01
8E-03	1E-02	1E-02	1E-02	2E-02	2E-02	2E-02	1.00	1.01	1.01	1.01	1.01	1.01	1.01
8E-03	1E-02	1E-02	1E-02	2E-02	2E-02	2E-02	1.00	1.01	1.01	1.01	1.01	1.01	1.01
8E-03	1E-02	1E-02	1E-02	2E-02	2E-02	2E-02	1.00	1.01	1.01	1.01	1.01	1.01	1.01
8E-03	1E-02	1E-02	1E-02	2E-02	2E-02	2E-02	1.00	1.01	1.01	1.01	1.01	1.01	1.01
8E-03	1E-02	1E-02	1E-02	2E-02	2E-02	2E-02	1.00	1.01	1.01	1.01	1.01	1.01	1.01
8E-03	1E-02	1E-02	1E-02	2E-02	2E-02	2E-02	1.00	1.01	1.01	1.01	1.01	1.01	1.01
8E-03	1E-02	1E-02	1E-02	2E-02	2E-02	2E-02	1.00	1.01	1.01	1.01	1.01	1.01	1.01
8E-03	1E-02	1E-02	1E-02	2E-02	2E-02	2E-02	1.00	1.01	1.01	1.01	1.01	1.01	1.01
8E-03	1E-02	1E-02	1E-02	2E-02	2E-02	2E-02	1.00	1.01	1.01	1.01	1.01	1.01	1.01
8E-03	1E-02	1E-02	1E-02	2E-02	2E-02	2E-02	1.00	1.01	1.01	1.01	1.01	1.01	1.01
8E-03	1E-02	1E-02	1E-02	2E-02	2E-02	2E-02	1.00	1.01	1.01	1.01	1.01	1.01	1.01
8E-03	1E-02	1E-02	1E-02	2E-02	2E-02	2E-02	1.00	1.01	1.01	1.01	1.01	1.01	1.01
8E-03	1E-02	1E-02	1E-02	2E-02	2E-02	2E-02	1.00	1.01	1.01	1.01	1.01	1.01	1.01
8E-03	1E-02	1E-02	1E-02	2E-02	2E-02	2E-02	1.00	1.01	1.01	1.01	1.01	1.01	1.01
8E-03	1E-02	1E-02	1E-02	2E-02	2E-02	2E-02	1.00	1.01	1.01	1.01	1.01	1.01	1.01
8E-03	1E-02	1E-02	1E-02	2E-02	2E-02	2E-02	1.00	1.01	1.01	1.01	1.01	1.01	1.01
8E-03	1E-02	1E-02	1E-02	2E-02	2E-02	2E-02	1.00	1.01	1.01	1.01	1.01	1.01	1.01
8E-03	1E-02	1E-02	1E-02	2E-02	2E-02	2E-02	1.00	1.01	1.01	1.01	1.01	1.01	1.01
8E-03	1E-02	1E-02	1E-02	2E-02	2E-02	2E-02	1.00	1.01	1.01	1.01	1.01	1.01	1.01
8E-03	1E-02	1E-02	1E-02	2E-02	2E-02	2E-02	1.00	1.01	1.01	1.01	1.01	1.01	1.01
8E-03	1E-02	1E-02	1E-02	2E-02	2E-02	2E-02	1.00	1.01	1.01	1.01	1.01	1.01	1.01
8E-03	1E-02	1E-02	1E-02	2E-02	2E-02	2E-02	1.00	1.01	1.01	1.01	1.01	1.01	1.01
8E-03	1E-02	1E-02	1E-02	2E-02	2E-02	2E-02	1.00	1.01	1.01	1.01	1.01	1.01	1.01
8E-03	1E-02	1E-02	1E-02	2E-02	2E-02	2E-02	1.00	1.01	1.01	1.01	1.01	1.01	1.01
8E-03	1E-02	1E-02	1E-02	2E-02	2E-02	2E-02	1.00	1.01	1.01	1.01	1.01	1.01	1.01
8E-03	1E-02	1E-02	1E-02	2E-02	2E-02	2E-02	1.00	1.01	1.01	1.01	1.01	1.01	1.01
8E-03	1E-02	1E-02	1E-02	2E-02	2E-02	2E-02	1.00	1.01	1.01	1.01	1.01	1.01	1.01
8E-03	1E-02	1E-02	1E-02	2E-02	2E-02	2E-02	1.00	1.01	1.01	1.01	1.01	1.01	1.01
8E-03	1E-02	1E-02	1E-02	2E-02	2E-02	2E-02	1.00	1.01	1.01	1.01	1.01	1.01	1.01
8E-03	1E-02	1E-02	1E-02	2E-02	2E-02	2E-02	1.00	1.01	1.01	1.01	1.01	1.01	1.01
8E-03	1E-02	1E-02	1E-02	2E-02	2E-02	2E-02	1.00	1.01	1.01	1.01	1.01	1.01	1.01
8E-03	1E-02	1E-02	1E-02	2E-02	2E-02	2E-02	1.00	1.01	1.01	1.01	1.01	1.01	1.01
8E-03	1E-02	1E-02	1E-02	2E-02	2E-02	2E-02	1.00	1.01	1.01	1.01	1.01	1.01	1.01
8E-03	1E-02	1E-02	1E-02	2E-02	2E-02	2E-02	1.00	1.01	1.01	1.01	1.01	1.01	1.01
8E-03	1E-02	1E-02	1E-02	2E-02	2E-02	2E-02	1.00	1.01	1.01	1.01	1.01	1.01	1.01
8E-03	1E-02	1E-02	1E-02	2E-02	2E-02	2E-02	1.00	1.01	1.01	1.01	1.01	1.01	1.01
8E-03	1E-02	1E-02	1E-02	2E-02	2E-02	2E-02	1.00	1.01	1.01	1.01	1.01	1.01	1.01
8E-03	1E-02	1E-02	1E-02	2E-02	2E-02	2E-02	1.00	1.01	1.01	1.01	1.01	1.01	1.01

$e^{2\grave{A}c}$							F_{EDL} (Newtons) = $4pR^* / ee_O\grave{A} [s_1s_2 / e^{-\grave{A}c} + 0.5 (s_1^2+s_2^2) / e^{-2\grave{A}c})$						
4 nm	5 nm	6 nm	7 nm	8 nm	9 nm	10 nm	4 nm	5 nm	6 nm	7 nm	8 nm	9 nm	10 nm
1.01	1.01	1.01	1.01	1.02	1.02	1.02	2.4E-22	2.4E-22	2.4E-22	2.4E-22	2.4E-22	2.4E-22	2.4E-22
1.01	1.01	1.01	1.01	1.02	1.02	1.02	1.5E-22	1.5E-22	1.5E-22	1.5E-22	1.5E-22	1.5E-22	1.5E-22
1.01	1.01	1.01	1.01	1.02	1.02	1.02	1.0E-22	1.0E-22	1.0E-22	9.9E-23	9.9E-23	9.9E-23	9.9E-23
1.01	1.01	1.01	1.01	1.02	1.02	1.02	6.4E-23	6.4E-23	6.4E-23	6.4E-23	6.4E-23	6.4E-23	6.4E-23
1.01	1.01	1.01	1.01	1.02	1.02	1.02	4.1E-23	4.1E-23	4.1E-23	4.1E-23	4.1E-23	4.1E-23	4.1E-23
1.01	1.01	1.01	1.01	1.02	1.02	1.02	2.7E-23	2.7E-23	2.7E-23	2.7E-23	2.6E-23	2.6E-23	2.6E-23
1.01	1.01	1.01	1.01	1.02	1.02	1.02	1.7E-23	1.7E-23	1.7E-23	1.7E-23	1.7E-23	1.7E-23	1.7E-23
1.01	1.01	1.01	1.01	1.02	1.02	1.02	1.1E-23	1.1E-23	1.1E-23	1.1E-23	1.1E-23	1.1E-23	1.1E-23
1.01	1.01	1.01	1.01	1.02	1.02	1.02	7.1E-24	7.1E-24	7.1E-24	7.1E-24	7.1E-24	7.0E-24	7.0E-24
1.01	1.01	1.01	1.01	1.02	1.02	1.02	4.6E-24	4.6E-24	4.6E-24	4.6E-24	4.5E-24	4.5E-24	4.5E-24
1.01	1.01	1.01	1.01	1.02	1.02	1.02	3.0E-24	2.9E-24	2.9E-24	2.9E-24	2.9E-24	2.9E-24	2.9E-24
1.01	1.01	1.01	1.01	1.02	1.02	1.02	1.9E-24	1.9E-24	1.9E-24	1.9E-24	1.9E-24	1.9E-24	1.9E-24
1.01	1.01	1.01	1.01	1.02	1.02	1.02	1.2E-24	1.2E-24	1.2E-24	1.2E-24	1.2E-24	1.2E-24	1.2E-24
1.01	1.01	1.01	1.01	1.02	1.02	1.02	7.9E-25	7.9E-25	7.9E-25	7.8E-25	7.8E-25	7.8E-25	7.8E-25
1.01	1.01	1.01	1.01	1.02	1.02	1.02	5.1E-25	5.1E-25	5.1E-25	5.0E-25	5.0E-25	5.0E-25	5.0E-25
1.01	1.01	1.01	1.01	1.02	1.02	1.02	3.3E-25	3.3E-25	3.3E-25	3.2E-25	3.2E-25	3.2E-25	3.2E-25
1.01	1.01	1.01	1.01	1.02	1.02	1.02	2.1E-25	2.1E-25	2.1E-25	2.1E-25	2.1E-25	2.1E-25	2.1E-25
1.01	1.01	1.01	1.01	1.02	1.02	1.02	1.4E-25	1.4E-25	1.3E-25	1.3E-25	1.3E-25	1.3E-25	1.3E-25
1.01	1.01	1.01	1.01	1.02	1.02	1.02	8.7E-26	8.7E-26	8.7E-26	8.7E-26	8.6E-26	8.6E-26	8.6E-26
1.01	1.01	1.01	1.01	1.02	1.02	1.02	5.6E-26	5.6E-26	5.6E-26	5.6E-26	5.6E-26	5.5E-26	5.5E-26
1.01	1.01	1.01	1.01	1.02	1.02	1.02	3.6E-26	3.6E-26	3.6E-26	3.6E-26	3.6E-26	3.6E-26	3.6E-26
1.01	1.01	1.01	1.01	1.02	1.02	1.02	2.3E-26	2.3E-26	2.3E-26	2.3E-26	2.3E-26	2.3E-26	2.3E-26
1.01	1.01	1.01	1.01	1.02	1.02	1.02	1.5E-26	1.5E-26	1.5E-26	1.5E-26	1.5E-26	1.5E-26	1.5E-26
1.01	1.01	1.01	1.01	1.02	1.02	1.02	9.6E-27	9.6E-27	9.6E-27	9.6E-27	9.6E-27	9.5E-27	9.5E-27
1.01	1.01	1.01	1.01	1.02	1.02	1.02	6.2E-27	6.2E-27	6.2E-27	6.2E-27	6.2E-27	6.1E-27	6.1E-27
1.01	1.01	1.01	1.01	1.02	1.02	1.02	4.0E-27	4.0E-27	4.0E-27	4.0E-27	4.0E-27	4.0E-27	4.0E-27
1.01	1.01	1.01	1.01	1.02	1.02	1.02	2.6E-27	2.6E-27	2.6E-27	2.6E-27	2.6E-27	2.5E-27	2.5E-27
1.01	1.01	1.01	1.01	1.02	1.02	1.02	1.7E-27	1.7E-27	1.7E-27	1.6E-27	1.6E-27	1.6E-27	1.6E-27
1.01	1.01	1.01	1.01	1.02	1.02	1.02	1.1E-27	1.1E-27	1.1E-27	1.1E-27	1.1E-27	1.1E-27	1.1E-27
1.01	1.01	1.01	1.01	1.02	1.02	1.02	6.9E-28	6.9E-28	6.9E-28	6.8E-28	6.8E-28	6.8E-28	6.8E-28
1.01	1.01	1.01	1.01	1.02	1.02	1.02	4.4E-28	4.4E-28	4.4E-28	4.4E-28	4.4E-28	4.4E-28	4.4E-28
1.01	1.01	1.01	1.01	1.02	1.02	1.02	2.8E-28	2.8E-28	2.8E-28	2.8E-28	2.8E-28	2.8E-28	2.8E-28
1.01	1.01	1.01	1.01	1.02	1.02	1.02	1.8E-28	1.8E-28	1.8E-28	1.8E-28	1.8E-28	1.8E-28	1.8E-28
1.01	1.01	1.01	1.01	1.02	1.02	1.02	1.2E-28	1.2E-28	1.2E-28	1.2E-28	1.2E-28	1.2E-28	1.2E-28
1.01	1.01	1.01	1.01	1.02	1.02	1.02	7.6E-29	7.6E-29	7.6E-29	7.6E-29	7.5E-29	7.5E-29	7.5E-29
1.01	1.01	1.01	1.01	1.02	1.02	1.02	4.9E-29	4.9E-29	4.9E-29	4.9E-29	4.9E-29	4.8E-29	4.8E-29
1.01	1.01	1.01	1.01	1.02	1.02	1.02	3.2E-29	3.1E-29	3.1E-29	3.1E-29	3.1E-29	3.1E-29	3.1E-29
1.01	1.01	1.01	1.01	1.02	1.02	1.02	2.0E-29	2.0E-29	2.0E-29	2.0E-29	2.0E-29	2.0E-29	2.0E-29
1.01	1.01	1.01	1.01	1.02	1.02	1.02	1.3E-29	1.3E-29	1.3E-29	1.3E-29	1.3E-29	1.3E-29	1.3E-29
1.01	1.01	1.01	1.01	1.02	1.02	1.02	8.4E-30	8.4E-30	8.4E-30	8.4E-30	8.3E-30	8.3E-30	8.3E-30
1.01	1.01	1.01	1.01	1.02	1.02	1.02	5.4E-30	5.4E-30	5.4E-30	5.4E-30	5.4E-30	5.4E-30	5.4E-30
1.01	1.01	1.01	1.01	1.02	1.02	1.02	3.7E-30	3.7E-30	3.7E-30	3.7E-30	3.7E-30	3.7E-30	3.7E-30

Particle Density (kg m^{-3}) ρ_P	Fluid Density (kg m^{-3}) ρ_F	Gravitational Acceleration (m s^{-1}) g	**F_G (Newtons) = $1/6\pi d\emptyset_p^3(\rho_P - \rho_F)g$**
1.250E+03	9.982E+02	9.810E+00	5.0E-21
1.250E+03	9.982E+02	9.810E+00	7.8E-21
1.250E+03	9.982E+02	9.810E+00	1.2E-20
1.250E+03	9.982E+02	9.810E+00	1.9E-20
1.250E+03	9.982E+02	9.810E+00	2.9E-20
1.250E+03	9.982E+02	9.810E+00	4.5E-20
1.250E+03	9.982E+02	9.810E+00	7.0E-20
1.250E+03	9.982E+02	9.810E+00	1.1E-19
1.250E+03	9.982E+02	9.810E+00	1.7E-19
1.250E+03	9.982E+02	9.810E+00	2.6E-19
1.250E+03	9.982E+02	9.810E+00	4.1E-19
1.250E+03	9.982E+02	9.810E+00	6.3E-19
1.250E+03	9.982E+02	9.810E+00	9.8E-19
1.250E+03	9.982E+02	9.810E+00	1.5E-18
1.250E+03	9.982E+02	9.810E+00	2.4E-18
1.250E+03	9.982E+02	9.810E+00	3.7E-18
1.250E+03	9.982E+02	9.810E+00	5.7E-18
1.250E+03	9.982E+02	9.810E+00	8.9E-18
1.250E+03	9.982E+02	9.810E+00	1.4E-17
1.250E+03	9.982E+02	9.810E+00	2.1E-17
1.250E+03	9.982E+02	9.810E+00	3.3E-17
1.250E+03	9.982E+02	9.810E+00	5.2E-17
1.250E+03	9.982E+02	9.810E+00	8.0E-17
1.250E+03	9.982E+02	9.810E+00	1.2E-16
1.250E+03	9.982E+02	9.810E+00	1.9E-16
1.250E+03	9.982E+02	9.810E+00	3.0E-16
1.250E+03	9.982E+02	9.810E+00	4.7E-16
1.250E+03	9.982E+02	9.810E+00	7.3E-16
1.250E+03	9.982E+02	9.810E+00	1.1E-15
1.250E+03	9.982E+02	9.810E+00	1.7E-15
1.250E+03	9.982E+02	9.810E+00	2.7E-15
1.250E+03	9.982E+02	9.810E+00	4.2E-15
1.250E+03	9.982E+02	9.810E+00	6.6E-15
1.250E+03	9.982E+02	9.810E+00	1.0E-14
1.250E+03	9.982E+02	9.810E+00	1.6E-14
1.250E+03	9.982E+02	9.810E+00	2.5E-14
1.250E+03	9.982E+02	9.810E+00	3.8E-14
1.250E+03	9.982E+02	9.810E+00	5.9E-14
1.250E+03	9.982E+02	9.810E+00	9.2E-14
1.250E+03	9.982E+02	9.810E+00	1.4E-13
1.250E+03	9.982E+02	9.810E+00	2.2E-13
1.250E+03	9.982E+02	9.810E+00	3.2E-13

Deposition Inhibiting $F_{DI} = (F_{VD}^2 + F_L^2)^{0.5}$			Depostion Promoting $F_{DP} = F_{VDW} + F_G + F_{FD} - F_{EDL}$		
2.5 m s^{-1}	3.1 m s^{-1}	3.6 m s^{-1}	100	200	300
8.5E-13	1.2E-12	1.7E-12	9.8E-12	9.8E-12	9.8E-12
1.1E-12	1.6E-12	2.3E-12	1.1E-11	1.1E-11	1.1E-11
1.5E-12	2.2E-12	3.0E-12	1.3E-11	1.3E-11	1.3E-11
2.1E-12	2.9E-12	4.1E-12	1.5E-11	1.5E-11	1.5E-11
2.8E-12	3.9E-12	5.5E-12	1.8E-11	1.8E-11	1.8E-11
3.7E-12	5.3E-12	7.3E-12	2.0E-11	2.0E-11	2.0E-11
5.0E-12	7.1E-12	9.8E-12	2.4E-11	2.4E-11	2.4E-11
6.6E-12	9.5E-12	1.3E-11	2.7E-11	2.7E-11	2.7E-11
8.9E-12	1.3E-11	1.8E-11	3.2E-11	3.2E-11	3.2E-11
1.2E-11	1.7E-11	2.4E-11	3.7E-11	3.7E-11	3.7E-11
1.6E-11	2.3E-11	3.2E-11	4.2E-11	4.2E-11	4.2E-11
2.2E-11	3.1E-11	4.3E-11	4.9E-11	4.9E-11	4.9E-11
2.9E-11	4.1E-11	5.7E-11	5.7E-11	5.7E-11	5.7E-11
3.9E-11	5.5E-11	7.7E-11	6.6E-11	6.6E-11	6.6E-11
5.2E-11	7.4E-11	1.0E-10	7.6E-11	7.6E-11	7.6E-11
7.0E-11	9.9E-11	1.4E-10	8.8E-11	8.8E-11	8.8E-11
9.3E-11	1.3E-10	1.9E-10	1.0E-10	1.0E-10	1.0E-10
1.3E-10	1.8E-10	2.5E-10	1.2E-10	1.2E-10	1.2E-10
1.7E-10	2.4E-10	3.3E-10	1.4E-10	1.4E-10	1.4E-10
2.3E-10	3.2E-10	4.5E-10	1.6E-10	1.6E-10	1.6E-10
3.0E-10	4.3E-10	6.0E-10	1.8E-10	1.8E-10	1.8E-10
4.0E-10	5.8E-10	8.0E-10	2.1E-10	2.1E-10	2.1E-10
5.4E-10	7.7E-10	1.1E-09	2.5E-10	2.5E-10	2.5E-10
7.3E-10	1.0E-09	1.4E-09	2.9E-10	2.9E-10	2.9E-10
9.8E-10	1.4E-09	1.9E-09	3.3E-10	3.3E-10	3.3E-10
1.3E-09	1.9E-09	2.6E-09	3.8E-10	3.8E-10	3.8E-10
1.8E-09	2.5E-09	3.5E-09	4.4E-10	4.4E-10	4.4E-10
2.4E-09	3.4E-09	4.7E-09	5.1E-10	5.1E-10	5.1E-10
3.2E-09	4.5E-09	6.3E-09	5.9E-10	5.9E-10	5.9E-10
4.2E-09	6.0E-09	8.4E-09	6.9E-10	6.9E-10	6.9E-10
5.7E-09	8.1E-09	1.1E-08	8.0E-10	8.0E-10	8.0E-10
7.7E-09	1.1E-08	1.5E-08	9.2E-10	9.2E-10	9.2E-10
1.0E-08	1.5E-08	2.1E-08	1.1E-09	1.1E-09	1.1E-09
1.4E-08	2.0E-08	2.8E-08	1.2E-09	1.2E-09	1.2E-09
1.9E-08	2.7E-08	3.7E-08	1.4E-09	1.4E-09	1.4E-09
2.5E-08	3.6E-08	5.0E-08	1.7E-09	1.7E-09	1.7E-09
3.4E-08	4.8E-08	6.8E-08	1.9E-09	1.9E-09	1.9E-09
4.5E-08	6.5E-08	9.2E-08	2.2E-09	2.2E-09	2.2E-09
6.1E-08	8.9E-08	1.3E-07	2.6E-09	2.6E-09	2.6E-09
8.3E-08	1.2E-07	1.7E-07	3.0E-09	3.0E-09	3.0E-09
1.1E-07	1.6E-07	2.4E-07	3.5E-09	3.5E-09	3.5E-09
1.5E-07	2.2E-07	3.1E-07	3.9E-09	3.9E-09	3.9E-09

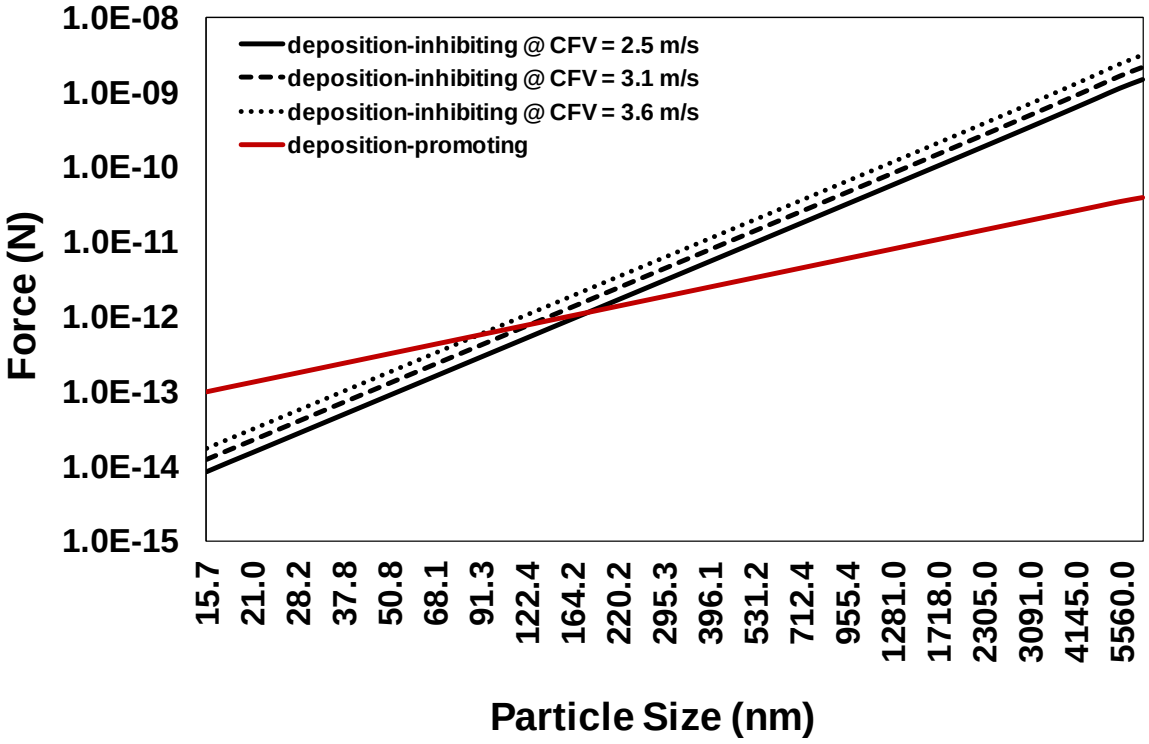
1.0E-08
1.0E-09
1.0E-10
1.0E-11
1.0E-12
1.0E-13
1.0E-14
1.0E-15
Force (N)
deposition-inhibiting @ CFV = 2.5 m/s
deposition-inhibiting @ CFV = 3.1 m/s
deposition-inhibiting @ CFV = 3.6 m/s
deposition-promoting
15.7
21.0
28.2
37.8
50.8
68.1
91.3
122.4
164.2
220.2
295.3
396.1
531.2
712.4
955.4
1281.0
1718.0
2305.0
3091.0
4145.0
5560.0
Particle Size (nm)

Appendix 6.7: Calculations for the model fitting using Hermia's fouling equations

Cake filtration

100 kPa

Time (sec)	$J_{S,20°C}$ ($m^3 m^{-2} s^{-1}$) @ 2.5 m s^{-1}	Filtrate Volume, V (m^3)	t/V (s/m^3)	$J_{S,20°C}$ ($m^3 m^{-2} s^{-1}$) @ 3.1 m s^{-1}	Filtrate Volume, V (m^3)	t/V (s/m^3)	$J_{S,20°C}$ ($m^3 m^{-2} s^{-1}$) @ 3.6 m s^{-1}	Filtrate Volume, V (m^3)	t/V (s/m^3)
300	0.000005	7.6E-06	3.9E+07	0.000006	8.5E-06	3.5E+07	0.000006	8.9E-06	3.4E+07
600	0.000005	1.5E-05	4.0E+07	0.000006	1.7E-05	3.6E+07	0.000006	1.8E-05	3.4E+07
900	0.000005	2.2E-05	4.1E+07	0.000005	2.5E-05	3.6E+07	0.000006	2.6E-05	3.5E+07
1200	0.000005	2.9E-05	4.1E+07	0.000005	3.3E-05	3.6E+07	0.000006	3.4E-05	3.5E+07
1500	0.000005	3.6E-05	4.2E+07	0.000005	4.1E-05	3.7E+07	0.000006	4.3E-05	3.5E+07
1800	0.000005	4.3E-05	4.2E+07	0.000005	4.9E-05	3.7E+07	0.000006	5.1E-05	3.5E+07
2100	0.000005	5.0E-05	4.2E+07	0.000005	5.6E-05	3.7E+07	0.000005	5.9E-05	3.5E+07
2400	0.000004	5.6E-05	4.3E+07	0.000005	6.4E-05	3.8E+07	0.000005	6.7E-05	3.6E+07
2700	0.000004	6.3E-05	4.3E+07	0.000005	7.1E-05	3.8E+07	0.000005	7.5E-05	3.6E+07
3000	0.000004	6.9E-05	4.3E+07	0.000005	7.9E-05	3.8E+07	0.000005	8.3E-05	3.6E+07
3300	0.000004	7.6E-05	4.3E+07	0.000005	8.6E-05	3.8E+07	0.000005	9.1E-05	3.6E+07
3600	0.000004	8.2E-05	4.4E+07	0.000005	9.3E-05	3.9E+07	0.000005	9.8E-05	3.7E+07
3900	0.000004	8.9E-05	4.4E+07	0.000005	1.0E-04	3.9E+07	0.000005	1.1E-04	3.7E+07
4200	0.000004	9.5E-05	4.4E+07	0.000005	1.1E-04	3.9E+07	0.000005	1.1E-04	3.7E+07
4500	0.000004	1.0E-04	4.4E+07	0.000005	1.1E-04	3.9E+07	0.000005	1.2E-04	3.7E+07
4800	0.000004	1.1E-04	4.4E+07	0.000005	1.2E-04	4.0E+07	0.000005	1.3E-04	3.8E+07
5100	0.000004	1.1E-04	4.5E+07	0.000005	1.3E-04	4.0E+07	0.000005	1.3E-04	3.8E+07
5400	0.000004	1.2E-04	4.5E+07	0.000005	1.4E-04	4.0E+07	0.000005	1.4E-04	3.8E+07
5700	0.000004	1.3E-04	4.5E+07	0.000005	1.4E-04	4.0E+07	0.000005	1.5E-04	3.8E+07
6000	0.000004	1.3E-04	4.5E+07	0.000005	1.5E-04	4.0E+07	0.000005	1.6E-04	3.8E+07
6300	0.000004	1.4E-04	4.5E+07	0.000005	1.6E-04	4.0E+07	0.000005	1.6E-04	3.8E+07
6600	0.000004	1.5E-04	4.5E+07	0.000005	1.6E-04	4.1E+07	0.000005	1.7E-04	3.9E+07
6900	0.000004	1.5E-04	4.5E+07	0.000005	1.7E-04	4.1E+07	0.000005	1.8E-04	3.9E+07
7200	0.000004	1.6E-04	4.6E+07	0.000004	1.8E-04	4.1E+07	0.000005	1.9E-04	3.9E+07
7500	0.000004	1.6E-04	4.6E+07	0.000004	1.8E-04	4.1E+07	0.000005	1.9E-04	3.9E+07
7800	0.000004	1.7E-04	4.6E+07	0.000004	1.9E-04	4.1E+07	0.000005	2.0E-04	3.9E+07
8100	0.000004	1.8E-04	4.6E+07	0.000004	2.0E-04	4.1E+07	0.000005	2.1E-04	3.9E+07
8400	0.000004	1.8E-04	4.6E+07	0.000004	2.0E-04	4.1E+07	0.000005	2.1E-04	3.9E+07
8700	0.000004	1.9E-04	4.6E+07	0.000004	2.1E-04	4.2E+07	0.000005	2.2E-04	4.0E+07
9000	0.000004	2.0E-04	4.6E+07	0.000004	2.2E-04	4.2E+07	0.000005	2.3E-04	4.0E+07
9300	0.000004	2.0E-04	4.6E+07	0.000004	2.2E-04	4.2E+07	0.000005	2.3E-04	4.0E+07
9600	0.000004	2.1E-04	4.6E+07	0.000004	2.3E-04	4.2E+07	0.000005	2.4E-04	4.0E+07
9900	0.000004	2.1E-04	4.6E+07	0.000004	2.4E-04	4.2E+07	0.000005	2.5E-04	4.0E+07
10200	0.000004	2.2E-04	4.7E+07	0.000004	2.4E-04	4.2E+07	0.000005	2.5E-04	4.0E+07

10500	0.000004	2.3E-04	4.7E+07	0.000004	2.5E-04	4.2E+07	0.000005	2.6E-04	4.0E+07
10800	0.000004	2.3E-04	4.7E+07	0.000004	2.5E-04	4.2E+07	0.000005	2.7E-04	4.0E+07
11100	0.000004	2.4E-04	4.7E+07	0.000004	2.6E-04	4.2E+07	0.000005	2.7E-04	4.0E+07

200 kPa

Time (sec)	$J_{S,\ 20°C}$ ($m^3\ m^{-2}\ s^{-1}$) @ 2.5 m s^{-1}	Filtrate Volume (m^3)	t/V (s/m^3)	$J_{S,\ 20°C}$ ($m^3\ m^{-2}\ s^{-1}$) @ 3.1 m s^{-1}	Filtrate Volume (m^3)	t/V (s/m^3)	$J_{S,\ 20°C}$ ($m^3\ m^{-2}\ s^{-1}$) @ 3.6 m s^{-1}	Filtrate Volume (m^3)	t/V (s/m^3)
300	0.000006	9.1E-06	3.3E+07	0.000007	1.0E-05	3.0E+07	0.000008	1.3E-05	2.4E+07
600	0.000006	1.7E-05	3.4E+07	0.000006	1.9E-05	3.1E+07	0.000008	2.4E-05	2.5E+07
900	0.000005	2.5E-05	3.6E+07	0.000006	2.8E-05	3.2E+07	0.000008	3.6E-05	2.5E+07
1200	0.000005	3.3E-05	3.7E+07	0.000006	3.7E-05	3.3E+07	0.000008	4.7E-05	2.5E+07
1500	0.000005	4.0E-05	3.8E+07	0.000005	4.5E-05	3.3E+07	0.000008	5.9E-05	2.6E+07
1800	0.000005	4.7E-05	3.8E+07	0.000005	5.3E-05	3.4E+07	0.000007	7.0E-05	2.6E+07
2100	0.000005	5.4E-05	3.9E+07	0.000005	6.1E-05	3.5E+07	0.000007	8.1E-05	2.6E+07
2400	0.000005	6.0E-05	4.0E+07	0.000005	6.9E-05	3.5E+07	0.000007	9.2E-05	2.6E+07
2700	0.000004	6.7E-05	4.0E+07	0.000005	7.7E-05	3.5E+07	0.000007	1.0E-04	2.6E+07
3000	0.000004	7.4E-05	4.1E+07	0.000005	8.5E-05	3.5E+07	0.000007	1.1E-04	2.6E+07
3300	0.000004	8.0E-05	4.1E+07	0.000006	9.3E-05	3.5E+07	0.000007	1.2E-04	2.6E+07
3600	0.000004	8.7E-05	4.1E+07	0.000006	1.0E-04	3.5E+07	0.000007	1.4E-04	2.7E+07
3900	0.000004	9.4E-05	4.2E+07	0.000005	1.1E-04	3.5E+07	0.000007	1.5E-04	2.7E+07
4200	0.000004	1.0E-04	4.2E+07	0.000005	1.2E-04	3.6E+07	0.000007	1.6E-04	2.7E+07
4500	0.000004	1.1E-04	4.2E+07	0.000005	1.3E-04	3.6E+07	0.000007	1.7E-04	2.7E+07
4800	0.000004	1.1E-04	4.2E+07	0.000006	1.3E-04	3.6E+07	0.000007	1.8E-04	2.7E+07
5100	0.000004	1.2E-04	4.3E+07	0.000005	1.4E-04	3.6E+07	0.000007	1.9E-04	2.7E+07
5400	0.000004	1.3E-04	4.3E+07	0.000005	1.5E-04	3.6E+07	0.000007	2.0E-04	2.7E+07
5700	0.000004	1.3E-04	4.3E+07	0.000005	1.6E-04	3.6E+07	0.000007	2.1E-04	2.7E+07
6000	0.000004	1.4E-04	4.3E+07	0.000005	1.7E-04	3.6E+07	0.000007	2.2E-04	2.7E+07
6300	0.000004	1.5E-04	4.3E+07	0.000005	1.7E-04	3.6E+07	0.000007	2.3E-04	2.7E+07
6600	0.000004	1.5E-04	4.3E+07	0.000005	1.8E-04	3.6E+07	0.000007	2.4E-04	2.7E+07
6900	0.000004	1.6E-04	4.3E+07	0.000005	1.9E-04	3.6E+07	0.000007	2.5E-04	2.7E+07
7200	0.000004	1.7E-04	4.3E+07	0.000005	2.0E-04	3.6E+07	0.000007	2.6E-04	2.7E+07
7500	0.000004	1.7E-04	4.3E+07	0.000005	2.1E-04	3.6E+07	0.000007	2.7E-04	2.7E+07
7800	0.000004	1.8E-04	4.4E+07	0.000005	2.1E-04	3.6E+07	0.000007	2.8E-04	2.7E+07
8100	0.000004	1.9E-04	4.4E+07	0.000005	2.2E-04	3.6E+07	0.000007	2.9E-04	2.7E+07
8400	0.000005	1.9E-04	4.4E+07	0.000005	2.3E-04	3.6E+07	0.000007	3.1E-04	2.8E+07
8700	0.000005	2.0E-04	4.4E+07	0.000005	2.4E-04	3.6E+07	0.000007	3.2E-04	2.8E+07
9000	0.000005	2.1E-04	4.4E+07	0.000005	2.5E-04	3.7E+07	0.000007	3.3E-04	2.8E+07
9300	0.000005	2.1E-04	4.4E+07	0.000005	2.5E-04	3.7E+07	0.000007	3.4E-04	2.8E+07
9600	0.000005	2.2E-04	4.4E+07	0.000005	2.6E-04	3.7E+07	0.000007	3.5E-04	2.8E+07

9900	0.000005	2.3E-04	4.4E+07	0.000005	2.7E-04	3.7E+07	0.000007	3.6E-04	2.8E+07
10200	0.000005	2.3E-04	4.4E+07	0.000005	2.8E-04	3.7E+07	0.000007	3.7E-04	2.8E+07
10500	0.000005	2.4E-04	4.4E+07	0.000005	2.9E-04	3.7E+07	0.000007	3.8E-04	2.8E+07
10800	0.000004	2.5E-04	4.4E+07	0.000005	2.9E-04	3.7E+07	0.000007	3.9E-04	2.8E+07
11100	0.000004	2.5E-04	4.4E+07	0.000005	3.0E-04	3.7E+07	0.000007	4.0E-04	2.8E+07

300 kPa

Time (sec)	$J_{S,20°C}$ (m^3 m^{-2} s^{-1}) @ 2.5 m s^{-1}	Filtrate Volume (m^3)	t/V (s/m^3)	$J_{S,20°C}$ (m^3 m^{-2} s^{-1}) @ 3.1 m s^{-1}	Filtrate Volume (m^3)	t/V (s/m^3)	$J_{S,20°C}$ (m^3 m^{-2} s^{-1}) @ 3.6 m s^{-1}	Filtrate Volume (m^3)	t/V (s/m^3)
300	0.000006	9.3E-06	3.2E+07	0.000007	1.1E-05	2.8E+07	0.000009	1.3E-05	2.2E+07
600	0.000006	1.8E-05	3.4E+07	0.000007	2.1E-05	2.8E+07	0.000009	2.6E-05	2.3E+07
900	0.000005	2.5E-05	3.6E+07	0.000007	3.1E-05	2.9E+07	0.000008	3.9E-05	2.3E+07
1200	0.000005	3.2E-05	3.7E+07	0.000007	4.1E-05	2.9E+07	0.000008	5.1E-05	2.3E+07
1500	0.000005	3.9E-05	3.8E+07	0.000006	5.1E-05	3.0E+07	0.000008	6.4E-05	2.4E+07
1800	0.000004	4.6E-05	3.9E+07	0.000006	6.0E-05	3.0E+07	0.000008	7.6E-05	2.4E+07
2100	0.000004	5.2E-05	4.0E+07	0.000006	7.0E-05	3.0E+07	0.000008	8.7E-05	2.4E+07
2400	0.000004	5.8E-05	4.1E+07	0.000006	7.9E-05	3.0E+07	0.000008	9.9E-05	2.4E+07
2700	0.000004	6.5E-05	4.2E+07	0.000006	8.9E-05	3.0E+07	0.000008	1.1E-04	2.4E+07
3000	0.000004	7.1E-05	4.2E+07	0.000006	9.9E-05	3.0E+07	0.000008	1.2E-04	2.5E+07
3300	0.000004	7.7E-05	4.3E+07	0.000006	1.1E-04	3.1E+07	0.000008	1.3E-04	2.5E+07
3600	0.000004	8.4E-05	4.3E+07	0.000006	1.2E-04	3.1E+07	0.000008	1.4E-04	2.5E+07
3900	0.000004	9.0E-05	4.3E+07	0.000006	1.3E-04	3.1E+07	0.000007	1.6E-04	2.5E+07
4200	0.000004	9.7E-05	4.3E+07	0.000006	1.4E-04	3.1E+07	0.000008	1.7E-04	2.5E+07
4500	0.000004	1.0E-04	4.4E+07	0.000006	1.5E-04	3.1E+07	0.000008	1.8E-04	2.5E+07
4800	0.000004	1.1E-04	4.4E+07	0.000006	1.6E-04	3.1E+07	0.000008	1.9E-04	2.5E+07
5100	0.000004	1.2E-04	4.4E+07	0.000006	1.6E-04	3.1E+07	0.000008	2.0E-04	2.5E+07
5400	0.000004	1.2E-04	4.4E+07	0.000006	1.7E-04	3.1E+07	0.000008	2.1E-04	2.5E+07
5700	0.000004	1.3E-04	4.4E+07	0.000006	1.8E-04	3.1E+07	0.000008	2.2E-04	2.5E+07
6000	0.000004	1.4E-04	4.4E+07	0.000006	1.9E-04	3.1E+07	0.000008	2.4E-04	2.5E+07
6300	0.000004	1.4E-04	4.4E+07	0.000006	2.0E-04	3.1E+07	0.000008	2.5E-04	2.6E+07
6600	0.000004	1.5E-04	4.4E+07	0.000006	2.1E-04	3.1E+07	0.000007	2.6E-04	2.6E+07
6900	0.000004	1.6E-04	4.4E+07	0.000006	2.2E-04	3.1E+07	0.000007	2.7E-04	2.6E+07
7200	0.000005	1.6E-04	4.4E+07	0.000006	2.3E-04	3.1E+07	0.000007	2.8E-04	2.6E+07
7500	0.000005	1.7E-04	4.4E+07	0.000006	2.4E-04	3.1E+07	0.000007	2.9E-04	2.6E+07
7800	0.000005	1.8E-04	4.4E+07	0.000006	2.5E-04	3.1E+07	0.000007	3.0E-04	2.6E+07
8100	0.000005	1.8E-04	4.4E+07	0.000006	2.6E-04	3.1E+07	0.000007	3.1E-04	2.6E+07
8400	0.000005	1.9E-04	4.4E+07	0.000006	2.7E-04	3.1E+07	0.000007	3.2E-04	2.6E+07
8700	0.000004	2.0E-04	4.4E+07	0.000006	2.8E-04	3.1E+07	0.000007	3.4E-04	2.6E+07

9000	0.000004	2.0E-04	4.4E+07	0.000006	2.9E-04	3.2E+07	0.000007	3.5E-04	2.6E+07
9300	0.000005	2.1E-04	4.4E+07	0.000006	2.9E-04	3.2E+07	0.000007	3.6E-04	2.6E+07
9600	0.000005	2.2E-04	4.4E+07	0.000006	3.0E-04	3.2E+07	0.000007	3.7E-04	2.6E+07
9900	0.000004	2.2E-04	4.4E+07	0.000006	3.1E-04	3.2E+07	0.000007	3.8E-04	2.6E+07
10200	0.000004	2.3E-04	4.4E+07	0.000006	3.2E-04	3.2E+07	0.000007	3.9E-04	2.6E+07
10500	0.000004	2.4E-04	4.4E+07	0.000006	3.3E-04	3.2E+07	0.000007	4.0E-04	2.6E+07
10800	0.000004	2.4E-04	4.4E+07	0.000006	3.4E-04	3.2E+07	0.000007	4.1E-04	2.6E+07
11100	0.000004	2.5E-04	4.4E+07	0.000006	3.5E-04	3.2E+07	0.000007	4.2E-04	2.7E+07

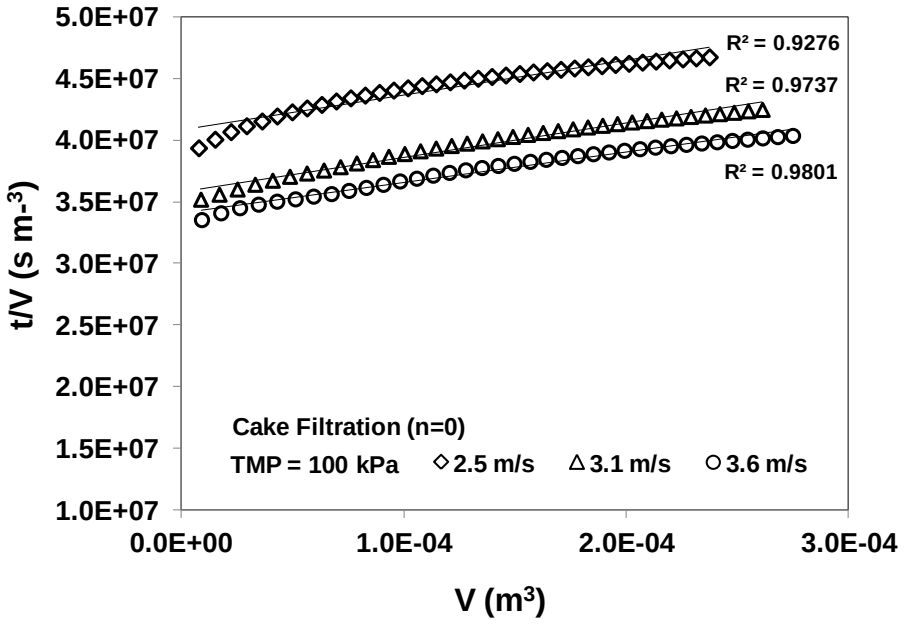

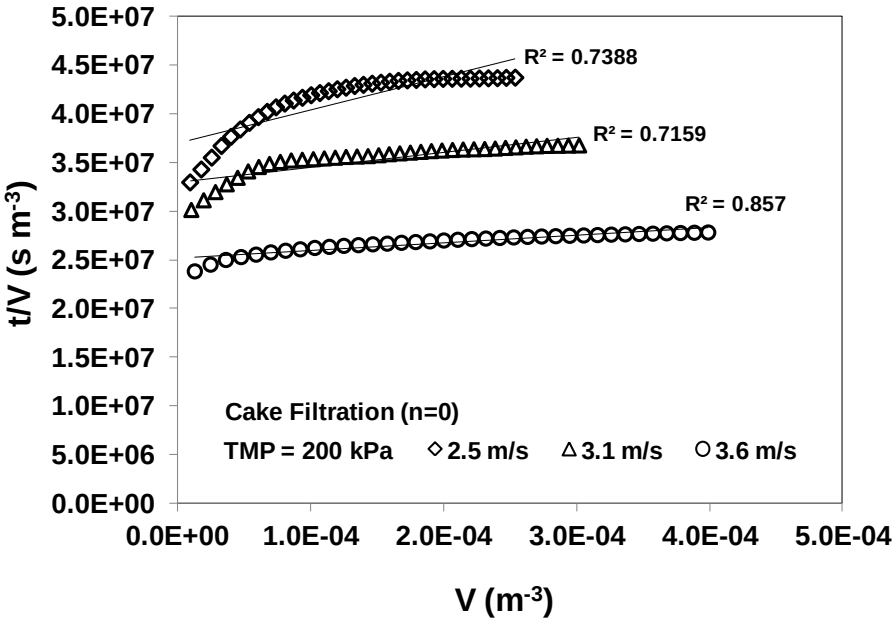

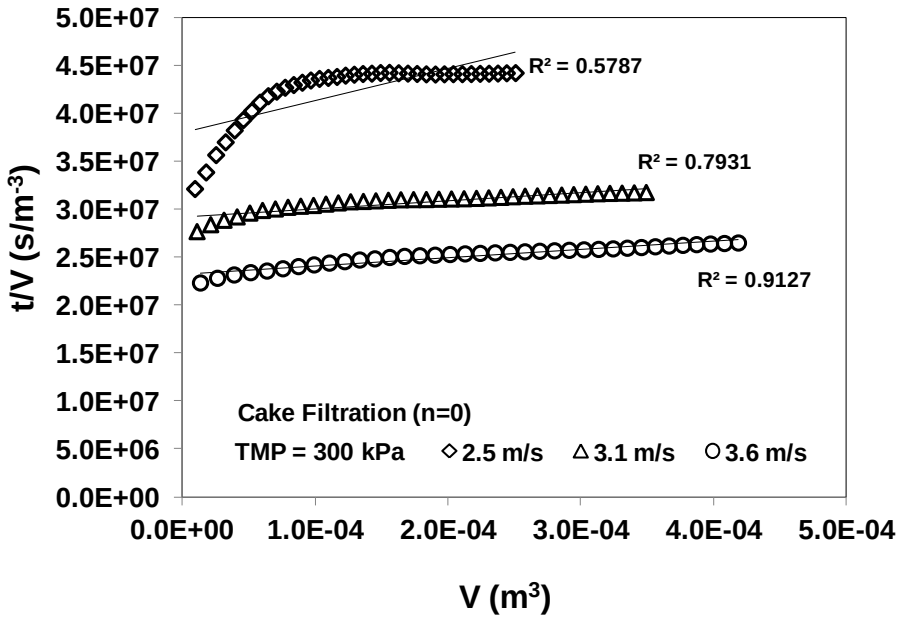

Complete blocking

100 kPa

Time (sec)	$J_{S,20°C}$ ($m^3 m^{-2} s^{-1}$) @ 2.5 m s^{-1}	Q ($m^3 s^{-1}$)	Filtrate Volume (m^3)	$J_{S,20°C}$ ($m^3 m^{-2} s^{-1}$) @ 3.1 m s^{-1}	Q ($m^3 s^{-1}$)	Filtrate Volume (m^3)	$J_{S,20°C}$ ($m^3 m^{-2} s^{-1}$) @ 3.6 m s^{-1}	Q ($m^3 s^{-1}$)	Filtrate Volume (m^3)
300	0.000005	2.5E-08	7.6E-06	0.000006	2.8E-08	8.5E-06	0.000006	3.0E-08	8.9E-06
600	0.000005	2.5E-08	1.5E-05	0.000006	2.8E-08	1.7E-05	0.000006	2.9E-08	1.8E-05
900	0.000005	2.4E-08	2.2E-05	0.000005	2.7E-08	2.5E-05	0.000006	2.8E-08	2.6E-05
1200	0.000005	2.3E-08	2.9E-05	0.000005	2.7E-08	3.3E-05	0.000006	2.8E-08	3.4E-05
1500	0.000005	2.3E-08	3.6E-05	0.000005	2.6E-08	4.1E-05	0.000006	2.8E-08	4.3E-05
1800	0.000005	2.3E-08	4.3E-05	0.000005	2.6E-08	4.9E-05	0.000006	2.8E-08	5.1E-05
2100	0.000005	2.3E-08	5.0E-05	0.000005	2.6E-08	5.6E-05	0.000005	2.7E-08	5.9E-05
2400	0.000004	2.2E-08	5.6E-05	0.000005	2.5E-08	6.4E-05	0.000005	2.7E-08	6.7E-05
2700	0.000004	2.2E-08	6.3E-05	0.000005	2.5E-08	7.1E-05	0.000005	2.6E-08	7.5E-05
3000	0.000004	2.2E-08	6.9E-05	0.000005	2.4E-08	7.9E-05	0.000005	2.6E-08	8.3E-05
3300	0.000004	2.2E-08	7.6E-05	0.000005	2.4E-08	8.6E-05	0.000005	2.6E-08	9.1E-05
3600	0.000004	2.2E-08	8.2E-05	0.000005	2.4E-08	9.3E-05	0.000005	2.5E-08	9.8E-05
3900	0.000004	2.1E-08	8.9E-05	0.000005	2.4E-08	1.0E-04	0.000005	2.5E-08	1.1E-04
4200	0.000004	2.1E-08	9.5E-05	0.000005	2.4E-08	1.1E-04	0.000005	2.5E-08	1.1E-04
4500	0.000004	2.1E-08	1.0E-04	0.000005	2.3E-08	1.1E-04	0.000005	2.4E-08	1.2E-04
4800	0.000004	2.1E-08	1.1E-04	0.000005	2.3E-08	1.2E-04	0.000005	2.4E-08	1.3E-04
5100	0.000004	2.1E-08	1.1E-04	0.000005	2.3E-08	1.3E-04	0.000005	2.4E-08	1.3E-04
5400	0.000004	2.1E-08	1.2E-04	0.000005	2.3E-08	1.4E-04	0.000005	2.4E-08	1.4E-04

5700	0.000004	2.1E-08	1.3E-04	0.000005	2.3E-08	1.4E-04	0.000005	2.4E-08	1.5E-04
6000	0.000004	2.1E-08	1.3E-04	0.000005	2.3E-08	1.5E-04	0.000005	2.4E-08	1.6E-04
6300	0.000004	2.1E-08	1.4E-04	0.000005	2.3E-08	1.6E-04	0.000005	2.4E-08	1.6E-04
6600	0.000004	2.1E-08	1.5E-04	0.000005	2.3E-08	1.6E-04	0.000005	2.4E-08	1.7E-04
6900	0.000004	2.1E-08	1.5E-04	0.000005	2.3E-08	1.7E-04	0.000005	2.4E-08	1.8E-04
7200	0.000004	2.1E-08	1.6E-04	0.000004	2.2E-08	1.8E-04	0.000005	2.3E-08	1.9E-04
7500	0.000004	2.1E-08	1.6E-04	0.000004	2.2E-08	1.8E-04	0.000005	2.3E-08	1.9E-04
7800	0.000004	2.1E-08	1.7E-04	0.000004	2.2E-08	1.9E-04	0.000005	2.3E-08	2.0E-04
8100	0.000004	2.1E-08	1.8E-04	0.000004	2.2E-08	2.0E-04	0.000005	2.3E-08	2.1E-04
8400	0.000004	2.0E-08	1.8E-04	0.000004	2.2E-08	2.0E-04	0.000005	2.3E-08	2.1E-04
8700	0.000004	2.1E-08	1.9E-04	0.000004	2.2E-08	2.1E-04	0.000005	2.3E-08	2.2E-04
9000	0.000004	2.0E-08	2.0E-04	0.000004	2.2E-08	2.2E-04	0.000005	2.3E-08	2.3E-04
9300	0.000004	2.0E-08	2.0E-04	0.000004	2.2E-08	2.2E-04	0.000005	2.3E-08	2.3E-04
9600	0.000004	2.0E-08	2.1E-04	0.000004	2.2E-08	2.3E-04	0.000005	2.3E-08	2.4E-04
9900	0.000004	2.0E-08	2.1E-04	0.000004	2.2E-08	2.4E-04	0.000005	2.3E-08	2.5E-04
10200	0.000004	2.0E-08	2.2E-04	0.000004	2.2E-08	2.4E-04	0.000005	2.3E-08	2.5E-04
10500	0.000004	2.0E-08	2.3E-04	0.000004	2.2E-08	2.5E-04	0.000005	2.3E-08	2.6E-04
10800	0.000004	2.0E-08	2.3E-04	0.000004	2.1E-08	2.5E-04	0.000005	2.3E-08	2.7E-04
11100	0.000004	2.0E-08	2.4E-04	0.000004	2.1E-08	2.6E-04	0.000005	2.3E-08	2.7E-04

200 kPa

Time (sec)	$J_{S,\ 20°C}$ ($m^3\ m^{-2}\ s^{-1}$) @ 2.5 m s^{-1}	Q ($m^3 s^{-1}$)	Filtrate Volume (m^3)	$J_{S,\ 20°C}$ ($m^3\ m^{-2}\ s^{-1}$) @ 3.1 m s^{-1}	Q ($m^3 s^{-1}$)	Filtrate Volume (m^3)	$J_{S,\ 20°C}$ ($m^3\ m^{-2}\ s^{-1}$) @ 3.6 m s^{-1}	Q ($m^3 s^{-1}$)	Filtrate Volume (m^3)
300	0.000006	3.0E-08	9.1E-06	0.000007	3.3E-08	1.0E-05	0.000008	4.2E-08	1.3E-05
600	0.000006	2.8E-08	1.7E-05	0.000006	3.1E-08	1.9E-05	0.000008	4.0E-08	2.4E-05
900	0.000005	2.6E-08	2.5E-05	0.000006	3.0E-08	2.8E-05	0.000008	3.8E-08	3.6E-05
1200	0.000005	2.4E-08	3.3E-05	0.000006	2.8E-08	3.7E-05	0.000008	3.8E-08	4.7E-05
1500	0.000005	2.4E-08	4.0E-05	0.000005	2.7E-08	4.5E-05	0.000008	3.8E-08	5.9E-05
1800	0.000005	2.3E-08	4.7E-05	0.000005	2.6E-08	5.3E-05	0.000007	3.7E-08	7.0E-05
2100	0.000005	2.3E-08	5.4E-05	0.000005	2.7E-08	6.1E-05	0.000007	3.7E-08	8.1E-05
2400	0.000005	2.3E-08	6.0E-05	0.000005	2.7E-08	6.9E-05	0.000007	3.7E-08	9.2E-05
2700	0.000004	2.2E-08	6.7E-05	0.000005	2.7E-08	7.7E-05	0.000007	3.6E-08	1.0E-04
3000	0.000004	2.2E-08	7.4E-05	0.000005	2.7E-08	8.5E-05	0.000007	3.7E-08	1.1E-04
3300	0.000004	2.2E-08	8.0E-05	0.000006	2.8E-08	9.3E-05	0.000007	3.6E-08	1.2E-04
3600	0.000004	2.2E-08	8.7E-05	0.000006	2.8E-08	1.0E-04	0.000007	3.7E-08	1.4E-04
3900	0.000004	2.2E-08	9.4E-05	0.000005	2.7E-08	1.1E-04	0.000007	3.6E-08	1.5E-04
4200	0.000004	2.2E-08	1.0E-04	0.000005	2.7E-08	1.2E-04	0.000007	3.6E-08	1.6E-04
4500	0.000004	2.2E-08	1.1E-04	0.000005	2.7E-08	1.3E-04	0.000007	3.6E-08	1.7E-04
4800	0.000004	2.2E-08	1.1E-04	0.000006	2.8E-08	1.3E-04	0.000007	3.6E-08	1.8E-04

5100	0.000004	2.2E-08	1.2E-04	0.000005	2.7E-08	1.4E-04	0.000007	3.6E-08	1.9E-04
5400	0.000004	2.2E-08	1.3E-04	0.000005	2.7E-08	1.5E-04	0.000007	3.5E-08	2.0E-04
5700	0.000004	2.2E-08	1.3E-04	0.000005	2.6E-08	1.6E-04	0.000007	3.5E-08	2.1E-04
6000	0.000004	2.2E-08	1.4E-04	0.000005	2.7E-08	1.7E-04	0.000007	3.5E-08	2.2E-04
6300	0.000004	2.2E-08	1.5E-04	0.000005	2.7E-08	1.7E-04	0.000007	3.5E-08	2.3E-04
6600	0.000004	2.2E-08	1.5E-04	0.000005	2.6E-08	1.8E-04	0.000007	3.5E-08	2.4E-04
6900	0.000004	2.2E-08	1.6E-04	0.000005	2.6E-08	1.9E-04	0.000007	3.5E-08	2.5E-04
7200	0.000004	2.2E-08	1.7E-04	0.000005	2.7E-08	2.0E-04	0.000007	3.5E-08	2.6E-04
7500	0.000004	2.2E-08	1.7E-04	0.000005	2.6E-08	2.1E-04	0.000007	3.5E-08	2.7E-04
7800	0.000004	2.2E-08	1.8E-04	0.000005	2.7E-08	2.1E-04	0.000007	3.5E-08	2.8E-04
8100	0.000004	2.2E-08	1.9E-04	0.000005	2.7E-08	2.2E-04	0.000007	3.5E-08	2.9E-04
8400	0.000005	2.3E-08	1.9E-04	0.000005	2.7E-08	2.3E-04	0.000007	3.5E-08	3.1E-04
8700	0.000005	2.3E-08	2.0E-04	0.000005	2.6E-08	2.4E-04	0.000007	3.5E-08	3.2E-04
9000	0.000005	2.3E-08	2.1E-04	0.000005	2.6E-08	2.5E-04	0.000007	3.4E-08	3.3E-04
9300	0.000005	2.3E-08	2.1E-04	0.000005	2.6E-08	2.5E-04	0.000007	3.5E-08	3.4E-04
9600	0.000005	2.3E-08	2.2E-04	0.000005	2.6E-08	2.6E-04	0.000007	3.5E-08	3.5E-04
9900	0.000005	2.3E-08	2.3E-04	0.000005	2.6E-08	2.7E-04	0.000007	3.5E-08	3.6E-04
10200	0.000005	2.3E-08	2.3E-04	0.000005	2.6E-08	2.8E-04	0.000007	3.5E-08	3.7E-04
10500	0.000005	2.3E-08	2.4E-04	0.000005	2.7E-08	2.9E-04	0.000007	3.5E-08	3.8E-04
10800	0.000004	2.2E-08	2.5E-04	0.000005	2.7E-08	2.9E-04	0.000007	3.5E-08	3.9E-04
11100	0.000004	2.2E-08	2.5E-04	0.000005	2.7E-08	3.0E-04	0.000007	3.5E-08	4.0E-04

300 kPa

Time (sec)	$J_{S,\ 20°C}$ ($m^3\ m^{-2}\ s^{-1}$) @ 2.5 m s^{-1}	Q ($m^3 s^{-1}$)	Filtrate Volume (m^3)	$J_{S,\ 20°C}$ ($m^3\ m^{-2}\ s^{-1}$) @ 3.1 m s^{-1}	Q ($m^3 s^{-1}$)	Filtrate Volume (m^3)	$J_{S,\ 20°C}$ ($m^3\ m^{-2}\ s^{-1}$) @ 3.6 m s^{-1}	Q ($m^3 s^{-1}$)	Filtrate Volume (m^3)
300	0.000006	3.1E-08	9.3E-06	0.000007	3.6E-08	1.1E-05	0.000009	4.5E-08	1.3E-05
600	0.000006	2.8E-08	1.8E-05	0.000007	3.4E-08	2.1E-05	0.000009	4.3E-08	2.6E-05
900	0.000005	2.5E-08	2.5E-05	0.000007	3.3E-08	3.1E-05	0.000008	4.2E-08	3.9E-05
1200	0.000005	2.4E-08	3.2E-05	0.000007	3.3E-08	4.1E-05	0.000008	4.1E-08	5.1E-05
1500	0.000005	2.3E-08	3.9E-05	0.000006	3.2E-08	5.1E-05	0.000008	4.1E-08	6.4E-05
1800	0.000004	2.2E-08	4.6E-05	0.000006	3.2E-08	6.0E-05	0.000008	4.0E-08	7.6E-05
2100	0.000004	2.1E-08	5.2E-05	0.000006	3.2E-08	7.0E-05	0.000008	3.9E-08	8.7E-05
2400	0.000004	2.1E-08	5.8E-05	0.000006	3.2E-08	7.9E-05	0.000008	3.9E-08	9.9E-05
2700	0.000004	2.1E-08	6.5E-05	0.000006	3.2E-08	8.9E-05	0.000008	3.8E-08	1.1E-04
3000	0.000004	2.1E-08	7.1E-05	0.000006	3.2E-08	9.9E-05	0.000008	3.8E-08	1.2E-04
3300	0.000004	2.1E-08	7.7E-05	0.000006	3.1E-08	1.1E-04	0.000008	3.8E-08	1.3E-04
3600	0.000004	2.2E-08	8.4E-05	0.000006	3.1E-08	1.2E-04	0.000008	3.8E-08	1.4E-04
3900	0.000004	2.2E-08	9.0E-05	0.000006	3.1E-08	1.3E-04	0.000007	3.7E-08	1.6E-04
4200	0.000004	2.1E-08	9.7E-05	0.000006	3.2E-08	1.4E-04	0.000008	3.8E-08	1.7E-04

4500	0.000004	2.2E-08	1.0E-04	0.000006	3.1E-08	1.5E-04	0.000008	3.8E-08	1.8E-04
4800	0.000004	2.2E-08	1.1E-04	0.000006	3.1E-08	1.6E-04	0.000008	3.8E-08	1.9E-04
5100	0.000004	2.2E-08	1.2E-04	0.000006	3.1E-08	1.6E-04	0.000008	3.8E-08	2.0E-04
5400	0.000004	2.2E-08	1.2E-04	0.000006	3.2E-08	1.7E-04	0.000008	3.8E-08	2.1E-04
5700	0.000004	2.2E-08	1.3E-04	0.000006	3.2E-08	1.8E-04	0.000008	3.8E-08	2.2E-04
6000	0.000004	2.2E-08	1.4E-04	0.000006	3.1E-08	1.9E-04	0.000008	3.8E-08	2.4E-04
6300	0.000004	2.2E-08	1.4E-04	0.000006	3.2E-08	2.0E-04	0.000008	3.8E-08	2.5E-04
6600	0.000004	2.2E-08	1.5E-04	0.000006	3.2E-08	2.1E-04	0.000007	3.7E-08	2.6E-04
6900	0.000004	2.2E-08	1.6E-04	0.000006	3.1E-08	2.2E-04	0.000007	3.7E-08	2.7E-04
7200	0.000005	2.3E-08	1.6E-04	0.000006	3.1E-08	2.3E-04	0.000007	3.7E-08	2.8E-04
7500	0.000005	2.3E-08	1.7E-04	0.000006	3.1E-08	2.4E-04	0.000007	3.7E-08	2.9E-04
7800	0.000005	2.3E-08	1.8E-04	0.000006	3.0E-08	2.5E-04	0.000007	3.7E-08	3.0E-04
8100	0.000005	2.3E-08	1.8E-04	0.000006	3.0E-08	2.6E-04	0.000007	3.7E-08	3.1E-04
8400	0.000005	2.3E-08	1.9E-04	0.000006	3.1E-08	2.7E-04	0.000007	3.6E-08	3.2E-04
8700	0.000004	2.2E-08	2.0E-04	0.000006	3.1E-08	2.8E-04	0.000007	3.6E-08	3.4E-04
9000	0.000004	2.2E-08	2.0E-04	0.000006	3.1E-08	2.9E-04	0.000007	3.5E-08	3.5E-04
9300	0.000005	2.3E-08	2.1E-04	0.000006	3.0E-08	2.9E-04	0.000007	3.5E-08	3.6E-04
9600	0.000005	2.3E-08	2.2E-04	0.000006	3.0E-08	3.0E-04	0.000007	3.5E-08	3.7E-04
9900	0.000004	2.2E-08	2.2E-04	0.000006	3.0E-08	3.1E-04	0.000007	3.5E-08	3.8E-04
10200	0.000004	2.2E-08	2.3E-04	0.000006	3.0E-08	3.2E-04	0.000007	3.4E-08	3.9E-04
10500	0.000004	2.2E-08	2.4E-04	0.000006	3.1E-08	3.3E-04	0.000007	3.5E-08	4.0E-04
10800	0.000004	2.2E-08	2.4E-04	0.000006	3.1E-08	3.4E-04	0.000007	3.5E-08	4.1E-04
11100	0.000004	2.2E-08	2.5E-04	0.000006	3.0E-08	3.5E-04	0.000007	3.5E-08	4.2E-04

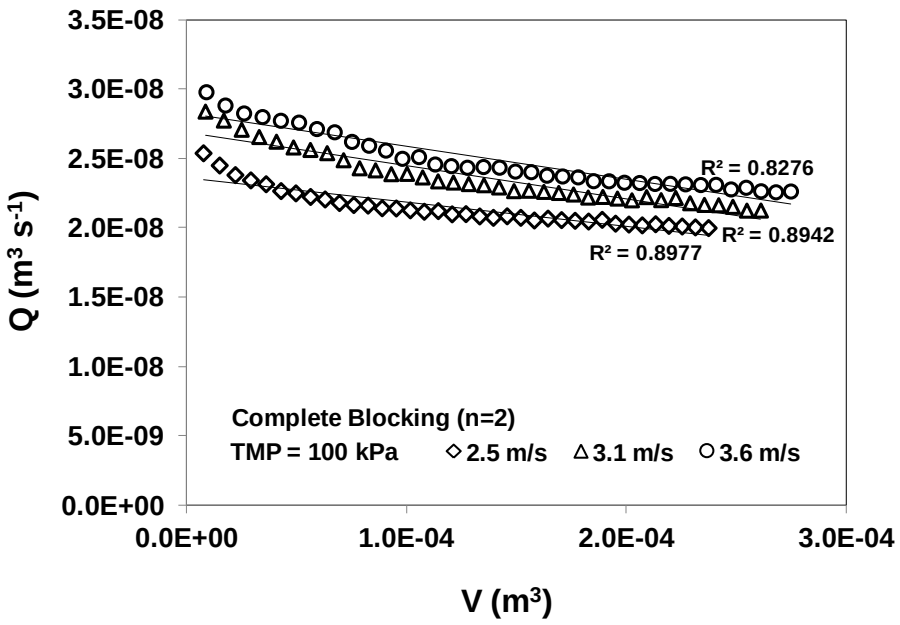

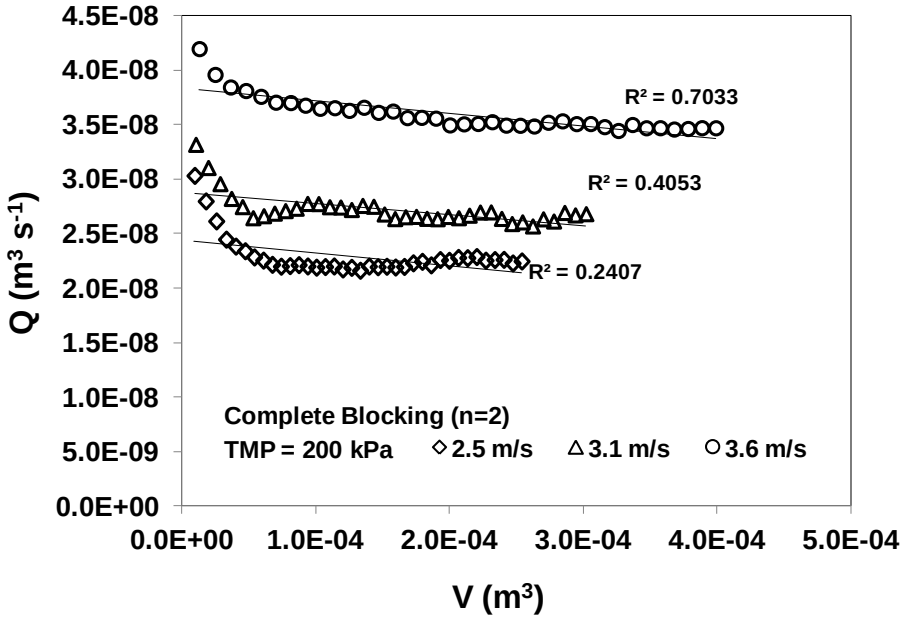

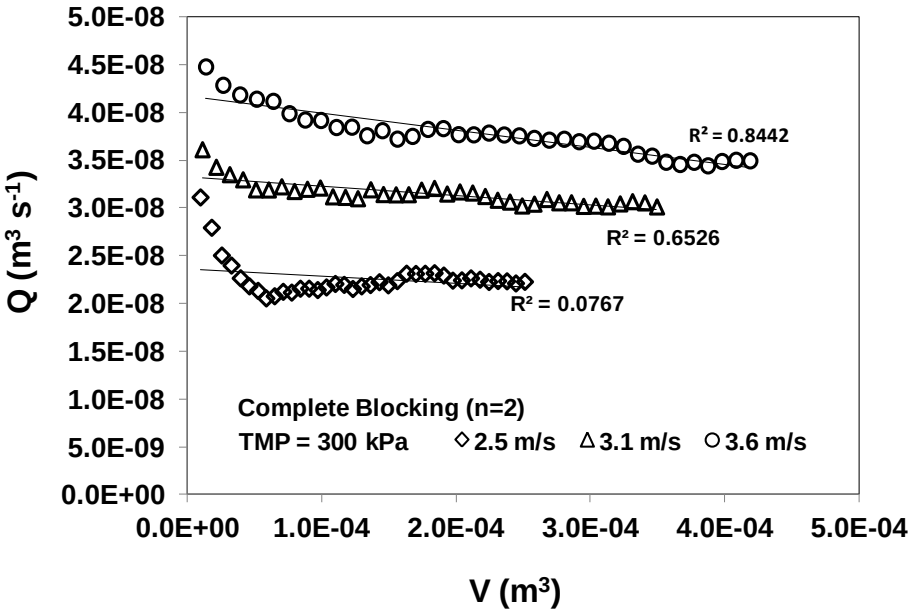

Intermediate blocking

100 kPa

Time (sec)	$J_{S,20°C}$ (m^3 m^{-2} s^{-1}) @ 2.5 m s^{-1}	1/Q	$J_{S,20°C}$ (m^3 m^{-2} s^{-1}) @ 3.1 m s^{-1}	1/Q	$J_{S,20°C}$ (m^3 m^{-2} s^{-1}) @ 3.6 m s^{-1}	1/Q

300	0.000005	3.9E+07	0.000006	3.5E+07	0.000006	3.4E+07
600	0.000005	4.1E+07	0.000006	3.6E+07	0.000006	3.5E+07
900	0.000005	4.2E+07	0.000005	3.7E+07	0.000006	3.5E+07
1200	0.000005	4.3E+07	0.000005	3.8E+07	0.000006	3.6E+07
1500	0.000005	4.3E+07	0.000005	3.8E+07	0.000006	3.6E+07
1800	0.000005	4.4E+07	0.000005	3.9E+07	0.000006	3.6E+07
2100	0.000005	4.4E+07	0.000005	3.9E+07	0.000005	3.7E+07
2400	0.000004	4.5E+07	0.000005	3.9E+07	0.000005	3.7E+07
2700	0.000004	4.5E+07	0.000005	4.0E+07	0.000005	3.8E+07
3000	0.000004	4.6E+07	0.000005	4.1E+07	0.000005	3.9E+07
3300	0.000004	4.6E+07	0.000005	4.1E+07	0.000005	3.9E+07
3600	0.000004	4.6E+07	0.000005	4.2E+07	0.000005	4.0E+07
3900	0.000004	4.7E+07	0.000005	4.2E+07	0.000005	4.0E+07
4200	0.000004	4.7E+07	0.000005	4.2E+07	0.000005	4.1E+07
4500	0.000004	4.7E+07	0.000005	4.3E+07	0.000005	4.1E+07
4800	0.000004	4.7E+07	0.000005	4.3E+07	0.000005	4.1E+07
5100	0.000004	4.7E+07	0.000005	4.3E+07	0.000005	4.1E+07
5400	0.000004	4.8E+07	0.000005	4.3E+07	0.000005	4.1E+07
5700	0.000004	4.8E+07	0.000005	4.4E+07	0.000005	4.2E+07
6000	0.000004	4.8E+07	0.000005	4.4E+07	0.000005	4.2E+07
6300	0.000004	4.8E+07	0.000005	4.4E+07	0.000005	4.2E+07
6600	0.000004	4.8E+07	0.000005	4.4E+07	0.000005	4.2E+07
6900	0.000004	4.8E+07	0.000005	4.4E+07	0.000005	4.2E+07
7200	0.000004	4.9E+07	0.000004	4.5E+07	0.000005	4.3E+07
7500	0.000004	4.8E+07	0.000004	4.5E+07	0.000005	4.3E+07
7800	0.000004	4.9E+07	0.000004	4.5E+07	0.000005	4.3E+07
8100	0.000004	4.9E+07	0.000004	4.5E+07	0.000005	4.3E+07
8400	0.000004	4.9E+07	0.000004	4.5E+07	0.000005	4.3E+07
8700	0.000004	4.9E+07	0.000004	4.5E+07	0.000005	4.3E+07
9000	0.000004	4.9E+07	0.000004	4.5E+07	0.000005	4.3E+07
9300	0.000004	4.9E+07	0.000004	4.5E+07	0.000005	4.3E+07
9600	0.000004	5.0E+07	0.000004	4.6E+07	0.000005	4.3E+07
9900	0.000004	4.9E+07	0.000004	4.6E+07	0.000005	4.4E+07
10200	0.000004	5.0E+07	0.000004	4.6E+07	0.000005	4.4E+07
10500	0.000004	5.0E+07	0.000004	4.6E+07	0.000005	4.4E+07
10800	0.000004	5.0E+07	0.000004	4.7E+07	0.000005	4.4E+07
11100	0.000004	5.0E+07	0.000004	4.7E+07	0.000005	4.4E+07

200 kPa

Time (sec)	$J_{S,\ 20°C}$ ($m^3\ m^{-2}\ s^{-1}$) @ 2.5 m s^{-1}	1/Q	$J_{S,\ 20°C}$ ($m^3\ m^{-2}\ s^{-1}$) @ 3.1 m s^{-1}	1/Q	$J_{S,\ 20°C}$ ($m^3\ m^{-2}\ s^{-1}$) @ 3.6 m s^{-1}	1/Q

300	0.000006	3.3E+07	0.000007	3.0E+07	0.000008	2.4E+07
600	0.000006	3.6E+07	0.000006	3.2E+07	0.000008	2.5E+07
900	0.000005	3.8E+07	0.000006	3.4E+07	0.000008	2.6E+07
1200	0.000005	4.1E+07	0.000006	3.5E+07	0.000008	2.6E+07
1500	0.000005	4.2E+07	0.000005	3.6E+07	0.000008	2.7E+07
1800	0.000005	4.3E+07	0.000005	3.8E+07	0.000007	2.7E+07
2100	0.000005	4.4E+07	0.000005	3.8E+07	0.000007	2.7E+07
2400	0.000005	4.4E+07	0.000005	3.7E+07	0.000007	2.7E+07
2700	0.000004	4.5E+07	0.000005	3.7E+07	0.000007	2.7E+07
3000	0.000004	4.5E+07	0.000005	3.7E+07	0.000007	2.7E+07
3300	0.000004	4.5E+07	0.000006	3.6E+07	0.000007	2.8E+07
3600	0.000004	4.5E+07	0.000006	3.6E+07	0.000007	2.7E+07
3900	0.000004	4.5E+07	0.000005	3.6E+07	0.000007	2.8E+07
4200	0.000004	4.6E+07	0.000005	3.6E+07	0.000007	2.8E+07
4500	0.000004	4.6E+07	0.000005	3.7E+07	0.000007	2.8E+07
4800	0.000004	4.5E+07	0.000006	3.6E+07	0.000007	2.8E+07
5100	0.000004	4.6E+07	0.000005	3.6E+07	0.000007	2.8E+07
5400	0.000004	4.6E+07	0.000005	3.7E+07	0.000007	2.9E+07
5700	0.000004	4.6E+07	0.000005	3.8E+07	0.000007	2.9E+07
6000	0.000004	4.5E+07	0.000005	3.8E+07	0.000007	2.9E+07
6300	0.000004	4.6E+07	0.000005	3.8E+07	0.000007	2.8E+07
6600	0.000004	4.5E+07	0.000005	3.8E+07	0.000007	2.9E+07
6900	0.000004	4.6E+07	0.000005	3.8E+07	0.000007	2.9E+07
7200	0.000004	4.6E+07	0.000005	3.8E+07	0.000007	2.9E+07
7500	0.000004	4.5E+07	0.000005	3.8E+07	0.000007	2.8E+07
7800	0.000004	4.5E+07	0.000005	3.7E+07	0.000007	2.8E+07
8100	0.000004	4.5E+07	0.000005	3.7E+07	0.000007	2.9E+07
8400	0.000005	4.4E+07	0.000005	3.7E+07	0.000007	2.9E+07
8700	0.000005	4.4E+07	0.000005	3.8E+07	0.000007	2.9E+07
9000	0.000005	4.4E+07	0.000005	3.9E+07	0.000007	2.9E+07
9300	0.000005	4.4E+07	0.000005	3.8E+07	0.000007	2.9E+07
9600	0.000005	4.4E+07	0.000005	3.9E+07	0.000007	2.9E+07
9900	0.000005	4.4E+07	0.000005	3.8E+07	0.000007	2.9E+07
10200	0.000005	4.4E+07	0.000005	3.8E+07	0.000007	2.9E+07
10500	0.000005	4.4E+07	0.000005	3.7E+07	0.000007	2.9E+07
10800	0.000004	4.5E+07	0.000005	3.7E+07	0.000007	2.9E+07
11100	0.000004	4.5E+07	0.000005	3.7E+07	0.000007	2.9E+07

300 kPa

Time (sec)	$J_{S,\ 20°C}$ ($m^3\ m^{-2}\ s^{-1}$) @ 2.5 m s^{-1}	1/Q	$J_{S,\ 20°C}$ ($m^3\ m^{-2}\ s^{-1}$) @ 3.1 m s^{-1}	1/Q	$J_{S,\ 20°C}$ ($m^3\ m^{-2}\ s^{-1}$) @ 3.6 m s^{-1}	1/Q
300	0.000006	3.2E+07	0.000007	2.8E+07	0.000009	2.23E+07
600	0.000006	3.6E+07	0.000007	2.9E+07	0.000009	2.33E+07
900	0.000005	4.0E+07	0.000007	3.0E+07	0.000008	2.39E+07
1200	0.000005	4.2E+07	0.000007	3.0E+07	0.000008	2.42E+07
1500	0.000005	4.4E+07	0.000006	3.1E+07	0.000008	2.43E+07
1800	0.000004	4.6E+07	0.000006	3.1E+07	0.000008	2.51E+07
2100	0.000004	4.7E+07	0.000006	3.1E+07	0.000008	2.55E+07
2400	0.000004	4.9E+07	0.000006	3.2E+07	0.000008	2.55E+07
2700	0.000004	4.8E+07	0.000006	3.1E+07	0.000008	2.60E+07
3000	0.000004	4.7E+07	0.000006	3.1E+07	0.000008	2.60E+07
3300	0.000004	4.7E+07	0.000006	3.2E+07	0.000008	2.66E+07
3600	0.000004	4.6E+07	0.000006	3.2E+07	0.000008	2.62E+07
3900	0.000004	4.6E+07	0.000006	3.2E+07	0.000007	2.69E+07
4200	0.000004	4.7E+07	0.000006	3.1E+07	0.000008	2.67E+07
4500	0.000004	4.6E+07	0.000006	3.2E+07	0.000008	2.62E+07
4800	0.000004	4.5E+07	0.000006	3.2E+07	0.000008	2.61E+07
5100	0.000004	4.6E+07	0.000006	3.2E+07	0.000008	2.65E+07
5400	0.000004	4.6E+07	0.000006	3.1E+07	0.000008	2.65E+07
5700	0.000004	4.6E+07	0.000006	3.1E+07	0.000008	2.64E+07
6000	0.000004	4.6E+07	0.000006	3.2E+07	0.000008	2.66E+07
6300	0.000004	4.5E+07	0.000006	3.2E+07	0.000008	2.66E+07
6600	0.000004	4.6E+07	0.000006	3.2E+07	0.000007	2.68E+07
6900	0.000004	4.5E+07	0.000006	3.2E+07	0.000007	2.69E+07
7200	0.000005	4.3E+07	0.000006	3.2E+07	0.000007	2.69E+07
7500	0.000005	4.3E+07	0.000006	3.3E+07	0.000007	2.71E+07
7800	0.000005	4.3E+07	0.000006	3.3E+07	0.000007	2.70E+07
8100	0.000005	4.3E+07	0.000006	3.3E+07	0.000007	2.72E+07
8400	0.000005	4.4E+07	0.000006	3.2E+07	0.000007	2.74E+07
8700	0.000004	4.5E+07	0.000006	3.3E+07	0.000007	2.81E+07
9000	0.000004	4.5E+07	0.000006	3.3E+07	0.000007	2.82E+07
9300	0.000005	4.4E+07	0.000006	3.3E+07	0.000007	2.87E+07
9600	0.000005	4.4E+07	0.000006	3.3E+07	0.000007	2.89E+07
9900	0.000004	4.5E+07	0.000006	3.3E+07	0.000007	2.87E+07
10200	0.000004	4.5E+07	0.000006	3.3E+07	0.000007	2.90E+07
10500	0.000004	4.5E+07	0.000006	3.3E+07	0.000007	2.87E+07
10800	0.000004	4.5E+07	0.000006	3.3E+07	0.000007	2.86E+07
11100	0.000004	4.5E+07	0.000006	3.3E+07	0.000007	2.86E+07

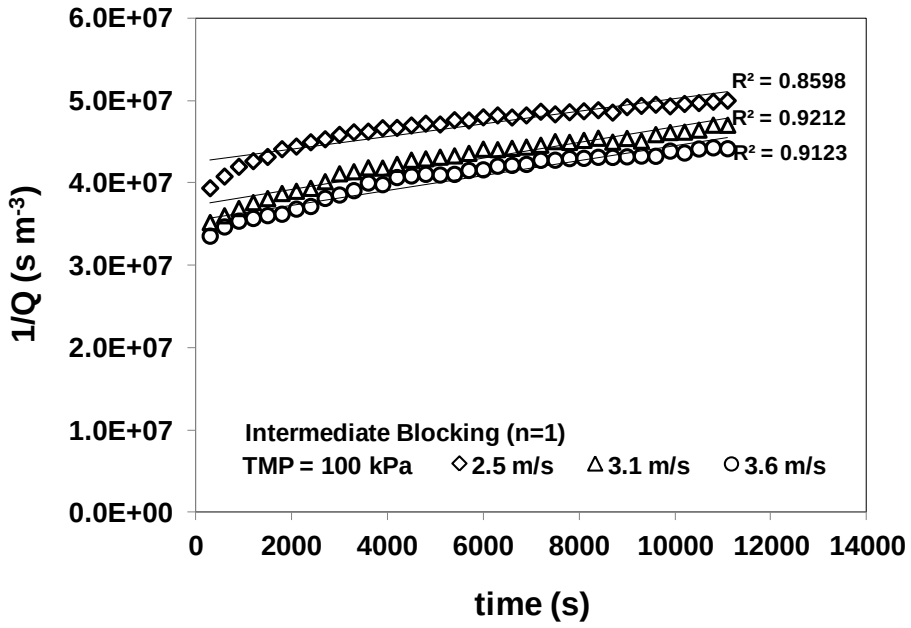
6.0E+07
5.0E+07
4.0E+07
3.0E+07
2.0E+07
1.0E+07
0.0E+00
1/Q (s m-3)
0
2000
4000
6000
8000
10000
12000
14000
time (s)
R² = 0.8598
R² = 0.9212
R² = 0.9123
Intermediate Blocking (n=1)
TMP = 100 kPa
2.5 m/s
3.1 m/s
3.6 m/s

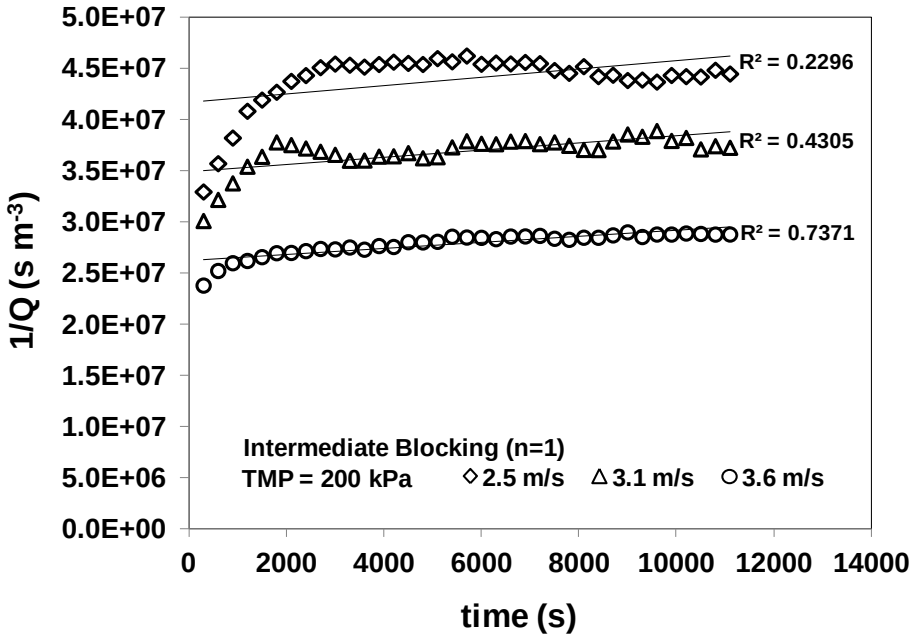
5.0E+07
4.5E+07
4.0E+07
3.5E+07
3.0E+07
2.5E+07
2.0E+07
1.5E+07
1.0E+07
5.0E+06
0.0E+00
1/Q (s m-3)
0
2000
4000
6000
8000
10000
12000
14000
time (s)
R² = 0.2296
R² = 0.4305
R² = 0.7371
Intermediate Blocking (n=1)
TMP = 200 kPa
2.5 m/s
3.1 m/s
3.6 m/s

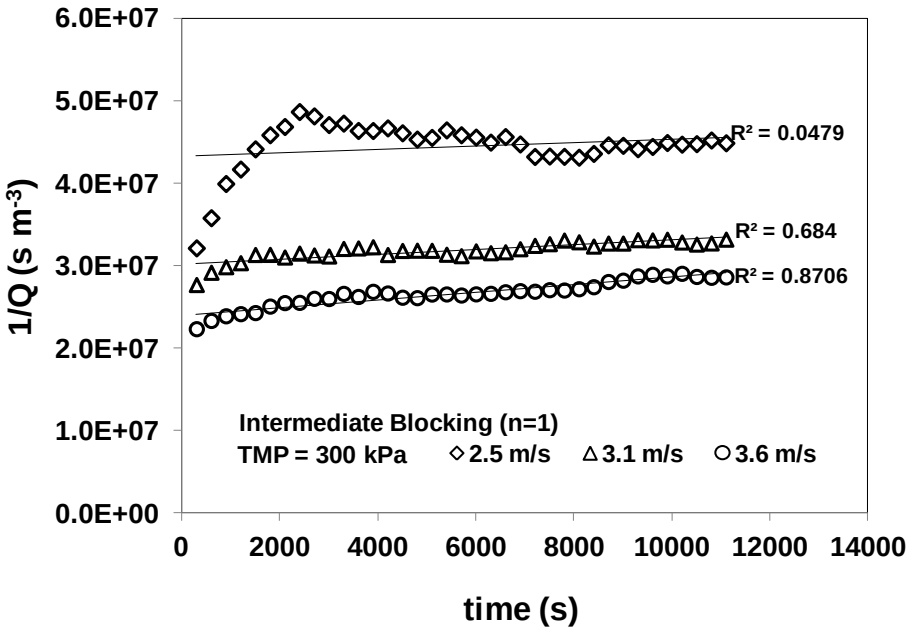

Standard blocking

100 kPa

Time (sec)	$J_{S,20°C}$ ($m^3 m^{-2} s^{-1}$) @ 2.5 m s^{-1}	t/V (s/m^3)	$J_{S,20°C}$ ($m^3 m^{-2} s^{-1}$) @ 3.1 m s^{-1}	t/V (s/m^3)	$J_{S,20°C}$ ($m^3 m^{-2} s^{-1}$) @ 3.6 m s^{-1}	t/V (s/m^3)
300	0.000005	3.94E+07	0.000006	3.52E+07	0.000006	3.36E+07
600	0.000005	4.01E+07	0.000006	3.56E+07	0.000006	3.41E+07
900	0.000005	4.07E+07	0.000005	3.60E+07	0.000006	3.45E+07
1200	0.000005	4.12E+07	0.000005	3.64E+07	0.000006	3.48E+07
1500	0.000005	4.16E+07	0.000005	3.68E+07	0.000006	3.51E+07
1800	0.000005	4.20E+07	0.000005	3.71E+07	0.000006	3.52E+07
2100	0.000005	4.23E+07	0.000005	3.73E+07	0.000005	3.55E+07
2400	0.000004	4.26E+07	0.000005	3.76E+07	0.000005	3.57E+07
2700	0.000004	4.29E+07	0.000005	3.79E+07	0.000005	3.59E+07
3000	0.000004	4.32E+07	0.000005	3.82E+07	0.000005	3.62E+07
3300	0.000004	4.34E+07	0.000005	3.84E+07	0.000005	3.64E+07
3600	0.000004	4.37E+07	0.000005	3.87E+07	0.000005	3.67E+07
3900	0.000004	4.39E+07	0.000005	3.89E+07	0.000005	3.69E+07
4200	0.000004	4.41E+07	0.000005	3.91E+07	0.000005	3.72E+07
4500	0.000004	4.42E+07	0.000005	3.94E+07	0.000005	3.74E+07
4800	0.000004	4.44E+07	0.000005	3.96E+07	0.000005	3.76E+07
5100	0.000004	4.46E+07	0.000005	3.98E+07	0.000005	3.78E+07
5400	0.000004	4.47E+07	0.000005	3.99E+07	0.000005	3.79E+07

5700	0.000004	4.49E+07	0.000005	4.01E+07	0.000005	3.81E+07
6000	0.000004	4.50E+07	0.000005	4.03E+07	0.000005	3.83E+07
6300	0.000004	4.52E+07	0.000005	4.05E+07	0.000005	3.84E+07
6600	0.000004	4.53E+07	0.000005	4.06E+07	0.000005	3.86E+07
6900	0.000004	4.54E+07	0.000005	4.08E+07	0.000005	3.87E+07
7200	0.000004	4.55E+07	0.000004	4.09E+07	0.000005	3.89E+07
7500	0.000004	4.56E+07	0.000004	4.11E+07	0.000005	3.90E+07
7800	0.000004	4.57E+07	0.000004	4.12E+07	0.000005	3.92E+07
8100	0.000004	4.58E+07	0.000004	4.13E+07	0.000005	3.93E+07
8400	0.000004	4.60E+07	0.000004	4.15E+07	0.000005	3.94E+07
8700	0.000004	4.60E+07	0.000004	4.16E+07	0.000005	3.96E+07
9000	0.000004	4.61E+07	0.000004	4.17E+07	0.000005	3.97E+07
9300	0.000004	4.62E+07	0.000004	4.18E+07	0.000005	3.98E+07
9600	0.000004	4.63E+07	0.000004	4.19E+07	0.000005	3.99E+07
9900	0.000004	4.64E+07	0.000004	4.20E+07	0.000005	4.00E+07
10200	0.000004	4.65E+07	0.000004	4.22E+07	0.000005	4.01E+07
10500	0.000004	4.66E+07	0.000004	4.23E+07	0.000005	4.02E+07
10800	0.000004	4.67E+07	0.000004	4.24E+07	0.000005	4.03E+07
11100	0.000004	4.68E+07	0.000004	4.25E+07	0.000005	4.04E+07

200 kPa

Time (sec)	$J_{S,\ 20°C}$ ($m^3\ m^{-2}\ s^{-1}$) @ 2.5 m s^{-1}	t/V (s/m^3)	$J_{S,\ 20°C}$ ($m^3\ m^{-2}\ s^{-1}$) @ 3.1 m s^{-1}	t/V (s/m^3)	$J_{S,\ 20°C}$ ($m^3\ m^{-2}\ s^{-1}$) @ 3.6 m s^{-1}	t/V (s/m^3)
300	0.000006	3.30E+07	0.000007	3.02E+07	0.000008	2.38E+07
600	0.000006	3.43E+07	0.000006	3.11E+07	0.000008	2.45E+07
900	0.000005	3.55E+07	0.000006	3.20E+07	0.000008	2.50E+07
1200	0.000005	3.67E+07	0.000006	3.28E+07	0.000008	2.53E+07
1500	0.000005	3.77E+07	0.000005	3.35E+07	0.000008	2.56E+07
1800	0.000005	3.84E+07	0.000005	3.41E+07	0.000007	2.58E+07
2100	0.000005	3.91E+07	0.000005	3.46E+07	0.000007	2.60E+07
2400	0.000005	3.97E+07	0.000005	3.49E+07	0.000007	2.61E+07
2700	0.000004	4.02E+07	0.000005	3.51E+07	0.000007	2.62E+07
3000	0.000004	4.07E+07	0.000005	3.52E+07	0.000007	2.64E+07
3300	0.000004	4.11E+07	0.000006	3.53E+07	0.000007	2.65E+07
3600	0.000004	4.14E+07	0.000006	3.54E+07	0.000007	2.65E+07
3900	0.000004	4.17E+07	0.000005	3.55E+07	0.000007	2.66E+07
4200	0.000004	4.20E+07	0.000005	3.55E+07	0.000007	2.67E+07
4500	0.000004	4.22E+07	0.000005	3.56E+07	0.000007	2.68E+07
4800	0.000004	4.24E+07	0.000006	3.56E+07	0.000007	2.69E+07

5100	0.000004	4.26E+07	0.000005	3.57E+07	0.000007	2.69E+07
5400	0.000004	4.27E+07	0.000005	3.58E+07	0.000007	2.70E+07
5700	0.000004	4.29E+07	0.000005	3.59E+07	0.000007	2.71E+07
6000	0.000004	4.30E+07	0.000005	3.60E+07	0.000007	2.72E+07
6300	0.000004	4.31E+07	0.000005	3.61E+07	0.000007	2.72E+07
6600	0.000004	4.32E+07	0.000005	3.61E+07	0.000007	2.73E+07
6900	0.000004	4.33E+07	0.000005	3.62E+07	0.000007	2.73E+07
7200	0.000004	4.34E+07	0.000005	3.63E+07	0.000007	2.74E+07
7500	0.000004	4.35E+07	0.000005	3.63E+07	0.000007	2.74E+07
7800	0.000004	4.35E+07	0.000005	3.64E+07	0.000007	2.75E+07
8100	0.000004	4.36E+07	0.000005	3.64E+07	0.000007	2.75E+07
8400	0.000005	4.36E+07	0.000005	3.64E+07	0.000007	2.75E+07
8700	0.000005	4.36E+07	0.000005	3.65E+07	0.000007	2.76E+07
9000	0.000005	4.36E+07	0.000005	3.65E+07	0.000007	2.76E+07
9300	0.000005	4.37E+07	0.000005	3.66E+07	0.000007	2.76E+07
9600	0.000005	4.37E+07	0.000005	3.67E+07	0.000007	2.77E+07
9900	0.000005	4.37E+07	0.000005	3.67E+07	0.000007	2.77E+07
10200	0.000005	4.37E+07	0.000005	3.67E+07	0.000007	2.77E+07
10500	0.000005	4.37E+07	0.000005	3.68E+07	0.000007	2.78E+07
10800	0.000004	4.37E+07	0.000005	3.68E+07	0.000007	2.78E+07
11100	0.000004	4.38E+07	0.000005	3.68E+07	0.000007	2.78E+07

300 kPa

Time (sec)	$J_{S,\ 20°C}$ ($m^3\ m^{-2}\ s^{-1}$) @ 2.5 m s^{-1}	t/V (s/m^3)	$J_{S,\ 20°C}$ ($m^3\ m^{-2}\ s^{-1}$) @ 3.1 m s^{-1}	t/V (s/m^3)	$J_{S,\ 20°C}$ ($m^3\ m^{-2}\ s^{-1}$) @ 3.6 m s^{-1}	t/V (s/m^3)
300	0.000006	3.21E+07	0.000007	2.77E+07	0.000009	2.23E+07
600	0.000006	3.39E+07	0.000007	2.84E+07	0.000009	2.28E+07
900	0.000005	3.57E+07	0.000007	2.89E+07	0.000008	2.32E+07
1200	0.000005	3.70E+07	0.000007	2.92E+07	0.000008	2.34E+07
1500	0.000005	3.82E+07	0.000006	2.96E+07	0.000008	2.36E+07
1800	0.000004	3.93E+07	0.000006	2.99E+07	0.000008	2.38E+07
2100	0.000004	4.03E+07	0.000006	3.01E+07	0.000008	2.40E+07
2400	0.000004	4.11E+07	0.000006	3.02E+07	0.000008	2.42E+07
2700	0.000004	4.18E+07	0.000006	3.03E+07	0.000008	2.44E+07
3000	0.000004	4.23E+07	0.000006	3.04E+07	0.000008	2.46E+07
3300	0.000004	4.27E+07	0.000006	3.06E+07	0.000008	2.47E+07
3600	0.000004	4.30E+07	0.000006	3.07E+07	0.000008	2.48E+07
3900	0.000004	4.32E+07	0.000006	3.08E+07	0.000007	2.50E+07
4200	0.000004	4.35E+07	0.000006	3.08E+07	0.000008	2.51E+07

4500	0.000004	4.36E+07	0.000006	3.09E+07	0.000008	2.52E+07
4800	0.000004	4.37E+07	0.000006	3.10E+07	0.000008	2.52E+07
5100	0.000004	4.38E+07	0.000006	3.10E+07	0.000008	2.53E+07
5400	0.000004	4.40E+07	0.000006	3.10E+07	0.000008	2.54E+07
5700	0.000004	4.41E+07	0.000006	3.10E+07	0.000008	2.54E+07
6000	0.000004	4.41E+07	0.000006	3.11E+07	0.000008	2.55E+07
6300	0.000004	4.42E+07	0.000006	3.11E+07	0.000008	2.55E+07
6600	0.000004	4.42E+07	0.000006	3.11E+07	0.000007	2.56E+07
6900	0.000004	4.43E+07	0.000006	3.12E+07	0.000007	2.56E+07
7200	0.000005	4.42E+07	0.000006	3.12E+07	0.000007	2.57E+07
7500	0.000005	4.42E+07	0.000006	3.13E+07	0.000007	2.57E+07
7800	0.000005	4.41E+07	0.000006	3.13E+07	0.000007	2.58E+07
8100	0.000005	4.41E+07	0.000006	3.14E+07	0.000007	2.58E+07
8400	0.000005	4.41E+07	0.000006	3.14E+07	0.000007	2.59E+07
8700	0.000004	4.41E+07	0.000006	3.15E+07	0.000007	2.60E+07
9000	0.000004	4.41E+07	0.000006	3.15E+07	0.000007	2.60E+07
9300	0.000005	4.41E+07	0.000006	3.16E+07	0.000007	2.61E+07
9600	0.000005	4.41E+07	0.000006	3.16E+07	0.000007	2.62E+07
9900	0.000004	4.42E+07	0.000006	3.16E+07	0.000007	2.63E+07
10200	0.000004	4.42E+07	0.000006	3.17E+07	0.000007	2.63E+07
10500	0.000004	4.42E+07	0.000006	3.17E+07	0.000007	2.64E+07
10800	0.000004	4.42E+07	0.000006	3.17E+07	0.000007	2.65E+07
11100	0.000004	4.42E+07	0.000006	3.18E+07	0.000007	2.65E+07

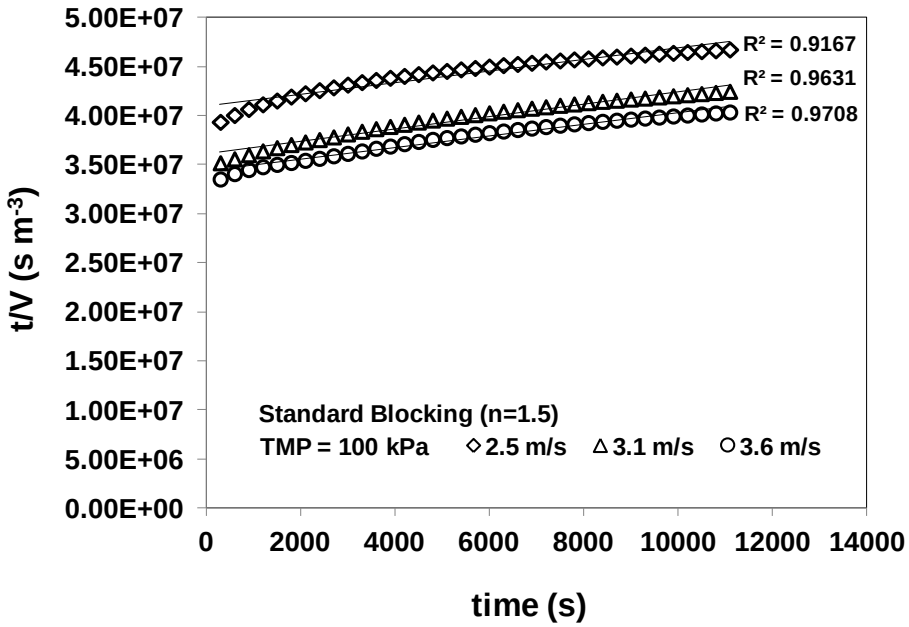

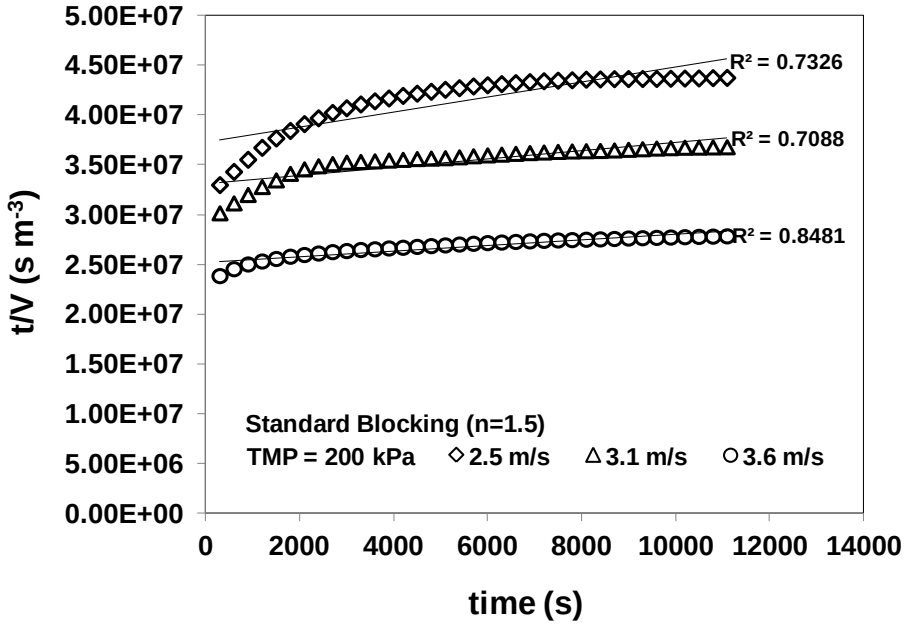
5.00E+07
4.50E+07
4.00E+07
3.50E+07
3.00E+07
2.50E+07
2.00E+07
1.50E+07
1.00E+07
5.00E+06
0.00E+00
t/V (s m-3)
0
2000
4000
6000
8000
10000
12000
14000
time (s)
R² = 0.7326
R² = 0.7088
R² = 0.8481
Standard Blocking (n=1.5)
TMP = 200 kPa
2.5 m/s
3.1 m/s
3.6 m/s

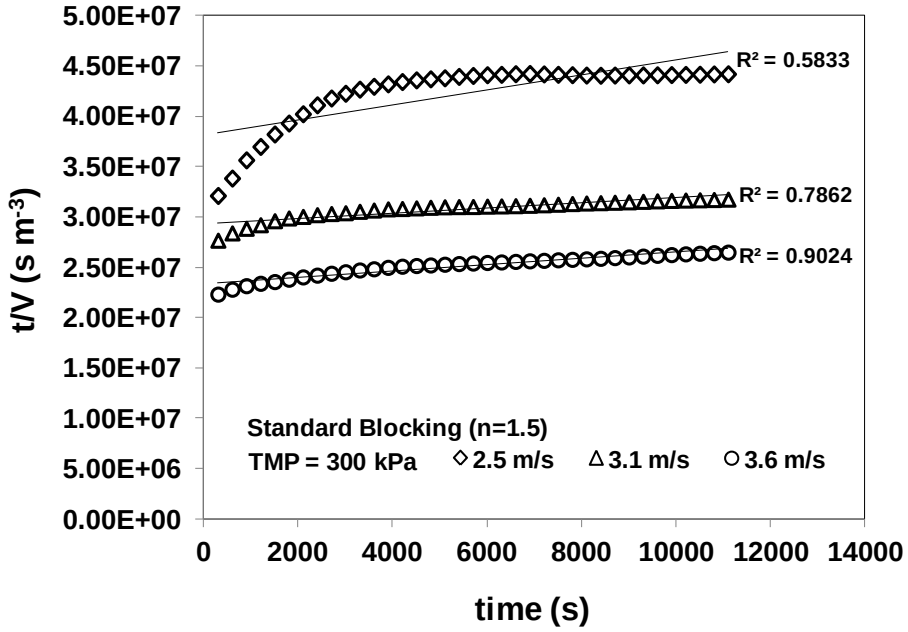
5.00E+07
4.50E+07
4.00E+07
3.50E+07
3.00E+07
2.50E+07
2.00E+07
1.50E+07
1.00E+07
5.00E+06
0.00E+00
t/V (s m-3)
0
2000
4000
6000
8000
10000
12000
14000
time (s)
R² = 0.5833
R² = 0.7862
R² = 0.9024
Standard Blocking (n=1.5)
TMP = 300 kPa
2.5 m/s
3.1 m/s
3.6 m/s

Appendix 7.1: Calculations for the membrane costs with reference to specific wastewater streams

			Treatment System								
			UF			NF		RO			
Feed Source	**Company**	**Ave. Volume of Wastewater Generated (m^3/day)**	% Recovery	Volume (m^3/day)	Volume/hr @ 18 hrs (m^3/hr)	% Recovery	Volume (m^3/day)	% Recovery	Volume (m^3/day)	Volume/hr @ 18 hrs (m^3/hr)	**% of wastewater generated**
Post ED rinse	A	253	10.0%	25	1.4						10.0%
			30.0%	76	4.2						30.0%
			50.0%	127	7.0						50.0%
			70.0%	177	9.8						70.0%
			90.0%	228	12.7						90.0%
Oily wastewater	A	578	10.0%	58	3.2			75.0%	43	2	7.5%
			30.0%	173	9.6				130	7	22.5%
			50.0%	289	16.1				217	12	37.5%
			70.0%	405	22.5				303	17	52.5%
			90.0%	520	28.9				390	22	67.5%
Metals wastewater	A	144	10.0%	14	0.8	75.0%	11				7.5%
			30.0%	43	2.4		32				22.5%
			50.0%	72	4.0		54				37.5%
			70.0%	101	5.6		76				52.5%
			90.0%	130	7.2		97				67.5%
General wastewater (combined with metals)	A	14	10.0%								
			30.0%								
			50.0%								
			70.0%								
			90.0%								
Beverage wastewater	B	942	10.0%	94	5.2			75.0%	71	4	7.5%
			30.0%	283	15.7				212	12	22.5%
			50.0%	471	26.2				353	20	37.5%
			70.0%	659	36.6				495	27	52.5%
			90.0%	848	47.1				636	35	67.5%

Note:

Recirculating pump for UF	
1-3 modules	1
4-6 modules	2
7-9 modules	3
10-12 modules	4
13-15 modules	5
16-18 modules	6
19-21 modules	7
1 recirculating pump	40 hp
1 feed pump	1 hp

Cost

Product Water for Reuse (m^3/day)	UF			RO		Total Equipment Cost ($AUD)	Total Operating Cost per year ($AUD/yr)
	Pall Clarisep 3 (2.4 m^3/hr permeate)	Electricity cost ($AUD/yr) @ 240 days	Cleaning chemicals ($AUD/yr) (@ 48 weeks)	Electricity cost ($AUD/yr) @ 240 days	Cleaning chemicals ($AUD/yr) (@ 12 months)		
25	$ 100,000.00	$ 12,445.49	$ 3,120.00			$ 100,000.00	$ 15,565.49
76	$ 200,000.00	$ 12,747.46	$ 3,120.00			$ 200,000.00	$ 15,867.46
127	$ 300,000.00	$ 13,049.43	$ 3,120.00			$ 300,000.00	$ 16,169.43
177	$ 400,000.00	$ 18,208.80	$ 6,240.00			$ 400,000.00	$ 24,448.80
228	$ 500,000.00	$ 25,796.88	$ 6,240.00			$ 500,000.00	$ 32,036.88
43	$ 200,000.00	$ 12,747.46	$ 3,120.00	$ 6,071.76	$ 1,440.00	$ 245,000.00	$ 23,379.22
130	$ 400,000.00	$ 25,494.92	$ 6,240.00	$ 6,071.76	$ 1,440.00	$ 445,000.00	$ 39,246.68
217	$ 700,000.00	$ 38,544.34	$ 9,360.00	$ 12,143.52	$ 2,880.00	$ 775,000.00	$ 62,927.86
303	$ 1,000,000.00	$ 51,593.77	$ 12,480.00	$ 12,143.52	$ 2,880.00	$ 1,075,000.00	$ 79,097.29
390	$ 1,200,000.00	$ 52,197.71	$ 12,480.00	$ 12,143.52	$ 2,880.00	$ 1,275,000.00	$ 79,701.23

UF + NF combined

	PRO AP GE (11 m^3/hr)	Electricity cost ($AUD/yr) @ 240 days	Cleaning chemicals ($AUD/yr) (@ 12 months)				
11	$90,000.00	$ 12,143.52	$ 2,880.00			$ 90,000.00	$ 15,023.52
32	$90,000.00	$ 12,143.52	$ 2,880.00			$ 90,000.00	$ 15,023.52
54	$90,000.00	$ 12,143.52	$ 2,880.00			$ 90,000.00	$ 15,023.52
76	$90,000.00	$ 12,143.52	$ 2,880.00			$ 90,000.00	$ 15,023.52
97	$90,000.00	$ 12,143.52	$ 2,880.00			$ 90,000.00	$ 15,023.52

	Pall Clarisep 3 (2.4 m^3/hr permeate)	Electricity cost ($AUD/yr) @ 240 days	Cleaning chemicals ($AUD/yr) (@ 48 weeks)	Electricity cost ($AUD/yr) @ 240 days	Cleaning chemicals ($AUD/yr) (@ 12 months)		
71	$ 300,000.00	$ 13,049.43	$ 3,120.00	$ 6,071.76	$ 1,440.00	$ 345,000.00	$ 23,681.19
212	$ 700,000.00	$ 38,544.34	$ 9,360.00	$ 12,143.52	$ 2,880.00	$ 775,000.00	$ 62,927.86
353	$ 1,100,000.00	$ 51,895.74	$ 12,480.00	$ 12,143.52	$ 2,880.00	$ 1,175,000.00	$ 79,399.26
495	$ 1,600,000.00	$ 65,549.10	$ 18,720.00	$ 14,977.01	$ 2,880.00	$ 1,690,000.00	$ 102,126.11
636	$ 2,000,000.00	$ 91,044.02	$ 21,840.00	$ 14,977.01	$ 2,880.00	$ 2,090,000.00	$ 130,741.03

			Freshwater savings		Wastewater reduction		
Factor	**Misc. Costs (Civil works, connection set-up, & freight)**		**Cost per year ($AUD/yr) @ 240 days**	**% of total freshwater consumption**	**Cost per year ($AUD/yr) @ 240 days**	**% of total wastewater generated**	**Factor**
5 % of Equipment Cost							x % of wastewater reduction cost/yr
0.05	$	5,000.00	$ 12,034.10	1.72%	$ 5,265.03	3.50%	0.2
0.05	$	10,000.00	$ 36,102.29	5.16%	$ 15,795.09	10.51%	0.2
0.05	$	15,000.00	$ 60,170.48	8.60%	$ 26,325.16	17.52%	0.2
0.05	$	20,000.00	$ 84,238.68	12.04%	$ 36,855.22	24.53%	0.2
0.05	$	25,000.00	$ 108,306.87	15.48%	$ 47,385.28	31.54%	0.2
0.05	$	12,250.00	$ 20,619.69	2.95%	$ 9,021.31	6.00%	0.2
0.05	$	22,250.00	$ 61,859.06	8.84%	$ 27,063.93	18.01%	0.2
0.05	$	38,750.00	$ 103,098.44	14.73%	$ 45,106.54	30.02%	0.2
0.05	$	53,750.00	$ 144,337.81	20.63%	$ 63,149.16	42.03%	0.2
0.05	$	63,750.00	$ 185,577.19	26.52%	$ 81,191.78	54.04%	0.2
0.05	$	4,500.00	$ 5,137.08	0.73%	$ 2,247.52	1.50%	0.2
			$ 15,411.25	2.20%	$ 6,742.57	4.49%	0.2
			$ 25,685.42	3.67%	$ 11,237.62	7.48%	0.2
			$ 35,959.59	5.14%	$ 15,732.66	10.47%	0.2
			$ 46,233.76	6.61%	$ 20,227.71	13.46%	0.2
0.05	$	17,250.00	$ 33,605.10	4.46%	$ 14,702.55	7.50%	0.3
0.05	$	38,750.00	$ 100,815.29	13.39%	$ 44,107.64	22.50%	0.3
0.05	$	58,750.00	$ 168,025.48	22.32%	$ 73,512.74	37.50%	0.3
0.05	$	84,500.00	$ 235,235.67	31.24%	$ 102,917.83	52.50%	0.3
0.05	$	104,500.00	$ 302,445.87	40.17%	$ 132,322.93	67.50%	0.3

Provision for increase in conc'n TMCA (TDS) SCH (BOD, TDS, SS)		Actual wastewater Cost savings per year ($AUD/yr)		Total savings from Freshwater & Wastewater ($AUD/yr)		Total Operating Cost per year ($AUD/yr)	
$	1,053.01	$	4,212.02	**$ 16,246.12**	-	**$**	**15,565.49**
$	3,159.02	$	12,636.07	**$ 48,738.37**	-	**$**	**15,867.46**
$	5,265.03	$	21,060.12	**$ 81,230.61**	-	**$**	**16,169.43**
$	7,371.04	$	29,484.17	**$ 113,722.85**	-	**$**	**24,448.80**
$	9,477.06	$	37,908.22	**$ 146,215.10**	-	**$**	**32,036.88**
$	1,804.26	$	7,217.05	**$ 27,836.73**	-	**$**	**23,379.22**
$	5,412.79	$	21,651.14	**$ 83,510.20**	-	**$**	**39,246.68**
$	9,021.31	$	36,085.23	**$ 139,183.67**	-	**$**	**62,927.86**
$	12,629.83	$	50,519.33	**$ 194,857.14**	-	**$**	**79,097.29**
$	16,238.36	$	64,953.42	**$ 250,530.61**	-	**$**	**79,701.23**
$	449.50	$	1,798.02	**$ 6,935.10**	-	**$**	**15,023.52**
$	1,348.51	$	5,394.06	**$ 20,805.31**		**$**	**15,023.52**
$	2,247.52	$	8,990.09	**$ 34,675.52**		**$**	**15,023.52**
$	3,146.53	$	12,586.13	**$ 48,545.72**		**$**	**15,023.52**
$	4,045.54	$	16,182.17	**$ 62,415.93**		**$**	**15,023.52**
$	4,410.76	$	10,291.78	**$ 43,896.88**	-	**$**	**23,681.19**
$	13,232.29	$	30,875.35	**$ 131,690.64**	-	**$**	**62,927.86**
$	22,053.82	$	51,458.92	**$ 219,484.40**	-	**$**	**79,399.26**
$	30,875.35	$	72,042.48	**$ 307,278.16**	-	**$**	**102,126.11**
$	39,696.88	$	92,626.05	**$ 395,071.92**	-	**$**	**130,741.03**

Actual Savings from Freshwater & Wastewater ($AUD/yr)	TOTAL COST ($AUD) (Misc. + Equipment)	Payback Period		
			yrs	months
$ 680.63	$ 105,000.00	154.3	154	4
$ 32,870.91	$ 210,000.00	6.4	6	5
$ 65,061.18	$ 315,000.00	4.8	4	10
$ 89,274.05	$ 420,000.00	4.7	4	9
$ 114,178.21	$ 525,000.00	4.6	4	8
$ 4,457.52	$ 257,250.00	57.7	57	9
$ 44,263.53	$ 467,250.00	10.6	10	8
$ 76,255.81	$ 813,750.00	10.7	10	8
$ 115,759.85	$ 1,128,750.00	9.8	9	10
$ 170,829.38	$ 1,338,750.00	7.8	7	10
			yrs	months
$ (8,088.42)	$ 94,500.00	-11.7		
$ 5,781.79	$ 94,500.00	16.3	16	4
$ 19,652.00	$ 94,500.00	4.8	4	10
$ 33,522.20	$ 94,500.00	2.8	2	10
$ 47,392.41	$ 94,500.00	2.0	2	0
			yrs	months
$ 20,215.69	$ 362,250.00	17.9	17	11
$ 68,762.78	$ 813,750.00	11.8	11	10
$ 140,085.14	$ 1,233,750.00	8.8	8	10
$ 205,152.05	$ 1,774,500.00	8.6	8	8
$ 264,330.89	$ 2,194,500.00	8.3	8	4